Novel Chemical Approach for the Site Selective Generation of Complex Self-Assembled Virus Derivatives

zur Erlangung des akademischen Grades eines
DOKTORS DER INGENIEURWISSENSCHAFTEN (Dr.-Ing.)

der Fakultät für Chemieingenieurwesen und Verfahrenstechnik des
Karlsruher Institut für Technologie (KIT)

genehmigte
DISSERTATION

von
MSc. Carlos Arturo Azucena Serrano
aus El Salvador

Referent: Prof. Dr. Matthias Franzreb
Korreferent: Prof. Dr. Jürgen Hubbuch
Tag der mündlichen Prüfung: 5.Dezember.2012

What we have made with our hands,
Planned with our heart,
And cared with our brain, be for the benefit
Of friends, foes and strangers.

"I do not believe in a fate that falls on men however they act;
But I do believe in a fate that falls on them unless they act"
G. K. Chesterton

Acknowledgments

I would like to wholehearted thank my supervisor, Dr. Hartmut Gliemann, for his scientific guidance, enthusiasm, encouragement and his absolute dedication and commitment to the challenges of this project and dissertation. I am indebted to him, for believing and giving me an opportunity to change some lives with this work including my own. I am also in great debt and completely beholden with Dr. Fabian Eber and Prof. Dr. Christina Wege from the Dept. of Molecular Biology and Plant Virology from the University of Stuttgart for all the great time we had preparing, planning, doing and discussing the project and experimental procedures. I would like to gratefully thank also to my doctorate advisor Prof. Dr.-Ing. Matthias Franzreb and my co-referent Prof. Dr. Jürgen Hubbuch for their valuable support, commitment and discussions. I would like to thank Vanessa Trouillet and Dr. Michael Bruns for the XPS measurements and friendly discussions. I am also grateful to Prof. Dr. Katja Schmitz for the introduction to the microspotter at the Institute of Toxicology and Genetics.

I would like to thank my family -which I owe eternally also respect and admiration for his work, ethics and manners- my mother, Haydee Anabell, my siblings Carlos Eduardo, Fatima and Veronica, my father Carlos Arturo, and my grandparents, Galileo, Haydee and Alicia for their love and support during my odyssey in Germany. Excellent guides, leaders themselves, they have always encouraged me towards excellence but above all compassion and kindness.

I am eternally obliged to my beloved wife, Ivonne, whose patience, commitment and encouraging words made every day of the journey an even more pleasant adventure. Thank you for giving me strength and support when I needed it the most.

I would like also to thank my friends, Tatjana and Andre, whose company along this project, the discussions, barbecues and the teaching-learning processes have been also invaluable to me during these years. I would like to thank also all the behind-the-scenes friends (I would not like to name anyone specifically for risk of leaving someone out), for the great and funny times, relax and enjoyable conversations. Special thanks go to Dr. Peter Weidler, Dr. Frank Friedrich, Stefan Heißler, Maria Buchholz, Peter Krolla-Sidenstein and Dr. Martin Silvestre, whose expertise, great instruction, discussions and support during the daily challenges, proved to be scientifically accurate with a high confidence level. I would to thank the Baden-Württemberg Stiftung for funding this research as well as, Dr. Anna Müller, Dr. Dr. Michael Hirtz, Dr. Stefan Walheim and Prof. Dr. Christof Wöll for their support and valuable discussion. This work was partly carried out with the support of the Institute of Functional Interfaces and the Karlsruhe Nano Micro Facility.

I declare hereby, that this dissertation has been elaborated by me and not used other than the sources, references and resources mentioned in the body of this manuscript. I present this work with the best of my knowledge and to fulfill the requisites of the Karlsruhe Institute of Technology to ensure good scientific practices.

Eggenstein/Leopoldshafen, October 2012

Abstract

The ability of self-assembly of biopolymers into functional virions – mature viral particles – combined with the modular quality of viral genomes, provides a vast potential for biologically based nano-engineering. One of the most promising biomolecule complexes is the Tobacco mosaic virus (TMV), which is a tube-shaped, exceptionally stable plant virus. Up to today it has been demonstrated that TMVs can be assembled in-vitro and adsorbed onto surfaces. However, this results in only weak binding forces and a far from optimum distribution and orientation of the TMVs. Therefore, the main goal of this dissertation is to develop a method which allows an efficient and site-selective immobilization of viral-RNA on oxidic and polymeric surfaces. By the help of these substrates cooperation partners at Stuttgart University were able to produce bottom-up self-assembled TMV-like particles with well-defined sequential order of coat proteins. Two new chemical approaches for the synthesis of substrates with covalently bound viral-RNA are introduced: Aldehyde converted alkoxysilanes and in-house synthesized isothiocyanate (ITC) alkoxysilanes. Both chemical strategies allow the activation of oxidic surfaces for the covalent immobilization of DNA oligomers, which, in turn, served as linkers for the viral RNA. By the use of the generated templates the site-selective bottom-up self-assembly of TMV-like particles is successfully demonstrated, for the first time. In comparison the newly developed isothiocyanate-terminated silane chemistry showed superior performance than the aldehyde-based surface chemistry. The successful conversion of 3-aminopropyltrimethoxysilane into 3-isothiocyanatepropyltrimethoxysilane was confirmed using infrared spectroscopy. In addition Raman spectroscopy was applied to follow up the behavior of the reactants consumption. The ITC-terminated silane was coupled to two different non-structured oxidic substrates: SiO_2 wafers and glass slides. Besides glass and Si wafers with a native oxide layer also the polymer polydimethylsiloxane (PDMS) was used as substrate material, whereby PDMS was irradiated with UV-light in order to create an oxidic layer on top of the polymer. In all cases, the substrates were prepared, chemically modified and characterized intensively by surface analytical methods, such as X-ray photon spectroscopy (XPS), atomic force microscopy (AFM), contact angle (CA) measurements and fluorescence microscopy. In order to achieve a spatial selective immobilization of the viral particles, the coupling strategies were combined with different structuring techniques, such as micro contact printing (μCP), Dip Pen Nanolithography (DPN) and UV-light irradiation. In all cases a site-selective bottom-up growth of TMV-like particles could be shown, however, substrates with native oxidic layers resulted in higher particle densities. Further goal will be to genetically modify the virus coat proteins in order to generate different functional groups, which can be arranged in a selected order along the longitudinal axis of the virus-like particles. In addition strategies should be developed, which allow the TMV-like particles to stand upright on the surface.

Zusammenfassung

Die Fähigkeit der Selbstorganisation von Biopolymeren zu funktionalen Virionen, d.h. reifen Viruspartikeln, kombiniert mit den modularen Eigenschaften des viralen Genoms, bietet ein großes Potenzial für biologisches Nano-Engineering. Eine der vielversprechendsten Biomolekülkomplexe ist das Tabakmosaikvirus (TMV), welches ein rohrförmiges, außergewöhnlich stabile Pflanzenvirus ist. Bis heute hat es sich gezeigt, dass TMVs in vitro zusammengebaut und an der Oberflächen adsorbiert werden kann. Dies führt jedoch zu nur schwachen Bindungskräfte und zu einer nicht-optimalen Verteilung und Orientierung des TMVs. Das Hauptziel dieser Dissertation ist daher eine Methode zu entwickeln, die eine effiziente und ortsselektiven Immobilisierung von Virus-RNA auf oxidischen und polymer-basierten Oberflächen ermöglicht. Mit Hilfe dieser Substrate produzieren unsere Kooperationspartner an der Universität Stuttgart bottom-up selbstorganisierte TMV-Partikel mit einer definierten Reihenfolge der Hüllproteine. Zwei neue Ansätze für die chemische Synthese von Substraten mit kovalent gebundenen viralen RNA konnte eingeführt werden: Aldehyde umgewandelt zu Alkoxysilane und in-house synthetisierte Isothiocyanat (ITC) Alkoxysilanen. Beide chemischen Strategien ermöglichen die Aktivierung oxidischer Oberflächen zur kovalenten Immobilisierung von DNA-Oligomeren, die ihrerseits als Anbindung der viralen RNA ermöglicht. Durch Verwendung von Schablonen konnte eine ortsselektive bottom-up-Selbstorganisation von TMV-ähnlichen Partikenn zum ersten Mal erfolgreich gezeigt werden. Im Vergleich zeigt die neu entwickelten Isothiocyanat-terminierte Silanchemie eine bessere Leistungsfähigkeit als der Aldehyd-basierte Oberflächenchemie. Die erfolgreiche Umwandlung von 3-Aminopropyltrimethoxysilan in 3-Isothiocyanatepropyltrimethoxysilan wurde unter Verwendung von Infrarot-Spektroskopie bestätigt. Darüber hinaus wurde Raman-Spektroskopie angewandt, um die Kinetik des Reaktantenverbrauchs zu untersuchen. Die ITC-terminierten Silane wurden auf zwei unterschiedlichen nicht-strukturierten oxidischen Substraten gekoppelt: SiO_2-Wafern und Glasobjektträgern. Neben Glas und Si-Wafern mit einer nativen Oxidschicht wurde auch das Polymer Polydimethylsiloxan (PDMS) als Trägermaterial benutzt, wobei PDMS mit UV-Licht bestrahlt wurde, um eine oxidische Schicht auf dem Polymer zu erzeugen. In allen Fällen wurden die Substrate vorbereitet, chemisch modifiziert und intensiv durch die Oberfläche analytische Methoden, wie X-ray Photonen-Spektroskopie (XPS), Rasterkraftmikroskopie (AFM), Kontaktwinkel (CA) Messungen und Fluoreszenzmikroskopie charakterisiert. Um eine ortsselektive Immobilisierung der viralen Partikel zu erreichen, wurden die Oberflächen mit unterschiedlichen Techniken strukturiert, wie micro contact printing (mCP), dip pen nanolithographie (DPN) und UV-Licht-Bestrahlung kombiniert. Ein ortsselektives bottom-up Wachstum von TMV-ähnlichen Partikeln konnte gezeigt werden, dabei führten Substrate mit nativem oxidischen Schichten zu höhere Teilchendichte. Weiteres Ziel ist die genetischen Modifizierung des Virus Hüllproteins, um verschiedene funktionelle Gruppen zu erzeugen, die in einer ausgewählten Reihenfolge entlang der Längsachse der virusähnlichen Partikel angeordnet werden. Zusätzlich Strategien werden entwickelt, die es erlauben, die TMV-ähnlichen Partikel senkrecht auf der Oberfläche zu fixieren.

TABLE OF CONTENTS

ABSTRACT I

ZUSAMMENFASSUNG II

1 .- INTRODUCTION AND OBJECTIVES 1-1

1.1 BACKGROUND OF THE PROJECT 1-1
1.2 CHALLENGES AND OBJECTIVES 1-4

2 METHODS AND TECHNIQUES FOR CHEMICAL FUNCTIONALIZATION AND STRUCTURING OF SURFACES. 2-1

2.1 CHEMICAL MODIFICATION OF SURFACES BY SELF ASSEMBLED MONOLAYERS (SAMS) 2-1
2.1.1 Introduction *2-1*
2.1.2 Silane-based Non-Patterned SAMs on Oxidic Substrates *2-3*
2.1.3 Silane-based Chemically Patterned SAMs on Oxidic Substrates *2-6*
2.1.3.1 Microcontact Printing 2-6
2.1.3.2 Ultraviolet Induced Lithography and Functionality Promotion 2-9
2.1.3.3 Polymer Blends 2-12
2.1.3.4 Dip Pen Nanolithography 2-13
2.2 BIOLOGICAL FUNCTIONALIZATION OF SURFACES- TOBACCO MOSAIC VIRUS SELF-ASSEMBLY ON A SURFACE. 2-15

3 .- EXPERIMENTAL METHODS 3-1

3.1 PROTOCOLS 3-1
3.1.1 Functionalization of Glass and Silicon Oxide surfaces *3-1*
3.1.1.1 Synthesis of ITCPTMS 3-3
3.1.1.2 Silanization of Silica Wafers and Glass Slides 3-5
3.1.1.3 Addition of Iron-cored Silica Nanoparticles and Fluoresceinamine 3-6
3.1.2 Functionalization of Polymers by UV/O_3 Irradiation *3-8*
3.1.3 Polymer blends as mask for selective functionalization of silica wafers *3-9*
3.1.4 Biofunctionalization of Substrates (Silicon Wafers and PDMS Oxidized Surface) *3-12*
3.1.4.1 DNA Linker Immobilization on Functionalized Isothiocyanate-Silanized Wafers. 3-12
3.2 MEASUREMENT TECHNIQUES 3-14
3.2.1 Atomic Force Microscopy *3-15*
3.2.2 X-ray Photospectroscopy *3-20*
3.2.3 Fourier Transform Infrared Spectroscopy *3-23*
3.2.4 Fourier Transform Raman Spectroscopy *3-26*
3.2.5 Contact Angle *3-28*

4 .- RESULTS AND DISCUSSION 4-1

4.1 ALDEHYDE-BASED SILANIZATION AND IMMOBILIZATION OF DNA-LINKER. 4-1
4.1.1 Characterization of Physical and Chemical Properties of Aldehyde-terminated Surfaces *4-4*
4.1.1.1 Morphology and Roughness 4-4
4.1.1.2 Wettability 4-6
4.1.1.3 Elementary Composition 4-7
4.1.1.4 Chemical Functionality 4-10
4.1.2 Application of Aldehyde-Based Silane Chemistry for Bottom-Up Assembly of Self-Assembled Tobacco Mosaic Virus. *4-13*
4.1.2.1 Homogeneously Coated Oxidic Substrates 4-13
4.1.2.2 Chemically Patterned SAMs on Oxidic Substrates 4-14
4.2 ISOTHIOCYANATE-BASED SILANIZATION AND IMMOBILIZATION OF DNA-LINKER. 4-20
4.2.1 Synthesis and Spectroscopic Characterization of 3-isothiocyanatepropyltrimethoxysilane *4-20*
4.2.1.1 Synthesis Procedures 4-21
4.2.1.2 Spectroscopic Characterization using FT-IR and FT-Raman 4-22
4.2.2 Characterization of Physical and Chemical Properties of Isothiocyanate-terminated Surfaces on Silica/glass Substrates. *4-32*
4.2.2.1 Morphology and Roughness 4-34
4.2.2.2 Wettability 4-35
4.2.2.3 Elementary Composition 4-39
4.2.2.4 Chemical Functionality 4-43

4.2.2.4.1 Microcontact Printing of Aminofluorescein on ITC-functionalized Glass Slides. 4-45
4.2.2.4.2 Isothiocyanate as a Reactive Agent for Microspotting Array Experiments. 4-47
4.2.2.4.3 Assessment of Isothiocyanate Silanization Homogeneity Using the Microarray Spotter Instrumentation....4-50
4.2.2.4.4 Dip-Pen Nanolithograpy (DPN)....4-55
4.2.3 Characterization of Physical and Chemical Properties of Isothiocyanate-terminated Surfaces on Polymeric Substrates (PDMS). 4-60
4.2.3.1 Morphology and Roughness....4-63
4.2.3.2 Wettability....4-73
4.2.3.3 Elementary Composition 4-75
4.2.3.4 Chemical Functionality 4-77
4.2.4 Application of Isothiocyanate-Based Silane Chemistry for Bottom-Up Assembly of Self-Assembled Tobacco Mosaic Virus. 4-82
4.2.4.1 Homogeneously Coated Oxidic Substrates....4-83
4.2.4.2 Chemically Patterned SAMs on Oxidic Substrates....4-94
4.2.4.3 Chemically Patterned SAMs on Polymeric Substrates....4-97

5 CONCLUSIONS 5-1

5.1 GENERAL CONCLUSIONS....5-1
5.2 OUTLOOK....5-4

6 REFERENCES 6-1

APPENDIX....A-1

A. VIRAL PARTICLES ASSEMBLY METHODOLOGY (STUTTGART UNIVERSITY- PLANT VIROLOGY GROUP) A-1
A.1 DNA Linker Immobilization on Aldehyde Functionalized Substrates A-1
A.2 RNA Ligation and Induced Assembly of TMV-like Nanotubes on Unstructured and Patterned Aldehyde Functionalized Surfaces A-2
A.3 Hybridization of assembly-directing RNA and surface associated assembly of TMV Coat Protein on Isothiocyanate silanized substrates A-3
A.4 Analysis of Intermediate RNA States in the Course of Bottom-Up Assembly. A-4
B. MICROCONTACT-PRINTING OF SILANES A-5

INDEX OF FIGURES

FIGURE 1.- PROJECT SCHEME OVERVIEW: ON AN OXIDIC SURFACE (GLASS, SILICA) (1) VIA SILANE CHEMISTRY (2) - A SELF-ASSEMBLED MONOLAYER TERMINATED BY A HIGHLY SPECIFIC REACTIVE CHEMICAL GROUP TOWARDS AN AMINO-TERMINATED DNA-LINKER IS COUPLED (3). THE DNA-LIGAND IS THEN SELECTIVELY COUPLED TO A VIRAL RNA BY HYBRIDIZATION FROM TOBACCO MOSAIC VIRUS (4). AFTERWARDS, COAT PROTEIN, WHICH CAN BE PREVIOUSLY MODIFIED IS ADDED SEQUENTIALLY TO THE SURFACE AND AN ENTROPY-DRIVEN SELF ASSEMBLY PROCESS E TAKES PLACE DURING THIS , THE VIRUS-LIKE, ROD-SHAPED NANOPARTICLE ASSEMBLES USING THE RNA AS A SCAFFOLD (5). THE BOX REPRESENTS THOSE PREPARATION STEPS WHICH WERE IN THE FOCUS OF THE WORK SUMMARIZED IN THIS THESIS. 1-3

FIGURE 2.- SCHEME OF SELF-ASSEMBLED MONOLAYERS. THE SAMS ARE COMONLY PREPARED BY DIPPING THE SUBSTRATES IN THE SOLUTION CONTAINING THE SAM MOLECULE. THE FIRST STEP CONSTITUTES GENERALLY AN ADSORPTION ONTO THE SUBSTRATE FOLLOWED BY A REORGANIZATION OF THE ALKYL CHAINS. GENERALLY THE SAMS ARE CREATED BY TWO DISTINCT MOLECULES: THIOLS AND SILANES. THE FIRST USES A SULFUR ATOM TO BIND ONTO GOLD AND SILVER PREFERABLY. THE SECOND USES AN ALKOXY GROUP TO BIND ON OXIDIC SURFACES SUCH AS SILICA OR GLASS. THEY ARE CONSTITUTED BY THREE COMPONENTS: A) THE ORGANIC FUNCTIONAL GROUP B) THE SPACER FORMED BY AN ALKYL CHAIN AND C) LIGAND OR TAIL GROUP WHICH BINDS TO THE SUBSTRATE DEPENDING ON THE CHEMICAL GROUP OF THE MOLECULE.....2-2

FIGURE 3.- SCHEME OF SILANIZATION PROCESS: A) THE SILANE UNDERGOES HYDROLISIS IN PRESENCE OF WATER RELEASING AN ALCOHOL RELATED TO ITS TAIL GROUP. IT CAN ALSO CONDENSATE STILL IN SOLUTION FORMING BIGGER POLYMERIC AGGREGATES. ONCE HYDROLIZED THE SILANOL GROUPS ATTACH TO THE SURFACE (DEPENDING OF THE PREVIOUS REACTION, HYDROLYSIS AND/OR CONDENSATION) EITHER IN B) SINGLE MOLECULES WHICH REARRANGE FURTHER INTO MONOLAYERS *VIA* ISLAND FORMATION (C) OR COMPLETE POLYMERIZED NETWORKS ATTACHED ON THE SUBSTRATE BY FEW HYDROXYLS (D). THE LATER CASE CAN ALSO HAPPEN AFTER THE MONOLAYER ISLANDS ARE FORMED BUT FURTHER CONDENSATION REACTIONS TAKES PLACE ON THE SURFACE ITSELF.....2-4

FIGURE 4.- DIFFERENT TYPES OF BONDING/INTERACTION BETWEEN AMINOPROPYLETHOXYSILANE MOLECULES AND SILICON OXIDE SUBSTRATES. ADAPTED FROM ASENATH, ET AL. 2008 [116]. A) VERTICALLY POSITIONED SILANE BONDED VIA SILANOL GROUP ON THE SURFACE. B) HORIZONTALLY POSITIONED SILANE BOUNDED *VIA* SILANOL INTERACTION PLUS HYDROGEN BOND BETWEEN THE AMINO AND THE HYDROXYL GROUP ON THE SURFACE. C) HYDROGEN BOND BETWEEN THE NON-HYDROLIZED ALKOXY GROUP AND THE HYDROXYL GROUP OF THE SURFACE. D) WEAK HYDROGEN BOND BETWEEN SILANOL AND HYDROXYL GROUPS ON THE SURFACE AND E) HEAD GROUP INTERACTION BETWEEN AMINO GROUP AND THE HYDROXYL OF THE SUBSTRATE. 2-6

FIGURE 5.- SCHEME OF THE PROCEDURE OF MICROCONTACT PRINTING (μCP) TO PATTERN SELF-ASSEMBLED MONOLAYERS (SAMS) ON A SUBSTRATE. THE PROCESS BEGINS WITH THE PREPARATION OF A MASTER FOR STAMP FABRICATION. THE MASTER IS CREATED BY THE IRRADIATION OF A PHOTORESIST LAYER BY AN E-BEAM, FOLLOWED BY A DEVELOPING AND AN ETCHING PROCESS. AFTER THE PDMS IS POURED ON TOP AND CURED AT INCREASED TEMPERATURE, THE STAMP IS PEELED OFF THE MASTER, IS INKED WITH THE PRECURSOR MOLECULE OF THE SAM AND IS BROUGTH IN CONTACT WITH THE SUBSTRATE. THE "INK" IS TRANSFERRED FORMING AN ORGANIZED MONOLAYER AT THE CONTACT AREAS. IN THIS WAY, SELECTIVE AREAS CAN BE PATTERNED WITH THE MOLECULE OF PREFERENCE. 2-9

FIGURE 6.- MECHANISM OF OXIDATIVE PROCESS ON PDMS USING UV/O_3 IRRADIATION IN AIR. A)THE METHYL GROUPS ARE SUCESSIVELY SUBSTITUTED BY HYDROXYL GROUPS. THE PDMS CHAINS ARE IN BLUE AND THE SUBSTITUTED SPECIE WITH SILANOL GROUPS (SI-OH) IS SHOWN IN RED. EVENTUALLY ALSO THE FORMATION OF ALDEHYDES OR CARBOXILIC ACID CAN OCCURR (ORANGE). ON B) ONCE THE POLYMER IS COMPLETELY OXIDIZE TO HYDROXYL GROUPS, THE REMOVAL OF WATER WILL TRANSFORM THE DECOMPOSED POLYMER TO INORGANIC SILICON OXIDE.....2-11

FIGURE 7.- POLYDIMETHYLSILOXANE OXIDATION AND FUNCTIONALITY SCHEME. FIRST THE CROSSLINKED PDMS (A) IS PLACED INSIDE A CHAMBER WHICH CONTAINS A UV/O_3 LAMP GENERATOR PLACING A PROTECTIVE MASK PREVIOUS TO THE IRRADIATION (B). AFTER THE SILICA LIKE LAYER IS CREATED (C), THEN THE SUBSTRATE CAN BE SILANIZED (D) FOLLOWING THE PROCEDURE TO FUNCTIONALIZE A NON-STRUCTURED SURFACE. 2-12

FIGURE 8.- SCHEME OF POLYMER BLEND LITHOGRAPHY. FIRST THE SUBSTRATE (A) IS COATED WITH A SOLUTION CONTAINING THE TWO IMMISCIBLE POLYMERS (PS AND PMMA), AFTER SOLVENT EVPORATION PHASE SEPARATION TAKES PLACE (B). SOLVING ONE OF THE POLYMERS (PS) SELECTIVELY WILL CREATE HOLES (C) WHICH CAN BE USED FOR SITE SELECTIVE FUNCTIONALIZATION (D).....2-13

FIGURE 9.- DIP PEN NANOLITHOGRAPHY CONCEPT SCHEME. FIRST THE AFM CANTILEVER IS DIPPED INTO A SOLUTION CONTAINING THE INK (SILANE OR THIOL). AFTER THE TIP IS DRIED, IT IS PLACED INTO CONTACT WITH THE SURFACE (B). DUE TO THE HUMIDITY OF THE ENVIRONMENT A WATER MENISCUS ON THE TIP IS FORMED, MAKING THE MOLECULES TO FLOW TOWARDS THE SUBSTRATE. ONCE THE MOLECULE IS DIRECTLY PLACED ON THE SUBSTRATE, FURTHER FUNCTIONALITY CAN BE ACHIEVED. IN THIS DISSERTATION, DNA LINKERS WHICH ARE COMPLEMENTARY TO A TMV-RNA SEQUENCE WILL BE COUPLED ON THE ISOTHIOCYANATE SURFACE. (C) THE AUTOMATED PROCESS MAKES THE REPETITION OF SEVERAL HUNDREDS OF FEATURES POSSIBLE USING DIFFERENT INKS SIMULTANEAOUSLY (D). 2-15

FIGURE 10.- SELF-ASSEMBLY PROCESS OF TMV MECHANISTIC MODEL FOR THE RNA-DIRECTED SELF-ASSEMBLY OF TMV-LIKE PARTICLES IN THE 5' DIRECTION. [BUTLER, 1984]. A) THE STRUCTURE OF THE PROTEIN DISK DERIVED FROM AN X-RAY DIFFRACTION PATTERN [BHYRAVBHATLA ET AL 1998]. B) SECONDARY STRUCTURE MODEL OF THE RNA SEQUENCE OF THE TMV GENOME [GOELET, 1982] WHERE THE INSET SHOWS THE ORIGIN OF ASSEMBLY HAIRPIN WITH THE NONANUCLEOTIDE LOOP [ZIMMERN AND BUTTLER , 1977]. C) THE INTERACTION OF THIS SECTION WITH A PREFORMED PROETIN DOUBLE-DISK AGGREGATE LEADS TO A TRANSITION OF THE COMPLEX INTO A LOCKWASHER COMFORMATION (D) WHEREAS THE ADDITION OF FURTHER DISKS TO THE GROWING POLE FORMS A CILINDRICAL STRUCTURE WHEN THE STRETCH OF THE RNA TAKES PLACE ALONG THE CENTRAL CHANNEL OF THE NASCENT VIRAL PARTICLE (E). THE SELF-ASSEMBLY PROCESS OF PROTEIN DISKS ALONG A RNA-TEMPLATE USED AS SCAFFOLD IS SHOWN. THE PROCESS IS SHOWN AS TAKEN PLACE IN SOLUTION WITH NO SPATIAL RESTRICTIONS. 2-17

FIGURE 11.- 3D AND AFM TOPOGRAPHY IMAGES PDMS STAMPS WITH TWO DIFFERENT PATTERNS: (A) LINES WITH 7.5 MICRON WIDTH DECREASING OVER A 60X60 μM^2 SCANNED AREA DOWN TO 5 MICRONS WIDTH. (B) PATTERN OF PYRAMIDAL FEATURE OVER A 20X20 μM^2 SCANNED AREA. THE COLOR SCALE IN BOTH IMAGES RANGE UP TO 1 MICRON.....3-8

FIGURE 12.- AFM TOPOGRAPHY IMAGE SHOWING SHOWING THE PS-PMMA STRUCTURED SUBSTRATE. A PARTIAL DISOLUTION OF THE PMMA MASK HAS BEEN DONE BY PLACING A DROP OF ACETIC ACID ON THE SURFACE REMOVING EXCLUSIVELY THE PMMA FROM THAT AREA. THE CIRCLES BELONG TO THE POLYSTYRENE POLYMER, AND THE MATRIX TO POLYMETHYLMETHACRYLATE. THE PS IS LOWER THAN THE PMMA BUT STILL HIGHER THAN THE SUBSTRATE. 3-10
FIGURE 13.- AFM TOPOGRAPHY OF A PS / PMMA POLYMER BLEND (1:1 MG) A) AFTER CASTING AND B) AFTER CYCLOHEXANE MEDIATED POLYSTYRENE REMOVAL, C) HIGHER MASS RATIO (1.5 MG PMMA:1 MG PS) SPIN COATED AND POLYSTYREN REMOVAL BY CYCLOHEXANE, D) REMOVAL OF BOTH POLYMERS BY TREATING THE SAMPLE WITH TOLUENE (FOR POLYSTYRENE) AND ACETIC ACID (FOR PMMA). 3-11
FIGURE 14.- ATOMIC FORCE MICROSCOPE INSTRUMENT DESCRIPTION. THE SAMPLE IS MEASURED BY THE TIP INTERACTING WITH THE SURFACE OF THE SAMPLE. THE SUBSTRATE IS PLACED ON TOP OF A SCANNER WHICH IS RESPONSIBLE TO MOVE THE SAMPLE IN XYZ DIRECTION. THE PIEZO RECEIVES A FEEDBACK SIGNAL FROM THE CONTROLLER WITH IN TURNS RECEIVES A SIGNAL FROM THE PHOTODIODE. THIS SIGNAL ADJUST THE FORCE/HEIGHT OF THE SAMPLE TO THE CANTILEVER AND SIMULTANEOUSLY IS PLOTTED IN THE PC VIA A DEDICATED PROGRAM. 3-16
FIGURE 15.- A) MFP-3D BIO AFM FROM ASSYLUM RESEARCH. B) DIGITAL INSTRUMENTS MULTIMODE AFM (IMAGES COURTESY OF ASSYLUM RESEARCH AND BRUKER NANO SURFACES DIVISION RESPECTIVELY) 3-19
FIGURE 16.- DIAGRAM EXPLANATION OF XPS PRINCIPLE. WHEN SURFACES ARE IRRADIATED WITH SOFT X-RAYS THE EMITTED PHOTOELECTRONS WITH A DETERMINED ENERGY ARE ANALYZED. THE INTERACTION BETWEEN AN X-RAY PHOTON AND THE CORE LEVEL ELECTRON OF AN ATOM CAUSES A COMPLETE TRANSFER OF THE PHOTON ENERGY TO THE ELECTRON WHICH HAS NOW ENOUGH ENERGY TO ESCAPE FROM THE SURFACE OF THE SAMPLE. THE DIFFERENCE BETWEEN THE X-RAY ENERGY AND THE PHOTOELECTRON ENERGIES GIVES THE BINDING ENERGIES (BES) OF THE CORE LEVEL ELECTRONS. 3-20
FIGURE 17.- AN EXAMPLE OF A TYPICAL XPS SURVEY SPECTRUM TAKEN FROM A ITC SILANIZED SAMPLE. INSET TILE SHOWS THE RANGE OF ENERGIES ASSOCIATED WITH THE BANDS TYPICAL FOR C 1S PHOTO ELECTRONS: SCAN A (C-C), SCAN B (C-O, C-N) AND SCAN C (-N=C=S) RESPECTIVELY. 3-22
FIGURE 18.- MICHELSON INTERFEROMETER SCHEME AS PART OF FTIR SPECTROMETER. 3-24
FIGURE 19.- SIMPLIFIED ENERGY LEVEL DIAGRAM OF THE DIFFERENT SCATTERING PROCESSES. THE WAVELENGTH DIFFERENCE BETWEEN THE EXCITATION LIGHT (λ_E) AND THE SCATTERED ONE (λ_S) IS RELATED TO RAMAN SHIFT ΔV GIVEN IN WAVENUMBERS ACCORDING TO $\Delta V = 1/\lambda_E + 1/\lambda_S$. IF THE DIFFERENCE IS 0 RAYLEIGH-SCATTERING OCCURS. 3-27
FIGURE 20.- MICHELSON INTERFEROMETER SCHEME AS PART OF FT-RAMAN SPECTROMETER. IN CONTRAST TO IR SPECTROSCOPY – FIRST THE SAMPLE IS IRRADIATED BY THE LASER LIGHT AND IT IS THE SCATTERED LIGHT WHICH IS COUPLED INTO THE MICHOLSEN INTERFEROMETER. THIS GUARANTEE THE COLECTION OF THE SCATTERED LIGHT THROUGH THE OPTICS/FILTER AND FURTHER ON THE INTERFEROMETER. THE INTERFEROGRAM IS THEN PROCESSED TO YIELD AN ABSORBANCE SPECTRUM AT THE COMPUTER. 3-28
FIGURE 21.- CONTACT ANGLE SCHEME SHOWING YOUNG'S EQUATION 3-29
FIGURE 22.- A) SCHIFF BASE (1) AND MICHAEL-TYPE (2) REACTIONS OF GLUTARALDEHYDE (PARTIALLY POLYMERIZED) WITH AMINO SILANE. B) IDEALIZED REACTION ON THE SURFACE. 4-2
FIGURE 23.- MECHANISM OF ALDEHYDE FUNCTIONALIZATION OF SURFACES. THE PATHWAYS FOLLOWS THE SAME REACTION MECHANISM AS THE SILANES BUT IN ADDITION A FINAL INCUBATION IN GLUTARALDEHYDE IS PERFORMED. THE FINAL PRODUCT IS A IDEALIZED MONOLAYER FORMATION WHICH LEAVES THE ALDEHYDE GROUPS ALSO FREE TO FURTHER COVALENT ATTACHEMENT OF ANOTHER MOLECULE CARRYING AN AMINO FUNCTIONALITY. 4-3
FIGURE 24.- AFM TOPOGRAPHY (UPPER ROW) AND PHASE (LOWER ROW) IMAGES FROM A) CLEAN WAFER, B) AMINO FUNCTIONALIZED WAFER AND C) ALDEHYDE COUPLED WAFER. PHASE IMAGES FROM D) CLEAN, E)AMINO AND F) ALDEHYDE FUNCTIONALIZED SUBSTRASTES ARE SHOWN 4-5
FIGURE 25.- CONTACT ANGLE MEASUREMENTS ON A SET OF AMINO/ALDEHYDE SILANIZED SLIDES. THE MEASUREMENTS WERE DONE ON THE SAME SLIDES BEFORE AND AFTER EACH STEP (AMINOSILANIZATION AND FURTHER ALDEHYDE CONVERSION). THE DOTS REPRESENT THE POSITION OF THE DROP FOR THE ASSESSMENT 4-6
FIGURE 26.- XPS SURVEY SPECTRA FROM THE SAMPLE IN THREE STAGES (CLEAN, AMINO FUNCTIONALIZED AND FINALLY ALDEHYDE FUNCTIONALIZED). THE SAMPLE WAS THE SAME ALONG THE PROCESS ON THE SAME SAMPLE. 4-7
FIGURE 27.- XPS SPECTRA ON AMINO (A AND C) AND SUBSEQUENTLY ALDEHYDE (B AND D) FUNCTIONALIZED SILICA WAFER. A) AND B) BELONGS TO CARBON 1S BINDING ENERGY WHILE C) AND D) BELONGS TO NITROGEN 1S BINDING ENERGY. 4-9
FIGURE 28.- FLUORESCENT REACTIVITY ASSESSMENT OF AMINO/ALDEHYDE TERMINATED GLASS SLIDES USING DNA-AMINO TERMINATED OLIGONUCLEOTIDE AS FLUOROPHORE BINDING MOLECULE. 4-12
FIGURE 29.- AFM TOPOGRAPHIC IMAGES OF TMV LIKE PARTICLES SELF-ASSEMBLED *VIA* RNA LIGATION ON THE SURFACE AFTER THE WHOLE PROCESS OF SURFACE FUNCTIONALIZATION WAS CARRIED OUT. 4-13
FIGURE 30.- AFM TOPOGRAPHY IMAGES OF DIFFERENT SiO_2 SUBSTRATES WHICH WERE PREPARED IDENTICALLY. ALL SUBSTRATES WERE STRUCTURED BY POLYMER BLEND LITHOGRAPHY AND UTILIZED FOR BOTTOM-UP SELF-ASSEMBLY OF TMV-LIKE NANOTUBES. ON THE TOP: A,B) POLYMER BLEND WITH THE POLYSTYRENE REMOVED AND READY FOR ASSEMBLY. ON THE BOTTOM: SAMPLES AFTER THE SILANIZATION, ALDEHYDE REACTION AND FURTHER TMV ASSEMBLY. INSET A DIFFERENT REGION OF EXAMINATION ON SAME SAMPLE AS THE BOTTOM. 4-15
FIGURE 31.- AFM TOPOGRAPHY IMAGE OF TMV-LIKE NANOTUBES PREASSEMBLED IN SOLUTION AND LATER DEPOSITED ON A) FLAT UNSTRUCTURED SI-WAFERS B) STRUCTURED WAFER WITH POLYMER MASK PS-PMMA 4-16
FIGURE 32.- COMPARISON OF THE LENGTH DISTRIBUTION OF BOTTOM-UP ASSEMBLED TMV-LIKE PARTICLES (AFM TOPOGRAPHY IMAGE A1 AND HISTOGRAM A2) WITH PARTICLES PREASSEMBLED IN SOLUTION (AFM TOPOGRAPHY IMAGE B1 AND HISTOGRAM B2). 4-17
FIGURE 33.- AFM TOPOGRAPHIC IMAGE OF A SILICA WAFER WITH SPOTTED PREASSEMBLED VIRUS-LIKE PARTICLES ON A STRUCTURED SAMPLE. ON A) THE SAME SAMPLE BEFORE AND B) AFTER THOUROUGHLY CLEAN WITH USE OF ULTRASOUND FOR 2 MINUTES AND 0.1% SDS FOR 30 SECONDS. 4-19
FIGURE 34.- KALUZA REACTION SCHEME. THE PRIMARY AMINE CONTAINING MOLECULE IS REACTED WITH CARBON DISULFIDE IN BASIC MEDIUM. THE INTERMEDIATE DITHIOCARBAMATE DERIVATIVE IS THEN DESULFURIZED USING ETHYLCHLOROFORMATE TO YIELD IN BASIC MEDIA AN STABLE FORM OF ISOTHIOCYANATE GROUP ON THE PREVIOUSLY AMINATED MOLECULE. 4-21

FIGURE 35.- MODIFIED KALUZA REACTION SCHEME. THE REACTION PROCEEDS IN THE SAME WAY UNTIL THE DITHIOCARBAMATE IS FORMED. AFTERWARDS, THE DESULFURIZING STEP IS DONE USING CYANAMIDE. THIS PROVIDES WITH ANOTHER ROUTE OF SYNTHESIS WHICH DOES NOT NEED A FURTHER SEPARATION PROCESS. 4-22
FIGURE 36.- RAMAN SPECTRA CM^{-1} OF THE PURE REACTANTS (DESCRIPTIONS AND MANUFACTURER IN CHAPTER 3). THE ENERGY INTERVAL IS CHOSEN AS THE INFLUENCE OF THE CARBON DISULFIDE IS MAXIMIZED IN THIS AREA AND NO FURTHER INFLUENCE FROM THE OTHER REACTANDS TAKES PLACE IN THIS AREA. 4-23
FIGURE 37.- RAMAN SPECTRA OF CARBON SISULFIDE VERSUS TIME IN (A). THE RAMAN INTENSITY OF THE SPECTRA IN THE WAVENUMBER REGION BETWEEN 640 AND 650 CM^{-1} CORRESPONDING TO THE CS_2 SIGNAL. ARE PLOTTED IN (B) TAKING INTO ACCOUNT THE AREA UNDER EACH CURVE IN THE SAME INTERVAL OF WAVENUMBERS (UNITS ARE ARBITRARY). THE CONDITION OF THE EXPERIMENTS FOLLOWS A CLOSE SYSTEM WITH NO EVAPORATION AND NO LOSSES. THE PROBE WAS NOT TAKEN OUT OF THE SPECTROMETER TO AVOID ANY ENVIRONMENTAL OR INSTRUMENTAL ERROR. 4-25
FIGURE 38.- INFRARED SPECTRA FROM REACTANTS INVOLVED IN THE ISOTHIOCYANATE SILANE SYNTHESIS. FROM TOP TO BOTTOM: 3-AMINOPROPYLTRIMETHOXYSILANE (APTMS), CARBON DISULFIDE (CS_2), ETHYLCHLOROFORMATE (ECF), TRIETHYLAMINE (TEA) AND FINAL PRODUCT 3-ISOTHIOCYANATEPROPYLTRIMETHOXYSILANE (ITCPTMS). THE EMERGENCE OF A DISTINCT BAND CENTERED AT 2100 CM^{-1} IS TYPICAL FROM ISOTHIOCYANATE DERIVATIVES. THIS BAND IS NOT PRESENT IN THE OTHER COMPONENETS OF THE REACTION. 4-26
FIGURE 39.- FTIR SPECTRA FROM 3-AMINOPROPYLTRIMETHOXYSILANE (BLUE) AND THE FINAL PRODUCT 3-ISOTHIOCYANATEPROPYLTRIMETHOXYSILANE (RED) AFTER KALUZA AND HODGKINGS REACTION [140, 228]. PARTICULARLY TO NOTE IS THE ARISING STRONG DOUBLET CENTERED AT ~2100 CM^{-1} CORRESPONDING TO AN -N=C=S ASYMMETRIC STRETCHING. 4-27
FIGURE 40.-IR SPECTRA OF REACTION SOLUTIONS FOLLOWING TWO DIFFERENT PREPARATION PATHS USING DIFFERENT SOLVENTS. A) ITCPTMS SYNTHESIS IN METHANOL, B) ITCPTMS SYNTHESIS IN CHLOROFORM FOLLOWING THE SAME PROCESS AND C) A SPECTRUM OF THE DITHIOCARBAMATE INTERMEDIATE. IN BOTH CASES ETHYLCHLOROFORMATE WAS USED AS AS DESULFURIZING AGENT FORMING THE INTERMEDIATE DITHIOCARBAMATE (RED LINE). 4-31
FIGURE 41.- FTIR SPECTRUM OF A IN-HOUSE SYNTHESIZED 3-ISOTHIOCYANATEPROPYLTRIMETHOXYSILANE IN CHLOROFORM MATRIX USING CYANAMIDE AS DESULFURIZING AGENT. THE SPECTRUM SHOWS SIMILAR BANDS ARISING CENTERED ON THE 2100 CM^{-1} WAVENUMBERS. 4-32
FIGURE 42.- MECHANISM OF COVALENT ATTACHMENT OF 3-ISOTHIOCYANATEPROPYLTRIMETHOXYSILANE TO THE SURFACE FOR FUNCTIONALIZATION. 4-33
FIGURE 43.- AFM IMAGES OF SILICA WAFERS AFTER CHEMICAL CLEANING (TOPOGRAPHY (A), PHASE (C)) AND AFTER FUNCTIONALIZATION WITH ITCPTES (TOPOGRAPHY (B), PHASE (D)). 4-35
FIGURE 44.- SINGLE CONTACT ANGLE MEASUREMENT ON A) CHEMICALLY CLEANED SILICON WAFER SURFACE (CA<5±0.5) AND B) ISOTHIOCYANATE-FUNCTIONALIZED SILICA WAFER (CA=65±6). 4-36
FIGURE 45.- AVERAGE CONTACT ANGLE DETERMINED FOR FOR SILICA WAFER SAMPLES CLEANED (BLUE LINE CA≤ 5°) AND AFTER SILANIZATION (ORANGE LINE CA= 70° ± 7). 4-37
FIGURE 46.- AVERAGE CONTACT ANGLE MEASUREMENTS FOR GLASS SLIDE SAMPLES. THE AVERAGE HAS BEEN CALCULATED BY MEASURING 3 POINTS IN 3 DIFFERENT SLIDES AND THEN PLOTTING THE AVERAGE. THE DOTS REPRESENTS THE POSITION OF THE DROPS ON THE GLASS SLIDE 4-38
FIGURE 47.- XPS SPECTRA OF A SILICA WAFER TREATED WITH IN-HOUSE-MADE ISOTHIOCYANATE SILANE (A-C) SHOWING THE C 1S, N 1S AND S 2P SIGNALS. AS A REFERENCE CLEAN, NON-SILANIZED SILICA WAS MEASURED (D-F). 4-40
FIGURE 48.- XPS SPECTRA OF C 1S AND N 1S COMPARING THE CUSTOM-MADE AVAILABLE ITCPTES (A, B) VERSUS THE SILANE SYNTHESIZED IN-HOUSE ITCPTMS (C, D). FOR ALL ELEMENTS NO SIGNIFICANT DIFFERENCES BETWEEN THE TWO SILANE SCAN BE FOUND AFTER THEY WERE BOUND TO THE SUBESTRATE. 4-42
FIGURE 49.- FLUORESCENT REACTIVITY ASSESSMENT OF AMINO/ISOTHIOCYANATE TERMINATED GLASS SLIDES USING DNA-AMINO TERMINATED OLIGONUCLEOTIDE AS FLUOROPHORE BINDING MOLECULE. 4-44
FIGURE 50.- ROAD MAP OF EXPERIMENTS IN SECTION 4.2.2.4 CHEMICAL FUNCTIONALITY ON ITC-BASED SILANIZATION. THE EXPERIMENTS HAVE BEEN DESIGN TO ASSESS: CHEMICAL REACTIVITY THROUGH FLUORESCENCE EVALUATION, HOMOGENEITY THROUGH FLUORESCENCE EVALUATION OF MICROARRAYS ON GLASS SLIDES AND ADHESION CAPABILITIES OF NANOPARTICLES AT SMALL SCALES. THE SECTION APPROACHES THIS ASSESSMENT THROUGH SCALING DOWN THE STRUCTURING TECHNIQUE FROM MACROSTRUCTURING UP TO MICRO/SUB-MICRON STRUCTURING. 4-45
FIGURE 51.- FLUORESCENCE IMAGE OF MICROCONTACT PRINTING PATTERNS FROM AMINOFLUORESCEIN ON ISOTHIOCYANATE SILANIZED GLASS SLIDES. A) AND C) REPRESENT STAMPING WITH THE SAME LINE THICKNESS BUT DIFFERENT SPACING BETWEEN THEM. B) AND D) ARE STAMPS REPRESENTING DIFFERENT LINE THICKNESS BUT SAME SPACING BETWEEN THEM. THE LINES REPRESENT THE PLACES WHERE THE FLUORESCENCE INTENSITY PROFILE MEASUREMENT WAS PERFORMED. 4-46
FIGURE 52.- FLUORESCENCE EVALUATION OF COMMERCIALLY AVAILABLE EPOXY SLIDES VERSUS ISOTHIOCYANATE IN-HOUSE PREPARED SILANE. A) EPOXY SLIDE TREATED WITH A STANDARD PROTOCOL FOR DNA COUPLING, B) ITC SLIDE TREATED WITH STANDARD PROTOCOL AS THE EPOXY SLIDE AND C) ITC SLIDE TREATED WITH AN OPTIMIZED PROCEDURE FOR DNA COUPLING ON GLASS SLIDES. ON THE GRAPH (D) THE RESULTS FROM THE FLUORESCENCE EVALUATION ARE PLOTTED AS SIGNAL INTENSITY IN ARBITRARY UNITS VERSUS CONCENTRATION OF THE OLIGONUCLEOTIDE USED. 4-50
FIGURE 53.- MICROARRAY HOMOGENEITY EXPERIMENTS. THREE REGIONS WERE EVALUATED ALONG THE LONGITUDINAL AXIS OF THREE SLIDES SILANIZED THE SAME WAY FOR STATISTICAL ANALYSIS. A) SLIDES USED FOR THE EXPERIMENT, IN ORDER SLIDE 1,2 AND 3. ON THE RIGHT B) ZOOM-INS ON SLIDE 2, ON THE FRAMED AREAS. 4-51
FIGURE 54.- NORMALIZED SURFACE PLOT OF FLUORESCENCE INTENSITY ALONG THE SLIDE. ON THE Z-AXIS, THE FLUORESCENCE INTENSITY, ON THE X-AXIS THE COLUMN NUMBER AND ON THE Y-AXIS THE ROW NUMBER FROM 1 TO 15 FOR EACH REGION OF EACH SLIDE. A,B AND C, CORRESPONDS TO SLIDE 1,2 AND 3 OF FIGURE 56 RESPECTIVELY. 4-53
FIGURE 55.- SUMARY OF STATISTICAL ANALYSIS ON FLUORESCENCE HOMOGENEITY EXPERIMENTS. THIS SUMMARIZED RESULTS ARE TAKEN FROM THE PLOTTED INTENSITY OF EACH DOT REGARDING THEIR POSITION ALONG THE SLIDE AS SHOWN IN FIGURE 53. 4-54

FIGURE 56.- SCHEME FOR DIP PEN NANOLITHOGRAPHY EXPERIMENTS. A) AMINOFLUORESCEIN DEPOSITION FOR ASSESS OF THE CHEMICAL REACTIVITY OF THE ITC-GROUP, AND B) AMINOFUNCTIONALIZED NANOPARTICLES DEPOSITION SELECTIVELY ON FUNCTIONALIZED SPOTS TO ADDRESS THE ABILITY OF THE ITCPTES TO IMMOBILIZE PARTICLES. 4-56
FIGURE 57.- DARK FIELD LIGHT MICROSCOPY IMAGES FROM DPN RECEIVED SAMPLE. ALL THE SAMPLES WERE DONE FOLLOWING THE SAME PROCEDURE. UPPER ROW OF SPOTS IN THE SAMPLE BELONG TO 20% R.H INCREASING UP TO 50% R.H 4-57
FIGURE 58.- A) FLUORESCENCE IMAGE OF DPN PRODUCED SPOT ARRAY ON SAMPLE 1. B) A 10X MAGNIFICATION PICTURE SHOWING ALSO THE SPOTTING PATTERNS OF THE ITCPTES VARYING WITH THE RELATIVE HUMIDITY OF THE CHAMBER. AFM TOPOGRAPHIC IMAGE OF A RANDOM PATTERN IN THE 50% R.H. ROW ON SAMPLE 1. ON THE TOP (C) A PROFILE OF THE MIDDLE ROW OF THE 5X5 ARRAY AND BOTTOM RIGHT (D) A TOPOGRAPHY AFM IMAGE OF AN ALEATORY PATTERNED AREA. 4-58
FIGURE 59.- AFM TOPOGRAFICAL EXAMINATION ON A DPN ARRAY PRODUCED WITH ISOTHIOCYANATE SILANE. A) IMAGES FROM THE SAMPLE 4 ARRAY AFTER THE WASHING AND INCUBATION STEP (ITCSILANE SITES ON WHITE). B) TOPOGRAPHICAL IMAGE OF A RANDOM SINGLE SPOT BEFORE ANY TREATMENT AND WASHING IS PERFORMED. C , D) FILTERED IMAGES USING THE SOFTWARE TO ENHANCE THE CONTRAST BETWEEN THE PARTICLES AND THE SUBSTRATE (IN D) CASE THE PARTICLES ARE SHOWN IN BLACK). UPPER ROW A 25X25 MICRON SCAN AREA WAS SELECTED (A,B) AND ON THE LOWER ROW A 3X3 MICRON ZOOM ON THE SPOT EXACTLY IN THE MIDDLE IS DONE. 4-60
FIGURE 60.- PROCEDURE OF SELECTIVE IRRADIATION AND FURTHER FUNCTIONALIZATION OF PDMS. A NON TRANSPARENT MASK COVERS PARTIALLY THE SUBSTRATE ALLOWING THE EXPOSED PART TO BE OXIDIZED AND TRANSFORMED INTO A SILICA LIKE LAYER WHICH IN TURN IS ISOTHIOCYANATE SILANIZED. AFTERWARDSS THE EVALUATION TAKES PLACE IN THE INTERFACE OF THE TWO REGIONS. 4-62
FIGURE 61.- REACTION SCHEME FOR THE PDMS IRRADIATION PROCESS USING AN UV/O_3 LAMP. I) THE UV LIGHT AT 185 NM WAVELENGHT TRANSFORMS THE OXYGEN IN THE AIR IN REACTIVE RADICAL AND OZONE. II) THE OZONE IN COMBINATION WITH THE UV ATTACKS THE METHYL GROUP OF THE UPPER LAYER OF CROSSLINKED PDMS LEADING TO FORMATION OF FURTHER OXIDIZED GROUPS. III) FURTHER REACTIONS LEAD THIS OXIDATED SPECIES TOWARDS THE FORMATION OF HYDROXYL GROUPS ON THE SURFACE. 4-62
FIGURE 62.- AFM TOPOGRAPHY IMAGES OF PDMS SUBSTRATE BEFORE (A) AND AFTER THE IRRADIATION WITH A UV/O_3 CHAMBER THROUGH A MASK AND FURTHER SILANIZATION (B). AFM PHASE CONTRAST IMAGES ARE SHOWN IN THE SAME LAYOUT C) FOR NON IRRATIATED SAMPLES AND D) AFTER IRRADIATED AND ITC-SILANIZED SUBSTRATE. 4-64
FIGURE 63.- AFM PHASE CONTRAST IMAGE OF PDMS SUBSTRATE BEFORE (A) AND AFTER THE IRRADIATION WITH A MASK (B). ON THE RIGHT, THE PICTURE CAN BE DIVIDED FURTHERMORE IN A IRRADIATED AREA ON THE RIGHT AND A PROTECTED AREA ON THE LEFT. 4-65
FIGURE 64.- SCHEME OF DIFFERENT REGIMES WHEN RECORDING AN AFM FORCE-DISTANCE CURVE. DURING THE APPROACH OF THE CANTILEVER ONTO THE SUBSTRATE, ATTRACTIVE FORCES CAUSE A SNAP-IN INTO THE SUBSTRATE, THE PIEZO CONTINUE THE HARD CONTACT REGIME ON THE CONSTANT COMPLIANCE REGION, AND WHEN IT REACHES THE DEFLECTION SET POINT, A RETRACTING MOVEMENT IS STARTED. THE ADHESION FORCE BETWEEN THE AFM TIP AND THE SUBSTRATE CAUSE THE BENDING OF THE CANTILEVER ON THE OPPOSITE DIRECTION UNTIL THE FORCE OF THE PIEZO RETRACTING OVERCOMES THE ADHESIVE FORCES. 4-66
FIGURE 65.- FORCE MAPPING OF A PARTIALLY IRRADIATED AND SILANIZED PDMS SUBSTRATE. A) TOPOGRAPHIC IMAGE OF THE AREA IN STUDY, B)PHASE CONTRAST IMAGE AND C)FORCE MAPPING IMAGE TAKEN FROM THE ADHESION FORCE CALCULATED ON THE SURFACE. ON THE LEFT, CURVES TAKEN RANDOMLY TO SHOW THE FORCE AND ADHESION ON THE CANTILEVER AFTER TREATMENT. ON THE RIGHT, A NON-TREATED AREA CURVES SHOWING A HIGHER ELASTIC DEFORMATION (SLOPE OF COMPLIANCE REGION). 4-68
FIGURE 66.- STATISTICAL ANALYSIS FOR TWO REGIONS OF THE SUBSTRATE. ON A) A HISTOGRAM SHOW THE ADHESION FORCE BI-MODAL DISTRIBUTION OF THE FORCE ALONG THE SAMPLE ON THE SILANIZED AREA AND THE NON-TREATED AREA. B) SHOWS THE ADHESION FORCE VARIATION ALONG THE Y-AXIS OF THE MEASURED FORCE PLOT. THE NUMBER OF POINTS LABEL INCREASE IN VERTICAL DOWNWARD DIRECTION. 4-70
FIGURE 67.- ELASTIC MODULUS MAP FROM SELECTIVE IRRADIATION ON PDMS SUBSTRATE. IN ACCORDANCE TO GUPTA ET AL. A) THE RIGHT AREA IS A SOFTER REGION WITH A 1.6 MPA ELASTIC MODULUS AND ON THE LEFT SIDE A HARDER MATERIAL WITH AROUND 16 MPA ELASTIC MODULUS. B) SHOWS A PROFILE CALCULATION ALONG THE RED LINE, SHOWING THE IRRRADIATED REGION AS A HIGHER YOUNG MODULUS ZONE, PLUS THE TRANSITIONAL REGION WHERE THE SURFACE CHANGE GRADUALLY ITS ELASTICITY AND THE SOFT NON-IRRADIATED AREA. ON C) IT CAN BE SEEN THE AVERAGE PLOT OF THE ELASTIC MODULUS VALUES ALONG THE TWO OUTER BORDERS OF THE IMAGE AS THEY ARE THE MOST REPRESENTATIVE FOR THEIR OWN AREAS OF MATERIAL PROPERTIES. 4-72
FIGURE 68.- SCHEMATIC REPRESENTATION OF THE PDMS SURFACE AFTER IRRADIATION. IT DEPICTS THE PRESENCE OF DIFFERENT ZONES, FROM CRYSTALLINE (SILICA-LIKE LAYER) TO AMORPHOUS (BULK POLYMER). THE CHAIN SCISSION ZONE IS ULTIMATELY RESPONSIBLE FOR THE HYDROPHOBICITY RECOVERY OF THE MATERIAL WITH TIME. 4-73
FIGURE 69.- CONTACT ANGLE ON PDMS COATED GLASS SLIDE IRRADIADET WITH UV-LIGHT SHOWING THE HYDROPHOBICITY RECOVERY OVER TIME AFTER IRRADIATION. IN THE FIRST TWO HOURS THE MIGRATION OF LOW MOLECULAR FRAGMENTS IS MORE PRONOUNCED AND THE INCREASE FLATS OVER TIME. INSET: LINEAR BEHAVIOR FROM RECOVERY IN THE FIRST TWO HOURS. AFTER THAT, THE RECOVERY WAS SLOWED DOWN SIGNIFICANTLY. IN THE INSET, THE X-AXIS HAS BEEN STRETCHED . THE Y-AXIS IS THE SAME FOR BOTH GRAPHS. 4-74
FIGURE 70.- X-RAY PHOTOELECTRON SPECTRA OF SUBSTRATES ITC-FUNCTIONALIZED PDMS (A,B,C), AND NON-TREATED PDMS (D, E, F) RESPECTIVELY. FOR ALL GRAPHS, THE VERTICAL AXIS IS EXPRESSED IN ARBITRARY UNITS ON NORMALIZED INTENSITY. 4-77
FIGURE 71.- SCHEME OF POLYDIMETHYLSILOXANE (PDMS) SUBSTRATE TREATED AND SILANIZED WITH ISOTHIOCYANATE GROUPS, WITH SUBSEQUENT FLUORESCEINAMINE COUPLING. 4-78
FIGURE 72.- FLUORESCENCE IMAGE OF AMINOFLUORESCEIN COUPLED TO A PDMS SUBSTRATE SELECIVELY IRRADIATED THROUGH A TEM GRID AS A MASK. THE GRID WAS REMOVED BEFORE ADDITION OF THE DYE BY COMPLETELY DIPPIMG THE SUBSTRATE INTO THE FLUROPHORE SOLUTION A) 60X MAGNIFICATION, B) 40X MAGNIFICATION AND C) 10X MAGNIFICATION. D) FLUORESCENCE INTENSITY PROFILE ALONG THE LINES. IT CAN BE NOTED THAT ALTHOUGH THE BRIGHTNESS OF THE IMAGES ARE DIFFERENT BETWEEN EACH OTHER, THE CONTRAST BETWEEN THE FUNCTIONALIZED AND THE NON-FUNCTIONALIZED REMAINS SIMILAR. 4-79
FIGURE 73.- FLUORESCENCE IMAGE OF PDMS IRRADIATED THROUGH A GRID AND AFTER THE ADDITION OF A SMALL DROP (<1µL) OF AMINOFLUORESCEIN TO THE CENTER OF THE PATTERNED AREA. THE BORDERS OF THE DROP CAN BE SEEN. THE DROP FOLLOWED A SQUARE SHAPE AS THE DROP FOLLOWED THE GRID PATTERN. A) TOP REGION OF THE DROP, B) UPPER-RIGHT REGION AND C) CENTER REGION OF THE TREATED AREA. 4-80

FIGURE 74.- AFM IMAGES (A,B) AND FLUORESCENCE IMAGE (C) OF STRUCTURED AND PARTLY IRRADIATED PDMS SUBSTRATE. A) SHOWS A TOPOGRAPHIC IMAGE OF THE TWO REGIONS (INDISTINGUISHABLE BY HEIGHT), B) A PHASE CONTRAST IMAGE IS SHOWN, ON WHICH THE RIGHT SIDE IS A IRRADIATED AND SILANIZED REGION AND THE LEFT SIDE IS THE NON-TREATED AREA. C) FLUORESCENCE IMAGE AFTER COUPLING OF AMINOFLUORESCEIN ON THE SILANIZED ISOTHIOCYANATE SIDE. THE PRE-STRUCTURED SUBSTRATE WAS CASTED FROM A DVD WHICH POSSESS TYPICALLY A WAVY PATTERN WITH 500 NM PITCH AND 100 NM DEPTH IN THE TRENCHES. 4-81
FIGURE 75.- SCHEME OF SITE-SELECTIVE BOTTOM-UP SELF-ASSEMBLY PROCESS OF TMV-LIKE PARTICLES ON AN OXIDIC FUNCTIONALIZED SURFACE. THE 5' END OF THE VIRAL RNA CAN BE FUNCTIONALIZED WITH ADDITIONAL CHEMICLA FUNCTIONS OR MOLECULES. 4-82
FIGURE 76.- AFM TOPOGRAPHIC IMAGES SHOWING THE RESULTS OF EXPERIMENT WITH DIFFERENT SILANIZATION TIMES (30S, 120S, 15MIN) COMBINED WITH DIFFERENT INDUCED CONDITIONS FOR THE FORMATION OF THE TMV-LIKE PARTICLES. FOR A BETTER UNDERSTANDING ALSO REFER TO TABLE 16. THE SCANS ARE 3X3 μM^2. 4-86
FIGURE 77.- AFM TOPOGRAPHIC IMAGES OF AN ASSEMBLY-RNA TIME EXPERIMENT. THE TIME FOR HYBRIDIZATION AND BONDING OF THE RNA TO THE DNA LINKER IS VARIED AND TESTED FOR A BOTTOM UP APPROACH AND FOR A SIMPLE TMV DEPOSITION. ALL THE IMAGES ARE 1X1 μM^2. 4-88
FIGURE 78.- AFM TOPOGRAPHIC IMAGES OF TMV-PARTICLES SELF ASSEMBLED WITH THEIR RESPECTIVELY HEIGHT PROFILES ALONG THE RED LINE ON EACH PICTURE. A) TMV PRE-ASSEMBLED IN SOLUTION AND THEN DEPOSITED ON THE SURFACE AND B) BOTTOM-UP TMV PARTICLES SELF ASSEMBLED DIRECTLY ON THE SURFACE. 4-89
FIGURE 79.- SCHEME SHOWING THE TWO AREAS IN THE SAME SAMPLE: 1) AN AREA INSIDE THE DROP OF DNA, WHICH HAS THE COMPLETE PREPARATION PROCEDURE AND 2) AN AREA WHICH WAS NOT WETTED BY THE DNA CONTAINING DROP, WHICH FOLLOWS EVERY STEP BUT THE DNA ADDITION. ALL SAMPLES WERE WASHED THOROUGHLY AFTER THE RNA+CP ADDITION. 4-90
FIGURE 80.- AFM TOPOGRAPHIC IMAGES OF TMV-LIKE PARTICLES BOTTOM-UP ASSEMBLED USING AN ITC-SILANE. THE SILANIZATION TOOK PLACE WITH SAME EXPERIMENTAL CONDITIONS VARYING ONLY THE SILANE MOLECULE: A) ITCPTES AND B) ITCPTMS. THE LATTER PREPARED FRESH WHILE THE FIRST WAS BOUGHT AND KEPT IN USE FOR ONE YEAR (AGED AND OXIDIZED). 4-90
FIGURE 81.- AFM TOPOGRAPHIC IMAGE SHOWING A TMV-LIKE PARTICLES BOTTOM-UP ASSEMBLY ON AN ITCPTMS FUNCTIONALIZED WAFER AFTER OPTIMIZATION. 4-91
FIGURE 82.- SELF-ASSEMBLY OF TMV-LIKE NANOROD STRUCTURES ON ITC-TERMINATED SILICON SUBSTRATES. REPRESENTATIVE AFM TOPOGRAPHY OF A SUBSTRATE (A) COATED WITH SELF-ASSEMBLED TMV-LIKE PARTICLE AFTER ALL PREPARATION STEPS, AND (B) STATISTICAL ANALYSIS OF THE PARTICLE LENGTH BASED ON (A). 4-92
FIGURE 83.- CONTROL EXPERIMENTS FOR BOTTOM UP ASSEMBLY OF TMV-LIKE PARTICLES ON A ITC FUNCTIONALIZED SILICA WAFER. A) AFM TOPOGRAPHIC IMAGE SHOWING RESULT FROM CONTROL EXPERIMENT OUTSIDE THE DROP, B) AFM TOPOGRAPHIC IMAGE SHOWING THE RESULT OF PREASSEMBLED VIRUS SPOTTED ON THE FUNCTIONALIZED SILICA WAFER BUT WASHED AWAY THOROUGHLY, C) TRANSMISSION ELECTRON MICROSCOPE IMAGE OF SELF-ASSEMBLED VIRUS IN SOLUTION THE SCALE BAR IS 500 NM D) AFM IMAGE SHOWING THE CONTROL EXPERIMENT INSIDE THE DROP WITHOUT RNA AND CP. ALL THE AFM IMAGES ARE 5X5 μM^2 4-93
FIGURE 84.- AFM TOPOGRAPHIC IMAGES OF DPN FUNCTIONALIZED SUBSTRATE SHOWING A HIGH SPECIFIC SELECTIVITY FOR VIRUS PARTICLES. ON THE UPPER ROW, SCAN AREAS OF 30X30 MICRONS (A,B,C) AND ON THE LOWER ROW SCAN AREAS OF 5X5 MICRONS (D,E,F). ITCPTMS DOTS WERE DEPOSITED (A,D) ON GLASS COVERSLIP, THEN A DNA-LINKER DROP COVERING THE WHOLE ARRAY AT THE SAME TIME WAS PLACED ON TOP (B,E) AND A FINAL STEP OF RNA COUPLING AND CP ADDITION (C,F) IN ORDER TO OBTAIN THE VIRUS-LIKE PARTICLES AS SHOWN. 4-95
FIGURE 85.- AFM IMAGES SHOWING A TOPOGRAPHIC EXAMINATION ON TWO DIFFERENT SUBSTRATES TREATED WITH THE SAME ITCPTMS USING DPN. A) COMPLETE PROCESS DONE AS EXPLAINED ABOVE (SILANIZATION-DNA LIGAND ATTACHAMENT- RNA HIBRIDIZATION- CP ADDITION - BU ASSEMBLY). B) SUBSTRATE WITH PREASSEMBLED VIRUS DEPOSITED ON THE SURFACE AND THEN WASHED OUT THE SAME WAY THE FINAL WASHING STEP FOR THE SELF ASSEMBLED VIRUS IS PERFORMED 4-96
FIGURE 86.- BOTTOM UP ASSEMBLY OF TMV-LIKE PARTICLES ON A ITC FUNCTIONALIZED DIP PEN NANOLITHOGRAPHY ESTRUCTURED SILICA WAFER. A) 3X3 μM SCAN AREA, B) STATISTICAL ANALYSIS ON PICTURE 4-96
FIGURE 87.-SCHEME OF POLYDIMETHYLSILOXANE (PDMS) SUBSTRATE TREATED AND SILANIZED WITH ISOTHIOCYANATE GROUPS, WITH SUBSEQUENT TMV ASSEMBLY 4-97
FIGURE 88.- AFM IMAGES SHOWING THE RESULTS FROM BOTTOM UP ASSEMBLY OF TMV-LIKE PARTICLES ON A SITE SELECTIVE ITC FUNCTIONALIZED PDMS SUBSTRATE. A) 90X90 μM SCAN AREA WITH THE IRRADIATED AND PROTECTED AREAS, B) 60X60 μM SCAN AREA WITH THE IRRADIATED AREA AND THE RIM AROUND DUE TO THE POSITIONING OF THE GRID C) ZOOM IN ON THE IRRADIATED AREA SHOWING TMV-LIKE PARTICLES D) ZOOM SCAN ON THE NON-IRRADIATED PARTS OF THE POLYMER WHERE NO PARTICLE CAN BE FOUND AND E) A 250X250 NM ZOOM SHOWING TMV-PARTICLES GROWN ON THE TREATED REGIONS AS ELONGATED RODS. 4-98
FIGURE 89.- DESCRIPTIVE STATISTICAL ANALYSIS OF TMV-LIKE PARTICLE LENGHTS GROWN ON PDMS SELECTIVELY IRRADIATED SUBSTRATES. A) HISTOGRAM SHOWING THE AMOUNT OF PARTICLES FOUND CORRESPONDING TO THEIR LENGTHS TAKEN FROM TWO DIFFERENT TREATED REGIONS. B) DISTRIBUTION OF THE PARTICLE LENGTH BY PERCENTAGE. 4-99
FIGURE 90.- FLUORESCENT REACTIVITY EVALUATION ON GLASS SLIDES SILANIZED WITH: I) AMINOPROPYLTRIMETHOXYSILANE, II) AMINOPROPYLTRIMETHOXYSILANE + ALDEHYDE COUPLING AND III) ISOTHIOCYANATEPROPYLTRIMETHOXYSILANE. AN ADDITIONAL CONTROL WAS DONE WITH A NON-FUNCTIONALIZED SILANE FOR BACKGROUND ASSESMENT. 5-2
FIGURE 91.- AFM TOPOGRAPHIC IMAGES, SHOWN AS A SUMMARY OF THE SILANIZED SUBSTRATES SUBMITTED TO THE TMV-LIKE PARTICLES BOTTOM UP ASSEMBLY . A-B) ALDEHYDE FUNCTIONAL SUBSTRATE ON SILICA WAFER WITH A PMMA MASKING FOR SELECTIVE ATTACHMENT. C-D) ISOTHIOCYANATE FUNCTIONALIZED SILICA WAFER WITH NO STRUCTURING. E-F) ISOTHIOCYANATE SILANIZED PDMS SUBSTRATE USING A CHEMICAL SELECTIVE STRUCTURING IRRADIATION TECHNIQUE. G-H) ISOTHIOCYANATE SILANIZED GLASS SLIDE USING A CHEMICAL STRUCTURING *VIA* DIP PEN NANOLITHOGRAPY FOR SELECTIVE DEPOSITION OF THE SILANE. THE SCALES IN THE A,C,E,G IMAGES IS 50 NM WHILE IN THE B,D,F,H IMAGES IS 500 NM. 5-4
FIGURE 92.- AFM TOPOGRAPHY IMAGES OF MICROCONTACT PRINTED ISOTHIOCYANATE SILANE ON SILICA WAFER. A) SURFACE PATTERN PRPARED WITH A LINE GRADIENT STAMP SHOWN IN FIGURE 6 , B) A ZOOM INTO THE LEFT LINE IN A). A-5

INDEX OF TABLES

TABLE 1.- CHEMICAL COMPONENTS AND AMOUNTS FOR ISOTHIOCYANATE PROPYLTRIMETHOXY SILANE SYNTHESIS 3-4
TABLE 2.- SURFACE SCIENCE TECHNIQUES FOR CHARACTERIZATION OF SELF-ASSEMBLED MONOLAYERS USED IN THIS DISSERTATION. 3-15
TABLE 3.- CANTILEVERS FREQUENCIES AND SPRING CONTANTS USED FOR THE CHARACTERIZATION OF SURFACES AND PARTICLES. 3-19
TABLE 4.- FTIR INSTRUMENTAL PARAMETERS USED IN MEASUREMENTS. 3-25
TABLE 5.- FT-RAMAN SPECTROMETER INSTRUMENTAL PARAMETERS USED IN MEASUREMENTS 3-28
TABLE 6.- ROUGHNESS DATA FOR THE CLEAN AND AFTER ALDEHYDE SILANIZATION SUBSTRATES. 4-5
TABLE 7.- XPS RESULTS ON A AMINOFUNCTIONALIZED SILICA WAFER AND ON A PARALLEL SAMPLE WHICH UNDERWENT ON THE GLUTARALDEHYDE COUPLING (-CHO). THE PEAK EVALUATION HAS BEEN PERFORMED REFERED TO THE CARBON 1S AT 285.0 EV. 4-8
TABLE 8.- FTIR ASSIGNMENTS FOR THE FUNDAMENTAL MODES OF 3-AMINOPROPYLTRIMETHOXYSILANE AND 3-ISOTHIOCYANATEPROPYLTRIMETHOXYSILANE. 4-28
TABLE 9.- ROUGHNESS EVALUATION DATA FOR THE CLEAN SUBSTRATES AND SUBSTRATES AFTER ITC SILANIZATION. 4-34
TABLE 10.- S 2P BINDING ENERGIES REPORTED FOR SULFUR SPECIES ON OXIDE SURFACES AND THEIR ASSIGNMENTS ACCORDING TO LITERATURE [395, 396]. 4-41
TABLE 11.- GRADIENT STAMP DIMENSIONS FOR MICROCONTACT PRINTING ASSESSMENT OF CHEMICAL REACTIVITY ON ISOTHIOCYANATE SILANIZED GLASS SLIDES. 4-46
TABLE 12.- OLIGONUCLEOTIDE CONCENTRATION AND RANDOM ARRANGEMENT FOR MICROSPOTTING COMPARISON BETWEEN COMMERCIALLY AVAILABLE EPOXY SLIDES AND ISOTHIOCYANATE SILANIZED SLIDES. 4-48
TABLE 13.- ROUGHNESS DATA FOR THE PDMS BEFORE AND AFTER UV/O_3 TREATMENT WITH FURTHER ISOTHIOCYANATE SILANIZATION SUBSTRATES. 4-64
TABLE 14.- AFM PARAMETERS USED FOR CALIBRATION OF THE SYSTEM IN ORDER TO PERFORM FORCE-DISTANCE MEASUREMENTS. 4-67
TABLE 15.- PDMS COMPOSITION BY ATOMIC PERCENTAGE BEFORE IRRADIATION, AFTER IRRADIATION AND AFTER SILANIZATION. THE REPRESENTATIVE SAMPLES ARE MARKED IN DIFFERENT COLORS. 4-76
TABLE 16.- EXPERIMENTAL LAYOUT TO ASSESS THE PROPER SILANIZATION TIME FOR TMV VIRUS ASSEMBLY AND FURTHER CONTROLS. A,B,D,E ARE NEGATIVE CONTROLS AS NEITHER RNA NOR CP IS PRESENT IN THE EXPERIMENT. SAMPLES C AND F HAVE THE MINIMUM REQUIRED CONDITIONS FOR A COMPLETE ASSEMBLY ON THE SUBSTRATE. 4-84

List of Abbreviations

AFM	ATOMIC FORCE MICROSCOPE/MICROSCOPY
APTES	3-AMINOPROPYLTRIETHOXYSILANE ($NH_2CH_2\,CH_2\,CH_2Si(OC_2H_5)_3$
APTMS	3-AMINOPROPYLTRIMETHOXYSILANE ($NH_2CH_2\,CH_2\,CH_2Si(OCH_3)_3$
CP	COAT PROTEIN
DNA	DEOXYRIBONUCLEIC ACID
DPN	DIP PEN NANOLITHOGRAPHY
DIPEA	N,N-DIISOPROPYLETHYLAMINE
ETO	ETHOXY
FITC	FLUORESCEIN ISOTHIOCYANATE
FTIR	FOURIER TRANSFORMED INFRARED SPECTROSCOPY
ITC	ISOTHIOCYANATE
ITCPTMS	3-ISOTHIOCYANATEPROPYLTRIMETHOXYSILANE ($SCNCH_2\,CH_2\,CH_2Si(OCH_3)_3$
MEO	METHOXY
μCP	MICRO CONTACT PRINTING
PDMS	POLYDIMETHYLSILOXANE
PMMA	POLYMETHYLMETHACRYLATE
PS	POLYSTYRENE
RNA	RIBONUCLEIC ACID
SAM	SELF-ASSEMBLED MONOLAYER
TMV	TOBACCO MOSAIC VIRUS
THF	TETRAHYDROFURANE
VLP	VIRUS LIKE PARTICLE
XPS	X-RAY PHOTOELECTRON SPECTROSCOPY

1 .- Introduction and Objectives

1.1 Background of the Project

Current trends in life sciences merge successfully the structuring of materials with the special properties of biofunctional molecules [1]. On recent years, one approach to take advantage of biological self-assembly in order to build synthetic materials is to employ virus capsids – the protein shells that encapsulate the genetic material of viruses – or even completely assembled viruses [2]. The ability of self-assembly of biopolymers into functional virions – mature viral particles – combined with the modular quality of viral genomes, provides vast potential for molecular-biological based engineering [3]. In material science, viruses are currently predominantly used as scaffolds for chemical synthesis, where molecules of interest are attached to the virions surface by bioconjugation chemistry. In this way, the viruses can be further used as frameworks for mineralization or metallization too [2].

Self-assembly is an effective method of nature to create nanostructured biological devices with high precision. The combination of the genetic modification of the repeatable coat of the protein virus [4, 5] - holding different organic groups [6, 7] - with a site-selective allocation of its scaffold RNA on a surface yields an ever increasing number of applications or close-to-application materials and devices.

The use of viral nanoparticles as carrier systems for metallic nanoparticles [8], the manufacturing of nanowires inside of the tubular arrangement of the coat protein of the virions [9], the production of virus-based nanoelectrodes [10, 11], novel designs of ferrofluids [12] or even the development of memory devices [13] are just some examples for the interaction between biology and material sciences. Viral particles consist of a well-defined number of coat protein (CPs) units arranged around the viral RNA in an exactly predetermined geometry. This approach of nature to form identical particles just by the combination of the required building blocks can be used to create well defined bio templates for further application. [14-16]. The formation of nanoscale particles from plant viral coat proteins prompted by the interaction with genomic nucleic acids [17, 18] is an example of a biologically directed self-assembly process.

In order to achieve control over the viral system, a site-selective highly specific interaction is desired. Site selective immobilization of the virions can be done e.g. by

using patterned self-assembled monolayers (SAMs). The concept of using SAMs in order to achieve an arrangement of functional molecules into higher ordered structures is not new [19]. SAMs are found in applications such as molecular and biomolecular recognition [20-22], lithography resists [23-25], sensing and electrode modification [26-28], corrosion prevention [29-31], and other fields where the tailoring of the physical and/or chemical properties of an interface is required. Amphiphilic molecules – which possess hydrophilic and hydrophobic properties at the same time – are able to organize themselves spontaneously into assemblies on metal or oxidic surfaces and they belong to a subset of self-assembled films that have been reported and characterized. Silanes and sulfur containing molecules (thiols, sulfides, disulfides etc.) in particular, being able to spontaneously organize to closely packed molecular arrays, have been preferentially used to tailor different kinds of surfaces for specific applications with different organic head groups [32]. Silanes, having hydrolysable groups on the anchors, have a strong affinity for oxides surfaces (glass [33-36], silica [37-42], quartz [43], aluminum oxide [44-46], amorphous iron [47]) and the thiols (the mostly studied and probably best understood SAM type formed by organosulfur compounds), possess a strong affinity for coin metals (silver [48-50], gold [48, 51-56], copper [49, 50, 57]).

The present work is a result from a close collaboration project financed by the Baden-Württemberg-Stiftung GmbH (Baden-Württemberg State Foundation). The project is divided in three main areas of interest: Biology (C. Wege and H. Jeske, Stuttgart University), Chemistry (H. Gliemann, M. Franzreb, Karlsruhe Institute of Technology) and Physics (S. Walheim and Th. Schimmel, Karlsruhe Institute of Technology). The idea behind the research project is to produce a robust bioactive self-assembled nano system with potential for biosensoring [26, 27, 58, 59] and diagnostic applications [60-62], which is based on substrate supported active molecules as e.g. enzymes. Important requirements for an optimized activity of the enzymes are: (1) a minimized cross sensitivity of the active molecules [63] (2) a high but controllable surface density on the supporting substrate, (3) good sterical access to the functionalities, and (4) low interactions between analytes/reactants and the technical environment. One possibility to address these requirements is the arrangement of the active molecules on a carrier system, whereby the density of the active molecules can be controlled. For this, we follow the approach of a site-selective, biologically driven self-assembly bottom-up process of viral-like nanorods on substrates. This system offers the opportunity to arrange the active molecules on well-

defined positions along the longitudinal axis of the viral particle by controlling the sequence of coat protein aggregates which are able to bind the active moieties. ("functionality on a stick"). Figure 1 shows a scheme of the approach: first a self-assembly monolayer holding a highly specific chemical group towards a DNA-amino terminated linker is coupled on an oxidic surface (glass, silica) *via* silane chemistry. This linker has a predetermined sequence of base pairs, which attach specifically to a complementary genetically engineered RNA from a Tobacco Mosaic Virus (TMV) mutant. Afterwards, the coat protein (CP) originally extracted from TMV-virions is added to the substrate. The coat protein self-assembles using the RNA as scaffold, producing a final virus-like particle with one end specifically and covalently attached to the substrate.

Framed in the box, is the part of the project investigated within this dissertation. The RNA and the coat protein (produced by the group in Stuttgart) are attached onto the substrates prepared at KIT. Afterwards the substrates are sent back to Karlsruhe for their characterization.

This novel approach may promote technically applicable production routes toward a controlled integration of multivalent biotemplates into miniaturized devices.

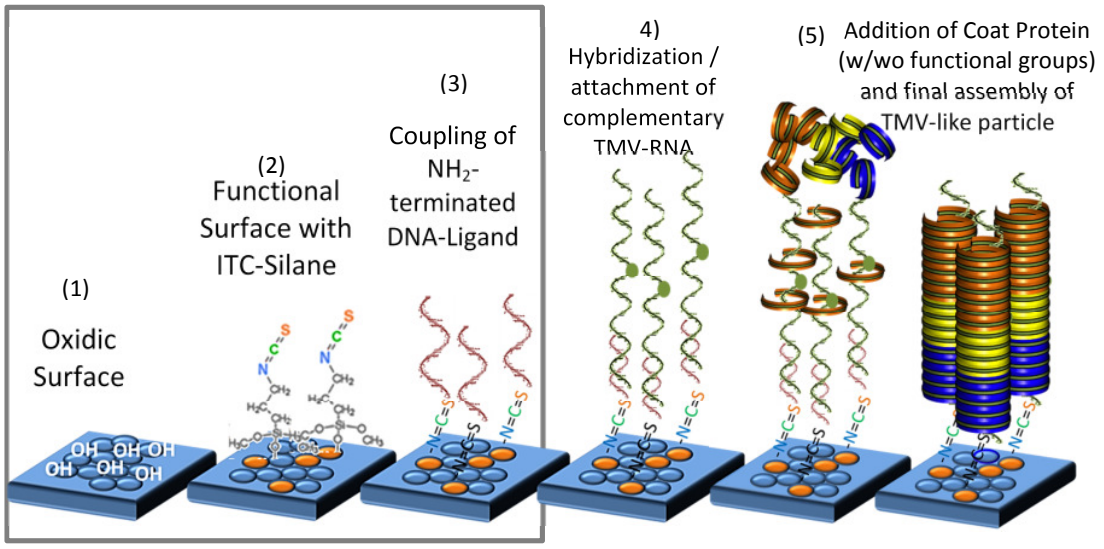

Figure 1.- Project scheme overview: on an oxidic surface (glass, silica) (1) via silane chemistry (2) - a self-assembled monolayer terminated by a highly specific reactive chemical group towards an amino-terminated DNA-linker is coupled (3). The DNA-ligand is then selectively coupled to a viral RNA by hybridization from tobacco mosaic virus (4). Afterwards, coat protein, which can be previously modified is added sequentially to the surface and an entropy-driven self assembly process e takes place during this , the virus-like, rod-shaped nanoparticle assembles using the RNA as a scaffold (5). The box represents those preparation steps which were in the focus of the work summarized in this thesis.

1.2 Challenges and Objectives

The main goal of the whole cooperative project is to produce site-selectively bottom-up self-assembled TMV-like particles with well-defined sequential order of differently chemically modified coat proteins along the longitudinal axis. To achieve this goal the following challenges had to be faced within the scope of this dissertation:

- Immobilization of viral-RNA on the surface via one-end terminus.
- The interaction between the viral-RNA and the surface - which might sterically hinder the subsequent bottom-up self-assembly of the nanorods - must be avoided.
- The chemical compatibility of the complete process with the experimental conditions e.g. pH, temperature, etc. for the self-assembly process of the viral particles must be achieved.
- A high density of the final produced TMV-viral particles must be realized while avoiding non-specific interactions of the bio-functional particles with the substrate or with each other.
- The assembly methodology should be able to be transferred onto a polymeric chemically stable and inert material.
- The compatible combination of bottom-up and top-down structuring techniques -either chemically or morphologically - in order to achieve site selective growth of the TMV-particles.

The following objectives give an outline of the approaches followed to address the previously stated challenges:

- A new method of the site selective bottom-up assembly of tobacco mosaic virus-like particles (VLPs) is introduced, whereby the VLPs are not preassembled before immobilizing but are prepared by the self-assembly of the coat proteins along the immobilized viral RNA.
- Within this framework one of the specific tasks of this thesis was the development of a suitable functional molecule with high specificity towards amino-terminated molecules with special emphasis on amino-modified DNA oligonucleotides. There are two common biofunctional silanes used commercially to immobilize single stranded oligonucleotides [64-66]: amino functional alkoxysilanes [67, 68] and the epoxy terminated silanes [69, 70]. The use of these silanes to anchor DNA oligomers non-covalently to a surface [70] has two advantages: the DNA-ligand retains its ability to hybridize to a complementary strand (which is required for the proper attachment of the

RNA belonging to the TMVs) and second they can be photolithographically patterned to fabricate high resolution patterned DNA surfaces using various approaches [64, 70, 71]. However, DNA films which were formed using this non-covalent attachment methods were susceptible to detachment from the surface under high salts concentration conditions and shear flows [66]. For applications where high ionic strength conditions are desirable, such as under physiological conditions, it is generally believed that a covalent attachment strategy will prove superior to one in which the nucleic acid is just adsorbed to the surface. This is accomplished by use of an aldehyde and an isothiocyanate-based (ITC), chemistry using self-assembled monolayers (SAMs). While the aldehyde modified silane is an already established approach [72] the isothiocyanate silane required a novel synthesis [73] which is why it is investigated in a higher extend. The isothiocyanate group possess a high reactivity toward amines and their derivatives (forming a strong and stable thiourea bond [74]).

- The ability to tailor both head and tail groups of the constituent molecules makes the SAMs excellent systems to study and understand phenomena affected by intermolecular, molecular-substrate or molecular-solvent interactions like ordering, growth, wetting and adhesion [75]. Additionally, our immobilization strategy is based on the use of oxidic surfaces as substrates. For this purpose the silanes offers a higher specificity towards the hydroxyl-rich surfaces, maintaining the self-organization properties while been able to be tailored with the organic specific group of our choice (isothiocyanate or aldehyde). Silanes are currently used with a very wide range of applications, from crosslinking of plastics [76], solar cells [77], adhesives [35, 78], and in our interest as biofunctionality promoters [79-81]. However, there are very few studies involving the application and eventual synthesis of isothiocyanate functional silanes [82-84]. Most of the applications come when the amino-terminated silane is converted into an isothiocyanate-terminated silane by treating it with a di-isothiocyanate derivative [85-88]. For that the surface must be functionalized previously with the amino silane. Important to mention is, that in this work, unlike the after-coupling reactions on the substrate (aldehyde conversion of amino-terminated silane), the ITC-terminated silane is synthesized stepwise in a single pot reaction. With this method stable isothiocyanate-terminated silanes can be produced and then used for other biological applications.
- Another objective of the thesis was to pattern the surface in order to immobilize the DNA-linker and subsequently artificial viral RNA immobilization, only at specific

locations: (1) on oxidic surfaces by using Dip Pen Nanolithography (DPN) [89] and microspotting, (2) on oxidic surfaces using a two-step polymer-blend masking technique [90], and (3) on polymers such as polydimethylsiloxane (PDMS) by UV-irradiation. The transfer of the immobilization protocol developed procedures from the oxidic surfaces onto an elastomer with the same capabilities as the homogeneous non-structured silanized substrates is executed when PDMS is oxidized by UV-light irradiation in air in order to promote the formation of a brittle silica-like layer suitable for functionalization.

- Finally the use of these techniques altogether should be able to provide an adequate surface for the bottom-up self-assembly of TMV-like particles using the RNA as a scaffold for the assembly. It should be shown that the chemistries and patterning techniques are able to fulfill for the first time, a site-selective bottom-up assembly of viral particles with stability sufficient for the systems to be employed in technical applications.
- In order to evaluate the success of each preparation step starting from the synthesis of the isothiocyanate up to the evaluation of the final self-assembled TMV particles, different characterization techniques should be employed. The synthesized molecules had to be investigated by vibrational spectroscopy (infrared and Raman spectroscopy). Chemical composition and coupling reactions on surfaces should be evaluated using X-ray photon spectroscopy (XPS) and fluorescence light microscopy. Finally the morphology and physical properties of the substrates should be evaluated using atomic force microscopy (AFM) and contact angle (CA) measurements.

2 Methods and Techniques for Chemical Functionalization and Structuring of Surfaces

2.1 Chemical Modification of Surfaces by Self Assembled Monolayers (SAMs)

2.1.1 Introduction

Self-assembled monolayers (SAMs) of organic molecules are highly ordered two-dimensional structures on a surface, with the particular property that they arrange spontaneously. There are different SAM systems which have been investigated. The first SAM was accredited and studied in 1946 by Zisman and Bigelow [91], adsorbing a surfactant onto a clean metal surface. This study went unnoticed until Nuzzo and Alara [92] showed that SAMs of alkanethiols on gold can be prepared by adsorption of di-n-alkyl sulphides from dilute solutions. In 1984 Maoz and Sagiv [93] introduced silanes as a second most popular SAM system, bringing interest to the scientific community. From there on, a distinction was made between molecules which are physisorbed to the surface and molecules which have an anchor group on one end (generally the hydrophilic one) which covalently binds it to a substrate [94]. Due to the particular interaction between molecule and substrate, the adsorption can often take place in a variety of solvents, polar and non-polar, allowing greater flexibility in molecular design and, therefore, in the types of surface properties that can be modified and controlled. The most common adsorbate/substrate combinations are sulfur-containing molecules on gold (forming Au-S bonds), organosilanes such as alkylchlorosilanes and alkylalkoxysilanes on oxide surfaces (forming Si-O-Si), alkenes on hydrogen terminated silicon surface (forming Si-C bonds) and alcohols on H-terminated silicon surface (forming Si-O-C bonds).

The main advantage of the monolayers is that - apart from the highly specific adsorption on a determined substrate - they have the ability to be custom-designed with the functional group of preference. Most common functional termini for the thiols or the silanes are: Amino-, alkyl-, polyethyleneglycol, fluoride-, methacrylate-, epoxy-, vinyl-, mercapto-, aldehyde-, keto-, and carboxy-groups [95-98].

The process to attach a SAM onto a substrate varies depending on the application. Commonly there are two ways to prepare them: a) in solution by immersion in a liquid, and b) in the gas phase. The immersion approach requires that the substrate is dipped in the solution containing the SAM molecule and incubating the sample until the monolayer is completed. There are two distinct phases in the assembly of a monolayer, first an disordered and non-oriented adsorption process takes place on the surface and second a surface organization process where the alkyl chains get out of the disordered state and into a parallel arrangement [75] (Figure 2 top). The kinetics of the first step is governed by the tail group-substrate interaction and its reactivity takes generally longer times for the silanes than for the thiols [56]. The SAMs are normally constituted by three key elements: a) the organic functional terminus which is responsible for the new surface properties and chemical reactivity, b) the spacer, which avoids the direct contact between the functional terminus and the surface and which also acts as a physical barrier or as a modifier of physical properties (e.g. conductivity or optical properties), c) the ligand or tail group which is responsible for the covalent bonding or chemisorption of the molecule to the surface and further stability of the surface atoms [48, 75, 99] (Figure 2, bottom). The interest in these monolayer films has continuously increased in recent years, and the development and application of surface-sensitive experimental techniques (e.g. scanning probe microscopy, vibrational spectroscopy, and synchrotron X-ray sources) has resulted in an improved understanding of the film structure and growth process. A more general review of SAM structure (with some information about film growth) can be found in the publications of Ullman [75].

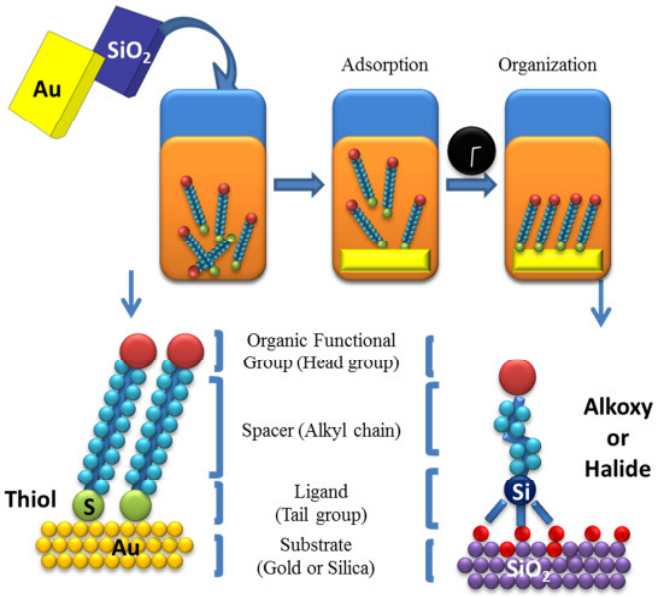

Figure 2.- Scheme of Self-assembled monolayers. The SAMs are comonly prepared by dipping the substrates in the solution containing the SAM molecule. The first step constitutes generally an adsorption onto the substrate followed by a reorganization of the alkyl chains. Generally the SAMs are created by two distinct molecules: thiols and silanes. The first uses a sulfur atom to bind onto gold and silver preferably. The second uses an alkoxy group to bind on oxidic surfaces such as silica or glass. They are constituted by three components: a) the organic functional group b) the spacer formed by an alkyl chain and c) ligand or tail group which binds to the substrate depending on the chemical group of the molecule.

2.1.2 Silane-based Non-Patterned SAMs on Oxidic Substrates

The coating with silicon dioxide has been widely used in the microelectronics industry for decades as a method to protect silicon surfaces, to control surface electronic and chemical properties and to pattern surfaces of SiO_2 with self-assembled monolayers (SAMs) [100].

The most common and effective route for deposition of SAMs on oxidic surfaces (glass, silica wafers, alumina,, etc.) is the silanization through the formation of Si-O-Si bonds between the silanol groups present on the oxidized silicon surface and the organosilanes molecules [26, 75, 101]. Silanes are chemical substances which consist of anchor groups used for the coupling to the substrate and a (heteroatomic) hydrocarbon rest which is terminated with a functional head group. Silanes are very useful in organic synthesis as crosslinkers, as coupling agents, and as support layers for introducing biological applications [68, 102, 103]. Despite the well-known applications of alkylsiloxane SAMs on SiO_2, the actual mechanism of monolayer formation on SiO_2 remains a subject of debate [101, 104-107] as various interfacial processes may be possible (covalent binding to the surface, lateral polymerization of adsorbed silanes, three-dimensional polymerization, etc.) depending on (i) the nature of the reactive moieties bound to the Si atoms in the silane (typically chloride or an alkoxy group), (ii) their number, and more generally (iii) the experimental parameters (Figure 3).

The question whether the formation process of SAMs is uniformly homogeneous or similar to an island-type is still under debate. Overall results favor the last situation depending significantly on the water content [39, 40]. This island growth however, is still found in situations where no water is available in solution [32].

Silanes integrate the alkoxy groups on the tail section of the molecule (-O-R^1 where R^1= -CH_3, -C_2H_5, -C_3H_7), so after they go under hydrolysis they create a silanol (-Si-OH) active compound or in case of an halogen to create a silicon halide (highest reactivity) [108]. Silanes are constituted basically of three parts: The non-hydrolysable head group, utilized for attachment of additional moieties [109-111] which provides the modified chemical character, the spacer and the anchor groups (hydrolysable), which are responsible for the attachment to the hydroxyl-groups of the oxidic surface. However, silanes are reactive not only towards the hydroxyl groups present on the surface but also to those of the solvent or other (silane) molecules. Their reactivity depends on the anchor groups, which first hydrolyze (Figure 3a) and then may condensate. Afterwards, the

silanols form intermolecular hydrogen bonds between each other or directly to the oxide surface [112-114] (Figure 3b). This adsorption mechanism has been studied before and will not be covered extensively in this introduction [112-115]. Schematically, silane grafting is expected to occur in two steps in the presence of water molecules [116]. First, hydrolysis reactions will cleave off the alcoholate which is then reacting to the corresponding alkohol (methoxy will yield methanol and ethoxy will produce ethanol respectively). Second, condensation reactions take place in solution, whereby either a coupling of the silanes to the surface, or a crosslinking with other molecules in solution or those molecules already immobilized on the surface takes place, the least resulting in the formation of a densely packed monolayer (Figure 3c). When excess humidity is found, these condensation reactions are responsible for the polymer network formation that takes place generally in the silanization process (Figure 3d).

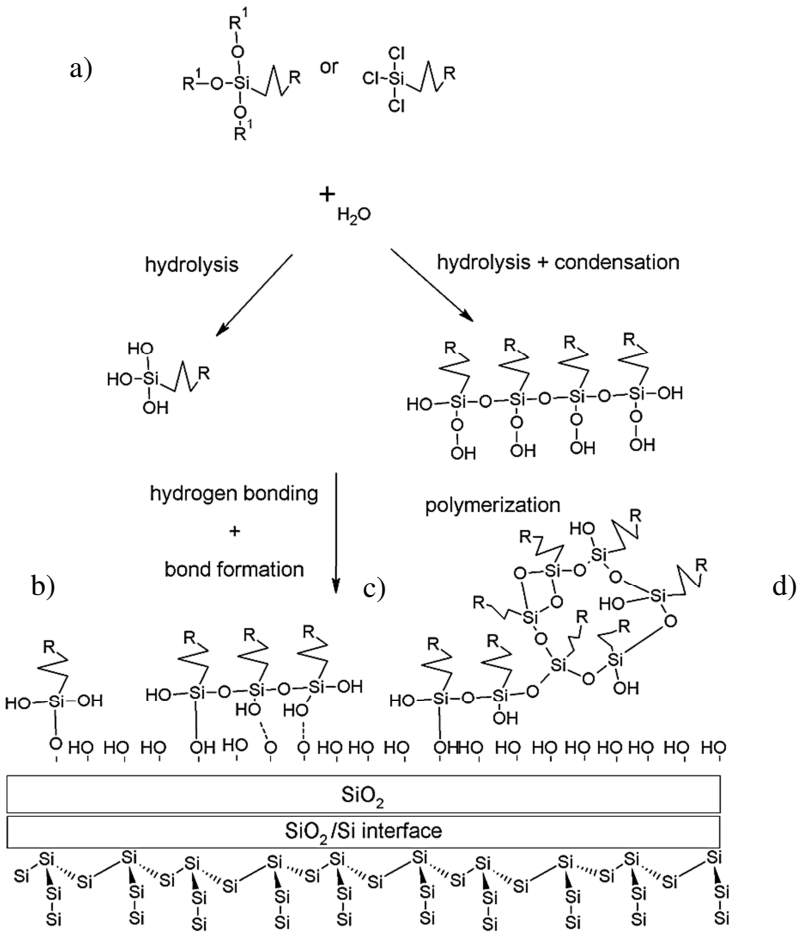

Figure 3.- Scheme of silanization process: a) the silane undergoes hydrolisis in presence of water releasing an alcohol related to its tail group. It can also condensate still in solution forming bigger polymeric aggregates. Once hydrolized the silanol groups attach to the surface (depending of the previous reaction, hydrolysis and/or condensation) either in b) single molecules which rearrange further into monolayers *via* island formation (c) or complete polymerized networks attached on the substrate by few hydroxyls (d). The later case can also happen after the monolayer islands are formed but further condensation reactions takes place on the surface itself.

This competition between condensation and adsorption reactions is very sensitive to the experimental conditions such as water content [117], temperature [118, 119] and additional energetic processes (ultrasonic treatment), concentration [120], substrate's nature [121], solvent [122] and aging of the solution [40, 123]. It is also argued that cross-linking and thin adsorbed water layers are required to form the silane based SAMs but some studies also argue that the bond between the silanes and substrate is not necessary [124, 125]. Infrared studies suggest that without water, an incomplete Silane SAM is formed on the substrate [126].

The aminosilanization of hydroxyl-terminated surfaces finds numerous applications in the field of biomolecule immobilization [127, 128]. The patterned amino-functionalized SAMs have been used as templates for adsorption of a wide variety of molecules on Si, SiO_2, and glass surfaces [129, 130]. Distinct to the SAMs from alkanethiols, the reactive head-groups in organosilanes introduce some potential lateral and disordered film growth mechanisms at the interface. The factors contributing to the stability of silanols have been reviewed by Arkles *et al.* [131]. Silanols are stabilized by: a) neutral conditions b) limited condensation (high dilution) c) presence of hydroxylic species (alcohols are stabilizers) d) silanes forming stable zwitterions. Amino silanes form such species and are among the most stable water borne species. They readily dissolve in water on stirring and are most stable at pH 10-11. This is the case for 3-aminopropyltrimethoxysilane (APTMS) in which the interaction between the $-NH_2$ group and the surface hydroxyl groups or other silanol groups makes it even more complex to form ordered layers. The amino group acts like a catalyst for the hydrolysis reaction of alkoxy- [132, 133] and chloro-silanes [134, 135]. For the same reason, aminoalkoxysilanes are more reactive than alkylalkoxysilanes toward water, which can cause uncontrolled polymerization/oligomerization of aminosilanes in solution (Figure 3d). Additionally, amino groups can form hydrogen bond with surface silanol groups, [116] thus covalently attached aminosilane layers typically have low grafting densities due to the presence of vertically (Figure 4a) as well as horizontally (Figure 4b) positioned silane molecules [136]. Hydrogen-bonding interactions with surface silanols alone might result in weakly attached silane molecules on silica surfaces (Figure 4c–e).

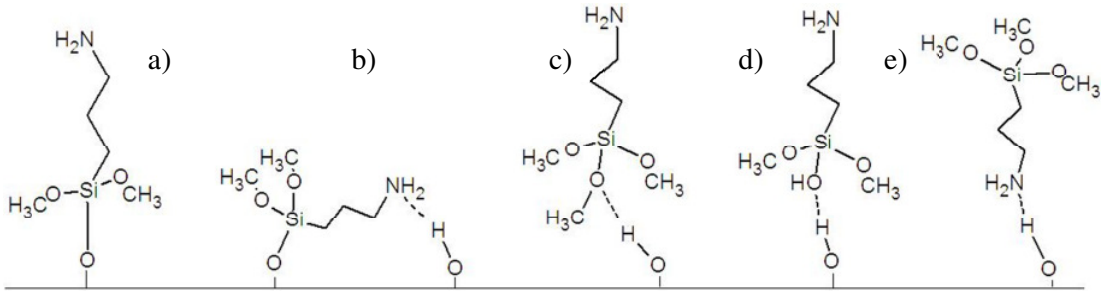

Figure 4.- Different types of bonding/interaction between aminopropylethoxysilane molecules and silicon oxide substrates. Adapted from Asenath, et al. 2008 [116]. a) vertically positioned silane bonded via silanol group on the surface. b) horizontally positioned silane bounded *via* silanol interaction plus hydrogen bond between the amino and the hydroxyl group on the surface. c) hydrogen bond between the non-hydrolized alkoxy group and the hydroxyl group of the surface. d) weak hydrogen bond between silanol and hydroxyl groups on the surface and e) head group interaction between amino group and the hydroxyl of the substrate.

These few disadvantages from this biocompatible silane are overcome when the amino silane is either 1) transformed into an aldehyde terminated silane *via* a reaction with glutaraldehyde [137] promoted on the silane which is already coupled on the surface or 2) transferred into an isothiocyanate (ITC) silane type *via* a one-pot synthesis, using a reaction developed first by Kaluza [138] and later by Hodgkins [139-141]. As it is within the focus of this dissertation, the application of surfaces functionalized with ITC-terminated silanes to prepare biofunctional interfaces will be discussed in more detail in the section 4.2. The terminal ITC group forms very stable thiourea bonds with NH_2-terminted molecules making it very useful for the preparation of biofunctional surfaces. Important applications of ITC silanes include the promotion of adhesion and immobilization of membranes [142] and biological molecules [143] either physically or chemically. ITC terminated surfaces can also be used, as we do in this work, for directing growth of nanoparticles and nanorods on the surface [7, 72], similar to aldehyde terminated silanes, with the exception, that this time, the amino group belonging to any of this moieties, which are adsorbed on the surface, can be attached to the ITC-silanized surface with higher selectivity.

2.1.3 Silane-based Chemically Patterned SAMs on Oxidic Substrates

2.1.3.1 Microcontact Printing

Some lithography methods have been developed (e-beam photolithography [144], electroforming [145], solid object printing [146], thermal printing [147]), mostly for preparing micron- to nanometer-sized features in polymeric materials [148], in applications such as medical devices (catheter tubes, drainage pipes) or industrial

components (adhesives, insulations) [149, 150]. Among different lithographic methods to produce patterned surfaces there is a family of techniques which are based on printing methodologies instead of an engraving one [52, 151]. Microcontact printing (μCP) is one representative of different soft lithography strategies which are commonly used for patterning materials directly. It constitutes a versatile and fast approach for creating laterally well-defined areas on large substrates up to square centimeters with micron to sub-micron resolution. Numerous applications of self-assembled monolayers (SAMs) in surface chemistry are based on patterning features with an elastomeric stamp, whereas polydimethylsiloxane (PDMS) is one of those polymers mostly used for that kind of application [151]. For the preparation of a structured stamp the monomer is casted on a master and allowed to cross link into a polymer (Figure 5). Whitesides et al. [152] developed the technique in 1993 and not even a year later it has already been used for patterning substrates for protein and cell adhesion. They used it for the first time for patterning of self-assembled monolayers (SAMs) of hexadecanethiols on gold surfaces [152]. In the early stages of microcontact printing, Singhvi et al. [153] created patterns of hexadecanethiol on gold surfaces followed by an incubation of a polyethylene glycol-terminated thiol. This resulted in a pattern, consisting of proteophilic and proteophobic areas, respectively. This patterning was used then to preferentially absorb cells on those regions functionalized with hexadecanethiol. Patterning of the SAMs at this level is probably still one of the best described printing techniques which is used extensively to study cell-substrate interactions at the single cell level [153]. The functional groups are essential to control some surface properties, such as wettability, roughness or chemical reactivity.

Historically for the preparation of stamps made out of PDMS different chemistries and preparation approaches were applied [154] but recently, most research has been done using the commercially available product Sylgard-184, manufactured from Dow Corning and Co. with a protocol recommended for the monomer-crosslinker ratio, as well as specific temperature and time conditions for curing. Silicon hydride groups present in the curing agent (which also contains platinum as a catalyst) react with vinyl groups present in the base material forming a cross-linked, elastomeric solid. The low surface free energy (γ = 22.1 dynes·cm^{-1}) [155] and the elasticity of PDMS allow it to be released from the masters after the cross linking step without any damage, although it is suffciently rigid to retain its shape. One of the advantages of the PDMS is that it can seal

to itself or other substrates, and this sealing can be reversible (when removing the stamp from the surface after the μCP process) or irreversible (e.g when the activated PDMS surface reacts chemically by forming a covalent boning with the substrate) without considerable distortion of the stamp features taking place. The polymeric nature of the PDMS plays an important role for the printing procedure, as the ink molecules are stored within the swollowed material - similar as in a sponge – and released again, as soon as the stamp contacts the substrate.

In this work, polydimethylsiloxane (PDMS) is used (i) to create replicas from different masters in order to use it as an elastomeric stamp for μCP or (ii) as base material for photochemical functionalization and patterning processes whereby the PDMS is converted to inorganic SiO_2 by the irradiation with UV-light [156-162].

Figure 5 outlines the procedure used in this work for fabricating a μCP elastomeric stamp. The masters can be prepared using standard lithographic techniques (e.g. UV-lithography, electron beam lithography [144], electroforming [145], solid object printing [146], thermal printing [147]). When employing electron beam (e-beam) lithography for the master fabrication, a photoresist is spin coated on the surface of a silica substrate, an e-beam is used to expose those areas of the resisit, which have to be removed afterards for the etching process. A developing step removes the irradiated precursor and the bare substrate is recovered which is then treated with an etching procedure (liquid etching or reactive ion etching) to form depressions. After a lift-off process where the non-irradiated photoresist is removed, the elastomer is poured over the structured substrate and is allowed to sit for some time to degas. After a curing step for 1-2 hours at 70°C the cross linked polymer is gently peeled off from the master. “Inking” of the elastomeric stamp is done by placing a drop of the SAM precursor on top of the featured surface. After the solution is dried (either under ambient conditions or by using a stream of nitrogen gas) the stamp is placed into contact with the substrate and SAM precursor molecules are allowed to react at the surface-stamp interface. Next the stamp is peeled off gently from the surface and the patterned surface can be subjected to further chemical treatments (e.g. etching, passivation, functional groups tailoring, biofunctional attachment, etc.).

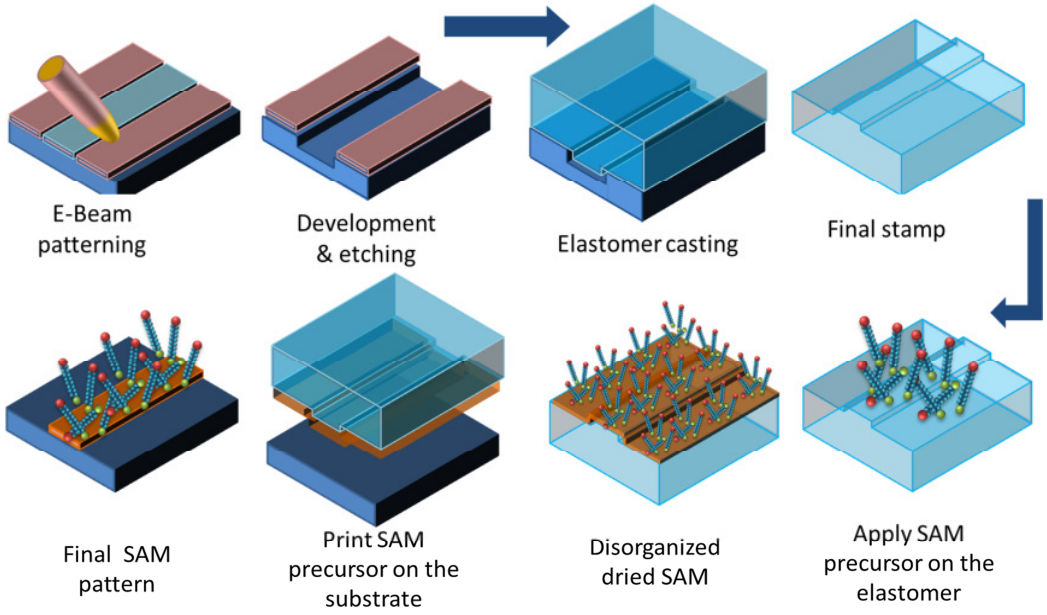

Figure 5.- Scheme of the procedure of microcontact printing (μCP) to pattern self-assembled monolayers (SAMs) on a substrate. The process begins with the preparation of a master for stamp fabrication. The master is created by the irradiation of a photoresist layer by an e-beam, followed by a developing and an etching process. After the PDMS is poured on top and cured at increased temperature, the stamp is peeled off the master, is inked with the precursor molecule of the SAM and is brougth in contact with the substrate. The "ink" is transferred forming an organized monolayer at the contact areas. In this way, selective areas can be patterned with the molecule of preference.

2.1.3.2 Ultraviolet Induced Lithography and Functionality Promotion

The materials and processes of semiconductor lithography are adopted from graphic-arts industry, where printing plates are prepared via lithography [163]. The basic idea of semiconductor lithography is to first coat (generally via spin-coating) the substrate which has to be patterned (e.g., a silicon wafer) with a photoresist. This radiation-sensitive material is then irradiated either through a mask with the desired pattern or by direct writing with the corresponding radiation beam such as e.g. ultraviolet (UV) light or electron beam (e-beam). After irradiation the sample is developed. Depending on the properties of the resist, either the exposed areas (positive resist) or the unexposed region (negative resist) can be dissolved or removed [163]. Then the patterned coating serves as a sealing during the structuring step of the uncoated substrate e.g. by etching. Finally, the resist can be stripped off the structured substrate. The mask needs to be morphologically stable under high-energy radiation and the lift-off of the resist should not damage the substrate surface. Therefore, it is a tedious, complicated and expensive process to form highly-ordered macro films using the conventional lithographic method.

The use of ultraviolet (UV) lithography means an overall irradiation of a substrate with light in the ultraviolet light spectrum. Selective irradiation is accomplished by using a

mask placed on top of the substrate. This mask protects certain regions of the surface where the chemical modification of the resist is avoided. Polymers have been used for decades to create chemically active regions and to generate morphological changes into it. This irradiation creates hydroxyl and other oxidic species on the top layer of the substrate through radical oxygen attack [164-169]. In this dissertation, an UV/ozone producing lamp is used (i) for the effective oxidation and (ii) for the topographic structuring of a polymer surface in presence of UV in one step. Silane chemistry can be applied on those hydroxyl- terminated polymer structures which were exposed to the UV light and - by that - a site selective second functionality can be achieved.

The polymer used in this work was Polydimethylsiloxane (PDMS). Due to its good optical, mechanical and chemical properties, this polymer is used in several applications, from protecting solar panels to contact lenses. As PDMS is a member of the group of silicones, by UV irradiation a silica-like layer on top of the substrate can be created, which can be used for further chemical treatment [170-172]. The presence of oxygen in the polymer matrix allows us to oxidize the upper layer of the polymeric bulk even in vacuum. A high intensity mercury vapor lamp with one emission maximum at 254 nm was used to cleave the bonds of organic molecules on the surface. Strong emission at 185 nm converts atmospheric oxygen into reactive ozone, which attacks the small molecular fragments and creates volatile organics. In this case, the Si–CH3 bond at the PDMS surface is cleaved and a Si –OH group is formed, resulting in a hydrophilic surface due to the newly silica-like layer created on the top. Figure 6 shows the UV/O3 induced oxidation mechanisms of PDMS. These mechanisms have already been discussed in literature [173-180]. Generally it is suggested that the abstraction of hydrogen is the first step. The resulting methylene radical reacts with oxygen to give a peroxy radical and rearranges to the silanol group. The ozone also photo dissociates to form oxygen atoms and molecules in the ground and excited state which in turn initiate also a bond breaking in the PDMS despite the UV irradiation playing a more important role in the oxidation process. It is also assumed that during the initial steps, a bond break is also occurring between the main chain (-Si-O-) or in the side groups of the polymer (-Si-C- and –C-H). Further reactions of the silicon and methylene radicals with oxygen lead to formation of other peroxy and oxidized radicals, as the cleaved bond of silicon with the $–CH_3$ is occupied by other oxidation products including –COOH, -COH and –OH groups resulting in a newly hydrophilic surface silica-like layer on the top [160, 170-172]. This fact has already been studied by Genzer [181], Chaudhury [182, 183], Ferguson [184] and

others [185] for 15 years, and they already used silanes for coupling to polymeric substrate [186] rearranging again to give silanol groups. It is mostly accepted that the side reactions end up with an oxygen radical attack on the -Si-C bond to create a new –Si-O-Si- bridge at the end of the mechanism [187, 188]. The silicon radical could also eventually react with a hydroxyl radical to form again a silanol group. This survey of possible reactions is shown in Figure 6.

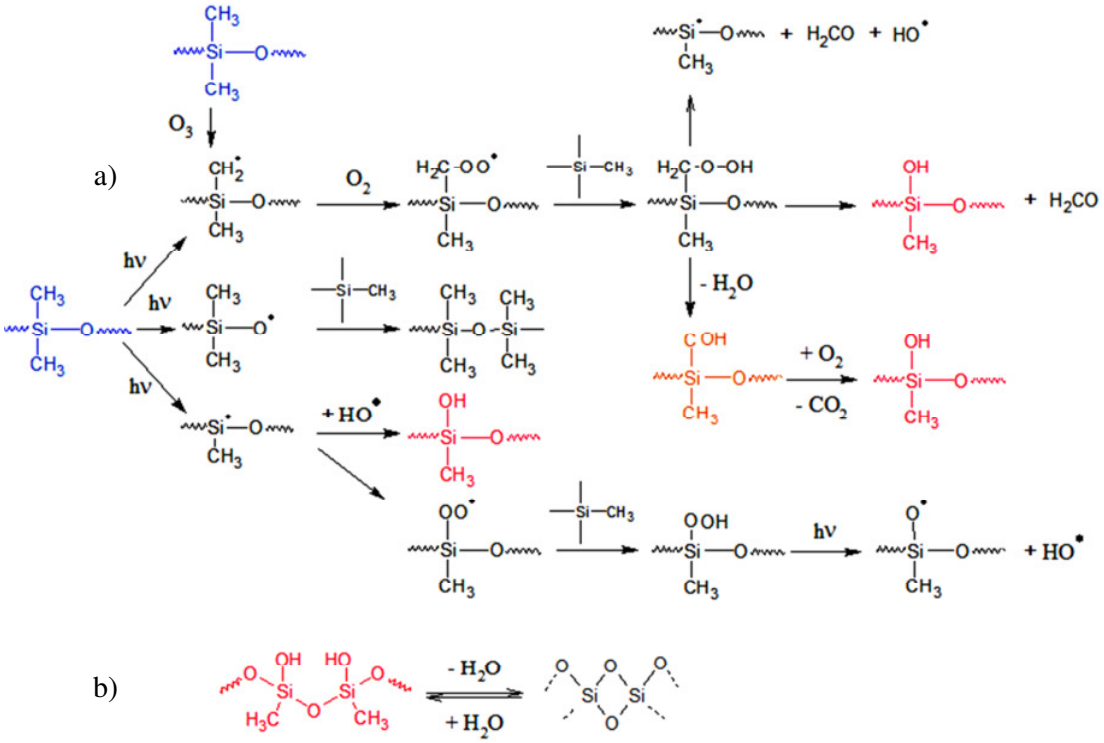

Figure 6.- Mechanism of oxidative process on PDMS using UV/O_3 irradiation in air. a)The methyl groups are sucessively substituted by hydroxyl groups. The PDMS chains are in blue and the substituted specie with silanol groups (Si-OH) is shown in red. Eventually also the formation of aldehydes or carboxilic acid can occurr (orange). On b) once the polymer is completely oxidize to hydroxyl groups, the removal of water will transform the decomposed polymer to inorganic silicon oxide.

After the polymer has been converted to a silica-like layer on the surface, further chemistry can be applied. On this case, silane chemistry is chosen due to the selective interaction toward oxidic materials containing hydroxyl groups. This fact has been already studied by Genzer [181], Chaudhury [183], Toth [189] and many others since 20 years. In Figure 7 a scheme of the process is shown: First the cross-linked PDMS substrate (created either flat or with topographical structures) is placed inside the irradiation chamber with a nickel grid (used for transmission electron microscopy) on top of it. The mask avoids the irradiation of the polymer on the covered areas, and in the exposed ones, silica-like layer with the incorporation of oxygen mostly from the environment is formed. Once the oxidized PDMS has been converted into a thin,

wettable, brittle silica-like layer, a further chemical functionality using silane (isothiocyanate-silane for this matter) can be achieved. In this research we use this technique to produce selectively oxidized substrate patterns on PDMS substrates providing a contrast of hydrophobic chemically inert areas and functionalized surface areas next to each other.

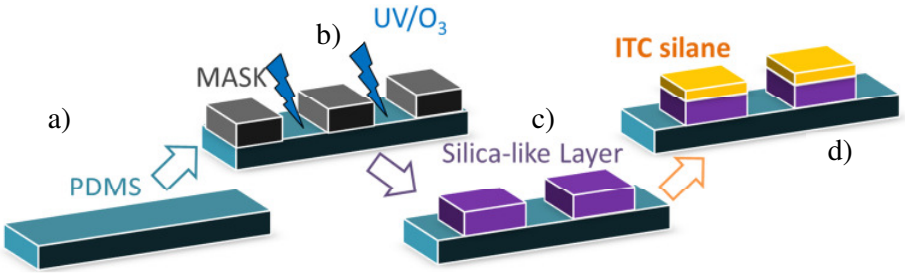

Figure 7.- Polydimethylsiloxane oxidation and functionality scheme. First the crosslinked PDMS (a) is placed inside a chamber which contains a UV/O_3 lamp generator placing a protective mask previous to the irradiation (b). After the silica like layer is created (c), then the substrate can be silanized (d) following the procedure to functionalize a non-structured surface.

However, hydrophobicity recovery has been observed in the substrates which have been modified under irradiation with UV/O_3. The following mechanisms for hydrophobicity recovery have been suggested: i) reorientation of polar groups from the surface to the bulk phase or reorientation of nonpolar groups from the bulk to the surface [189, 190], ii) diffusion of preexisting low-molecular weight non-crosslinked polymer towards the surface [191-205], iii) condensation of the surface hydroxyl groups [190] and iv) migration of low-molecular weight created during the irradiation or treatment to the surface [194, 195, 199, 200, 206, 207]. The commonly accepted explanation for this recovery is due to a diffusion of unoxidized low molar mass PDMS through cracks in the silica-like surface layer[175, 185, 205, 206]. Toth *et a.l* [189] studied silicone rubber surfaces exposed to radio frequency (RF) plasma or corona discharges in air. They found silica-like layer formed on the surface, with a thickness of less than 3 nm, using angle-resolved XPS. They concluded that the diffusion of low molar mass PDMS played a more important role for the hydrophobicity recovery than the reorientation of polar groups in the bulk of the rubber and other mechanisms. The importance of these phenomena lies in the stability of the brittle layer of silica on top and therefore it will be assessed in the experimental section.

2.1.3.3 Polymer Blends

A polymer blend is a mixture of at least two polymers with different characteristics which can be used e.g. as a coating to tailor physical properties of the coated substrate. A

mixture of two immiscible polymers - polystyrene (PS) and polymethylmethacrylate (PMMA) – can be used to prepare a binary polymer coating on top of a substrate. For that the two polymers were dissolved in a common solvent, a drop of the solution was placed on a substrate, and the thin film was prepared by rapid rotation of the substrate (spin-coating). Solvent evaporation during spin-coating causes an increase in the polymer concentration that leads to the demixing of the polymers [208]. After the selective removal of one of the polymers a hole-mask is formed on the surface and the bottom of the holes can be chemically functionalized. This patterning method is called polymer blend lithography. The produced polymer mask was mainly used to realize a site selective attachment of the isothiocyanate silane or aldehyde and TMV assembly on the surface (Figure 8).

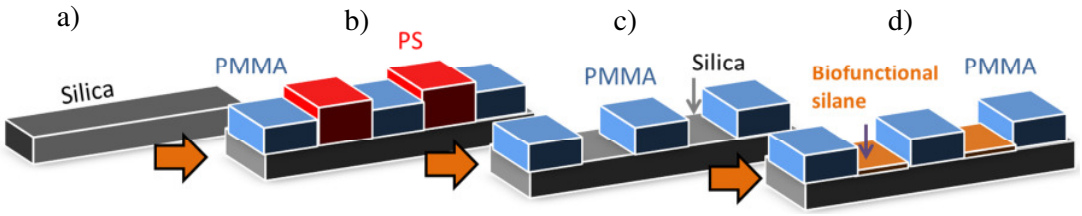

Figure 8.- Scheme of polymer blend lithography. First the substrate (a) is coated with a solution containing the two immiscible polymers (PS and PMMA), after solvent evporation phase separation takes place (b). Solving one of the polymers (PS) selectively will create holes (c) which can be used for site selective functionalization (d).

2.1.3.4 Dip Pen Nanolithography

Nanostructuring techniques are essential in developing further nanomaterials and nanoscience. Particularly, some are needed to work with soft and hard matter on a scale of sub- up to many micrometers. Methods such as e-beam lithography or ion beam lithography or nanoimprint lithography offer the ability to build hard structures but they do not allow the deposition of molecules in a nanopatterned way directly on the surface. Microcontact printing (μCP) allows doing the latter but it does not allow generating structures made of different inks with nanoscale resolution. Dip Pen Nanolithography allows making multicomponent structures with very high lateral resolution and by using arrays of several cantilevers, it is possible to achieve the massive parallel capabilities of the microcontact printing with the versatility of photolithographic techniques.

The use of atomic force microscopy as a nanofabrication device developed in the recent years with the promotion of the Dip Pen Nanolithography (DPN). This technique offers a very high lateral resolution (10 to 20 nm) and *in situ* imaging capabilities, ranging even to

manipulate matter at individual atom or molecular level [209]. It employs an ink-coated AFM tip to precisely create patterns with arbitrary shape and different sizes on a surface, and unlike other methods, DPN is a direct writing tool that allows the deposition of soft molecules and materials onto a surface with high nano and sub-micron resolution. Further exposure to any other conditions, or harsh UV or ion electron beam or solvents is not necessary [210]. Due to this advantage, it is employed in this work to selectively deposit isothiocyanate silane on a glass slide. The concept of the method is shown schematically in Figure 13. The ink, in this case isothiocyanate silane, can be transferred to the tip of the cantilevers by placing a drop on top of the chip or by dipping it into the solution. After drying, the AFM tip is approached to the surface, where the humidity from the environment creates a meniscus which fluidizes the silane molecules on the AFM tip towards the surface where it reacts with the –OH groups of the surface (Figure 9b). For the deposition of biomolecular patterns on solid surfaces, two strategies can be employed: a direct and an indirect method. They distinguish from each other depending on the chemical component which is been deposited. In this case, the isothiocyanate silane is directly deposited on the silica surface. Afterwards, a DNA linker solution is incubated on top of the substrate (accordingly to the goal specified previously in the introduction) and the DNA couples specifically to the silane. This is considered as an indirect deposition on the substrate as the molecule is adsorbed just on the pre-functionalized pattern. This second approach allows fabricating biomolecular patterns, but without any denaturation of fragile biomolecules caused by direct writing [211]. However, nonspecific binding effects of the biomolecules may influence the fidelity of the patterned structures.

As this technique writes directly onto the surface, it is very compatible for patterning biomolecules on surfaces. DPN can work in the same way as some chip-based array techniques or microarrays, which have become universally used in almost every area of health-related research [212, 213]. The advantage of this technique over microarray technology is the increase of density of dots available on the same area on almost 5 orders of magnitude and, with an appropriate readout system, this densities would allow an assay to screen for a correspondingly larger number of targets. Another important step forward is the advance in development of high-efficiency, high-resolution screening tools in order to read these nanoarrays. Using a chip containing several cantilevers (from 10 up to 25 tips), it can be used for a selective deposition of different inks or functionalities in a single process as illustrated in Figure 9d.

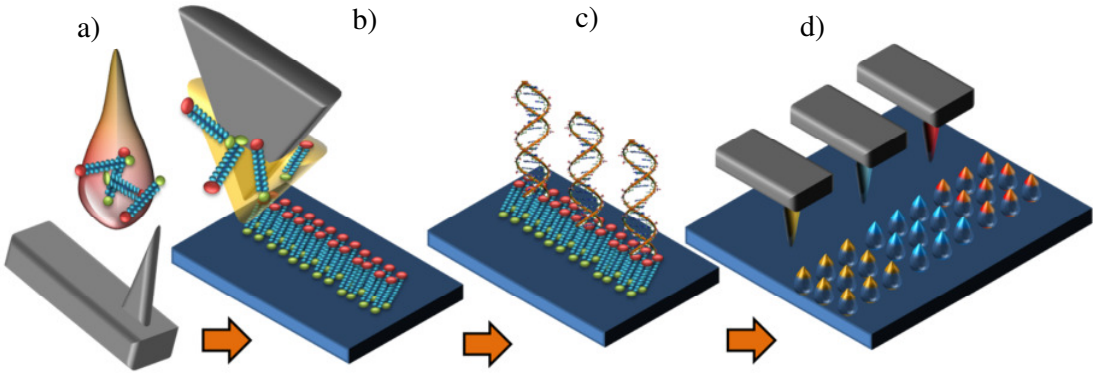

Figure 9.- Dip Pen Nanolithography concept scheme. First the AFM cantilever is dipped into a solution containing the ink (silane or thiol). After the tip is dried, it is placed into contact with the surface (b). Due to the humidity of the environment a water meniscus on the tip is formed, making the molecules to flow towards the substrate. Once the molecule is directly placed on the substrate, further functionality can be achieved. In this dissertation, DNA linkers which are complementary to a TMV-RNA sequence will be coupled on the isothiocyanate surface. (c) The automated process makes the repetition of several hundreds of features possible using different inks simultaneaously (d).

2.2 Biological Functionalization of Surfaces- Tobacco Mosaic Virus Self-assembly on a Surface.

Strategies for immobilizing different chemical groups on solid surfaces, with the purpose to act as templates for biological applications (biofunctionalized surfaces), range from non-specific adsorption of proteins to glass or polymers to oriented self-assembly monolayers and high density packed arrays on gold, silicon or other materials. It is desirable that these surfaces are stable, robust and reproducible. The high throughput preparation of nano-sized devices is a big challenge particularly when the resulting products have to be identical in shape, dimensions and functionality. Tobacco mosaic virus (TMV) particles have been used to direct arrange and functionalize specific sites on substrates. This biomolecule complex offers promising perspectives for nano application as a carrier of multiple functional molecules [58, 60, 214-216]. One of its advantages is the long-time stability in technical environments [12, 217].

Nature faces this challenge by using the principle of self-assembly whereby molecular building blocks are arranged “automatically” in a well-defined orientation just driven by the specific interactions between the different components. Bottom-up approach is the manufacturing of nanomaterials by manipulation and organization of individual atoms and molecules into determined configurations in a way similar to the processes done by molecular machines in nature. A classic example on the bottom-up approach for

constructing nanomaterials is the self-assembly of lipid molecules such as liposomes. Another example is the accommodation of protein along the RNA forming this way a virus, in its several particular structures. The advantage of the bottom-up approach would be the flexibility to create any substance, object or device through an atom by atom construction [218]. Therefore, the site selective bottom up assembly of the viral nanoparticles is desirable and was shown to be possible in a recent work by Müller et al. [72]. These characteristics would offer a high potential for application of the particles as biotemplates e.g. for the production of metallic nanorods [10, 219, 220] or virus-based solar cells [15, 221-223]. The self-assembly of the tobacco mosaic virus was first demonstrated by Fränkel-Conrat and Williams [224] in 1955. They started with isolated particles from some infected plants. Through a dialysis process using glycine buffer, they were able to degrade the virus into their two main components, ribonucleic acid (RNA) and coat protein. The separation from RNA and the protein takes place by precipitating the protein alone by saturation with ammonium sulfate [224]. Therefore two different solutions can be prepared, one containing the protein and the other one containing the RNA. Once they mixed again the two solutions they found fully assembled TMV-like particles and for the first time demonstrated that the tobacco mosaic virus could self-assemble in a test tube starting only with its basic protein and the RNA [225]. Therefore, a robust, well studied and non-pathological system is found in the TMV assembly for this research. The entropy-driven process [226] has been analyzed extensively by in vitro studies, resulting in a widely accepted mechanistic model as reviewed in detail by Butler et al [18]. Furthermore, the vertical sequence of the CPs can be modified by alternating coat proteins chemically functionalized at different steps. By this, different viral nanoparticles can be produced with sequences of different CPs [227, 228] which can – on their part – be used to bind other molecules as e.g. enzymes to the TMV-like particle [229].

Nucleation of TMV self-assembly is done by binding a specific stem-loop of the single-stranded viral RNA into the central hole of a two-ring sub-assembly of the coat protein (34 CP subunits), known as the “disk” [230] (Figure 10a). Elongation of the nanotube proceeds rapidly via the serial addition of further CP disks, each with subsequent incorporation of the following stretch of RNA located 5’ end of the origin of assembly [231]. During this process, the residual free 5’ tail of the RNA is threaded through the central channel of the nascent viral particle, with its foremost portion forming an RNA “travelling loop” at the fast-growing end of the virion [16]. Binding of the loop onto its

specific binding site, between the two rings of the disk, leads to melting of the stem so more RNA is available to bind (Figure 10b). The interaction of the RNA with the protein subunits in the disk cause this to dislocate into a proto-helix [232] (Figure 10c-d), rearranging the protein subunits in such a way that the axial gap between the rings at inner radii closes, entrapping the RNA with around 2200 identical protein subunits (Figure 10e) [18, 233, 234]. The resulting nanoparticle has a known geometry with an outer diameter of ~18 nm and a hollow channel with a diameter of ~4 nm. This in-vitro mechanism is essential for elucidating the bottom-up self-assembly of the virus-like particles on a surface when the RNA is fixed on one of the ends (5') by the DNA-complementary strand and ITC chemistry

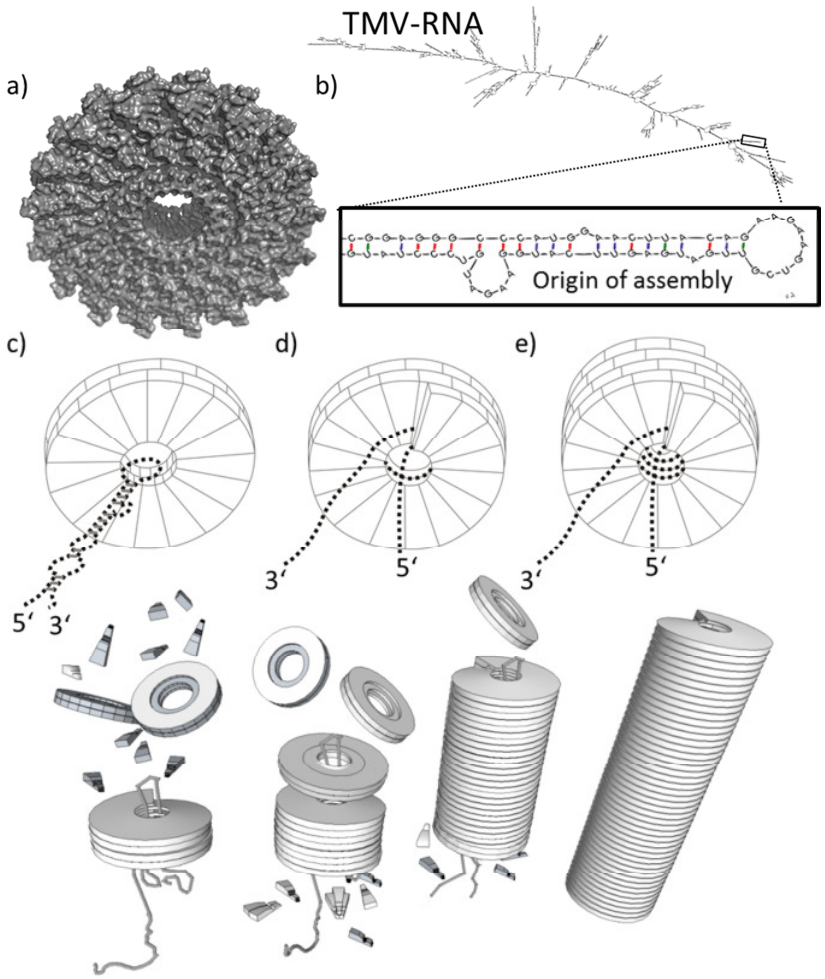

Figure 10.- Self-assembly process of TMV mechanistic model for the RNA-directed self-assembly of TMV-like particles in the 5' direction. [Butler, 1984]. a) the structure of the protein disk derived from an X-ray diffraction pattern [Bhyravbhatla et al 1998]. b) Secondary structure model of the RNA sequence of the TMV genome [Goelet, 1982] where the inset shows the origin of assembly hairpin with the nonanucleotide loop [Zimmern and Buttler , 1977]. c) the interaction of this section with a preformed proetin double-disk aggregate leads to a transition of the complex into a lockwasher comformation (d) whereas the addition of further disks to the growing pole forms a cilindrical structure when the stretch of the RNA takes place along the central channel of the nascent viral particle (e). the self-assembly process of protein disks along a RNA-template used as scaffold is shown. The process is shown as taken place in solution with no spatial restrictions.

3 .- Experimental Methods

3.1 Protocols

In this section, technical details for the characterizations and procedures followed to prepare the experiments are presented in the following layout: materials and methods, protocols, small review from some methods and for the measurement techniques, the most important operating parameters.

First it must be reminded that the focus of this thesis is on the surface selective modification and structuring of substrates for biological applications. As the project is a joint collaboration with the University of Stuttgart, several biological methods (Appendix A) used throughout the dissertation belong and are developed outside the reach of this work and done directly by the biology group in Stuttgart. Nevertheless, the procedures are also described even though they might be outside of the specific focus of this work.

For silicon dioxide surfaces, organosilane-based chemistry was applied. For polydimethylsiloxane also a silane-based chemistry is applied, granted a silicon oxide thin layer is formed previously on the polymer by UV/O_3 irradiation as explained in section 2.1.3.2.

3.1.1 Functionalization of Glass and Silicon Oxide surfaces

For the functionalization of oxidic surfaces, two main procedures from literature were tested and modified. First, a cleaning procedure of the substrate is necessary to achieve a successful adsorption of the monolayers, followed by the preparation of the 3-isothiocyanate propyl trimethoxy silane (ITCPMTS) and the silanization procedure. The selection of the experimental parameters (temperature, humidity, pressure) and the selection of the solvents play a very important role in the successful formation of a silane monolayer.

Preparation of the substrate- Cleaning

Materials

- Float-Zone grown Si (100), polished, with a 8-12 Ohm/cm resistance, and thickness about 525±20 µm, from Silchem (Freiberg, Germany) with a thin oxide layer (~60 Å) is used for silicon oxide based silanization.

- Microscope glass slides from VWR/ menzel glass (Germany) dimension LxWxT: 76x26x2 mm
- MilliQ water from a Millipore Milli-Q plus equipment. (Germany) of at least 18 MΩ quality
- Ammonium hydroxide 25% solution from Merck (Germany) for analysis
- Sulfuric acid ACS reagent, 95.0-98.0% from Sigma-Aldrich (Germany)

The wafers were received as small plates of 10 cm diameter and cut with a diamond pen to the required sizes (~1 cm^2) and cleaned with a snow-jet gun of CO_2 at high pressure.
This procedure alone is just a deficient cleaning procedure which was responsible for yield losses in our earlier experiments. According to several representative early papers published the effects of contaminants is very important in the application process of silicon wafer and devices [235].
The so called RCA wet cleaning sequence was developed by Werner Kern in the 1960 while he was working for Radio Corporation of America before the high temperature processing steps were used (oxidation and diffusion)[236], and still is used widely in semiconductor manufacturing as a critical cleaning steps for the removal of organic, metallic and particulate contamination on wafers surfaces prior to oxide growth, monolayer growth or any other surface treatments. The process consists of the consecutively application of two hot solutions known as RCA-standard cleaning solutions (SC-1 and SC-2) at 60°C for 30 minutes. In this dissertation the SC-1 solution for the first processing step consists of a mixture (1:1:5) of ammonium hydroxide (NH_4OH), hydrogen peroxide (H_2O_2) and water (H_2O). The second (modified: sulfuric acid instead of hydrochloric acid) cleaning solution SC-2m consists of a mixture (1:1:5) of sulfuric acid (H_2SO_4), hydrogen peroxide (H_2O_2) and water (H_2O).This is a diluted version of the so called piranha solution. In our case, the solutions were used to remove gross organic materials, particle contamination, and mainly for oxidation of the surface, as the monolayers formed by silane need the highest amount of hydroxyl groups possible. Unfortunately metallic and other inorganic contaminants are not desorbed. For handling of the solution extreme care needs to be enforced e.g. goggles, gloves and always a fume hood. Vigorous rinsing with milliQ water is necessary after each step. After the SC-1, the small chip of silicon wafer is not taken out from the cleaning vial, but overflown with water to avoid any contact with the environment and the re-deposition of organics. At the

end of the rinsing the chips remain immersed in the water until the silanization process takes place.

In case of cleaning microscope glass slides, the procedure remains the same, but using higher amounts of cleaning solutions for the slides to be kept always under solution (200 ml beakers).

3.1.1.1 Synthesis of ITCPTMS

Materials

- 3-aminopropyltrimethoxysilane (APTMS) (97%) and 3-aminopropyltriethoxysilane (APTES) (99%) was bought from ABCR (Germany) and used without further purification.
- Methanol (≥99.93%) was bought from Sigma-Aldrich (Germany) and used without further purification or treatment.
- Methanol anhydrous for analysis (99.8% and max 0.005%water) was bought from Applichem (Germany) and kept always under nitrogen atmosphere when used.
- Ethylchloroformate (97%) from Sigma-Aldrich (Germany) was used without further treatment.
- Chloroform (>99%) was bought from Sigma-Aldrich (Germany).
- Triethylamine (>99%) was bought from Sigma-Aldrich (Germany).
- Carbon disulfide anhydrous (>99%) was bought from Sigma-Aldrich (Germany).

Isothiocyanates have been prepared mainly by reaction of primary amines with thiophosgene [237], by the decomposition of 1,3 disubstituted thiourea with acids, and by the decomposition of dithiocarbamates from primary amines and carbon disulfide in presence of heavy metal salts [238], or dicyclohexylcarbodiimide [239].

In 1978, Halles described the reactions of amino groups with isothiocyanates onto silanized substrates[240]. Since then several kinds of isothiocyanates have been used for surface reactions: a phenylene di-isothiocyanate was used for linkage of amino-modified nucleic acids [241], peptides [88] or other amines [242] to an amino-functionalized surface. Benzophenone-4-isothiocyanate was used as a linker for antibody immobilization on a thiolated gold surface[243]. Fluorescein isothiocyanate (FITC) is one of the most common labeling dyes used for labeling amines. In the past, FITC was used to prove the successful coupling of amino siloxanes on modified gold nanoparticles [244], on amino silanized carbon nanotubes [78] or fluorinated polymer-coated surfaces [245] whereby

confocal microscopy was used for analysis [246]. For the work presented here, the 3-isothiocyanatepropyltrimethoxysilane (ITCPTMS) moiety is produced *via* a one-pot synthesis following the Kaluza [247] and Hodgkins [139-141] reaction and following Yamamoto et al. [248, 249] procedure from an amino terminated silane and immobilized on the surface without need of an additional incubation process as it is the case for the aldehyde terminated substrates, where the coupling of the 3-aminopropyltrimethoxysilane is required as a first step, followed by the dialdehyde coupling (see chapter 3.1.1.2).

This reaction uses a primary amine as nitrogen source and with carbon disulfide as the carbon and sulfur source. The reaction was prepared stoichiometrically adding 0.1 mol of amino silane (independently from the alkyloxy group) inside a balloon flask containing 20 ml of chloroform. The dithiocarbamate was prepared from the amine with a 0.1 mol of triethylamine as basic agent and carbon disulfide in excess to ensure the complete or most advance yield of the reaction. The carbon disulfide was added drop wise over a 10 minutes period. This mixture reacted at a temperature close to ~0° C or below with stirring for 3 hours. The reaction was completed by adjusting room temperature. Afterwards, the carboethoxylation was carried out adding an equivalent of ethyl chloroformate also drop wise at -5° C. The addition of triethylamine is also required as it serves as a base catalyst. A salt (triethylamine hydrochloride) is then separated from the liquid by filtration and the liquid is used without further purification. The product can be isolated by extraction with ether and evaporation of the solvent in vacuum.

Another option is to redissolve the salt into the same solution without the need for separation. In this sense, a lower purity is achieved but it can be treated as one-pot-synthesis nevertheless.

Table 1.- Chemical components and amounts for isothiocyanate propyltrimethoxy silane synthesis

	MW (g/mol)	Density (g/ml)	Molar concentration	Mass (g)	Volume (ml)	Purity (%)	final amount (ml)
aminopropyltrimethoxysilane	221.37	0.946	0.1	22.14	23.40	0.98	23.88
carbon disulfide	76.14	1.266	0.1	7.61	6.01	0.9999	6.01
ethylchloroformate	108.52	1.135	0.1	10.85	9.56	0.97	9.86
methanol	32.04	0.791				0.998	
triethylamine	101.19	0.726				0.99	3.0
chloroform	119.38	1.492				0.99	10.0

The procedure for the isothiocyanate synthesis using cyanamide as desulfurizing agent follows a very similar method to the previously developed from Kaluza. In this method, the reaction follows the same steps until the formation of the dithiocarbamate. From there instead of using ethylchloroformate as desulfurizing agent, cyanamide is used together with triethylamine as catalyst. A solution of cyanamide in tetrahydrofurane is added into the solution containing the dithiocarbamate and after stirring at ambient temperature for 3 hours, the residue is extracted with ether (4 times). Afterwards, the ethereal extract is evaporated to give the corresponding isothiocyanate silane as an oily yellowish residue.

3.1.1.2 Silanization of Silica Wafers and Glass Slides

Materials

- Silica wafer chips or glass slides cleaned using SC1-SC2m
- Methanol anhydrous for analysis (99.8% and max 0.005%water) was bought from Applichem (Germany) and kept always under nitrogen atmosphere when used.
- Isothiocyanatepropyltrimethoxysilane (ITCPTMS) (in-house prepared)
- Isothiocyanatepropyltriethoxysilane (ITCPTES) >90% in chloroform from ABCR (Germany) custom made according to Kaluza reaction. This will be referred as commercially available / custom-made silane.
- Aminopropyltriethoxysilane (APTES) from Sigma Aldrich (Germany) >97%
- Glutaraldehyde 25 wt. % in H_2O from sigma Aldrich (Germany) diluted in Millipore water up to 1% v/v.

Isothiocyanate silanization.

According to a modified procedure of Zeira et al.[35] preparation of a high quality monolayer is done following an improved two-step procedure. Using the freshly cleaned silica substrate, the water excess is blown with a nitrogen gun. A 3% v/v solution of ITCPTMS silane in dry methanol is freshly prepared and kept under nitrogen to avoid any water absorption into the solution. It is well known that silanization is very sensitive to many parameters, such as water content of solution, ambient humidity of the surrounding atmosphere, and even glassware which has been previously used for another purpose. Some parameters are hardly possible to be controlled e.g. how thick is the water layer physically adsorpted on the hydroxyl surface depends on the ambient humidity (summer

60% or more and winter 30% or less). In this sense, the layer was not able to be controlled in our set up for the experiments.

The chip is immersed inside the methanolic ITC solution and sonicated for 15 minutes followed by a 2 minutes sonication in pure solvent (dry methanol). The immersion of the sample and further rinsing is repeated three times. By exposing the chips to a humid atmosphere (100% r.H.) for 12 hours at 40°C, a further elimination of monolayer defects by densification and stabilization is achieved [54]. Furthermore, the silica wafers are taken out from the humid chamber and dipped again in the silane solution for 15 minutes and the corresponding 2 minutes rinsing step. This is done three times ending with a final thermal annealing of 10 minutes at 100°C. Finally the samples are packed under nitrogen for the further use.

Amine / Aldehyde silanization

Amino silanization of the cleaned or pre-structured Si wafers was done by gas phase silanization with aminopropyltriethoxysilane (APTES) under nitrogen atmosphere. Si wafer pieces were placed over a beaker containing pure APTES at room temperature (RT) in dry nitrogen for 40 min under 1 mbar vacuum. Afterward, the silanized samples were incubated in a 1% glutardialdehyde solution in ambient atmosphere for 30 min, washed with H_2O, and dried in a stream of nitrogen (procedure modified from Feng et al. [137]). The other suitable procedure is exactly the same as used above for the isothiocyanate functionalization following the wet route.

3.1.1.3 Addition of Iron-cored Silica Nanoparticles and Fluoresceinamine

Materials

- Magnetic nanoparticles (MagPrep®) of around 100 nm in aqueous suspension of 50 mg/ml were bought from Merck and diluted 1:100 in MilliQ water.
- Fluoresceinamine isomer I, was bought from Sigma-Aldrich (Germany) and prepared in an aqueous buffer solution of pH 9.0
- “DIG buffer wash and block” bought from Carl Roth (Germany).
- Sodium dodecylsulfate (SDS) Sigma-Aldrich, (Germany).
- Streptavidin-alkaline phosphatase Roche; Cat #11093266910 Germany
- Diisopropylethylamine ≥99.5% (DIPEA) from Sigma-Aldrich (Germany)

- Dimethylformamide (DMF) for molecular biology, ≥99% from Sigma-Aldrich (Germany)
- Potassium chloride from Sigma-Aldrich (Germany)
- Acetone from Sigma-Aldrich (Germany)
- Aminohexanol (≥97.0%) from Fluka (Germany)

For the experiments involving particle adhesion or the coupling of fluoresceinamine, the samples are dipped inside the solution containing the previously mentioned markers. In the case of the nanoparticles adsorption the samples were placed vertical on the solution containers to avoid any influence from gravity on the assembly.

In case a contrast area in the sample is required, a drop (smaller than the isothiocyanate silanized area) is placed on top of the substrate and left for 5 minutes in case of the aminofluorescein and 18 hours in case of the DNA-fluorophore addition. The concentrations vary from 0.01 mM to 0.1 mM. They will be specified in the experiment when discussed.After the treatment, the samples were washed with MilliQ water.

In the case of the microarray experiments (section 4.2.2.4.2) involving fluorescein, different concentrations were used. Nevertheless they were prepared following this procedure: The epoxy slide and one of the isothiocyanate slides were treated with a standard protocol for microarray oligonucleotide coupling (immobilization T°= 60°C, 30 minutes, washing step with 0.1% Triton buffer and 1mM HCl, 100 mM KCl, and H_2O, then a blocking step at 50°C, for 15 min with PEG blocking solution and final washing with H_2O). The other isothiocyanate functionalized slide was treated according to Manning et al. [250, 251], (immobilization T°= 37° C , 90 minutes, washing step with methanol and H_2O, then a blocking step at 27°C, for 60 min with a 50 mM aminohexanol/DIPEA blocking solution and final washing with DMF, Acetone and H_2O).

In case of the fluoresceinamine, microcontact printing was used on silanized substrates in order to provide an further structure and approach towards miniaturization goals.

Figure 11 shows AFM topography images of two PDMS stamps made in-house from different master. One of them was received from the group of Prof. Terfort (University of Frankfurt, Germany, Figure 6a) and a second was bought from Klarite ®, Renishaw Diagnostics (England, Figure 6b).

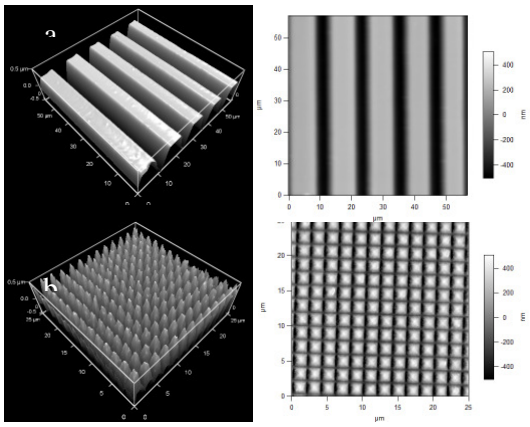

Figure 11.- 3D and AFM topography images PDMS stamps with two different patterns: (a) lines with 7.5 micron width decreasing over a 60x60 µm^2 scanned area down to 5 microns width. (b) pattern of pyramidal feature over a 20x20 µm^2 scanned area. The color scale in both images range up to 1 micron.

3.1.2 Functionalization of Polymers by UV/O_3 Irradiation

Materials

- Polydimethylsiloxane (PDMS) from Dow Corning (Belgium) and its crosslinker is prepared in a 10:1 volume ratio composition.
- Methanol anhydrous for analysis (99.8% and max 0.005%water) was bought from Applichem (Germany) and kept always under nitrogen atmosphere when used.
- Isothiocyanatepropyltrimethoxysilane (ITCPTMS) in-house prepared
- Isothiocyanatepropyltriethoxysilane (ITCPTES) >90% in chloroform from ABCR (Germany) custom made according to Kaluza reaction. This will be referred as commercial
- UV/O_3 Pro-cleaner from Bioforce
- Transmission Electron Microscopy (TEM) grids from Plano (Germany). Different sizes and patterns (400 square mesh nickel, 200 square mesh nickel, mixed mesh copper)

Polydimethilsiloxane (PDMS) from Dow Corning (Belgium) with its crosslinker was used in a 10:1 (monomer:crosslinker) ratio. PDMS is cured by an organometallic crosslinking reaction. The siloxane base oligomers contain vinyl groups. The cross-linking oligomers contain at least 3 silicon hydride bonds each. The curing agent contains a proprietary platinum-based catalyst that catalyzes the addition of the Si-H bond across the vinyl groups, forming Si-CH_2-CH_2-Si linkages. The multiple reaction sites on both the base and crosslinking oligomers allow for three-dimensional crosslinking. If the ratio of curing agent to base is increased, a harder, more cross-linked elastomer results. Heating will also accelerate the crosslinking reaction [252]. In our case 2 hours at 70°C has been used for every experiment. The density of the mixture does not change appreciably during

cross-linking because the monomer is non-volatile. The shrinkage in PDMS films during curing has been reported to be about 1% [253]. Furthermore the pot-life of the solution is around two hours and the mixture begins to solidify at longer durations. The cross-linking mechanism gives elastic stiffness to the PDMS film and the modulus of PDMS will increase with increasing mass fraction of the cross-linker. Conditions that favor the crosslinking reaction will also produce an increase in stiffness.

Silica wafer cleaned according to SC_1-SC_2m cleaning procedures was used as master for achieving nanometer roughness. The flat substrates were afterwards taken into the UV/O_3 cleaner and irradiated for 600 minutes. A high intensity mercury vapor lamp generates 254nm wavelength light which cleaves the bonds of organic molecules on the surface. Emission at 185nm converts atmospheric oxygen into reactive ozone, which attacks the small molecular fragments and creates volatile organics.

The substrate can be also selectively irradiated and therefore selectively oxidized previous to silanization. Patterning was carried out by placing transmission electron microscope (TEM) grids (nickel grid with 400 squares mesh and a copper 200 square mesh from PLANO, Germany) on top of the polymer surface before the substrate is treated in the UV/O_3 chamber. Irradiation takes place for two hour period for 3 up to 5 times with pauses of 60 minutes between the irradiation steps. This is for countermeasure the hydrophobicity recovery of the substrate after the irradiation took place (see section 2.1.3.2). Immediately after the substrate is finally treated, the sample is immersed in a 3% v/v solution of ITCPTMS in dry methanol. An alternative procedure is done just by pipetting a drop from the pure silane onto the irradiated area (in many cases over the grid in pure form) and for each cases, two hours waiting is necessary for a saturated silanization of the substrate. The silane also prevents further hydrophobic recovery of the substrate as the crosslinking between the silane molecules acts also as a reinforcing network for the surface.

3.1.3 Polymer blends as mask for selective functionalization of silica wafers

Materials

- Polymethylmethacrylate (PMMA) 100 kDa reference standard quality from Polymer Standards (Germany).
- Polystyrene (PS) 100 kDa reference standard quality from Polymer Standards (Germany).

- 2-Butanone / toluene / cyclohexane/ acetic acid bought from Sigma Aldrich (Germany) quality >99%

Silicon wafers were spin-coated with a solution of the two immiscible polymers polystyrene (PS) and polymethylmethacrylate (PMMA) dissolved in methyl–ethyl–ketone (MEK). A molar 1:1 mixture of polystyrene (PS) and polymethylmethacrylate (PMMA) in methyl–ethyl–ketone with a total polymer concentration of 2 mg/mL was prepared. Twenty microliters of this solution were coated with a spin coater at 50 rps for 30 s onto the Si wafers. Demixing of the polymers occurred upon fast evaporation of the solvent and resulted in patterns characteristic of the respective mixtures applied. The resulting polymer pattern was treated with a specific solvent in an ultrasonic bath for 10 min to selectively remove the desired polymer from the surface, which uncovers the Si wafer in these areas: acetic acid 10% vol. treatment for 10 minutes selectively removed PMMA, partially uncovering the Si wafer while cyclohexane treatment for 10 minutes removes selectively the PS. Figure 12 represents the same area of a wafer exhibiting a characteristic circular and meander structure, with a combined PMMA removal, respectively, leaving a PS mask 100 nm in height. The partial removal of the PMMA is due to an acetic acid drop placed on a small area of the substrate, dissolving selectively just the PMMA but not the PS in this case. On a different approach, the substrate was functionalized first with the amino silane and after it can be structured in the previously explained form. The last step in both cases is the aldehyde coupling. In the figure the three areas can be seen: the depressions (darker areas) arise due to the PMMA removal and the circular pattern corresponds to the PS islands. The elevated (brighter) area belongs to the remaining PMMA.

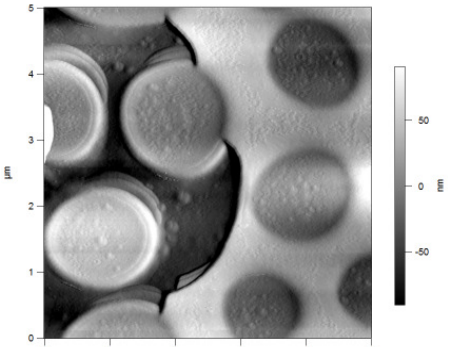

Figure 12.- AFM topography image showing showing the PS-PMMA structured substrate. A partial disolution of the PMMA mask has been done by placing a drop of acetic acid on the surface removing exclusively the PMMA from that area. The circles belong to the polystyrene polymer, and the matrix to polymethylmethacrylate. The PS is lower than the PMMA but still higher than the substrate.

AFM topographic images of the polymer blends cast from 2 mg/ml solution in butanone are shown in Figure 13. With the 50% mass ratio of PS:PMMA the substrate was coated with an island-type topography as shown in Figure 13a and b. These isolated islands have

a height of about 5–10 nm above the continuous surface, in this case silica, and they possess a diameter of around 200 nm. If the PS/PMMA ratio is decreased, then a continuous phase appears. Figure 13c) shows the topography of the 25% weight ratio of PS:PMMA. The islands tend to coalesce together to form large and bicontinuous areas. Since the continuous area fraction increases with PMMA bulk concentration, these islands are most probably composed of a PMMA-rich phase [254]. In the experiments described here the bigger islands were preferentially used as the selective removal of the polystyrene was favored in this situation. A complete removal of the PMMA layer was also investigated, yielding the acetic acid (99% purity) as the best removal solvent for PMMA (Figure 13d).

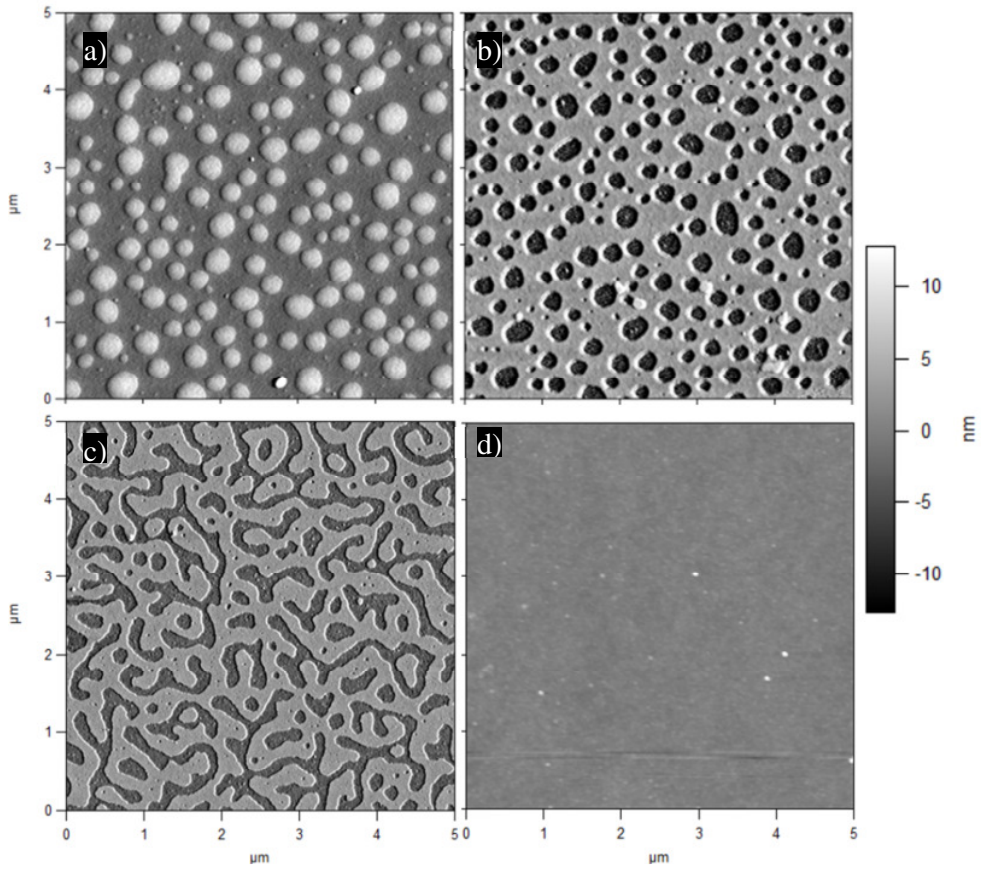

Figure 13.- AFM topography of a PS / PMMA polymer blend (1:1 mg) a) after casting and b) after cyclohexane mediated polystyrene removal, c) higher mass ratio (1.5 mg PMMA:1 mg PS) spin coated and polystyren removal by cyclohexane, d) removal of both polymers by treating the sample with toluene (for polystyrene) and acetic acid (for PMMA).

3.1.4 Biofunctionalization of Substrates (Silicon Wafers and PDMS Oxidized Surface)

In order to biofunctionalize the substrate following a self-assembly scheme as shown in section 2.2, DNA oligonucleotide strands have to be coupled first on the substrate and submitted to subsequent steps of ligation/hybridization for further RNA coupling. Once the RNA has been conjugated on the substrate, the final coat protein self-assembly takes place. The biofunctionalization of the substrates is carried out in the same way independently of the substrate (silica wafer, glass or PDMS). Therefore, the substrate type will not be mention in the materials list. As explained in the introduction, the part of the project carried out in this facility involves the DNA-linker immobilization in-house before the samples are sent to Stuttgart University for the RNA-CP assembly. For a more comprehensive list of the methods used in the bottom-up self-assembly of virus-like particles done in the University of Stuttgart involved in this dissertation please refer to Appendix 1A

3.1.4.1 DNA Linker Immobilization on Functionalized Isothiocyanate-Silanized Wafers.

Materials

- DNA oligonucleotide was ordered and assembled according to the necessary sequence for the RNA binding purchased from Metabion Martinsried, Germany, (USA); Martinsried (Germany). *sequence will be extended in the procedure
- RNA sequence in vitro with a MEGAscript Kit from Ambion (Austin USA).
- Only sterile 2x filtered HPLC water was used to prepare buffer solution.
- Spotting buffer 1M tris-HCl at pH 7 bought from Carl Roth (Germany).
- Saline-sodium citrate (SSC) buffer bought from Carl Roth (Germany).
- RNase inhibitor New England Biolabs (USA).
- Sodium dodecylsulfate (SDS) Sigma-Aldrich (Germany).
- Diisopropylethylamine ≥99.5% (DIPEA) from Sigma-Aldrich (Germany)
- Dimethylformamide (DMF) for molecular biology, ≥99% from Sigma-Aldrich (Germany).
- Aminohexanol (≥97.0%) from Fluka (Germany).

Generally, from this step on, MilliQ water which had been treated with dimethyl dicarbonate (DMDC, Merck, Germany) [255] was used for the preparation of aqueous solutions. A single-stranded DNA oligomer (ssDNA, from Metabion, Germany, nucleotide sequence:"5'-T_{15}-GCACCACGTGTGATTACGGACACAATCCG-3") with 5'-terminal amino modification (5' C6 Aminolink) was covalently bound to the isothiocyanate-functionalized areas of the wafers and the PDMS. The linker DNA oligomers were diluted in 1 M Tris-HCl buffer pH 7.0, 1 % *N*,*N*-Diisopropylethylamine (DIPEA) [256] to a concentration of (10 pmol/µl). 2 µl of this spotting solution were applied to the functionalized surfaces. After incubation in a humid chamber for 16 h, the surfaces were washed and blocked as reported [256]. Briefly, immobilization was followed by immersion in DMDC-treated MilliQ water for two times 2 min and 5 min in methanol under gentle agitation. Subsequently, the specimens were dried under a stream of nitrogen and residual isothiocyanate functionalities were blocked by treating them in a solution of 50 mM 6-amino-1-hexanol in DMF containing 150 mM DIPEA for 2 h. After final washing steps in DMF (2 min), in acetone (2 min) and in DMDC-treated MilliQ water (two times for 5 min), the specimens were dried under a stream of nitrogen.

3.2 Measurement Techniques

A summary of several surface analytical techniques used in this dissertation and their specific parameters is discussed in the following pages. Some topography evaluating techniques are often found in the biomaterial literature, including: (Environmental) scanning electron microscopy ((E)SEM), transmission electron microscopy (TEM), atomic force microscopy (AFM) and light microscopy / fluorescence light microscopy (LM/FLM). In this dissertation, a second group of techniques is used to reveal valuable information regarding the elements constituting the surface (or the solution) and to characterize the chemical structure near the surface region (or in solution) of a sample by using the interaction between mater and radiated energy. Included in this second group is X-ray spectroscopy (XPS), and time-of-flight secondary ion mass spectrometry (TOF-SIMS).

Numerous techniques for surface analysis including optical and spectroscopic methods are used to characterize the chemical composition of a material. Although for chemical characterization the use of microscopes such as environmental scanning electron microscope (ESEM) or atomic force microscope (AFM) or even a normal light microscope or fluorescence microscope is not suitable, secondary or indirect techniques are used to assess the chemical composition and structure of the molecules (mostly in solution) and functionalities. Some examples are: Fourier transform infrared spectroscopy (FT-IR) and Fourier transform Raman spectroscopy (FT-Raman).

When examining the efficiency of a surface reaction through light/fluorescence microscopy, an amino functional fluorophore is added to the complementary reactive group on the surface (either aldehyde or isothiocyanate). The intensity of the emitted light is measured in order to assess the presence of the functional group in the surface. Different structuring techniques are used in combination with the characterization techniques to help in the evaluation of the presence of the functional groups. A short summary of the techniques used in this dissertation, along with the useful information which can be withdrawn from them is shown in Table 2.

Table 2.- Surface science techniques for characterization of self-assembled monolayers used in this dissertation.

Experimental Technique	Information that can be obtained
X-ray photoemission spectroscopy (XPS)	Elemental composition, chemical state, impurities
Fourier transform Infrared spectroscopy (FT-IR)	Specific chemical groups, adsorption site, molecular tilt
Fourier transform Raman spectroscopy (FT Raman)	Specific chemical groups, adsorption site, adsorbate vibration.
Contact Angle (sessile-static drop)	Wettability, homogeneity of the surface, semi-quantitative change before/after chemical group coupling.
Light/Fluorescence microscopy	Visually distinguish spatial distributed chemically modified surfaces. Chemical reactivity, semi-quantitative change before/after chemical group coupling.
Atomic force microscopy (AFM)	Surface topography, surface structure (periodic and non-periodic), stiffness, elasticity.

3.2.1 Atomic Force Microscopy

Atomic Force Microscopy (AFM) uses a non-optical way to map the surface of the sample. It belongs to the techniques of scanning probe microscopy family. It can be also used for several other applications, including chemical [257], magnetic or potential probe microscopy, photothermal microspectroscopy, kelvin probe microscopy, etc. In this dissertation AFM was used for topographic investigation for biological purpose [258]. The AFM maps surfaces by raster scanning a fine silicon tip very smoothly over the surface, recording via a photodiode and a laser reflected on the back of a tip, a profile that can achieve atomic resolution (mica, HOPG, or freshly etched silica). As the tip of the cantilever finds any elevation change on the surface, the cantilever deflects. A laser pointed to the back of the cantilever and is aligned in that way that it - after reflection – irradiates a four-segment photo diode. If there is a deflection of the cantilever due to a change in topography, the laser hits the photodiode in the upper or lower field registering a difference in voltage. Feedback from the photodiode difference signal, through software control from the computer moves the piezoelectric element holding the sample in order for the tip to maintain either a constant force between the surface and the cantilever. If the

tip is bending upward because it has reached a feature, the scanner/piezo moves the whole probe downwards, enough to return the deflection of the cantilever to its original value. In the same way, when a "valley" is encountered, the scanner moves the probe upwards. In this way, the deflection of the cantilever, and hence the tip-sample interaction force is kept constant. The amount the scanner had to move to maintain the deflection is equivalent to sample topography, and is recorded by the computer, plotted and translated to a height image by knowing the deflection generated by any nanometer (see Figure 14) [259-262].

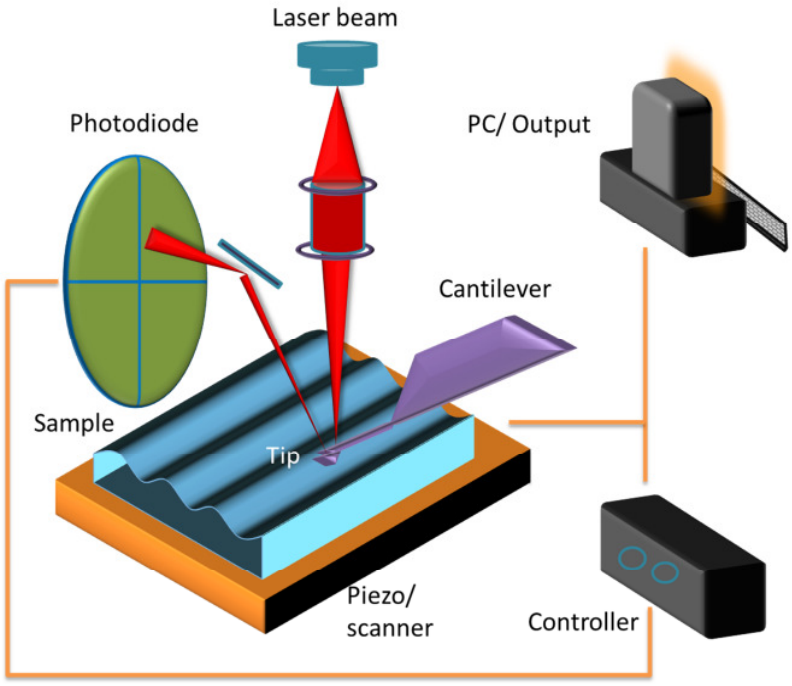

Figure 14.- Atomic force microscope instrument description. The sample is measured by the tip interacting with the surface of the sample. The substrate is placed on top of a scanner which is responsible to move the sample in XYZ direction. The piezo receives a feedback signal from the controller with in turns receives a signal from the photodiode. This signal adjust the force/height of the sample to the cantilever and simultaneously is plotted in the PC via a dedicated program.

Atomic force microscopy is a technique used today as one of the most common type of scanning microscopy used for imaging biomaterials [263]. It measures the interaction force between the tip and the surface. The tip may be moved contacting the surface permanently, or it may vibrate perpendicular to the substrate just “tipping” to the surface during the scan. The interaction force will depend on the nature of the sample, the probe tip and the distance between them. In this dissertation, the AFM is the preferred method for characterization of the surface. It is the most accurate method to assess the correct

TMV-like particle formation on the surface after the complete procedure has been made with respect to spatial resolution combined with height information. Therefore, a deeper explanation on how it works and the parameters used for the majority of the imaging will be carried out. The concept of resolution in this technique is different from light based microscopy techniques because AFM is a three dimensional, mechanical imaging technique. Spatial resolution is defined as the smallest distance between two adjacent points which can be distinguished as separated points. There is a clearly important distinction between images resolved by wave optics and scanning probe techniques. The first are limited by diffraction, and the second ones are limited by the geometry of the tip and the sample as well as by the mechanical properties of the whole setup. The technique is based on a silicon cantilever with a sharp tip at its end, sensing the surface by measuring the interaction between the attractive or repulsive forces between them both. The radius of curvature may vary between the 5 nm and 10 nm for the tips used. When the cantilever is brought into proximity of any sample surface, forces between the tip and the sample will deflect the cantilever according to Hooke's law. Depending on the case, the forces measured can be classified into long and short range interactions. Normally, the potential energy between the tip and sample V_{ts} causes a z component of the tip-sample force F_{ts}, whereby k_{ts} is the cantilever spring constant.

$$F_{ts} = -dV_{ts}/ dz \quad (1)$$

$$k_{ts} = -dF_{ts}/dz. \quad (2)$$

Depending on the mode of operation the AFM uses F_{ts} or some entity derived from F_{ts} as the imaging signal [264]. Under ambient air conditions, most surfaces are covered by a layer of adsorbed gases (condensed water and other contaminants) which is typically several nanometers thick. When the scanning tip touches this layer, two different atttractive forces occur which are oriented downward and influence the force between the AFM tip and the substrate. One is the capillary action which causes the formation of a meniscus and then the surface tension pulls the cantilever down into the layer. The second force is due to coulomb interactions based on trapped electrostatic charges on the tip and on the sample. These downward oriented forces increase the overall force on the sample and, when combined with lateral shear forces caused by the scanning motion, can distort measurement data and cause severe damage to the sample, including movement or tearing off surface features .

Two operating modes were used in this dissertation for the AFM characterization with different results. In contact mode the tip scans in the repulsive force regime with forces between 0.01 to 1.0 N/m in air and the cantilever is deflected by the interactions between the tip and the surface. This mode can be used for metal or hard polymers which are not damaged at all [265]. However, the cantilever exerts lateral shear force and the scanning motion may affect soft materials, distorting measurement data and causing some damage to the sample [266]. Therefore, as a second mode for AFM investigation the intermittent contact mode also called alternate current mode (AC-mode), as the cantilever is vibrated near its resonance frequency, and lightly taps the sample with an amplitude typically between 20 – 100 nm. This mode has the advantage that as there are no lateral friction forces applied to the surface there is no destruction or damage on the material. This mode works well with hydrophobic polymers in this case PDMS. Inside this AFM intermittent contact mode, the phase image mode can be used also to map the composition of a sample. The differences in materials drive a phase difference between the oscillations of the piezoelectric corresponding to each material interacting with the tip. This imaging mode can reveal fine structures that are concealed by a rough surface topography. Nonetheless the hardness and elasticity, adhesion or charge may affect the phase images obtained. Therefore it is used mostly to distinguish between two types of materials.

Microscopy Procedure Details.

Atomic force microscopy is the most appropriate technique to evaluate the final results on this dissertation taking into account the final biofunctionality approach by assembly the TMV-like particles on the surface. This technique provides sufficient lateral/spatial resolution when measuring the virus rods and other nanostructures.

The microscopes used in this dissertation are:

1) A commercially available MFP-3D Bio AFM (Figure 15a) from Asylum Research. This features an inverted optical microscope with fluorescence capabilities. It uses a closed loop sensor to move the probes along the three axes both in air as in liquid. The modes of operation used were: (i) AC mode (alternating current mode: generic name for an oscillatory probe technique of which intermittent contact mode is a subset. An AC-like signal is used to drive the piezoelectric actuator to produce a non–DC response of the cantilever to the drive signal (under the repulsive regime [267]) and (ii) contact mode (also known as quasi-static mode AFM, where interatomic van der Waals forces become repulsive as the AFM tip comes in close contact with the sample force).

2) A commercially available Digital Instruments Multimode AFM (Figure 15b). This AFM use the intermittent contact mode (Tapping ®) of operation which provides good spatial resolution on the TMV measurements. However sample size is limited to approximately 1 square centimeter and samples must be low profile.

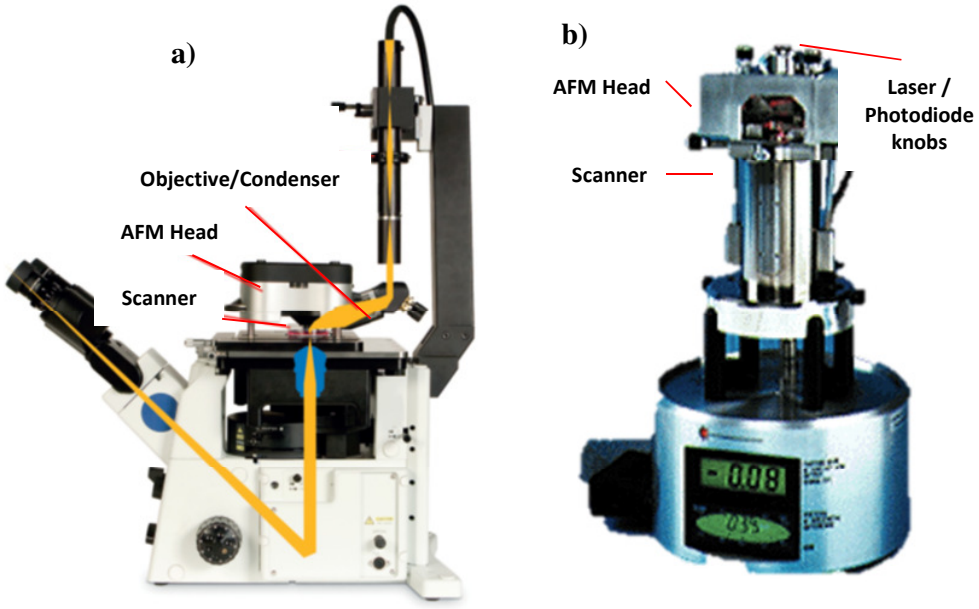

Figure 15.- a) MFP-3D Bio AFM from Assylum Research. b) Digital Instruments Multimode AFM (Images courtesy of Assylum Research and Bruker Nano Surfaces Division respectively)

The cantilevers were bought from Mikromasch (Germany) in different schemes. They are made from silicon (phosphorus doped) n-type with a typical probe tip radius of 10 nm and a full tip cone angle of 40°. The total tip height accounts for 20 to 25 µm according to the manufacturer. There were two types of cantilevers used: single lever probe and a three-lever probe. The probes showed different resonant frequencies and spring constants (see Table 3), but all of them were intended to be used with soft and medium soft samples in intermittent contact mode.

Table 3.- Cantilevers frequencies and spring contants used for the characterization of surfaces and particles.

	Resonant Frequency (kHz)			Spring Constant (N/m)		
Cantilever	A	B	C	A	B	C
NSC-18	75			3.5		
NSC-35	210	315	150	7.5	14	4.5
NSC-36	105	155	75	0.95	1.75	0.6

3.2.2 X-ray Photospectroscopy

The photo emission process is based on the photoelectric effect discovered by Heinrich Herzt and was applied in the mid 1960's by Kai Siegbahn to develop further the technical equipment in order to record the first high-energy- resolution X-ray photospectroscopy spectra.

X-ray photospectroscopy (XPS) is a surface characterization technique used for chemical assessment. Photons of a specific energy are used to excite the electronic states of atoms on the surface of the sample. The material is irradiated with a beam of X-rays, which excites the electrons on the upper 10-100 nm of the sample. The interaction between an X-ray photon and the core level electron of an atom causes a complete transfer of the photon energy to the electron (see Figure 16). Then the electron has enough energy to escape from the surface of the sample. These electrons are collected and their kinetic energy distribution is determined. Since their energies are quantized, the resulting spectra exhibit bands whose energetic position is characteristic for the corresponding chemical elements present at the surface [268, 269]. Additionally the chemical environment of the atom results in a defined band peak shift which gives a precise idea about the binding state of an atom (e.g. single, double, triple bond), the neighboring elements and the oxidation state of the atom [270-272]. The kinetic energy distribution of the emitted photoelectrons E_k for an electrically conductive solid can be calculated by:

$$E_k = h\nu - \phi_{sp} - E_B \qquad (3)$$

where h is Planck constant (6.62 x10^{-34} J.s), ν is frequency of the radiation in Hz and ϕ_{sp} is the work function of the spectrometer where the kinetic energy of electrons is measured [273]. E_B is the electron binding energy representing the difference in energy between the ionized and neutral atoms.

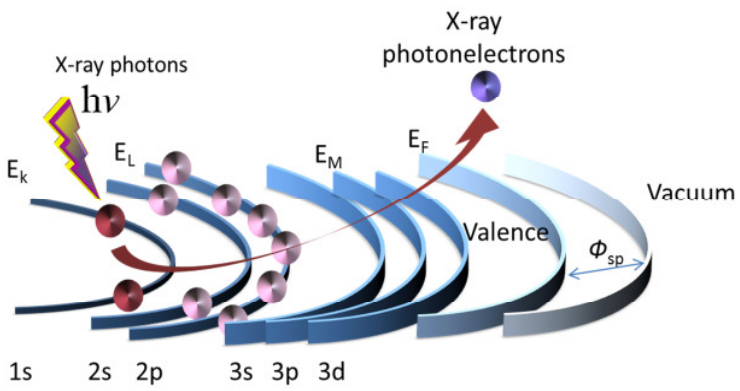

Figure 16.- Diagram explanation of XPS principle. When surfaces are irradiated with soft X-rays the emitted photoelectrons with a determined energy are analyzed. The interaction between an X-ray photon and the core level electron of an atom causes a complete transfer of the photon energy to the electron which has now enough energy to escape from the surface of the sample. The difference between the X-ray energy and the photoelectron energies gives the binding energies (BEs) of the core level electrons.

In case of conducting samples, the electron energies can be referenced to the Fermi level of the element, giving the possibility to create an absolute energy scale aiding in the identification process of different species. However for non-conductive samples (such as PDMS and other polymers) the problem of energy calibration is significant. Electrons leaving the sample surface cause a potential difference resulting in a retarding effect acting on the electrons to be measured. This can account for shifted peaks in energy by as much as 150 eV. XPS is a quantitative technique in the sense that the number of electrons recorded is proportional to the number of atoms at the surface. In practice however, to produce accurate atomic concentrations from XPS spectra is not straightforward. The precision of the intensities measured by XPS is doubtless as the repeatability on similar samples giving good precision. What might me doubtful are the results reporting to be atomic concentrations for the elements at the surface. In this sense, for quantification based on standard relative sensitivity factors, precision is achieved and not accuracy. Therefore, a quantitative atomic percentage analysis of the surface is not possible for the samples tested in this work. Since in the dissertation, the samples were treated and changed chemically, monitoring the changes in the binding energies from the atoms provides the precision of XPS as a very powerful technique for qualitative analysis.

Basic quantification procedure

XPS counts the electrons of a certain energy coming from the sample surface when they are emitted by X-rays. The spectrum representing the amount of electrons hitting the detector plotted versus a sequence of energies includes also contributions from a background signal and resonance peaks.

The spectra are quantified primarily in terms of peak intensities (area below the signal) and peak positions. The area below the curve (counts p/second) measures how much of the element is at the surface, while the positions indicate which element in which environment is present. Other values, such as the full width at half maximum (FWHM) is a useful indicator for the changes of chemical state of the element or physical influences. The assumption when quantifying spectra is that the number of electrons recorded is proportional to the number of atoms in a given state; therefore, an atomic percentage is very commonly used for quantification. The intensity of an XPS peak (I_A) strongly depends on: a) the incoming photon flux, b) the concentration of the element on the surface, c) the ionization cross-section (excitation-energy dependent), d) the mean free path of the emitted photoelectron and e) further instrumental parameters (detection

efficiency). Figure 17 illustrates an example XPS spectrum measured from an ITC-silanized sample on a silica wafer sample done in this dissertation. The inset tile within Figure 17 shows the range of energies associated with the bands typical for C 1s photo electrons. It can be shown by peak model fitting that the spectrum describes three different carbons, labeled with scan A (C-C), scan B (C-O, C-N) and scan C (-N=C=S) which have different chemical environments. The degree of correlation between the peaks in the model influences the accuracy of the peak area computation.

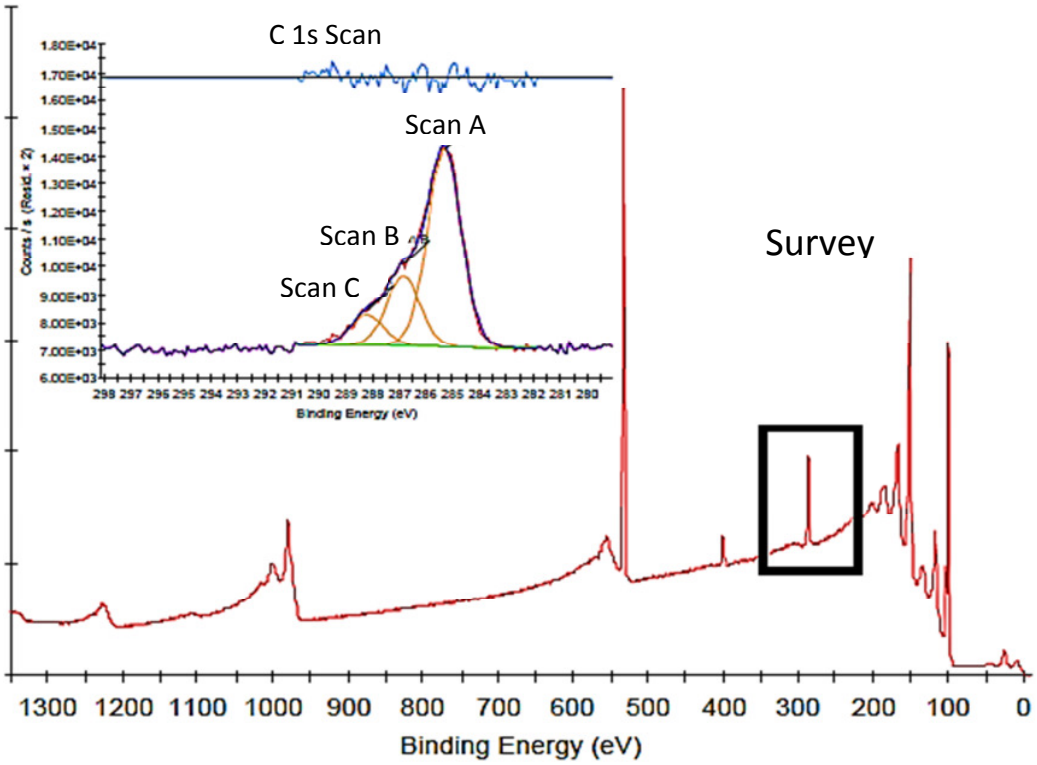

Figure 17.- An example of a typical XPS survey spectrum taken from a ITC silanized sample. inset tile shows the range of energies associated with the bands typical for C 1s photo electrons: scan A (C-C), scan B (C-O, C-N) and scan C (-N=C=S) respectively.

X-ray photon spectroscopy (XPS) measurements were performed using a K-Alpha XPS spectrometer (ThermoFisher Scientific, East Grinstead, UK). Data acquisition and processing using the Thermo Advantage software is described elsewhere [274]. All thin films were analyzed using a microfocused, monochromated Al Kα X-ray source (400 µm spot size). The kinetic energy of the electrons was measured by a 180° hemispherical energy analyzer operated in the constant analyzer energy mode (CAE) at 50 eV pass energy for elemental spectra. The K-Alpha charge compensation system was employed during analysis, using electrons of 8 eV energy, and low-energy argon ions to prevent any localized charge build-up. The spectra were fitted with one or more Voigt profiles (BE uncertainty: +0.2eV) and Scofield sensitivity factors were applied for quantification

[275]. All spectra were referenced to the C1s peak of hydrocarbon at 285.0 eV binding energy controlled by means of the well-known photoelectron peaks of metallic Cu, Ag, and Au, respectively.

3.2.3 Fourier Transform Infrared Spectroscopy

Fourier transform infrared spectroscopy (FTIR) is a technique which is used to detect the molecular vibrations excited by infrared radiation at a specific wavelength For a molecule to absorb IR, the vibrations or rotations within a molecule must cause a net change in the dipole moment of the molecule [276].

The infrared region (10-14000 cm^{-1}) of the electromagnetic spectrum is divided into three regions: the near-, mid- and far- infrared. The mid-IR (400-4000 cm^{-1}) is the most common used region for analysis as all molecules possess characteristic absorbance frequencies and primary molecular vibrations in this region [277]. As the beam is passed through a sample, specific wavelengths are absorbed causing the chemical bonds in the material to undergo vibrations such as stretching, and bending. Functional groups present in a molecule tend to absorb IR radiation in a characteristic wavenumber range regardless of other structures in the molecule, and spectral peaks are derived from the absorption of those wavelengths which are responsible for the excitation of the corresponding bond vibration in the molecules. For instance the C=O stretch of a carbonyl group occurs at ~1700 cm^{-1} and small shifts of the bands can be detected depending whether this group is implemented e.g. in ketones, aldehydes and carboxylic acids.

An IR spectrum is measured by calculating the intensity of the IR radiation before and after it passes through a sample and the spectrum is plotted with Y-axis units as absorbance or transmittance and the X- axis as wavenumber units. For quantitative purposes it is necessary to plot the spectrum in absorbance units.

FT-IR absorbance spectra follow Beer‘s law, which relates concentration to absorbance as in Eq. 4

$$A_\lambda = l\,\varepsilon_\lambda\,c \qquad (4)$$

Where A_λ = Absorbance, l = path length, $\mathcal{E}_\lambda$ = absorptivity and c= concentration

The transmittance is not directly proportional to the concentration and is defined by:

$$T = \frac{I_S}{I_r} \qquad (5)$$

Where I_s= intensity of IR beam after passing through the sample and I_r = the intensity of IR beam before passing through the sample, T= transmittance.

Infrared spectroscopy (IR) is a useful technique to analyze which molecules, and eventually determine at which concentrations are present in a sample. This can be done in solid, on a surface, in gas and liquid. The accessibility, speed and reliability of the results, give the infrared spectroscopy an advantage over other spectroscopic techniques [278]. A general scheme of an FT-IR spectrometer is shown in Figure 18. An interference pattern is produced by splitting a beam of light into two paths, bouncing the beams back and recombining them. The different paths may be of different lengths or be composed of different materials to create interference fringes on a back detector. This configuration was first developed by Abraham Michelson and is still one of the most common optical interferometers in use. The moving mirror in the interferometer scans forward and backward in a rapid and continuous way. During the mirror scan, the path length of the IR beam from the beam splitter to the moving mirror changes relative to the path length of the IR beam to the fixed mirror. This path traversal difference for the light beams in the two arms of the interferometer is known as optical path difference (OPD) or optical retardation. When the two parts of the IR beam recombine on the other side of the beam splitter and form an image at the detector the intensity of the composite beam is an interference pattern depending very strongly upon the optical path difference (See Figure 18). The plot of this intensity variation as a function of optical retardation i.e. the intensity registered at the detector as a function of moving mirror position is known as an interferogram.

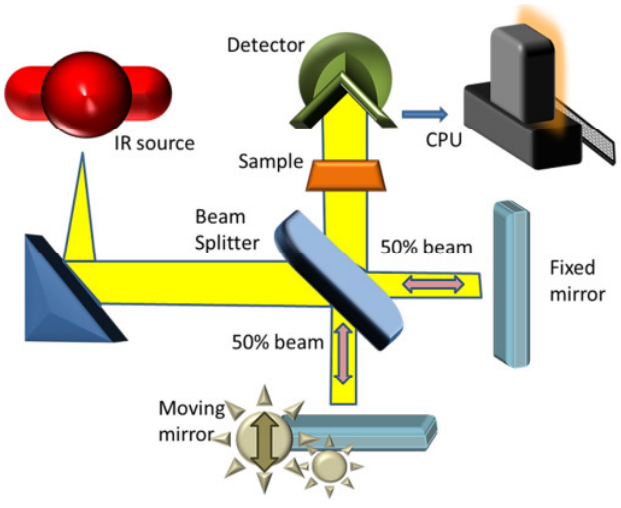

Figure 18.- Michelson interferometer scheme as part of FTIR spectrometer.

First a background spectrum is measured just with the clean support substrate (clean wafer or clean KBr pellet). Then the molecule is placed on the substrate and its single

channel is measured and divided by the background. This results in the absorption bands which belong only to the molecule under investigation. [277, 279-282]

In this work for the characterization of the functional groups in solution as well as on a surface a rapid scan FT-IR spectrometer Tensor 27 (Bruker, Germany) is used. The HeNe laser interferogram is monitored by the FTIR spectrometer at any mirror position during the course of the scan, yielding a plot of intensity versus frequency. This interferogram and the sample interferogram are then Fourier transformed to yield a spectrum of frequency dependent intensity. As this instrument is a single beam spectrometer, a background spectrum should be run first. Normally it is done with the same KBr pellet which will serve afterwards as the support for the substance. The procedure to measure the different liquids in a reproducible way is to place a drop (5µl) of the substance (silanes, ethylchloroformate, solvents, etc.) on its own KBr pellet followed by the recording of the spectra. Then this spectrum is divided by the background and consequently an absorbance spectrum is obtained.

To prove the success of the Kaluza reaction for ITC-silane synthesis, IR spectroscopy was carried out. For that purpose, absorption spectra were recorded in the mid-infrared spectral region monitoring the change in vibrational frequency on the NCS stretch at 2100 cm^{-1} showing a very strong but broad band. Spectra in this region were recorded using a FT-IR spectrometer Tensor 27 from Bruker Optics (Germany). IR spectra were recorded in the frequency range of 400–4000 cm^{-1}, which covers the absorption range of gaseous H_2O and CO_2. The IR radiation source is a Globar^{tm} emitter and the standard IR detector is at room temperature a DTGS (deuterated tri-glycine sulfate) detector. Also for the majority of the experiments potassium bromide (KBr) was chosen for the matrix sample, as it has an increased infrared transparency (ranging from 7500 to 370 cm^{-1}. However, it is highly hygroscopic so measures were taken to ensure the system was not exposed to atmospheric water.

The parameters used in the experiments are shown in the table below:

Table 4.- FTIR Instrumental parameters used in measurements.

Technical Parameters	Value
Laser Wavenumber	15799.4 cm^{-1}
Instrument Type	TENSOR 27
Aperture Setting	6 mm
Result Spectrum	Absorbance
Resolution	4 cm^{-1}

3.2.4 Fourier Transform Raman Spectroscopy

Raman spectroscopy is quite similar to FTIR except Raman can detect vibrational modes corresponding to symmetric stretches that do not cause a change of the dipole moment. Infrared and Raman spectroscopy are used as complementary techniques, because each method looks at different aspects of a given sample. IR-spectroscopy is a method which is sensitive to functional groups and to highly polar bonds and where the absorbed light is measured after a light spectrum passes the sample or is reflected on the sample surface. In contrast to IR, Raman spectroscopy is more sensitive to backbone structures and symmetric bonds, whereby the sample is irradiated with monochromatic laser light and the spectrum of the scattered light is detected. Using both techniques provides more detailed information about the vibrational structure than can be obtained by using either alone [283].There are two types of scattering: elastic (Rayleigh) and inelastic (Raman). The latter occurs when there is an exchange of energy between the incident photon and the molecule [279, 284]. If the molecule gains energy after the irradiation, the transition is referred to as Stokes transitions; if the molecule loses energy, the transition is referred to as anti-Stokes transitions. As shown in the following simplified diagram in Figure 19, a molecule at rest, resides in the ground vibrational and electronic states. The electric field of the laser beam raises the energy of the system for an instant by inducing a vibration in the molecule [285, 286]. The excited state is named a “virtual” state. Relaxation from the virtual state occurs almost instantaneously and is mainly back to the initial ground state. This results in the Rayleigh scattered photon, which has the same wavelength as the exciting one. Relaxation towards the first excited vibrational state of the molecule results in a Stokes-Raman shift [283] and the scattered light is of longer wavelength (lower energy) than that from the laser light. In addition, most systems have also at least a small population of molecules that are initially in an excited vibrational state. When the process initiates from this excited level, relaxation to the ground state is possible, producing scattered light whose energy is higher (has shorter wavelength) than that of the incoming laser. This process is called anti-Stokes Raman scattering [283]. The different scattering processes are summarized schematically in Figure 21.

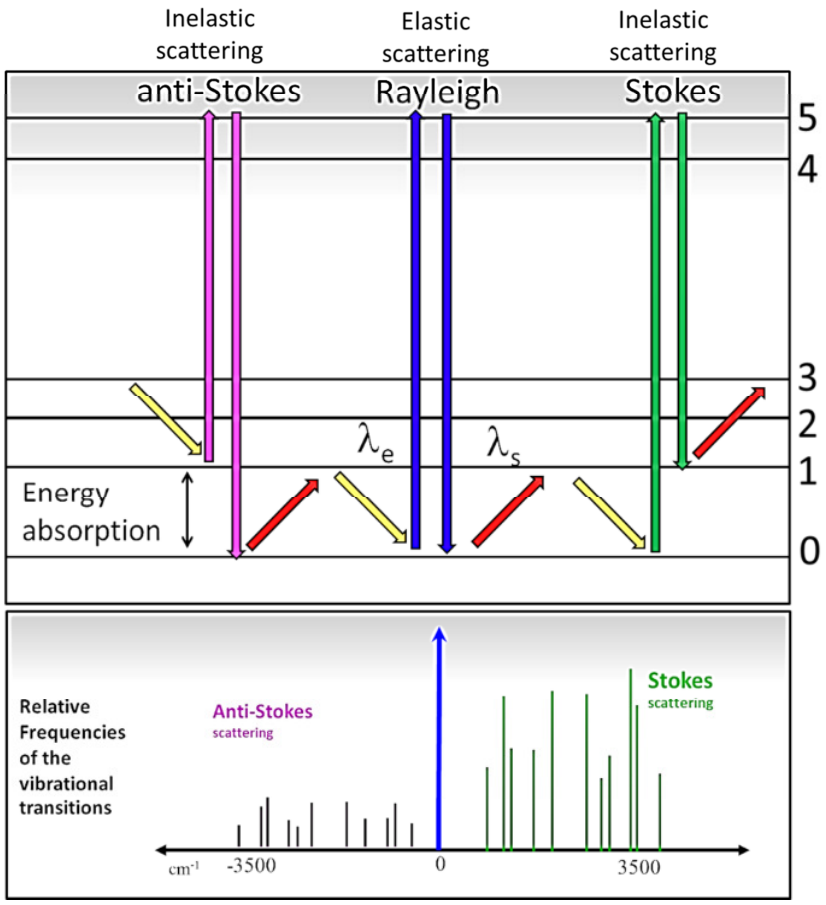

Figure 19.- Simplified energy level diagram of the different scattering processes. The wavelength difference between the excitation light (λ_e) and the scattered one (λ_s) is related to Raman shift ΔV given in wavenumbers according to $\Delta V = 1/\lambda_e + 1/\lambda_s$. If the difference is 0 Rayleigh-scattering occurs.

For the experiments described within this work a Fourier transform (FT)-Raman spectrometer was used. The basic set-up of an FT Raman spectrometer is shown in Figure 20. The detector is usually placed perpendicular to the direction of the incident radiation so as to observe only the scattered light. The setup of the instrument is very similar to that of the FTIR, but instead of the beam to pass through the sample after the interferometer, it does so before it in order to collect the scattered light from the sample through the interferometer. Also a laser source is used instead of an IR source, as the intensity of the Raman scattering is proportional to $1/\lambda^4$, so short excitation laser wavelengths deliver a much stronger Raman signal. In our experiments, a RAM II FT-Raman Module was used. It is an add-on module coupled to a Bruker's vertex 80. The instrument parameters are shown in the following table.

Table 5.- FT-Raman spectrometer instrumental parameters used in measurements

Technical Parameters	Value
Laser Wavenumber	15799.4 cm^{-1}
Instrument Type	Vertex 80
Aperture Setting	6 mm
Detector	LN_2 Germanium
Result Spectrum	Raman scattering
Resolution	4 cm^{-1}

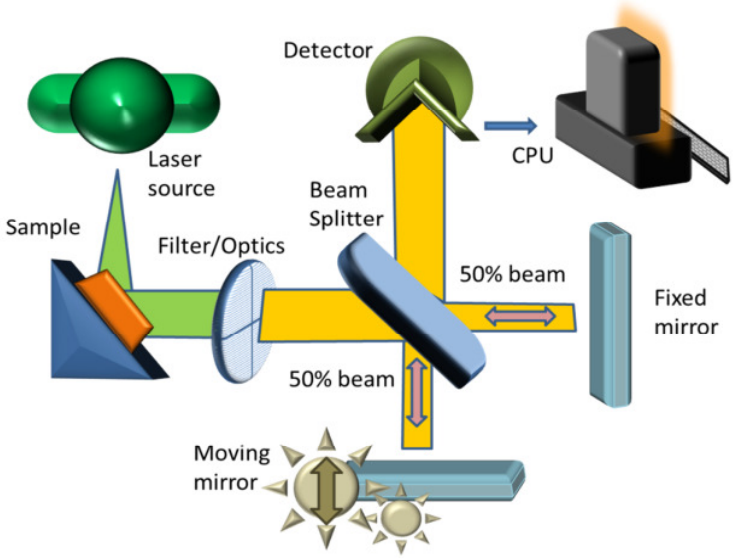

Figure 20.- Michelson interferometer scheme as part of FT-Raman spectrometer. In contrast to IR spectroscopy – first the sample is irradiated by the laser light and it is the scattered light which is coupled into the Micholsen interferometer. This guarantee the colection of the scattered light through the optics/filter and further on the interferometer. The interferogram is then processed to yield an absorbance spectrum at the computer.

3.2.5 Contact Angle

Contact angle is a useful technique to provide firsthand information if the functionalization of the surface has been performed or not, by measuring the spreading of a drop on the surface. The contact angle results from the interaction between different surface and interface tensions (surface free energies) usually between liquid, solid and surrounded by a gas. It is measured according to the Young's equation shown in Figure 21 [287]. The technique is very useful to evaluate the surface energy of a solid substrate, in this dissertation mostly a silicon oxide layer on top of a silicon wafer or glass. Polar solid materials like glass, silica and metals, have large surface free energies and water

droplets should form small contact angles [288, 289]. On the other hand when the solid surface is contaminated with organics or other impurities the angle will increase. Some special operations or procedures are not necessary for the preparation. The contact angle machine is a self-built device using an optical commercially available system with a back light camera, a computer with a dedicated software routine to calculate the angle from the picture taken and a precision needle which delivers the same amount of liquid every time. Physical properties of different interactions between solid and liquid like wettability, affinity, adhesiveness and repellency can be studied [290, 291]. Small contact angles normally mean a better wettability and adhesiveness and a larger free surface energy and vice versa. In our case we use a static drop method which measures the angle after a predefined time on the surface to allow some spreading of the drop while it is been placed on top [291-294].

If a droplet changes its contact angle with time due to any property of the surface even after it has been completely deposited and the needle removed (as in case of polymers or porous materials) then the static drop method might lead to some errors over time. The drop movement on top of a porous layer is caused by an interaction of two processes: i) the spreading of the drop over already saturated (filled with liquid) parts of the porous layer, which results in the growth of the drop base and ii) the embedment of the liquid from the drop into the porous substrate, which results in a reduction of the drop base and an expansion of the wetted region inside the porous layer [295]. Due to the fact that silanes, if they are over polymerized they will create a polymeric porous network (PN) [111, 296] care has to be taken when interpreting the contact angle measurements.

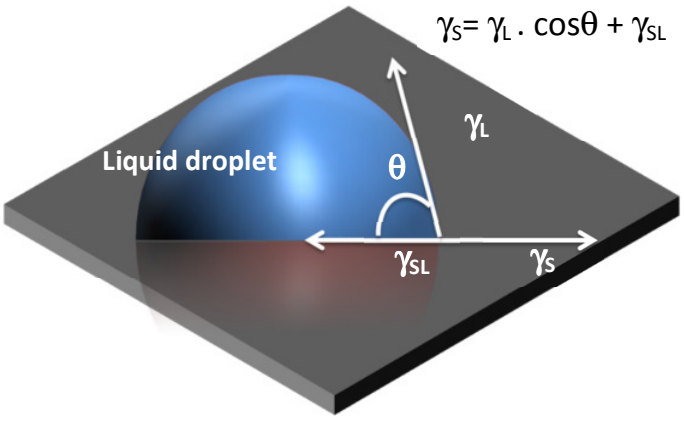

$$\gamma_S = \gamma_L \cdot \cos\theta + \gamma_{SL} \quad \text{[Young's Equation]} \qquad (6)$$

γ_S= Solid surface free energy

γ_L= Liquid surface free energy

γ_L= Solid/Liquid interfacial free energy

θ = Contact angle

Figure 21.- Contact angle scheme showing Young's equation.

4 .- Results and Discussion

4.1 Aldehyde-based Silanization and Immobilization of DNA-linker.

Aldehyde reacts reversibly with amines to form Schiff's base (imine group). In order to obtain sustainable immobilization, imine groups must be reduced into stable secondary amines e.g. by borohydrides treatment. The stabilization deactivates residual unreacted aldehyde groups into alcohol groups that do not cause nonspecific adsorption. Aldehydes are moisture sensitive and are easily oxidized into carboxylic acids [297]. The functionalization of solid supports by aldehyde reactive groups is classically done by three procedures: i) oxidation of alcohol functions [297], ii) oxidation of olefinic groups [298] and iii) modification of aminated surface by glutaraldehyde [299, 300]. In this dissertation the latter method is used for the amino silane conversion into aldehyde functionality. Glutaraldehyde (GA) is an organic compound with the formula $CH_2(CH_2CHO)_2$ and used commonly as a fixation or ligation agent towards proteins or as an amine-reactive homobifunctional crosslinker. Glutaraldehyde was used for the first time at the beginning of the 1960's for tissues fixation, and since it has been developed for many other applications. The high reactivity of glutaraldehyde toward proteins at around neutral pH is based on the presence of several reactive residues in proteins and different molecular forms of glutaraldehyde in solution, producing a variety of reaction mechanisms. GA can react with several functional groups belonging to the proteins, such as amines, thiols, phenols and imidazoles[301] because the most reactive aminoacid side-chains are nucleophiles. Various data on the reactivity (at pH from 2.0 to 11.0) with the following amino acids have been reported in literature already: lysine[302], tyrosine, tryptophane, and phenyl alanine [303], histidine, cysteine, proline, serine, glycine, glycylglycine and arginine[304]. This is important as these authors ranked the ability of different aldehydes to react with aminoacids in this decreasing order: Ɛ-amino, α-amino, guanidinyl, secondary amino, and hydroxyl groups.

For the specific aldehyde functionalization of oxidic surfaces, a common procedure is followed. First the oxidic surface is cleaned and subsequently amino silanized. The amine functionalized surface is then reacted with glutaraldehyde, generating a Schiff base functional aldehyde intermediate. This intermediate is then further reacted with the amino

groups of the DNA-oligonucleotid, generating a bis-Schiff base functional structure. This adduct is very hydrolytically labile, and often must be reduced with sodium cyanoborohydride to generate hydrolytically stable amines. As in this work the use of DNA and further RNA for biofunctionalization is within the main focus, the unspecific interaction with this various groups makes the approach with the aldehyde relatively difficult. The glutaraldehyde additionally reacts reversibly with amino groups over a pH range (>pH 3.0), except between pH 7.0 and 9.0 where only little reversibility is observed [305]. Kawahara et al. [306] reported that most of the studies which accounted for the different polymerization stages of glutaraldehyde neglected possible solvent effects on the glutaraldehyde structure. In fact, water is the medium in which commercial glutaraldehyde is supplied and in which the crosslinking reaction with proteins is carried out, and glutaraldehyde was found to react with this solvent in various ways. Accordingly to their studies, they found that in a dilute solution (1 to 10% v/v) and in the range of pH 3-8, the glutaraldehyde is almost monomeric, predominantly in cyclic hemiacetal form [306]. In summary, several studies [301, 307-314] have shown that commercially available glutaraldehyde represents multicomponent mixtures, but knowing which of these components is the most efficient for reactions with proteins is debatable. In fact, in aqueous solution, glutaraldehyde can exist in its simplest form, a monomeric dialdehyde, but also as a dimer, trimer, and polymer. Therefore, the effectiveness of glutaraldehyde immobilization and the controversies surrounding its chemical behavior could be rationalized with the multiplicity of structures, which depends on the solution conditions. Figure 22 shows two different reaction paths of (polymeric) glutaraldehyde resulting in the formation of a Schiff base (path 1) or – according to the Michael-type reaction - a secondary amine (path 2).

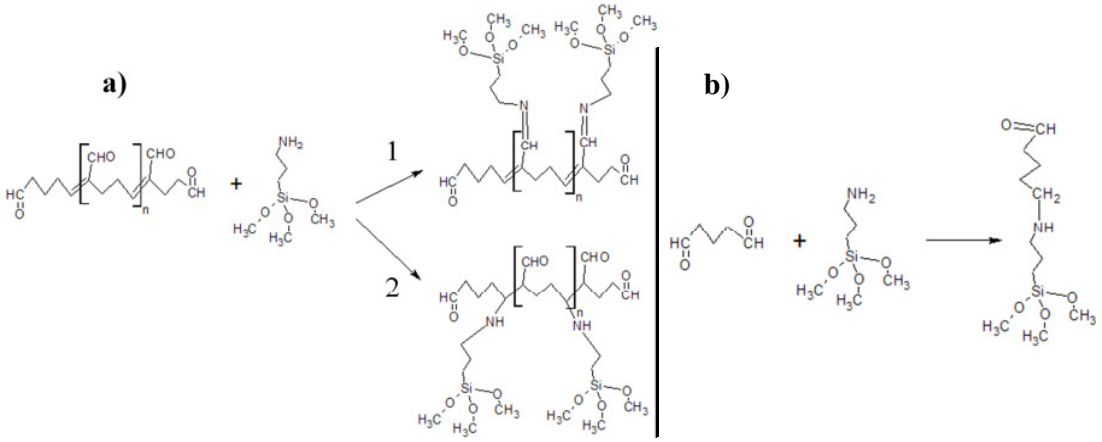

Figure 22.- a) Schiff base (1) and Michael-type (2) reactions of glutaraldehyde (partially polymerized) with amino silane. b) idealized reaction on the surface.

The aldehyde biofunctionality was performed by transforming an already silanized sample with 3-aminopropyl trimethoxysilane into an aldehyde group. This reaction takes place when samples are incubated in glutaraldehyde solution in water (1% v/v) at room temperature for 40 minutes and then dried under a nitrogen stream.

Suitable surfaces were generated by coating Si-wafers with aminopropyltriethoxysilane, the amino functions of which were reacted with glutardialdehyde [137]. In this sense, as the previously discussed topic on the multiple mechanisms and conformations that the glutaraldehyde can take, AFM, fluorescence essays and XPS measurements were performed on an aminosilanized substrate and after the treatment with the GA.

An idealized process of the preparation of the surface and reactions mechanisms are explained in

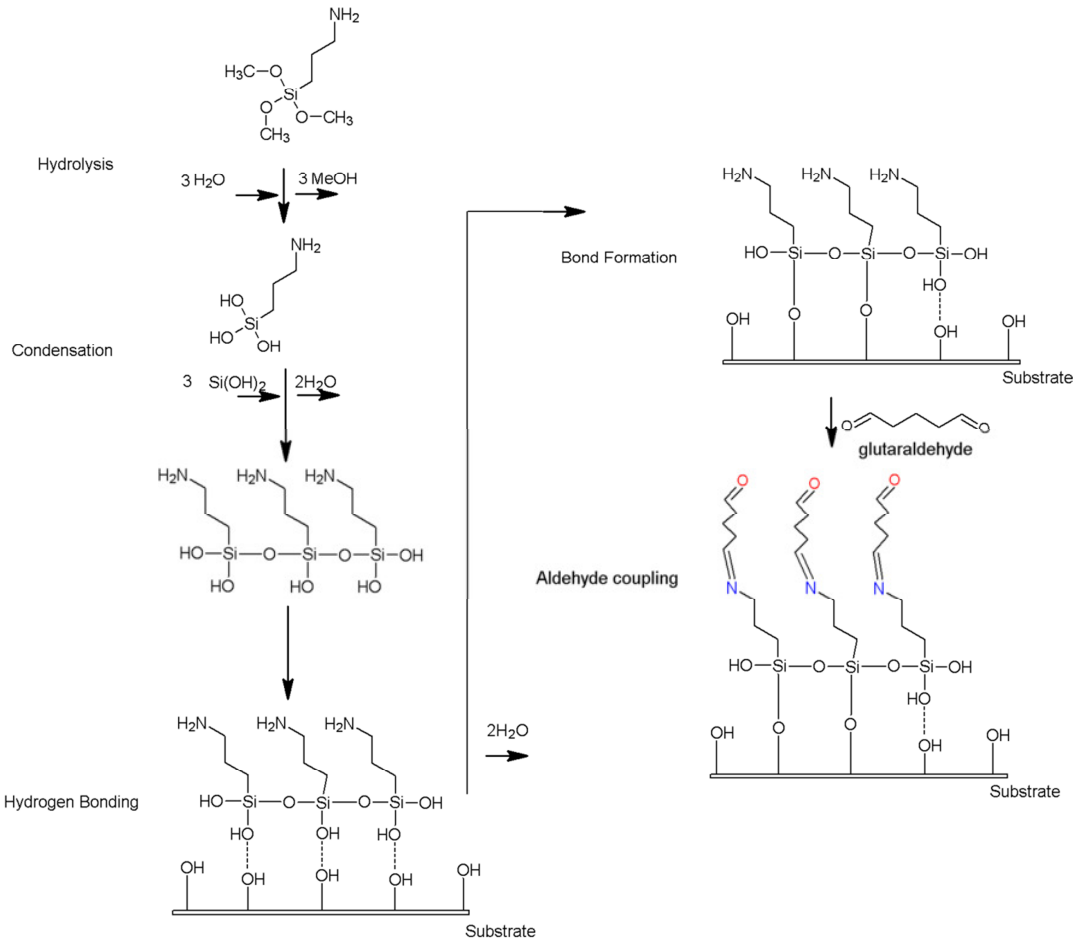

Figure 23.- Mechanism of aldehyde functionalization of surfaces. The pathways follows the same reaction mechanism as the silanes but in addition a final incubation in glutaraldehyde is performed. the final product is a idealized monolayer formation which leaves the aldehyde groups also free to further covalent attachement of another molecule carrying an amino functionality.

4.1.1 Characterization of Physical and Chemical Properties of Aldehyde-terminated Surfaces.

In this section different characterization techniques of amino-terminated samples after silanization and further reaction with GA are described and discussed. The sample preparation and characterization has been carried out in the following way: silica wafers and glass slides were cleaned, amino silanized and aldehyde incubated. AFM was used to characterize the influence of the chemical treatment on the morphology and roughness of the functionalized substrate. As the native roughness of the glass might influence the results, silica wafers with a roughness of less than 0.5 nm over a 25 μm^2 area were used as substrates. As XPS was used to investigate the elementary composition of the surface, silica wafers were used as substrate material, because in this case Si or SiO_2 will be the only material which will be detected as a background, while in the case of glass a huge number of other elements will be detected additionally. For the investigation of the influence of the aldehyde coupling on amino-terminated oxidic surfaces on the wettability and reactivity, amino-functionalized glass slides before and after the incubation in the aldehyde solution were characterized by contact angle and fluorescence microscopy, respectively. In all the cases, the same sample was used for the evaluation of every step to avoid any further experimental error to be added to the measurements.

The goal is to provide a chemical functionality on an oxidic substrate which can react with functional groups of biomolecules, such as peptides, oligonucleotides or DNA fragments.

4.1.1.1 Morphology and Roughness

As there are no visually noticeable changes in the surface once the silanization and further incubation of the sample in glutaraldehyde are performed, AFM morphology investigations were carried out. The results are summarized in Table 5 and Figure 24.

Changes in surface roughness monitored by the AFM can be correlated to the chemical changes of the sample surface. An increase in surface roughness appears when going from a completely clean (Figure 24a) to a glutaraldehyde functionalized surface (Figure 24c). The corresponding AFM images show no visible features after the amino silanization step (Figure 24b), but the surface root mean square roughness results obtained from the AFM images during this period reveal a small roughness increase, indicating that the surface

morphology was changed. The values of roughness after the aldehyde coupling change significantly compared to that of the amino functionalized surface (Table 6). Possible explanations are: the water incubation promotes silane motility and further molecules are condensed on the surface. Furthermore it could be attributed to the polymerization reactions taking place in an aqueous solution due to the glutaraldehyde [303].

Table 6.- Roughness data for the clean and after aldehyde silanization substrates.

Roughness Data	Clean	Amino silanized	Aldehyde incubated
Parameter	Full Image Values	Full Image Values	Full Image Values
RMS:	**228 pm**	**423 pm**	**3.02 nm**
Average Deviation:	177 pm	94 pm	376 pm

Sample roughness monitored by the AFM appears to follow qualitatively the chemical changes, reasonably well for the stepwise reaction.

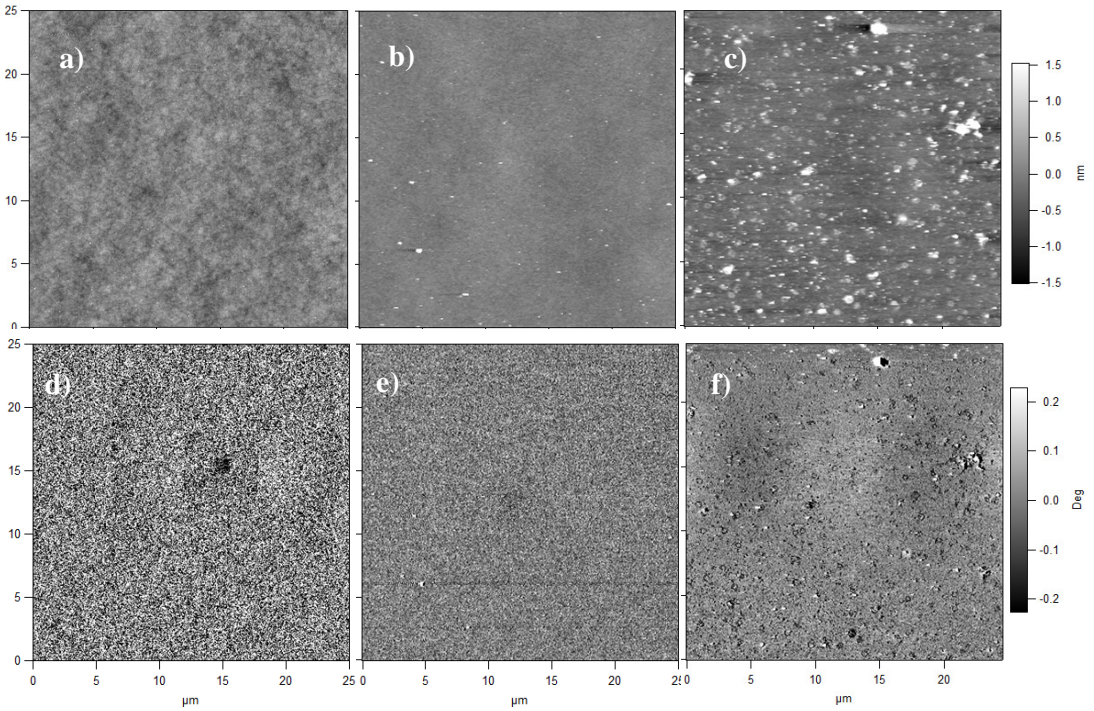

Figure 24.- AFM topography (upper row) and phase (lower row) images from a) clean wafer, b) amino functionalized wafer and c) aldehyde coupled wafer. Phase images from d) clean, e)amino and f) aldehyde functionalized substrastes are shown.

4.1.1.2 Wettability

The wettability of each functionalized surface was determined by contact angle measurement at the same sample before and after coupling of the aldehyde. A lower water contact angle indicates a more hydrophilic and polar material surface. The contact angle was calculated by averaging the contact angles of three drops positioned along the longitudinal axis, whereby the drops were placed side by side as shown in the sketch of Figure 25. The measured value is plotted as a function of the drop position along the slide (as shown in Figure 25). These measurements can be considered also as an indirect measurement of the homogeneity of the coating.

The average contact angle measured over the aminosilanized substrate was 62 ± 6°. The uncertainty of the values has been calculated taking into account the instrumental error of the device. After the coupling of aldehyde to the amino-terminated surface, the final contact angle measured was 68 ± 7°.

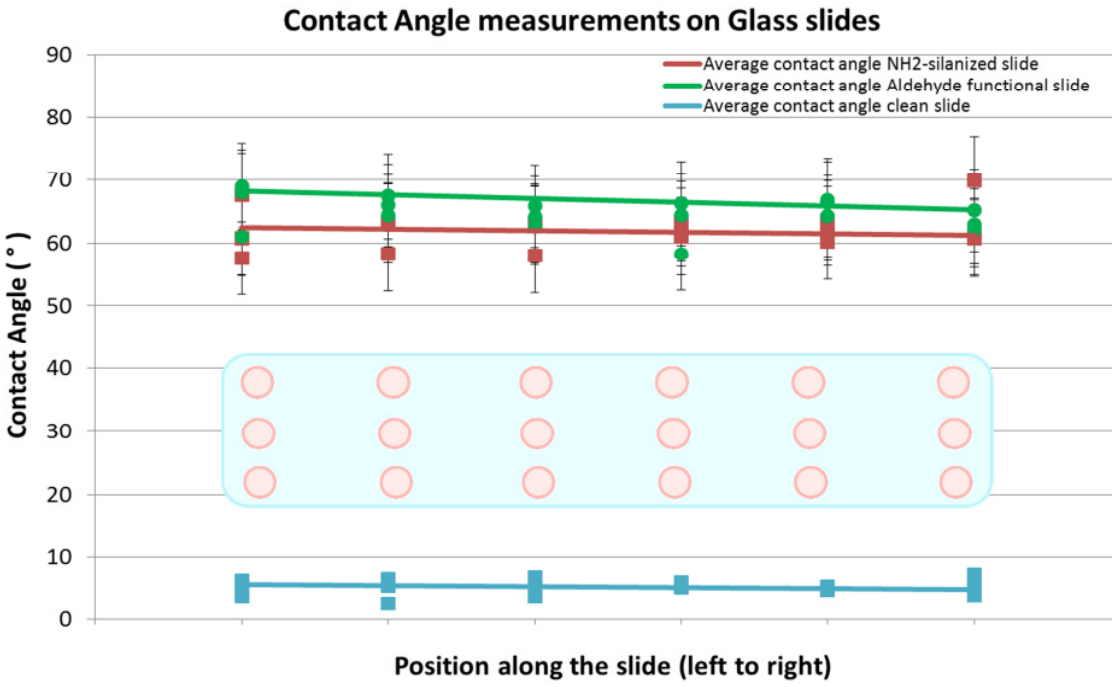

Figure 25.- Contact angle measurements on a set of amino/aldehyde silanized slides. The measurements were done on the same slides before and after each step (aminosilanization and further aldehyde conversion). The dots represent the position of the drop for the assessment.

In literature values of 54±0.5 ° are mentioned for amino silanized glass used in DNA microarray essays [315]. In the same study, the silanized glass was converted using the same technique (*via* glutaraldehyde coupling) into an aldehyde terminated substrate and again, the contact angle measured after the transformation is 50.5±2 ° [315]. In our case,

the small increase in the contact angle from the aldehyde silane (from 62±6° to 68±7°), might be due to polymerization reactions of both the silane and the glutaraldehyde, which was explained in the section before [303, 316].

4.1.1.3 Elementary Composition

The elementary characterization of the sample surface is performed using X-ray photoelectron spectroscopy (i) before and after the amino silanization and (ii) after the coupling of the glutaraldehyde to the amino-terminated substrate to prove the success of the corresponding surface reaction. The measurements on the clean silicon wafer showed no carbon and no nitrogen. After the silanization a sharp increase in the carbon signal and a mild increase in the nitrogen signal could be observed (this can be seen in the survey spectra on Figure 26). The spectra have been normalized and referenced to the 285.0 eV binding energy of C 1s spectrum of the amino functionalized substrate. It can be seen the clean substrate shows no traces of carbon or nitrogen, thus allowing the proper evaluation of the sample after each step.

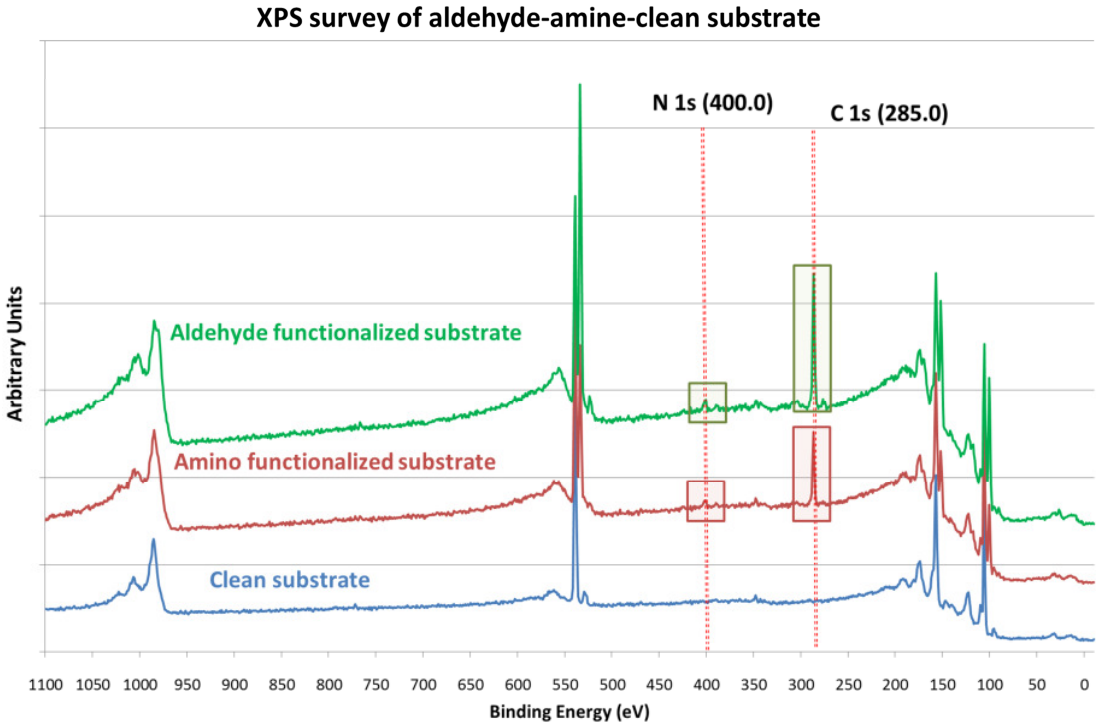

Figure 26.- XPS survey spectra from the sample in three stages (clean, amino functionalized and finally aldehyde functionalized). The sample was the same along the process on the same sample.

Carbon 1s scans showed mainly three energies accordingly to the fitted curves. This curves can be assigned to the carbons of a C-C (~285 eV), of a O=C-O (~289.5 eV) and of a -C-N bond (~288 eV). As shown in Table 7, a very small increase in the carbon content is observed after the glutaraldehyde reaction. This can be the result of a less effective and incomplete reaction of the amino groups of the substrate surface with the GA or due to a reversible reaction of the Schiff base back to the educts (see Figure 27).

As it was discussed previously, the glutaraldehyde can produce reversible reactions whenever the pH is above pH 3.0. In this case, the reversibility would be responsible for a shift of the relative position of the N 1s peaks along the energy scale due to different electronic stages of the nitrogen in the amine and the Schiff base. Based on the literature published we assume that the conversion into the Schiff base is very likely to happen. When the aldehyde coupling was performed, the peaks showed a very small widening in the area below the spectra. This might be due to the change in the electronic environment of the carbon 1s and nitrogen 1s. As the spectrum for oxygen 1s measured could also be a combination from the oxygen belonging to the substrate and the oxygen belonging to the silane, any change will not be considered. Even if there would be a complete monolayer formation which accounts for only a few nanometers, the XPS is able to measure up to 10 nm through the substrate's surface and it is possible that this oxygen peaks are mostly due to the silicon oxide substrate.

In Table 7 the values from the XPS examination are presented. It is noticeable in this sense the proportional increase of the areas due to the widening of the peaks. While the signal remains mostly in the same position, a proportional change in N 1s (deconvoluted areas) also as it can be seen in the Figure 27c-d, shows the change in the electronic binding energy from the nitrogen oxidized (402.4).

Table 7.- XPS results on a aminofunctionalized silica wafer and on a parallel sample which underwent on the Glutaraldehyde coupling (-CHO). The peak evaluation has been performed refered to the Carbon 1s at 285.0 eV.

Scan	Peak BE (eV)		Area (N)	
	$-NH_2$	-CHO	$-NH_2$	-CHO
C 1s Scan A	285.0	285.0	156479	24672
C 1s Scan B	286.2	286.5	15235	4107
C 1s Scan C	287.8	288.1	1186	1537
N 1s Scan A	400.0	400.1	26985	13965
N 1s Scan B	402.4	401.7	5385	9130
O 1s Scan	533.2	533.1	304403	323670

In the Figure 27, Carbon 1s and Nitrogen 1s spectra of the aldehyde converted amino silane are shown. The appearance of a second species in the nitrogen spectrum, with energy level and intensity found similarly in both samples might indicate a relative oxidation of the silane previous the glutaraldehyde coupling. The relatively proportional increase in the second area peak from the nitrogen, points toward a more oxidative state than before, which might be due to the glutaraldehyde coupling. It has to be pointed out that the measurements are in no manner quantitative.

The shape of the fitted curves remained similar before and after aldehyde coupling and a very small change in intensities could be picked up from the experiment. This might hint toward a lower condensation and polymerization of the silane on the surface after the glutaraldehyde reaction.

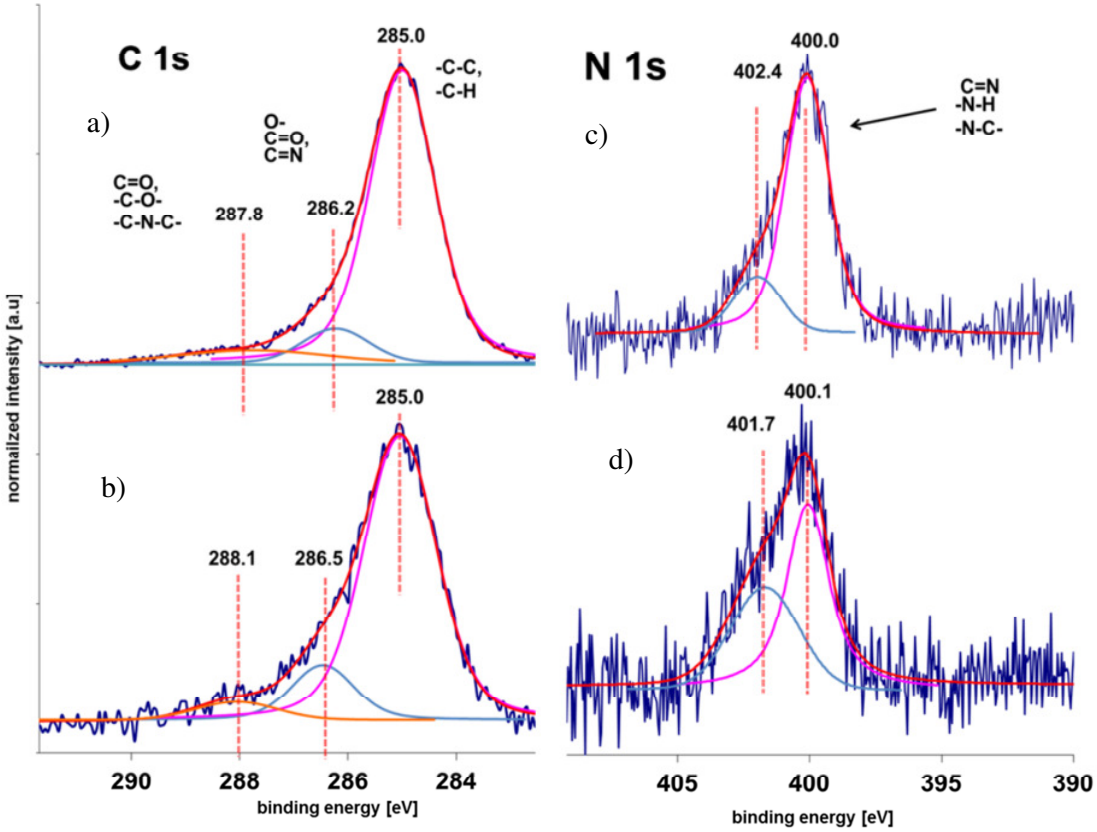

Figure 27.- XPS spectra on amino (a and c) and subsequently aldehyde (b and d) functionalized silica wafer. a) and b) belongs to carbon 1s binding energy while c) and d) belongs to nitrogen 1s binding energy.

4.1.1.4 Chemical Functionality

Aldehydes can undergo a variety of reactions leading towards many different products. The most common reactions are nucleophilic addition reactions which lead in turn to the formation of alcohols, alkenes, diols, cyanohydrins and imines to mention some representative examples. Due to differences in electronegativities, the carbonyl group is polarized [317]. The carbon atom has a partial positive charge, and the oxygen atom has a partially negative charge. This makes the aldehyde more reactive toward nucleophilic substitutions and as the hydrogen is attached also to the carbon, less steric hindrance affects the reactions taking place. Ammonia and primary amines react with the carbonyl group of the aldehydes to give an imine, often referred to as a Schiff base. The imines are usually unstable unless the C=N group is part of an extended system of conjugation (e.g rhodopsin) [318]. The mechanism follows four steps: i) an unshared pair of electrons on the nitrogen of the primary amine is attracted to the partial-positive carbon of the carbonyl group (R-CHO), ii) then a proton is transferred from the nitrogen to the oxygen, iii) the hydroxyl group is protonated, which iv) easily liberates a water molecule and finally a proton from the positively charged nitrogen is transferred to the water molecule, leading to the imine formation [319].

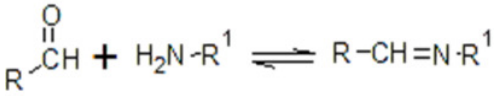

This acid catalyzed process is explained in more detail in the following set of chemical equations.

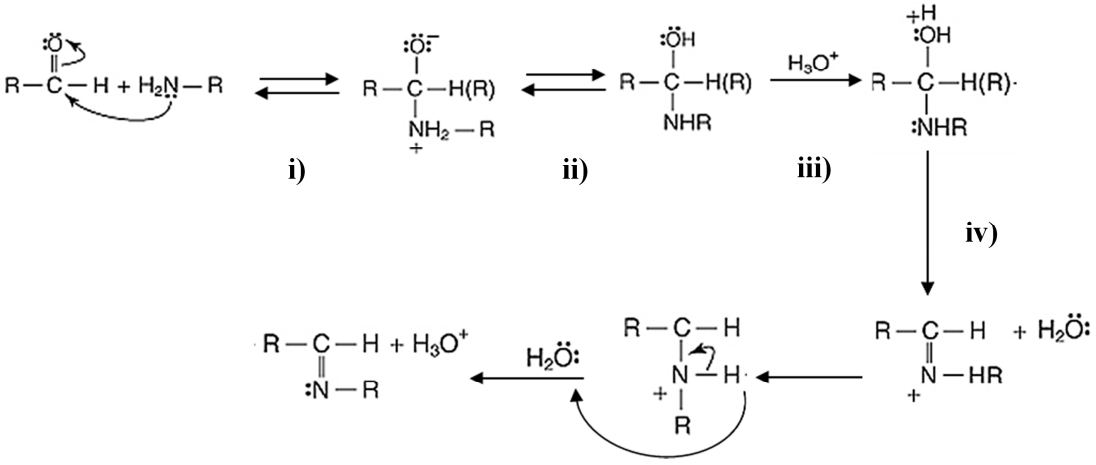

In this section the functionality of the substrate before and after the aldehyde coupling is tested using an amino terminated fluorescent oligonucleotide (DNA single strand). Here it should be mentioned that "functionality" in this context means the relative amount of

target molecules bound to a defined surface area. The substrates are prepared following section 3.1.1.2 protocols for the silanization of glass slides and silica wafers. In this case, the silanization takes place on glass slides as the fluorescence probe is more easily readable using a conventional microarray scanner (GenePix 4000B, Molecular Devices, Germany), able to resolve up to 5 µm/pixel. The samples are manually spotted using drops with 2 µl volume. The spotting solution is prepared using a DNA-fluorescent probe diluted 1:10 in a tris-HCL-buffer (7.0 pH) and 1% di-isopropylethylamine (DIPEA). The samples are spotted sequentially and incubated for 18 hours within a humid chamber to avoid drying of the droplets.

Two samples are prepared simultaneously in the same solution containing NH_2 silane. In addition two clean samples containing no functionality were used as control samples.

The evaluation of the fluorescence is done using the native software from the microarray scanner (GenePix Pro 4.0). Ideally the DNA-linker will covalently react with the surface within the specified time of incubation of 18 hours. This time is exactly the same for the incubation using the other silanes. With this it can be assumed that the fluorescence intensity, while maintaining the same conditions and the same procedures along the different glass slides, will be in direct relationship with the amount of fluorescent oligonucleotide covalently bounded on the surface. The spotting results showed that in average an increased fluorescence was noticeable along the slide containing the aldehyde modified head group silane compared to the amino-terminated substrate. Unfortunately the immobilization of oligonucleotides around the spotted areas during the rinsing step could not be avoided in case of the aldehyde terminated substrate due to the high affinity of those molecules to the substrate (Figure 28, green labeled sample). Nevertheless, the mean values for each row is taken and plotted along with the standard deviation (see Figure 28). The rinsing is done with abundant water and without use of any other buffer systems. After this rinsing, in the case of the aldehyde functionalized slide, the fluorescence in the center of the contact areas of the drops is significantly lower than that of the area around the center. This might be because of the instability of the newly formed Schiff based, which can be hydrolyzed and break apart the imine bond of the DNA-oligonucleotide. Further assessment of the reactivity of the surface will be performed using biomolecules and bottom-up self-assembled viruses.

A very weak interaction could be found between the fluorescent probe and the non-functionalized spotted surface. The values were considerably lower than those from the amino terminated silane.

Amino terminated substrates are also very useful for the non-covalent attachment of oligonucleotides [320]. Aminosilane coated slides have a high concentration of primary amino groups available at the surface. These groups become protonated and therefore positively charged when placed in contact with a near-neutral, aqueous solution. Negatively charged probe molecules, such as DNA, will initially form multiple ionic interactions with the positively charged amino surface coating. In this case no additional amino-modifications of the nucleic acids are required, After spotting, the probes are covalently linked to the slide surface by either heating, or a brief exposure to ultraviolet (UV) light [319, 321, 322].

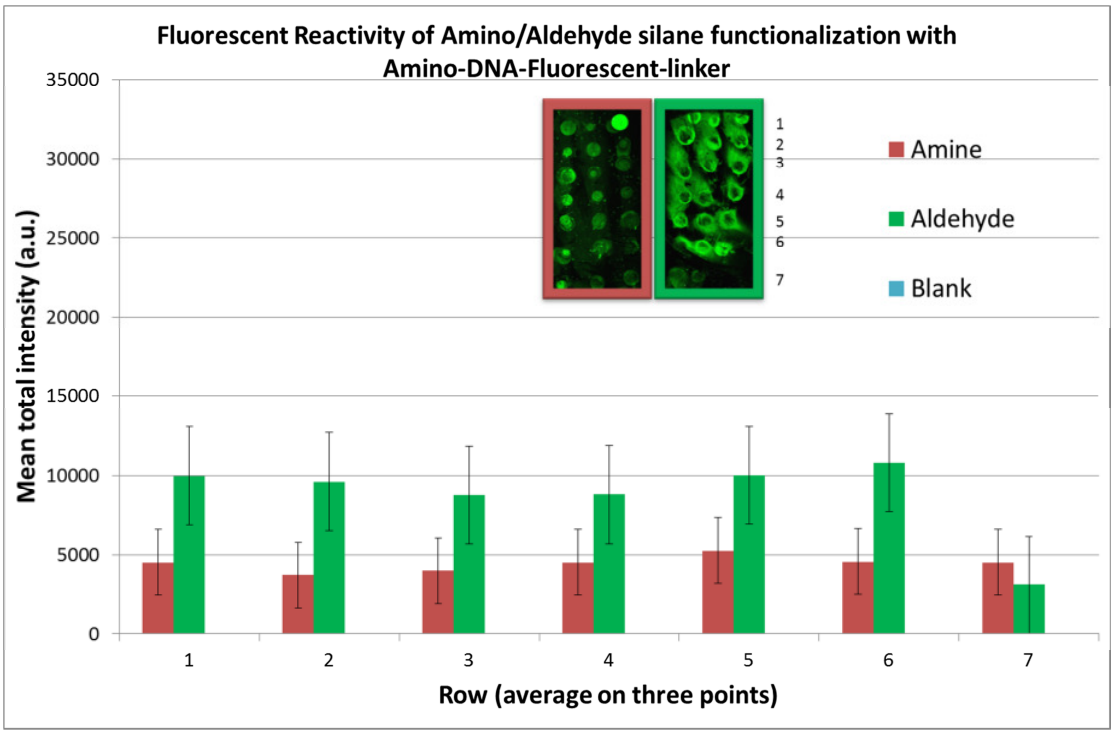

Figure 28.- Fluorescent reactivity assessment of amino/aldehyde terminated glass slides using DNA-amino terminated oligonucleotide as fluorophore binding molecule.

4.1.2 Application of Aldehyde-Based Silane Chemistry for Bottom-Up Assembly of Self-Assembled Tobacco Mosaic Virus.

4.1.2.1 Homogeneously Coated Oxidic Substrates

Silica wafers were set up for the initiation of RNA-guided viral nanotube self-assembly process. Single stranded (ssDNA) linker molecules ("RNA-anchor") with 3'-terminal amino modification were covalently bound to the aldehyde functionalized areas of the wafers by condensation to Schiff bases (imines), the reaction conditions of which were optimized in the system investigated here. 5'-phosphate residues of the DNA linkers permitted subsequent enzymatic ligation of assembly-triggering single-stranded RNA (ssRNA) strands via their 3'-terminal hydroxyl groups by T4 RNA ligase directly on the Si-wafers. The ssRNA utilized contained the TMV OAs sequence and was derived from in vitro transcription reactions with accordingly cloned and digested plasmid constructs. Its size of 2884 nucleotides was expected to direct the self-assembly of TMV-like nanotubes with a predicted maximum final length of 135 nm [7].

AFM examination was performed on flat surfaces to check if the functionalized substrates were proper for the bottom-up self-assembly of the virus like particles. In Figure 29 it can be seen that the self-assembly of the TMV derivatives are successful after the substrates undergoes the whole preparation procedure according to chapter 3.

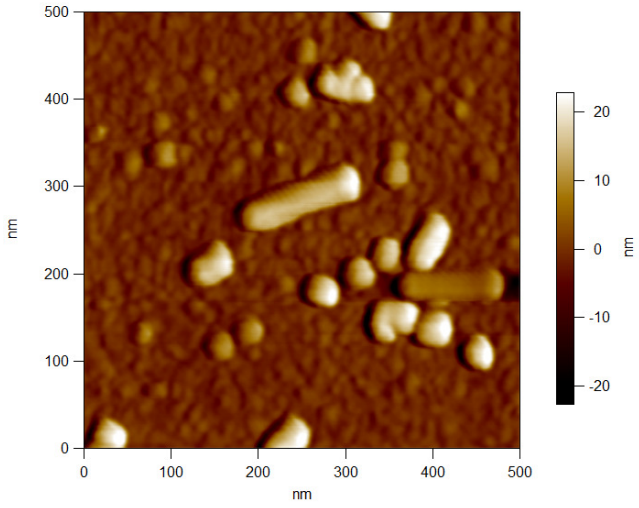

Figure 29.- AFM topographic images of TMV like particles self-assembled *via* RNA ligation on the surface after the whole process of surface functionalization was carried out.

4.1.2.2 Chemically Patterned SAMs on Oxidic Substrates

In order to achieve spatially selective biotemplate growth, pre-structured surfaces allowing site-specific binding of the DNA linkers were prepared. To this goal, Si wafers were patterned by polymer blend lithography [323-325] prior to the chemical functionalization. The technique is suitable to create chemical surface textures of highly different dimensions and shapes. Parameters influencing the morphology of the resulting patterns have been discussed elaborately [90, 326] and include the choice of solvents, polymer concentration, substrate coating speed, and humidity of the atmosphere. Polymer blend lithography can be used with almost any substrate sizes ranging from millimeters to meters and thus makes up a method of choice also for the high-throughput production of large-area array devices to be equipped with nanoscaled functions.

An alternative strategy toward patterned substrates selectively functionalized with aldehyde, started with homogeneous wet-route amino silanization of cleaned Si wafer pieces. The silanized surfaces were then patterned by coating a 1:1 (PS/PMMA) polymer blend onto the aminopropyltriethoxysilane film (experimental conditions as before). Treatment with cyclohexane for 10 min in an ultrasonic bath developed the desired PMMA masks. The Si wafer pieces structured in such a manner were then immersed in a 1% glutardialdehyde solution in water for 30 min. Afterwards the ssDNA linkers were coupled to the aldehyde terminus of the silanized surfaces followed by the ligation of RNA scaffolds, and bottom-up self-assembly experiments.

AFM images of wafers subjected to the CP multimerization step revealed that indeed, rod-like structures of homogeneous diameter had been assembled in the aldehyde-functionalized areas of the homogeneous as well as of the pre-patterned wafers. According to the AFM data the rod-shaped nanoscopic elements had the expected width, after tip deconvolution, of approximately 20 nm. To ensure assembly competence of the virus-derived building blocks applied to the solid substrates, also non-immobilized RNA was incubated with coat protein in solution under conditions favoring nanotube growth in all experiments. This demonstrates that a two-phase assembly of virus-like particles (VLP) from TMV-derived building blocks is mechanistically and energetically possible, with a guiding RNA's end linked to the solid substrate at predetermined sites of a solid-liquid interface.

The polymer-patterned substrates allowed for a control of spatial selectivity of TMV assebly down to areas in the 100 nm range: TMV-like nanosticks were observed exclusively in the non passivated "holes" (see Figure 30).

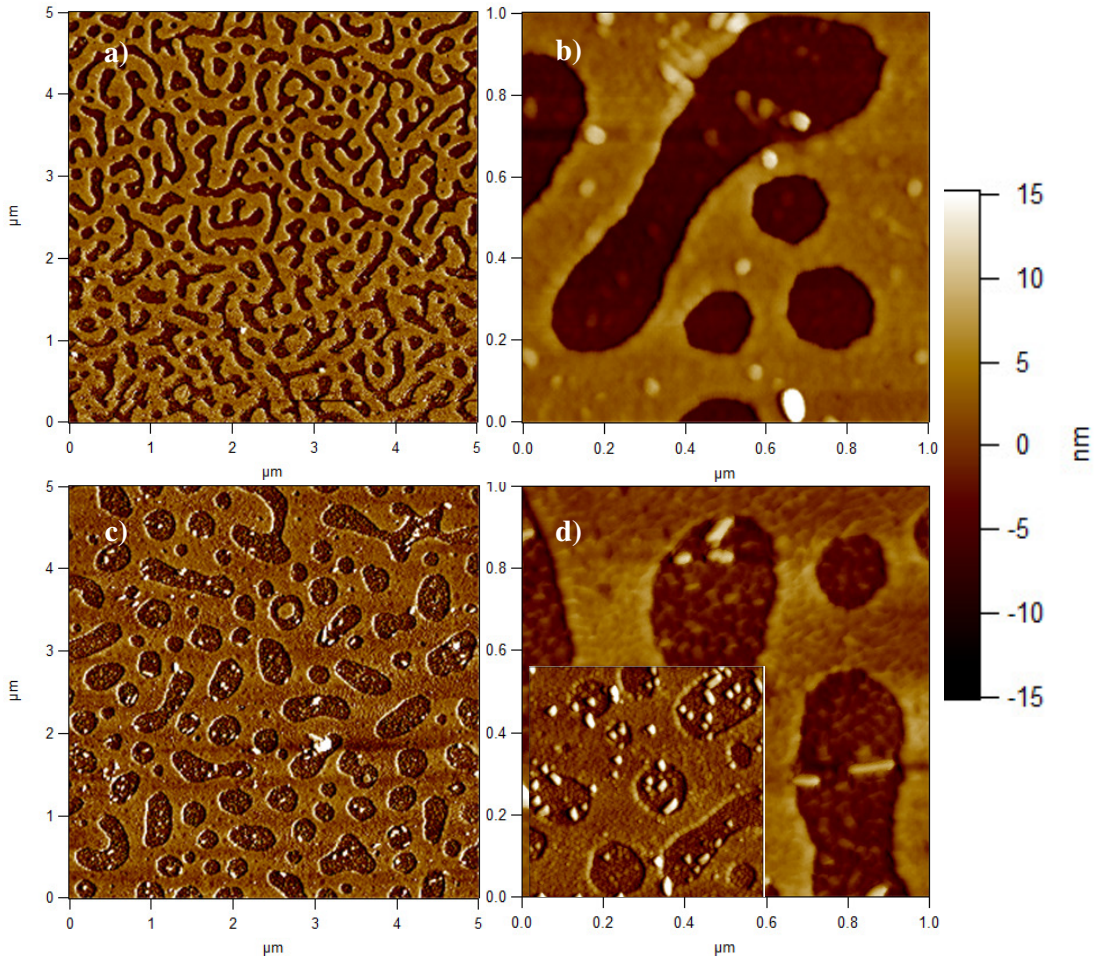

Figure 30.- AFM topography images of different SiO_2 substrates which were prepared identically. All substrates were structured by polymer blend lithography and utilized for bottom-up self-assembly of TMV-like nanotubes. On the top: a,b) polymer blend with the Polystyrene removed and ready for assembly. On the bottom: samples after the silanization, aldehyde reaction and further TMV assembly. Inset a different region of examination on same sample as the bottom.

To allow for direct comparisons, VLPs grown in solution with the same RNA template (scaffolding 135 nm length upon complete encapsidation) were deposited on equally prepared substrates and measured in parallel. For this controls, the substrate was prepared as previously explained, however, no RNA was immobilized on the DNA-functionalized areas, but preassembled VLPs were adsorbed, resulting in a non-specific adhesion all over the substrate without spatial selectivity (see Figure 31a). Further negative experiments were done placing the preassembled virus in solution onto the structured substrate as if they were used for bottom-up assembly (see Figure 31b).

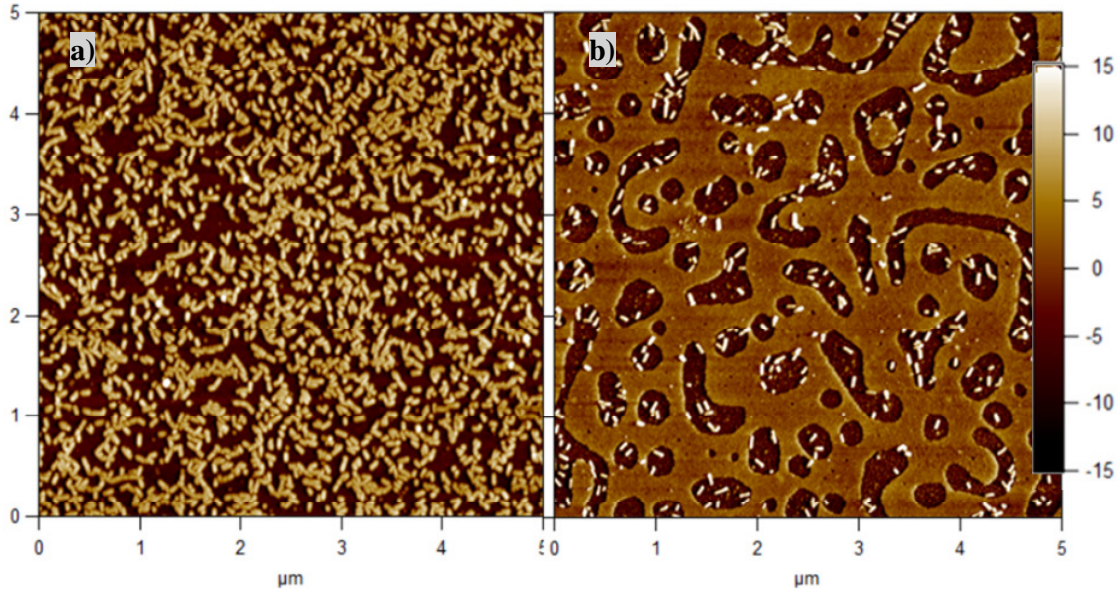

Figure 31.- AFM topography image of TMV-like nanotubes preassembled in solution and later deposited on a) Flat unstructured Si-wafers b) structured wafer with Polymer mask PS-PMMA

To test the deviation of length between bottom-up assembled TMV derivatives and those which were preassebled in solution a statistical comparison is carried out. The final lengths of the rods assembled on solid substrates were determined from AFM images processed to verify flat positioning of analyzed particles (Figure 32) by help of the software ImageJ. The average median apparent length of particles assembled bottom-up on surfaces was 96 nm (±4nm), with 17 % between 115 and 135 nm, which significantly differed from 110 nm (±4nm) determined for rods constituted in solution (Perror <0.0001 delimited by Mann-Whitney rank sum test), with 32 % between 115 and 135 nm, respectively. These deviating length distributions are detailed for one experiment in the Figure 32. In both cases, the VLPs were assembled/deposited on structured Si wafers. The box plot (top middle) shows the different length distributions obtained by the distinct assembly strategies, with median values (black dot), 50% particle populations between second/third quartiles (gray boxes), and lowest/largest values (lines) indicated. The expected maximum particle length of 135 nm, corresponding to the RNA template used, is labeled by the dotted line in the plot. For particle length determination, AFM tip convolution was taken into account.

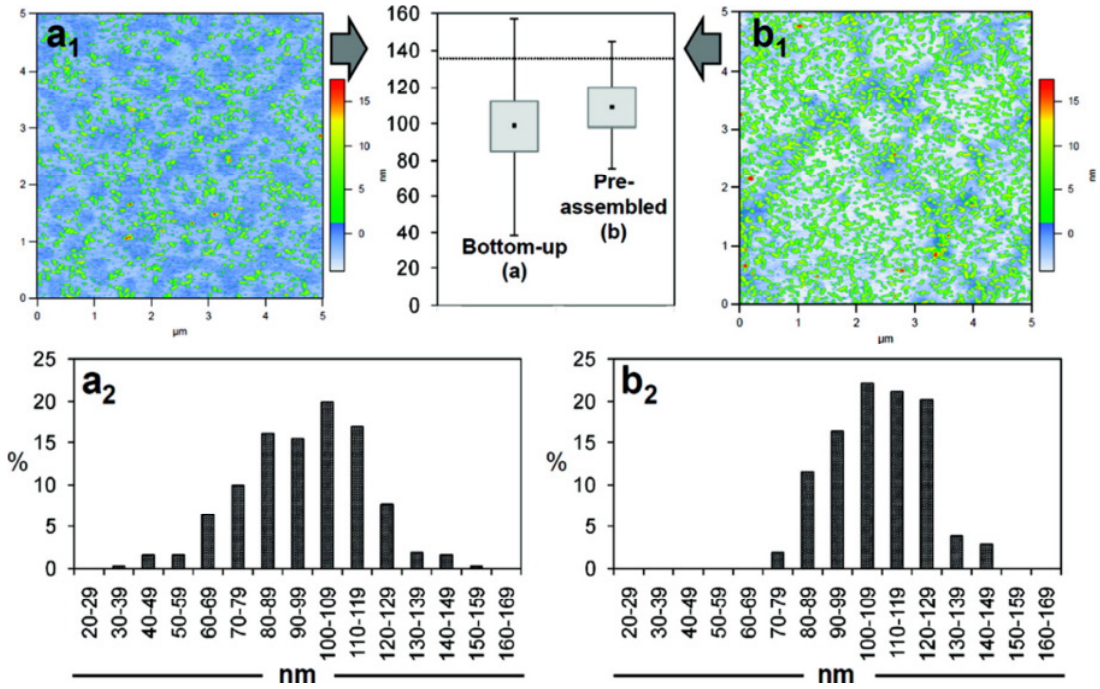

Figure 32.- Comparison of the length distribution of bottom-up assembled TMV-like particles (AFM topography image a1 and histogram a2) with particles preassembled in solution (AFM topography image b1 and histogram b2).

On the other hand, surface coverage with TMV-like particles in no case reached saturation, irrespective of whether grown in situ, or deposited in assembled state (in amounts sufficient to form 16 closed layers) from the same buffer as a control. Alleged molecular reasons encompass limited availability of DNA linker or RNA strands, respectively, as well as physical constraints during the in situ assembly process. The incomplete coverage of wafers even after treatment with preformed TMV-like nanotubes, however, yielded strong evidence for a major contribution of physical limitations on TMV CP enrichment at target sites. Helically assembled as well as mono- or oligomeric protein subunits exhibit a negative net charge under conditions of multimerization [327] and therefore are subject to repulsive electrostatic interactions with surfaces equipped with nucleic acids as well as with adjacent coat protein aggregates. Suci et al. [328] have investigated comparable inter-relationships between differently charged Si and polymer substrates, and Cowpea chlorotic mottle virus (CCMV) icosahedral particles with a pI of 3.8 similar to that of TMV. Their experiments have underscored the pivotal influence of electrostatic interactions on the resulting spatial distribution of viruses, the kinetic adsorption behavior of which could be described well by use of the Langmuir model with limitations found for conditions close to equilibrium [328]. TMV particle densities

obtained in other studies on different surfaces are mostly in agreement with this suggestion: hybridization of partially disassembled virus rods via an exposed 5′ portion of their RNA to oligodesoxynucleotides on solid substrates resulted in arrays quite comparable to those observed on patterned wafers in our study [329, 330] whereas high-density deposition of TMV or M13 phage arrays was achieved by different technologies: planar self-organization into closed films occurred upon diffusion through polyelectrolyte multilayers; [331, 332] densely packed arrays with rod orientation predominantly normal to the surface were generated by metal-to-thiol-linkage of the viral protein coat,[11, 60] a method also applied, for example, to the icosahedral Cowpea mosaic virus CPMV; [333] and by photolithographic lift-off technology [10]. Close to complete coverage with random rod orientation was also possible by microcontact printing [334] and, interestingly, by hybridization of partially "stripped" TMV with their RNA ends to ssDNA probes on chitosan-modified surfaces [335].

Although the whole process will therefore need further optimization, these experiments demonstrate that micropatterned, nucleic acid equipped technical substrates offer a so far unique opportunity for an inducible, kinetically controlled, and site-selective bottom-up growth of true nanostructures.

The DNA-mediated linkage of the assemblies to sites of interest prove to withstand extended washing of the freshly grown nanorods with 60 mL/min flow, corresponding to 2.4 cm/s buffer stream inverting direction three times per second, in all experiments. This harsh treatment exceeded flow rates routinely applied in many lab-on-a-chip microfluidic devices.[336-338] Dried arrays even remained unaffected by flowing water of 25 mL/s for 2 min or streaming 0.1% sodium dodecyl sulfate (SDS) for 30 s, being removed from the wafers only after two min ultrasound exposure at 40 kHz, which completed test series on the robustness of the ensembles. On the other side, a very poor adhesion of the pre-assembled virus particles (assembled *in vitro*) on the substrate was observed when they were just spotted on the surface. After a washing with 10 seconds in an ultrasonic bath the virus are completely washed away. This can be observed in the following AFM images from the same substrate before and after washing with sonification (see Figure 33).

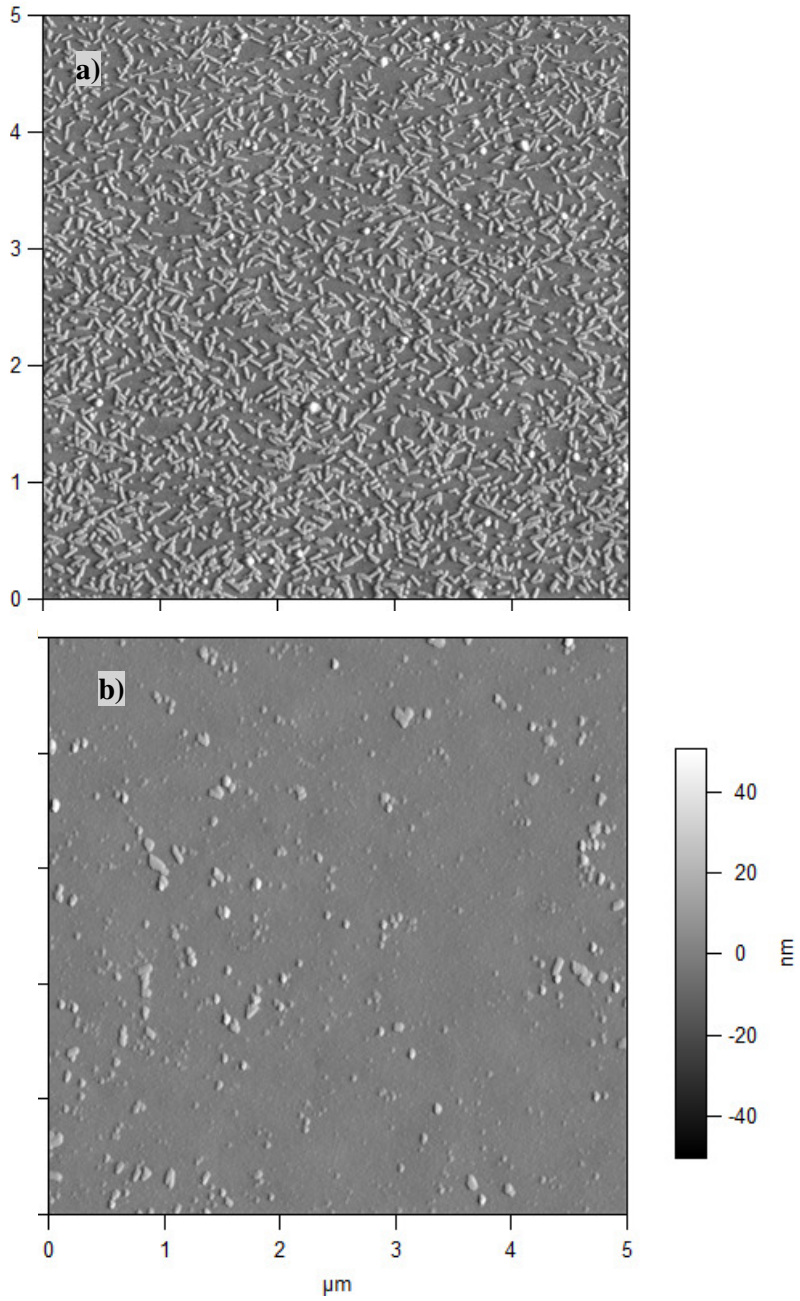

Figure 33.- AFM topographic image of a silica wafer with spotted preassembled virus-like particles on a structured sample. On a) the same sample before and b) after thouroughly clean with use of ultrasound for 2 minutes and 0.1% SDS for 30 seconds.

4.2 Isothiocyanate-based Silanization and Immobilization of DNA-linker.

In this section the isothiocyanate-based silanization of substrates is discussed. The first part, unlike the discussion with the aldehyde chemistry, is focused on the synthesis of the silane in-house. This is due to the special synthesis required for this silane and the lack of commercial availability. Further assessment of the reaction is done using Fourier-transform infrared and Raman spectroscopy. The second section follows the same layout as the previously discussed one, involving aldehyde based silanization. Morphology, wettability, elementary composition and chemical functionality is assessed for the isothiocyanate functionalized substrate after coupling the silane to the silica wafer, the glass substrates and the UV-irradiated polydimethylsiloxane surfaces.

4.2.1 Synthesis and Spectroscopic Characterization of 3-isothiocyanatepropyltrimethoxysilane

An isothiocyanate head-group is employed for further covalent functionalization as its reactions towards amines is basic for the covalent attachment of the DNA-linker onto the surface. Isothiocyanates are defined when the oxygen in the isocyanate family compounds is substituted by a sulfur atom and therefore they can also be defined as esters of isothiocyanic acid. In the general formula R-N=C=S, the group R can be aliphatic, alicyclic, aromatic, acyl, or heterocyclic [339].

Many of this isothiocyanates can be found naturally in plants, commonly known as “mustard oils” [138]. Isothiocyanates (ITC’s) are believed to inhibit carcinogenesis and tumorigenesis and as such are useful chemopreventive agents against the development and proliferation of cancers [340, 341]. Also the ITCs are used worldwide in the determination and quantification of proteins and aminated substances in the form of Fluorescein isothiocyanate (FITC).

Isothiocyanides have been prepared commonly by the reaction of primary amines with thiophosgene [237], by decomposition of thioureas by acids, by the decomposition of dithiocarbamates from primary amines and carbon disulfide in the presence of heavy metal salts [239], by reaction of alkyl and acyl halides with salts of thiocyanic acid [342, 343] and the addition of thiocyanic acid to unsaturated amino containing compounds [344]. To synthesize isothiocyanates in this research, an amino modification by

desulfurization of a dithiocarbamate derivative route was selected not only because it is a safer option (no extremely dangerous components are necessary) but also because this method can reach high yields (above 90% for alkyl silanes) and purities (above 95%) [140, 141].

4.2.1.1 Synthesis Procedures

For the synthesis of the isothiocyanate silane, two procedures have been used. Both progress in the same way until the production of the dithiocarbamate derivative. The difference consists just in the variation of the desulfurizing agent to yield the isothiocyanate functional group on the molecule once the derivative intermediate is reached. In more detail, the first synthesis is described by Kaluza [138] and later by Hodgkins [139-141] who showed that intermediate carbethoxydithiocarbamates, are decomposed into isothiocyanates readily at room temperature by aqueous alkali or by triethylamine in chloroform solution using a desulfurizing agent as ethylchloroformate. In this case the conversion of a 3-aminopropyl trimethoxy silane into a 3-isothiocyanatepropyltrimethoxysilane using the Kaluza reaction is shown in the Figure 34 below:

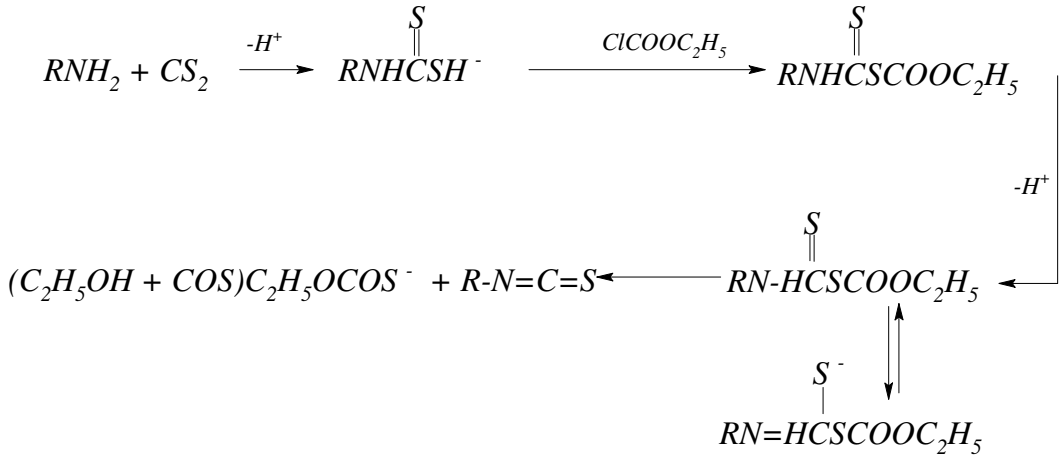

Figure 34.- Kaluza reaction scheme. The primary amine containing molecule is reacted with carbon disulfide in basic medium. The intermediate dithiocarbamate derivative is then desulfurized using ethylchloroformate to yield in basic media an stable form of isothiocyanate group on the previously aminated molecule.

The second method used was a one-pot synthesis which uses the desulfurizing effect of the carbodiimide tautomeric form of the cyanamide to yield the isothiocyanate as described by Yamamoto et al. [249]. The advantage of this method is that a further refining or even any intermediate separation is not necessary (see Figure 35).

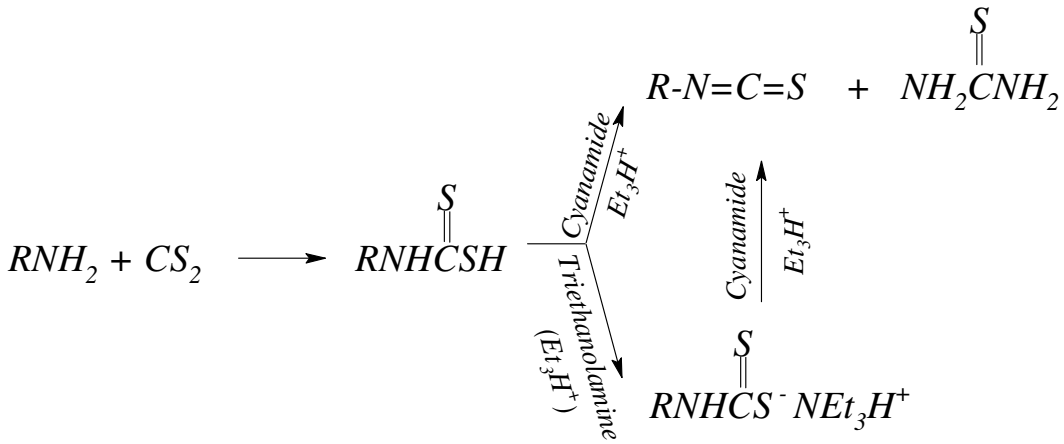

Figure 35.- Modified Kaluza reaction scheme. The reaction proceeds in the same way until the dithiocarbamate is formed. Afterwards, the desulfurizing step is done using cyanamide. This provides with another route of synthesis which does not need a further separation process.

An oily yellowish but clear liquid is obtained when methanol or chloroform is used as matrix solvent. A further purification can be performed, although it is not necessary. The smell is related to mustards oils and sweet. It is soluble in methanol, ethanol, toluene, tetrahydrofurane and dimethylformamide. It possesses a high boiling point at approximately 290° C. Density = 1.02 g/ml and a molecular weight calculated of 263.43 g/mol (data extracted from the custom-made -ABCR,Germany- available 3-isothiocyanate propyl triethoxy silane MSDS).

4.2.1.2 Spectroscopic Characterization using FT-IR and FT-Raman

During the synthesis of isothiocyanate silane, the primary amine used was respectively a commercial 3-aminopropyltrimethoxysilane (APTMS) (Sigma Aldrich, Germany). Using Fourier transform infrared spectroscopy and Fourier transform Raman spectroscopy, a follow up of the reaction yielding the intermediate and a final assessment on the isothiocyanate functional group was performed.

FT-Raman spectroscopy on isothiocyanate silane.

Continuous Raman spectroscopy of the reaction solution was carried out and the presence of carbon disulfide versus time is determined in order to assess the proper times for the reaction to take place, in order to guarantee that the silane used in the further experiments has been converted into the isothiocyanate propyl alkoxysilane successfully. The reactants were introduced in a quartz cuvette and immediately placed inside the spectrometer. The measurement were done without any removal of the contents or

alteration of the reactant vessel, therefore a further normalization was not required as no quantitative follow up was done. The amounts used for the reactions are specified in the Table 1 (chapter 3).

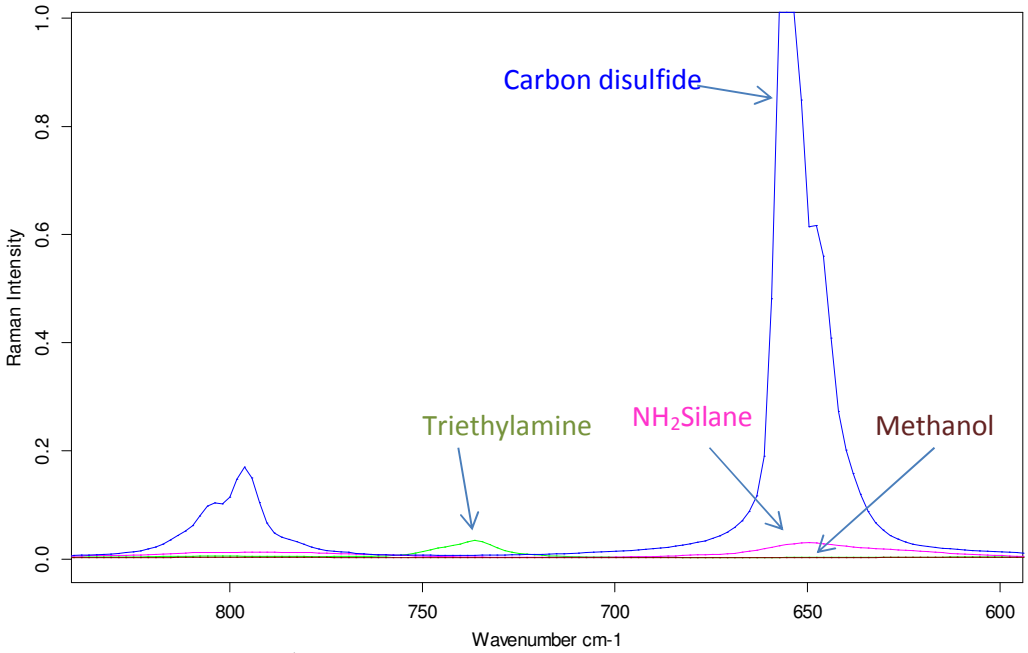

Figure 36.- Raman spectra cm^{-1} of the pure reactants (descriptions and manufacturer in chapter 3). The energy interval is chosen as the influence of the carbon disulfide is maximized in this area and no further influence from the other reactands takes place in this area.

Figure 36 shows the Raman spectra of 3-aminopropyltrimethoxysilane, triethylamine (Et_3N), methanol and carbon disulfide (CS_2). CS_2 is the only reactant which shows Raman bands in the spectral range between 600 cm^{-1} and 700 cm^{-1}. Therefore, carbon disulfide is selected as probe molecule to investigate the progress of the reaction. In Figure 37a, the consumption of CS_2 is plotted versus time, until the concentration of the carbon disulfide remains constant. The carbon disulfide was added in a 10% excess in relation to the amine. During the first 10 minutes the reaction is very fast and consumes approximately 90% of the reactant (CS_2) (calculation based in the initial value of the area beneath the curve when extrapolated to t = 0 in the progression curve Figure 37b). The initial carbon disulfide spectrum for t = 0 is not shown in the graph, (being concentrated as 100 % the intensity is much higher than the scale which is used to show the reaction progress). In the spectra in Figure 37a it can be seen that, for the two silanes (amino and isothiocyanate), as well as for the methanol and triethylamine, there is no band that arise on the 650 cm^{-1} wavenumbers. Following up the conversion reaction, by recording a spectrum of the solution every 7 minutes, the curve in Figure 37b shows after 100

minutes the concentration of carbon disulfide remains almost constant. Qualitatively, the optimal time to leave the carbon disulfide reacting with the primary amine is when the intensity values from the reaction followed reach a plateau point. Therefore the Raman intensity value reaches this stable point after 2 hour. The fast reaction at the beginning in the first 10 minutes ensures a high conversion from the amine to the dithiocarbamate salt without a further reaction between the remaining dithiocarbamate and the amino terminated silane.

Assuming the 100% of CS_2 is available for the reaction in the cuvette, it is necessary at least 100 minutes to reach a equilibria point as discussed before. The amino terminated silane is still reacting towards the dithiocarbamate but with a much slower rate. From literature, it is possible to achieve a high degree of conversion, above 90% of the primary aliphatic amine to isothiocyanate and above 70% when converting amino terminated aromatic compounds [141, 239, 249, 339, 345]. For the calculation of the follow up curve, the area below the curve was taken into consideration. The limits for the integrals were fixed between 630 and 660 cm^{-1} for all the curves. At the beginning it can be seen that the reaction progress at a linear speed, until after 40 minutes it has reached already a nonlinear decelerating rate.

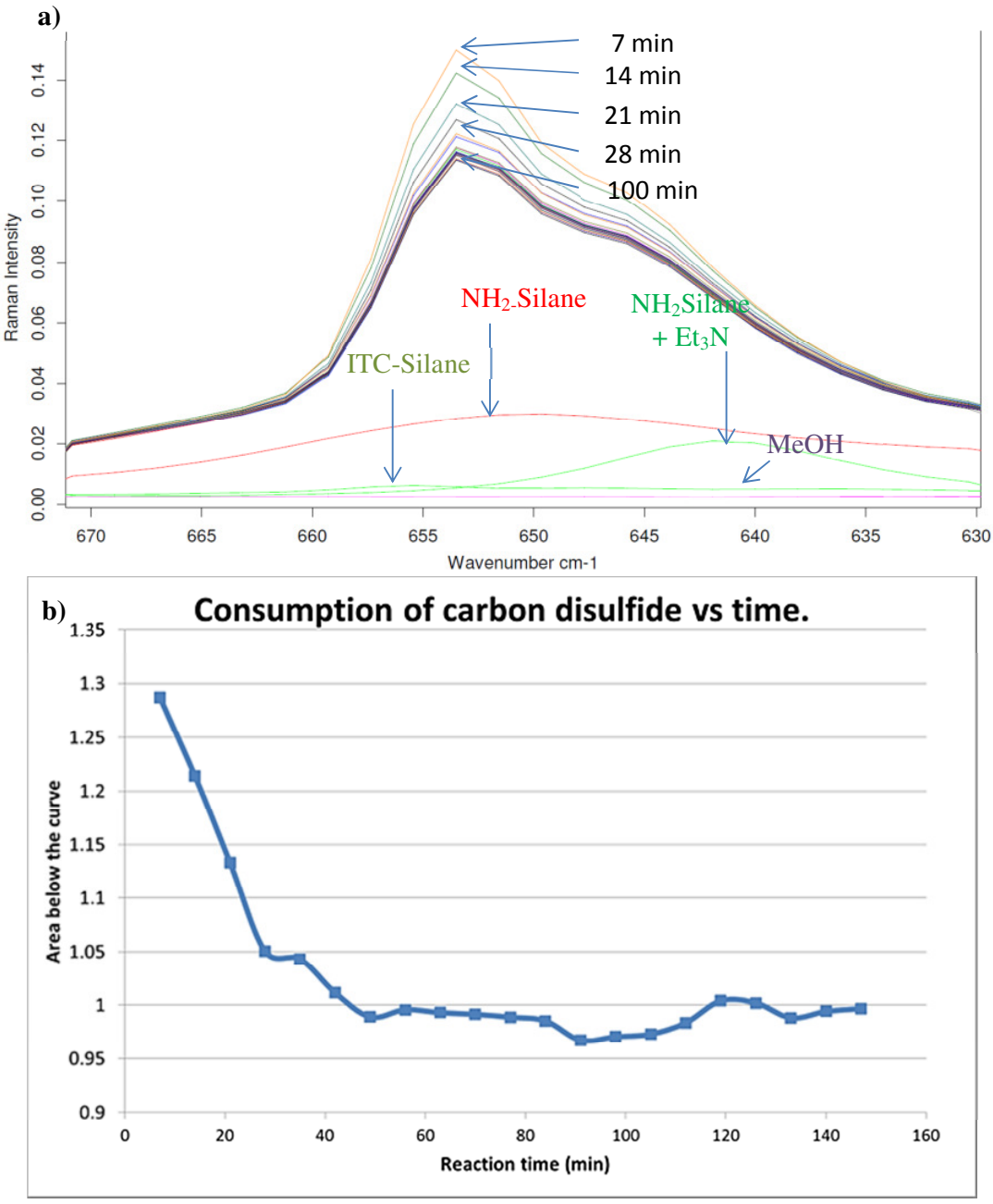

Figure 37.- Raman spectra of carbon sisulfide versus time in (a). The Raman intensity of the spectra in the wavenumber region between 640 and 650 cm^{-1} corresponding to the CS_2 signal. are plotted in (b) taking into account the area under each curve in the same interval of wavenumbers (units are arbitrary). The condition of the experiments follows a close system with no evaporation and no losses. The probe was not taken out of the spectrometer to avoid any environmental or instrumental error.

Fourier Transform Infrared Spectroscopy of isothiocyanate-silane.

Fourier transform infrared (FT-IR) spectroscopy in the transmission mode was used to investigate the substances involved in the Kaluza reaction. A 5 µl drop of the substance was placed on top of a potassium bromide (KBr) pellet, previously produced by adding

300 mg of the KBr powder into a press cylinder and dried afterwards The KBr pellet was measured before (background) and after the placement of a drop. After the measurements the single channel spectra was divided by the background to produce the absorbance spectra, corresponding to the dried liquid. Organic isothiocyanates (ITC) show a broad and strong band centered around 2100 cm^{-1} [346, 347]. With a strong doublet occurring near 2150 cm^{-1}, Badger [348] suggested that one of this bands aroused is a fundamental transition of the linear –N=C=S group while the other arises from a second excited state. This might be due to internal stretching modes of the -N=C=S group. A correct assignment of the three vibrations modes ν_a (NCS), ν_s(NCS) and ν_a (C –N) is essential to a correct interpretation of the spectra where a= asymmetric and s= symmetric.

Further reading and explanation on how the group got its bands assigned can be found in Kniseley et al. [347]. In Figure 38 the FT-IR spectra for the main reactants involved in the synthesis reaction according to Kaluza and Hodgkins [141, 247] using ethylchloroformate as desulfurizing agent are shown. After the addition of the reactants, several bands were also found corresponding to the intermediate, and then afterwards disappear as the reaction progress towards the isothiocyanate final stable product (Figure 38). The strong band centered around 2100 cm^{-1} is - according to Kniseley et al. [347] - characteristic for the asymmetric stretching of the NCS group and can, therefore, be used as probe to follow the progress of the reaction of the amino silane to the isothiocyanate.

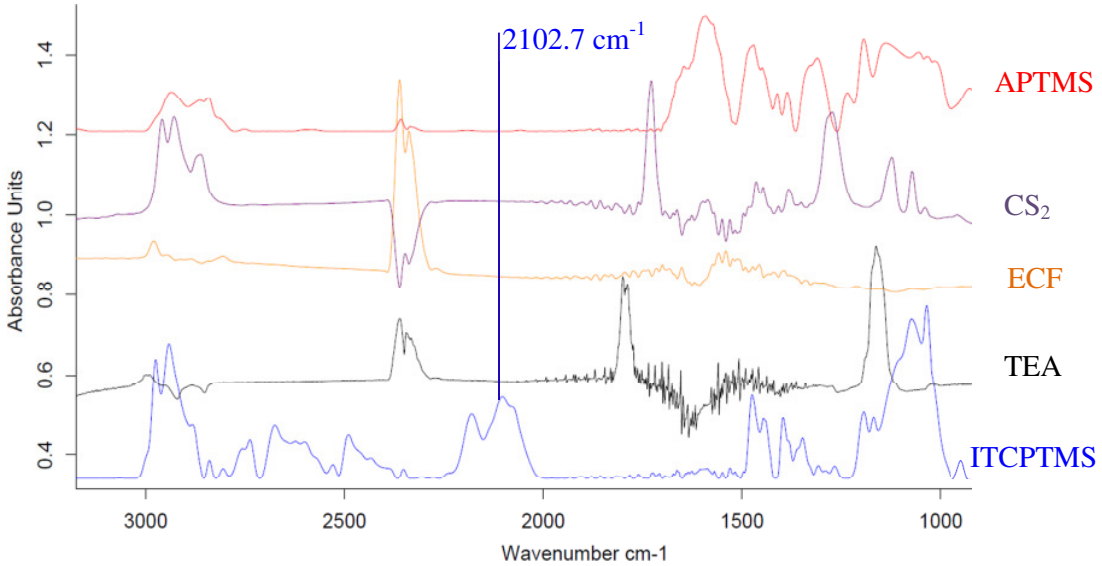

Figure 38.- Infrared spectra from reactants involved in the isothiocyanate silane synthesis. from top to bottom: 3-aminopropyltrimethoxysilane (APTMS), carbon disulfide (CS_2), ethylchloroformate (ECF), triethylamine (TEA) and final product 3-isothiocyanatepropyltrimethoxysilane (ITCPTMS). The emergence of a distinct band centered at 2100 cm^{-1} is typical from isothiocyanate derivatives. This band is not present in the other componenets of the reaction.

On the following Figure 39, the direct comparison between the aminosilanes and the isothiocyanate silane with a more specific band assignment is done. The FT-IR technique is used as a tool in this case to characterize the silane and its reaction. A complete spectroscopic discussion will not be done in this thesis as it is out of its scope. It is important to note, that while the NH_2-silane has been commercially acquired and therefore a silane with higher purity is used, the conversion of this silane towards the ITC-silane is carried out in a single-pot synthesis way. As explained in the experimental chapter, the amino silane purity is determined as 97% pure amino silane from the fabricant. Therefore, we will assign the vibrations in this region of the spectrum (~3350 cm^{-1}) exclusively to the amino group and assume that only few hydroxyl groups might be present in enough quantity to interfere in this analysis, which can be neglected. The isothiocyanate silane final solution was produced mixing all the reactants in a single pot without separation steps in between, and because of this, some reactants might still be present at the end of the reactions as non-reacted components in the same solution when the FTIR analysis is performed. Thus an assignment based exclusively on the difference between bands belonging to each of the reactants and the isothiocyanate silane cannot be obtained, as some bands might not even belong to the ITC silane but to other reactants present. Therefore, an analysis of the strongest peaks is done and the assignment of them to specific groups is implemented.

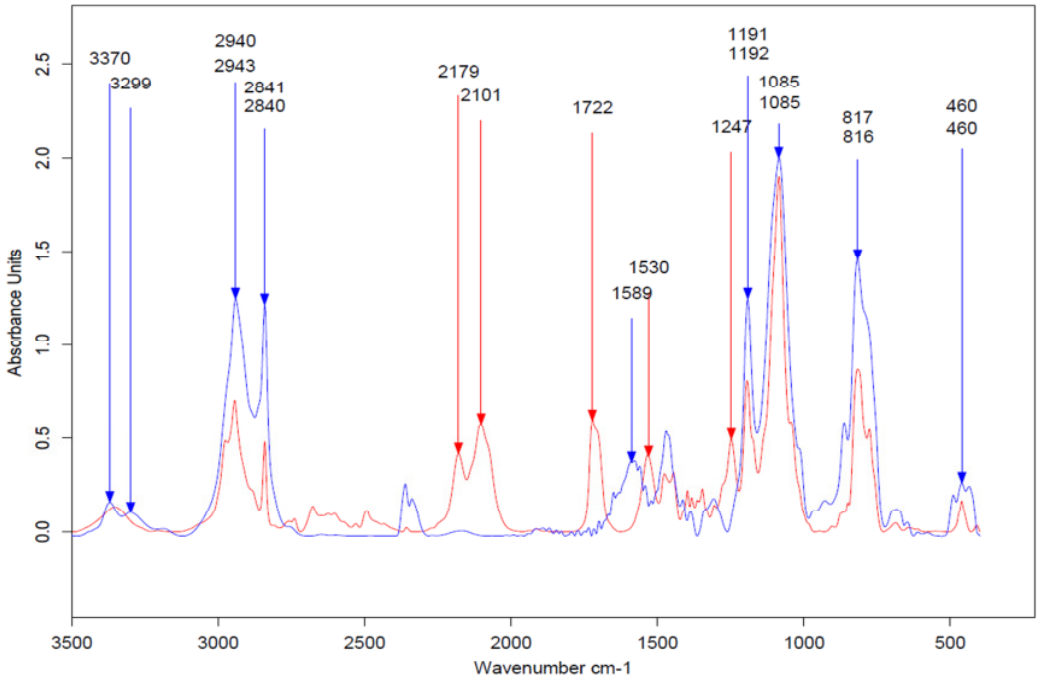

Figure 39.- FTIR spectra from 3-aminopropyltrimethoxysilane (blue) and the final product 3-isothiocyanatepropyltrimethoxysilane (red) after Kaluza and Hodgkings reaction [140, 228]. Particularly to note is the arising strong doublet centered at ~2100 cm^{-1} corresponding to an -N=C=S asymmetric stretching.

The analysis of the aminosilanes done by White and Tripp [349] provides a tabulated assignment of bands for a monoalkoxysilane. We will use this information as an approximation for our interpretation of the bands belonging to both silanes when referred to the NH assignments, the silicon atom and the alkyl chain interpretation from the spectra (shown in Figure 39). A more recent examination on the 3-aminopropyltriethoxysilane using FT-IR was done by Peña-Alonso et al. [350] who uses the technique to study the hydrolysis and condensation reactions of the amino silane on its attachment to glass. Parallel from experiments done by Ishida and Koenig [351] on the effect of hydrolysis and drying of the siloxane bonds of a silane couple agent, a summarized table for the assignments on the silicon atom and the alkyl chain is shown.

Table 8.- FTIR assignments for the fundamental modes of 3-aminopropyltrimethoxysilane and 3-isothiocyanatepropyltrimethoxysilane.

Assignment	Bands (cm^{-1})	Comment	Band found from experimental (cm^{-1}) (Figure 39)
N-H_2 asym.	3370 [38, 349, 352, 353]	NH asymmetric stretching of H-bonded NH_2 group	3370
N-H sym	3305 [38, 349, 352, 353]	NH symmetric stretching of H-bonded NH_2 group	3299
CH_2 asym.	2928 [278, 281, 354, 355]	CH_2 asymmetric modes for the carbon backbone	2940
CH_2 sym.	2885 [278, 281, 354, 355]	CH_2 asymmetric modes for the carbon backbone	2840
-N=C=S asym.	2000-2200 [347, 356]	Strong and broad asymmetric stretch with a doublet centered at 2150 cm^{-1}	2179 and 2101
-N=C=S sym.	1090-925 [347, 356]	Symmetrical stretch very weak in IR	1085
C=O	1740-1720 [357]	Carbonyl group stretch	1722
-NH_2 bend.	1602 [350]		1589
R-NCSN-R	1560-1500 [358, 359]		1530
CH_3 rocking	1190 [360]		1191
-Si-OCH_3	1085 [361]		1085
-Si-C bend	830-800 [276, 350, 358, 362]		815
-CCN	500-400 [347, 349]	fingerprint	460

In the spectra above, sweeping the most notorious bands from the higher to the lower wavenumber are examined. The discussion is also summarized in Table 8. Likewise, Figure 39 shows two small peaks located at 3370 and 3299 cm^{-1} due to the N-H asymmetric and symmetric stretching of the amino group respectively on the amino silane [353, 363]. Due to the appearance of this band and further on the ones related to the amino groups in both silanes, it is probable that, although the reaction has progressed toward the ITC, it is not 100% completed. Further quantitative analysis might be difficult due to the fact, that the reaction takes place following a single-pot synthesis procedure.

In Figure 39, the FTIR spectra for the amino silane and the reaction solution for ITC silane synthesis are presented. It shows a cluster of bands between 2800 and 3000 cm^{-1}, which arise from the overlap of several CH symmetric and asymmetric stretch modes from backbone. More specifically, bands arising at 2940 cm^{-1} and 2840 cm^{-1} correspond to the asymmetrical and symmetrical stretching of C-H in CH_2 respectively [349, 352, 354, 362, 363]. The appearance of the doublet at 2179 cm^{-1} and 2101 cm^{-1} is typical of a cumulated double bond system attributed to the isothiocyanate asymmetrical stretching. Fermi resonance is probably responsible for the presence of these two bands in the 2150 cm^{-1} region [362]. This region is of special interest as it is the region in which cumulated double bonds arise and this is very exclusive from the rest of the vibrational and rotational modes.

The appearance of the band at 1722 cm^{-1} is an indication for the presence of a carbonyl group which belongs to the ethylchloroformate. This is attributed to the presence of the desulfurizing agent, necessary for the change of the dithiocarbamate intermediate into the isothiocyanate.

Further on the aminosilane shows a weak band at 1589 cm^{-1}, which can be assigned to the NH_2 bending mode of the primary amine [349, 350]. This band is present only on the amino silane and is not perceivable on the isothiocyanate mixture. In the latter, the 1530 cm^{-1} according to some authors [349, 352, 354, 362, 363], can be attributed to an amide formation (in this case a thiourea bond formation) occurring between the first isothiocyanate compounds forming and the rest of the amino silane still in the solution which did not react towards the dithiocarbamate intermediate. The thiourea group is very similar to the amide group and it is comparable as this band is also attributed – according to some authors - to a –C-N-C bond [279, 349, 354, 359, 364].

From the infrared results, an indication that the isothiocyanate synthesis was successful using as precursor the amino silane is found. Some bands that appear to be common on

both silanes are in the region of 700 – 1300 cm^{-1}. This accounts for the silicon atom vibration with a carbon $\delta(Si\text{-}CH_2)$ at 815 cm^{-1} and other carbon related vibrations [350, 358]. The range of 1000-1200 cm^{-1} shows a high density of peaks which accounts also for CH_2 and CH_3 vibrations [350]. The band at 1191 cm^{-1} is assigned to the rocking in the CH_3 group present in the alkoxy terminal end. $Si\text{-}OCH_3$ vibrations might also be found in that area representing an asymmetric stretching at 1085 cm^{-1} [38, 349-355, 365]. Finally in the fingerprint region of the spectra, a band arising at 460 cm^{-1} is attributed to the –C-C=N- bending which some authors have attributed to a isopropyl isothiocyanate compound [347, 349].

With this analysis we can account that the aminosilane transformed mainly the functional primary amine, leaving the body of the silane linker intact and the tail groups slightly hydrolyzed. On the following figures a full band examination using native software from the spectrometer has been done.

Figure 40 shows the IR spectra of reaction solutions according to Figure 34 following two different preparation paths using different solvents and the dithiocarbamate intermediate arising from the methanol assisted synthesis. A very reproducible spectrum can be obtained from the same conditions changing only the matrix solvent. It shows the main characteristic bands of the isothiocyanate in the 2100-2200 cm^{-1} wavenumber region, and additionally the bands related to the silicon and methoxy groups. Figure 40 shows a full range (400-4000 cm^{-1}) spectrum of a synthesized ITCPTMS as standard preparation with ethylchloroformate used as a desulfurizing agent. A very sharp and broad band on the 2102 cm^{-1} and 2179 cm^{-1} characteristic of the NCS stretching are shown again.

On the upper spectrum in Figure 40 (a), methanol (Sigma Aldrich 99.9% dried) was used as matrix solvent, while on the middle spectrum on Figure 40 (b) can be seen, on a different preparation date, that chloroform (sigma Aldrich, Germany) was used as solvent. A very weak band arises on the 1789 cm^{-1} on the spectrum in the middle (ITC on chloroform), which can be additionally assigned to acid chlorides coming from the decomposition of the chloroform and ethylchloroformate or to carbonyl groups [366]. The spectrum at the bottom on Figure 40 (c) shows the intermediate component of the reaction (dithiocarbamate salt).

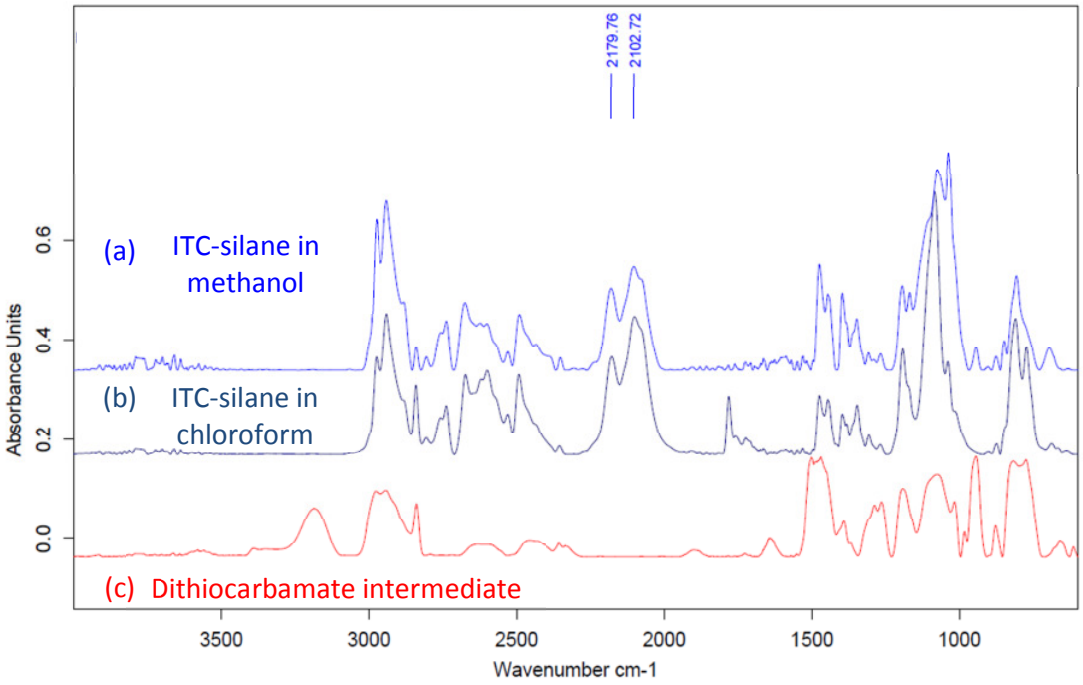

Figure 40.-IR spectra of reaction solutions following two different preparation paths using different solvents. a) ITCPTMS synthesis in methanol, b) ITCPTMS synthesis in chloroform following the same process and c) a spectrum of the dithiocarbamate intermediate. In both cases ethylchloroformate was used as as desulfurizing agent forming the intermediate dithiocarbamate (red line).

For the second route synthesis according to Figure 35, the desulfurizing agent ethylchloroformate was substituted with cyanamide. Although the procedure is relatively similar to that of the ethylchloroformate route shown in Figure 34, the difference is the avoidance of higher amounts of solvent to solubilize some of the dithiocarbamate salts produced by the addition of carbon disulfide on the primary amine under basic conditions. A separation from the salts was performed using ether as an extracting solvent and a further separation was performed using a separation funnel. The infrared spectrum in Figure 41 shows the final isothiocyanate silane product and its corresponding bands. The analysis of the bands will not be repeated in this section, and the assessment of the isothiocyanate bands will be done using the native software again (OPUS 6.0 from Bruker). On Figure 41 the bands corresponding to the ITC silane can be seen centered at 2100 cm^{-1}. The third band appearing on the 2250 cm^{-1} can also be a hint for some cyanamide residual compounds as this band is not visible in the other route of synthesis.

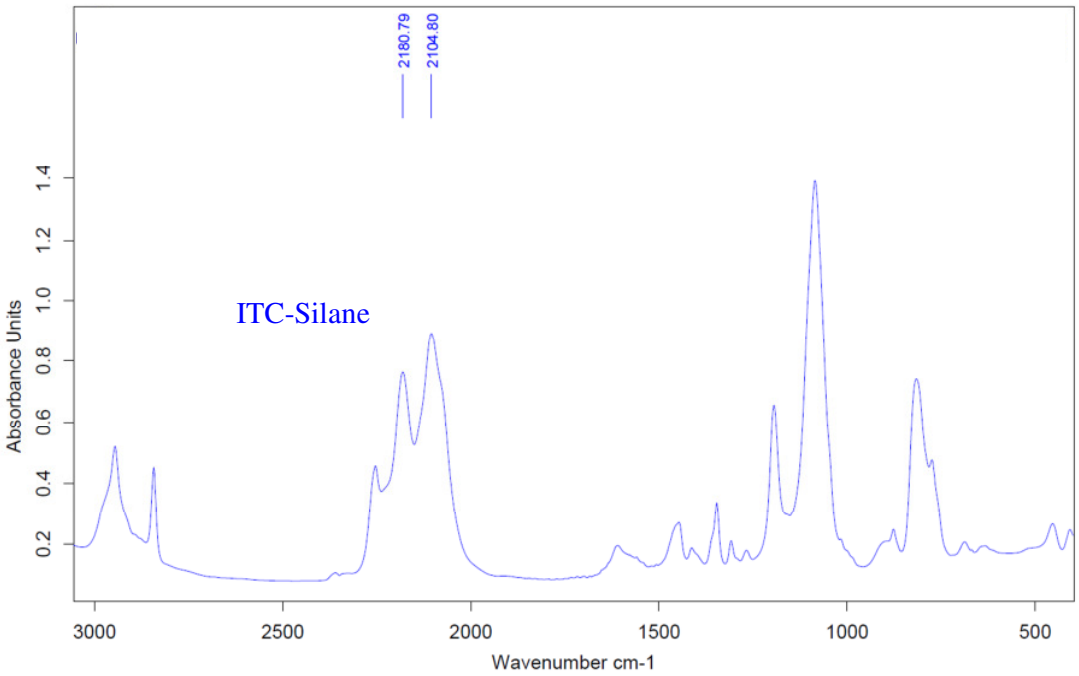

Figure 41.- FTIR spectrum of a in-house synthesized 3-isothiocyanatepropyltrimethoxysilane in chloroform matrix using cyanamide as desulfurizing agent. The spectrum shows similar bands arising centered on the 2100 cm^{-1} wavenumbers.

4.2.2 Characterization of Physical and Chemical Properties of Isothiocyanate-terminated Surfaces on Silica/glass Substrates.

Silanization of surfaces follows mostly the same rules independently from the head non-hydrolysable group when it is transfer onto the surfaces. The hydrolysable groups are mostly divided in halides and alkoxy ones. In this work, methoxy and ethoxy groups are used as they offer a relatively fast reaction time and methanol and ethanol result as sub products whenever silica wafers or glass slides are used [111]. The mechanism which the 3-isothiocyanatepropyltrimethoxysilane (ITCPTMS) follows for its coupling on the oxidic surface of silica is shown in Figure 42. First a hydrolysis of the three alkoxy groups takes place, absorbing water and releasing methanol, creating a "silanol" molecule. It is necessary to note that the alkoxy group has no influence in the overall adsorption mechanism towards the surface, but it influences the speed on which the hydrolysis of the tail groups takes place. The rates of hydrolysis of the alkoxy groups are generally related to their steric bulk forces and decreases in the order CH_3O > C_2H_5O > *t*-C_4H_9O [131]. A methoxysilane hydrolyzes at 6-10 times the rate of an ethoxysilane, but given enough time for complete hydrolysis, the final silanol tail groups are the same

either if they come from the methoxy or the ethoxy groups. After hydrolysis reactions have taken place, the oligomers couple with each other via their hydrolyzed tail groups using the available -OH groups for condensation. This polymerization reaction is taking place parallel to the condensation reaction toward the surface hydroxyl groups. Consequently some of the remaining hydroxyl groups can condensate on the surface via hydrogen bonding, which ultimately forms both a $Si_{substrate} - O - Si_{silane}$ and $Si_{silane} - O - Si_{silane}$ cross linking covalent bonds [367]. Experimental results from AFM display the substrate before any silanization procedure and after cleaning. The process for cleaning is explained in the protocols of section 3.1.1. Additionally X-ray photoelectron spectroscopy was performed on the substrates. On the first set of experiments, silica wafers were prepared for the attachment of ITCPTMS. As AFM is neither an optical nor a chemical characterization technique, the use of fluorescence microscopy was also useful to characterize the reactivity of the surface.

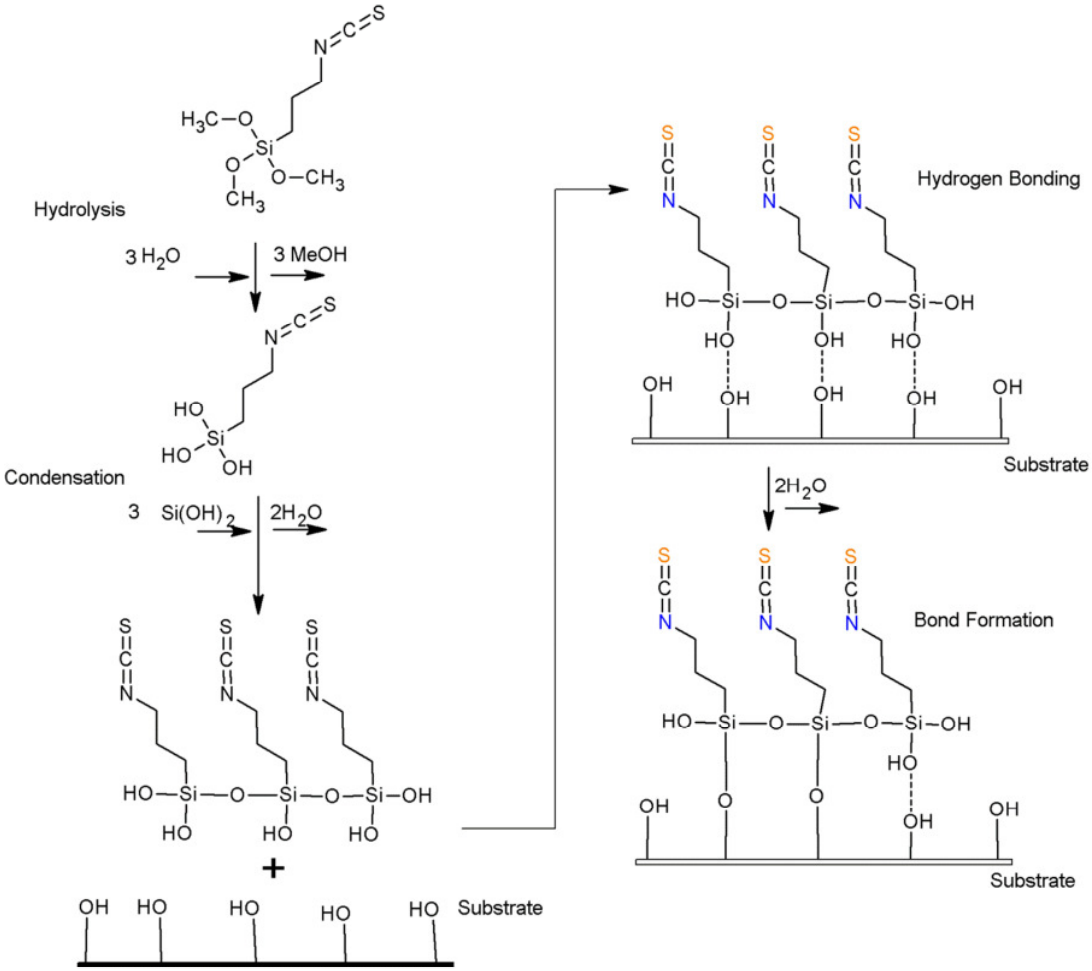

Figure 42.- Mechanism of covalent attachment of 3-isothiocyanatepropyltrimethoxysilane to the surface for functionalization.

4.2.2.1 Morphology and Roughness

After silanization the investigation of samples roughness and topography is necessary to assess also the ability of the silane to form flat SAM layers or - on the contrary - rough interfaces by the formation of aggregates, which in turn will influence the reactivity with respect to further coupling of other molecules. In Figure 43a the AFM topography images can be seen, showing the morphology of the silica wafer substrate after it is cleaned. Roughness was calculated for the clean sample, giving a 0.229 nm root mean square (RMS) value taking the full image into account. After silanization procedure (see section 3.1.1), AFM examination was also performed, resulting in an increase in roughness (RMS) up to 1.867 nm. The comparison is shown in the Table 9 below. It can be seen on the AFM images that the coverage of the silane is not homogeneous, but it assembles in islands [368-370]. This island formation can be explained by two probable mechanisms: first the silane condensate one molecule to the surface and then the rest of molecules attached to the further hydrolysable groups [81, 102]. A second idealized mechanism (as proposed on the Figure 42) follows a pre-condensation reaction of the silane forming polymerized molecules with different lengths and geometries before the silane multimers (clusters) couples to any interfacial hydroxyl group. This latter model is one of the most accepted mechanisms by literature and it will be adopted for this dissertation [371-373]. Due to this polymerized molecules with different lengths and molecular weights, a plausible explanation for the increase in roughness and the appearing of islands (see Figure 43b) on the surface of different shapes and sizes is found [368-370].

The results from the AFM roughness investigations are summarized in the following Table 9. The increase in the island formation and roughness is due to the condensation of the silane on the surface or even in the reaction solution. The silane is synthesized from the amino group using a base catalyzed process [114]. This basic environment promotes the condensation reactions of the silanol groups on the silane anchor groups.

Table 9.- Roughness evaluation data for the clean substrates and substrates after ITC silanization.

Roughness Data	Clean	ITC silanized
Parameter	Full Image Values	Full Image Values
RMS:	**229 pm**	**1.8 nm**
Average Deviation:	177 pm	755 pm

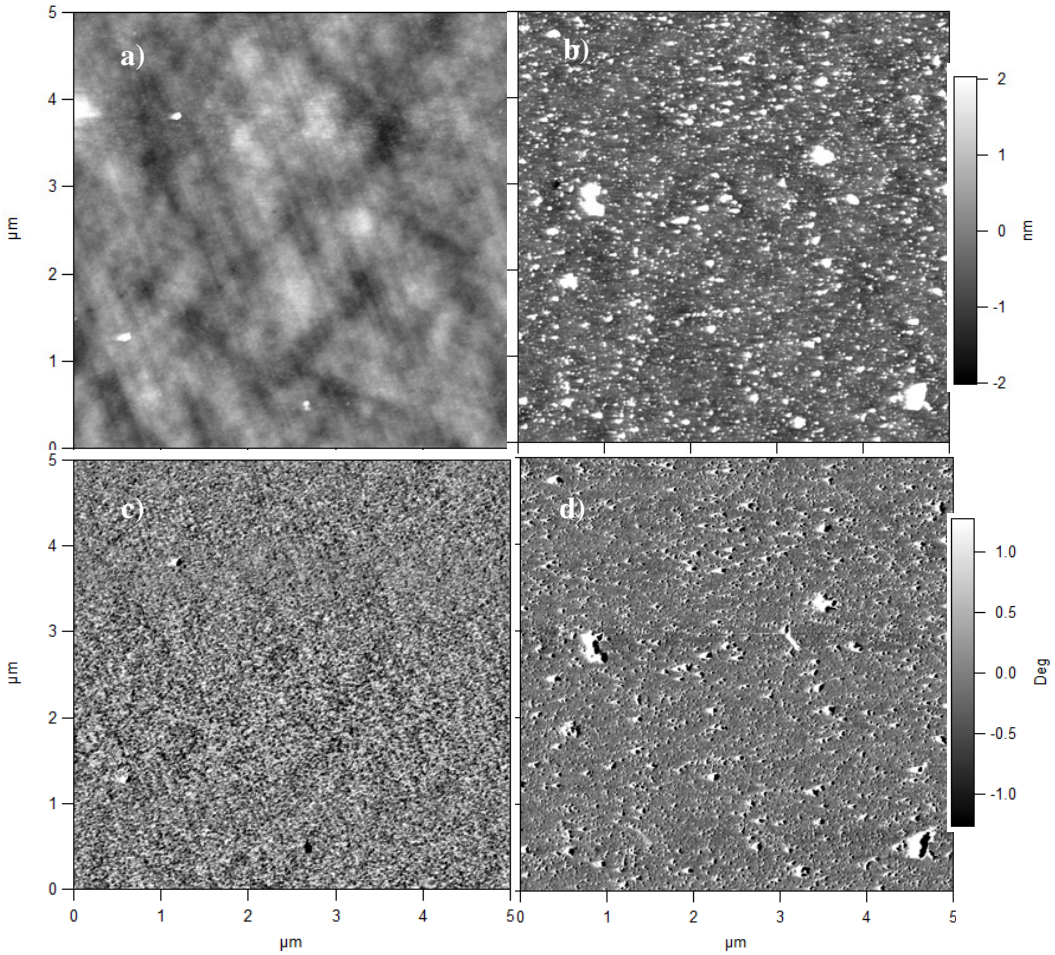

Figure 43.- AFM images of silica wafers after chemical cleaning (topography (a), phase (c)) and after functionalization with ITCPTES (topography (b), phase (d)).

4.2.2.2 Wettability

Contact angle measurements were used to characterize the change in the chemical functionality of the terminal groups of the silica wafer before and after silanization (Figure 44). The silane in this case was the 3-isothiocyanatepropyltriethoxysilane in a methanolic solution at 3% volume percentage. The substrates were cleaned following the procedure described in chapter 3 and then immediately used for measurement resulting in a CA<5±0.5 (Figure 44a). After silanization, a steep increase of the contact angle (sessile drop method) due to the addition of organosilanes is observed (CA=65±6) (Figure 44b).

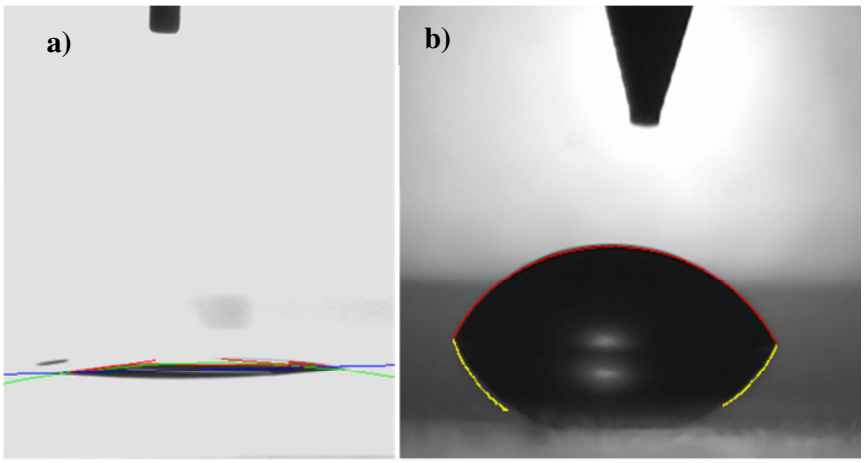

Figure 44.- Single contact angle measurement on a) chemically cleaned silicon wafer surface (CA<5±0.5) and b) isothiocyanate-functionalized silica wafer (CA=65±6).

In Figure 45 the advancing contact angles on a silica wafer using the sessile drop method are presented. Each value represents an average on 5 measurements on different areas of the same sample for three different silanized silica wafer substrates. A value of 5° was assigned to the measurements of the clean wafers prior silanization, due to the lack of precision of the instrument to measure properly contact angles below that value. The error associated with the machine is around 10% of the measured value, therefore the error bars in the values assigned to the clean wafers are almost unnoticeable at the scale of the graph. A very steep increase of the angle up to 70° was observed, after silanization. This can be due to the reaction (reduction of number) of the hydrophilic hydroxyl groups of the substrate with the silanol groups of the hydrophobic silane molecules. [109]). Several groups have already investigated the contact angle of silica and glass substrates which were functionalized with several other silanes [102, 374-376] and, therefore, a complete analysis on the mechanisms of attachment is not necessary. Factors which contribute to the ability of an organosilane to generate a hydrophobic/hydrophilic surface are: i) its organic substituent, ii) the extent of surface coverage iii) residual unreacted groups (both from the silane and the surface), iv) the distribution and orientation of the silane molecules on the surface as well as substrate roughness (including roughness due to cluster formation). Fadeev and McCarthy [377] reported data, which indicates that the contact angle of water on a silica substrate treated with alkylsilanes are independent of the alkylsilane length. Compared to the contact angle measured for the Si wafer functionalized with 3-isothiocyanatepropyltrimethoxysilane (CA ~70°) the same silane moiety (propyltrimethoxysilane) without ITC terminus has a contact angle of 82.4° [378,

379]. Therefore, the change in the hydrophilicity behavior of the silica layer might be due to the coverage of the surface by the silane, but more specifically by the presence of the isothiocyanate group independent of the organic spacer.

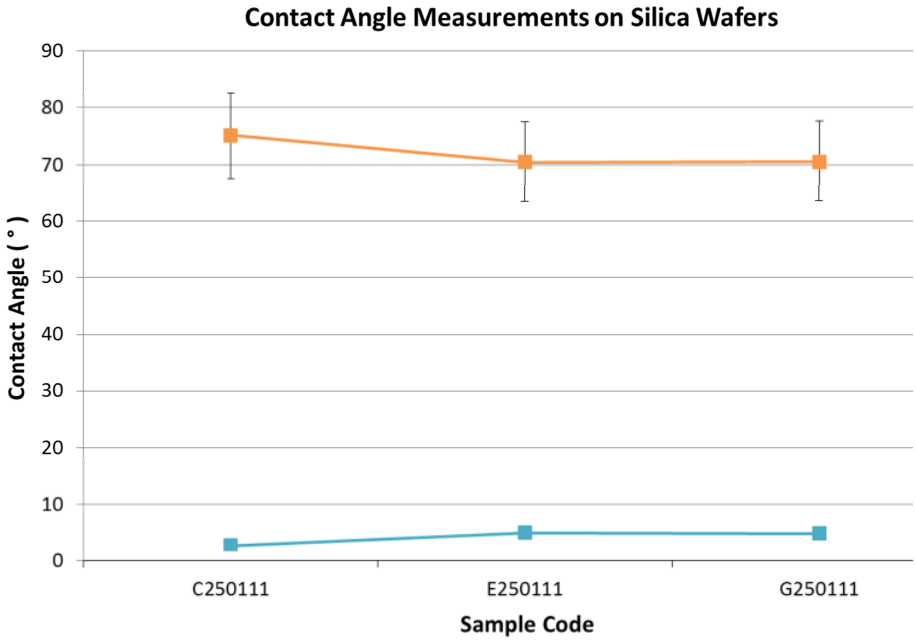

Figure 45.- Average contact angle determined for for silica wafer samples cleaned (blue line CA≤ 5°) and after silanization (orange line CA= 70° ± 7).

Similar experiments were done on glass slides to check the homogeneity of the silane layer on the surface. Following what Fripiat et al. [380, 381] investigated before, a higher number of hydroxyls are present in the glass than on the silica wafer. This should result in a lower contact angle of water for glass after cleaning compared to that of a silica wafer. However, with the contact angle instrument it is not possible to determine precisely contact angles below 5°. Literature on the adsorption of water and the role of the OH groups on a silica surface, covering the temperature ranges from the hydroxylation or dehydroxilation of silica surfaces has been reviewed by Zhuravlev [33, 382]. From his work, an average number of 4.9 OH-groups/nm^2 is calculated to be found in silica oxide substrates. After the ITC silanization of the glass the contact angle determined was 65° in average which is smaller than that determined for the Si wafer (70°, see Figure 45). As an explanation we will assume that a full surface coverage by the silane was not completely achievable in the case of glass resulting in a contact angle value between that of a non-silanized glass and a glass substrate with all of the –OH groups reacted with the silane. Figure 46 shows that the resulting sessile drop contact angle was in average 65°.

Although this experiment had the intention to compare the substrates, the control of the homogeneity of the silanization along the slide can also be assessed approximately. For that purpose a mapping of 9 points along the longer axis of the slide in three different positions was done (left, middle and right). From these points an average was calculated (65°). The lowest calculated angle was 53.6° and the highest was 73°. It means the silanization procedure using a liquid strategy is slightly variable in itself. The tendency of the contact angle to shift towards one side of the slide can be explained by the higher concentration of the silane on the higher end of the silanization beaker due to the higher evaporation rate of the methanol at that point. The variability of the silanization in liquid has been already studied and is still a point of discussion for several authors [102, 374, 383]. Other strategies have been developed in order to reduce the polymerization and over condensation reactions of the silanes in solution, either with themselves or with the surface. These strategies includes: i) limiting the concentration of the silane before the modification, ii) using chemical vapor deposition, iii) using anhydrous solvents and use of some monoalkoxysilanes [34, 38, 42, 384]. For biological use, a highly ordered and homogeneous surface is desired. Further homogeneity experiments are performed using fluorescence microscopy (see section 4.2.4.2)

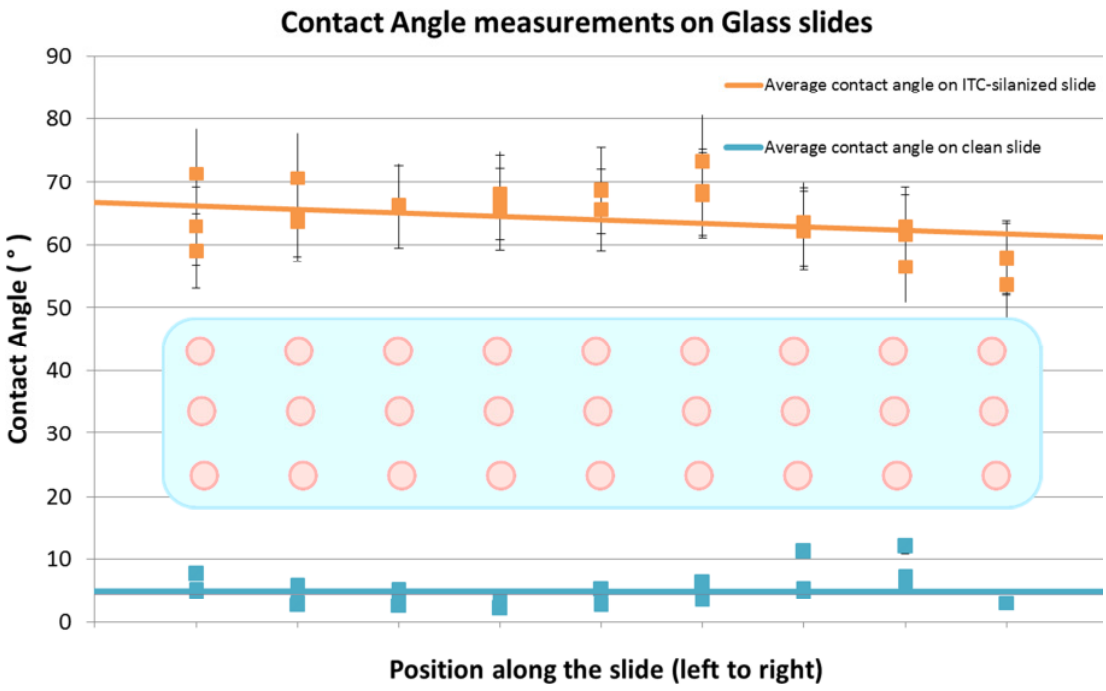

Figure 46.- Average contact angle measurements for glass slide samples. The average has been calculated by measuring 3 points in 3 different slides and then plotting the average. The dots represents the position of the drops on the glass slide

In an effort to reduce the reaction time and to improve the reaction yield, other reaction conditions were tested. In this context the addition of a base to the silanization solution increased the rate of hydrolysis significantly. With an average time of approximately 2 hours to accomplish a silanization on a wafer, the basic conditions improved the total silanization time to just 15 minutes. This could be tested by contact angle and AFM characterizations. Unfortunately the rapid hydrolysis of the methoxy groups was also responsible for a higher degree of cluster formation on the surface, resulting in a noticeable less clean wafer at the end of the treatment. This behavior has been already tested and studied by Osterholtz [385] and Kallury [114] and it can be explained in the case of the basic catalysis as a bimolecular nucleophilic displacement reaction in which negative charge development on the silicon atom is considerable. Electron withdrawing substitution on the methyl groups will eventually stabilize the developing negative charge and lower the energy of the intermediate state. This will produce an increase in the rate of hydrolysis as the methyl group becomes more electron withdrawing [385]. Likewise, the higher hydrolysis rate, the higher the rate of parallel condensation reactions which can take place [131]. This multimerization reaction is too fast to be controlled properly hindering this base-catalyzed method for suitable use.

4.2.2.3 Elementary Composition

To prove the successful chemical functionalization of the silica wafers, XPS measurements before (Figure 47d-f) and after (Figure 47a-b) the treatment with 3-isothiocyanatepropyltrimethoxysilane prepared by the in-house synthesis method were carried out. In a second experiment the XPS results of wafers treated with the silane prepared by the in-house method and of wafers treated by the silane bought from a chemical company were compared (Figure 47e-f). The advantage of using a custom-made reactant is the purity that can be achieved (>97% volume) and the opportunity to compare the silane synthesized in house with a commercial standard. For comparison C 1s, N 1s, and S 2p are selected taking into account that these elements should come from the silane.

First experiment remarks the comparison between an ITCPTMS silanized and a clean surface. In Figure 47 it can be noted, that adventitious carbon can be found on clean silicon wafers, but the intensity of the peaks shown are much lower than those on the silanized wafers. The carbon peak C 1s (Figure 47a-d) can be deconvoluted in several components: 285.0 eV (C-C, C-H), 286.7 eV (C-O, C-N), 287.8 eV (N=C=S) and 289.4

eV (O-C=O) which are in agreement to the experiments from Graf [386, 387]. These components indicate the presence of ITCPTMS but show an oxidation of the molecule as well. The S 2p doublet at 163,2 eV shows the presence of isothiocyanate whereas the doublet at 169,0 eV (Figure 47c) is also a hint for oxidation [388]. The N 1s peak (Figure 47b) can be deconvoluted into one peak rising at 400.6 eV that can be attributed to the -N=C=S bond [386, 389].

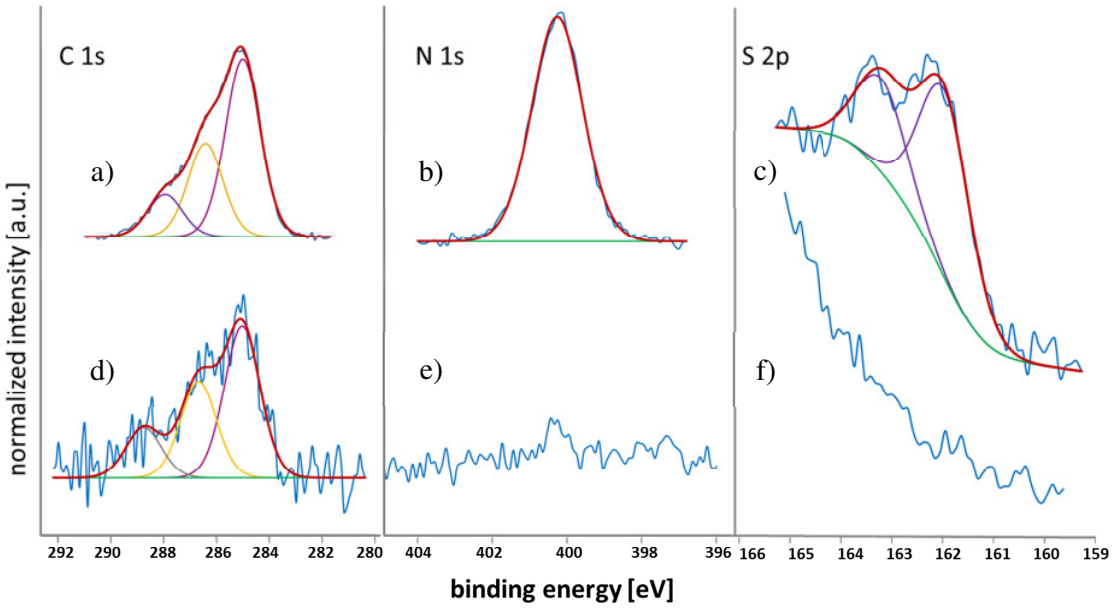

Figure 47.- XPS spectra of a silica wafer treated with in-house-made isothiocyanate silane (a-c) showing the C 1s, N 1s and S 2p signals. As a reference clean, non-silanized silica was measured (d-f).

Aided by the FTIR measurements described before, and the contact angle measurements, we can conclude that the isothiocyanate group is present on the surface of the examined samples. As there is no XPS information available for the isothiocyanate silane as pure substance in literature, we will compare the ITCPTMS with the XPS spectra of ammonium isothiocyanate from literature and try to identify the elements of the ITC group. It has to be mentioned additionally that the analysis of S 2p is complex as this peak is masked by the silicon peak signal. A direct comparison of the isothiocyanate groups between the two different chemical substances might not be as straightforward as it seems. The chemical environment of the group is different in both molecules, affecting in this way the measured binding energy of the corresponding sulfur atom. The S 2p peak doublets expected for ammonium isothiocyanate are found close to 161 eV according to Ciszek et al. [390, 391]. The higher binding energy for oxidized sulfur, ranging from 165 eV and more (SO^{2-}), is not found in ITCPTMS, meaning that the sulfur in the

isothiocyanate group is in the lower valence state and it is not oxidized. While a peak at around 163 eV has been consistently assigned to the S^{2-} species [392], different authors have assigned a peak around 168 eV as S^{+6}/ S^{+4} species. Alternatively Umebayashi et al. [393] identify it as a peak of absorbed SO_2 in the same region of the binding energy (even from 166-169eV) [394, 395]. The lower binding energy corresponds to a sulfur atom with lower valence. Sayago et al. [395] also gathered literature values of S 2p peaks for many sulfur based species absorbed on different surfaces and oxides in particular. Their results are presented in Table 10. From literature, a large variation in the energy values can be noted, partially because the binding energies within the SO_2 molecule significantly depend on the used oxidic surfaces. From this survey, we can conclude that the sample shows bound non-oxidized sulfur which corresponds neither to a decomposed sulfur atom on the surface nor to a physisorbed species. Consequently it can be concluded that it belongs to the isothiocyanate group.

Table 10.- S 2p binding energies reported for sulfur species on oxide surfaces and their assignments according to literature [395, 396].

Compound type	Binding energy range (eV)
Sulfides (S^{2-})	162.1–163.6
S_n	162.4–164.8
SO_2 (chemisorbed)	163.5–165.7
$(SO_3)^{-2}$ (S^{4+})	164.9–167.6
$(SO_4)^{-2}$ (S^{6+})	166.1–169.0
SO_2 (physisorbed or multilayers)	166.6–171.0

The second experiment focused on a further comparison between the behavior of the ITCPTMS synthesized in-house versus the 3-isothiocyanatepropyltriethoxysilane custom-made silane (ABCR, Germany) (shown in Figure 48). The carbon 1s examination (Figure 48a,c) show similar spectral peaks for both silanes corresponding to the previously discussed analysis (285,0 eV (C-C, C-H), 286,7 eV (C-O, C-N), 287,8 eV (N=C=S) and 289,4 eV (O-C=O) which are in agreement to the experiments from Graf [386, 387]) in a very reproducible way. In the case of N 1s, a sharp peak on the custom-made available silane can be assigned exclusively to the –N=C=S group as the

purity value of the silane is >90% (Figure 48b). On the in-house synthesized ITCPMTS an appearance of two bands can be explained due to an incomplete conversion of the 3-aminopropyltrimethoxysilane to isothiocyanate or a further dithiocarbamate derivative formation (Figure 48d). The conversion from the primary amine to the isothiocyanate functional group is above 70% as described by Hodgkins [141].

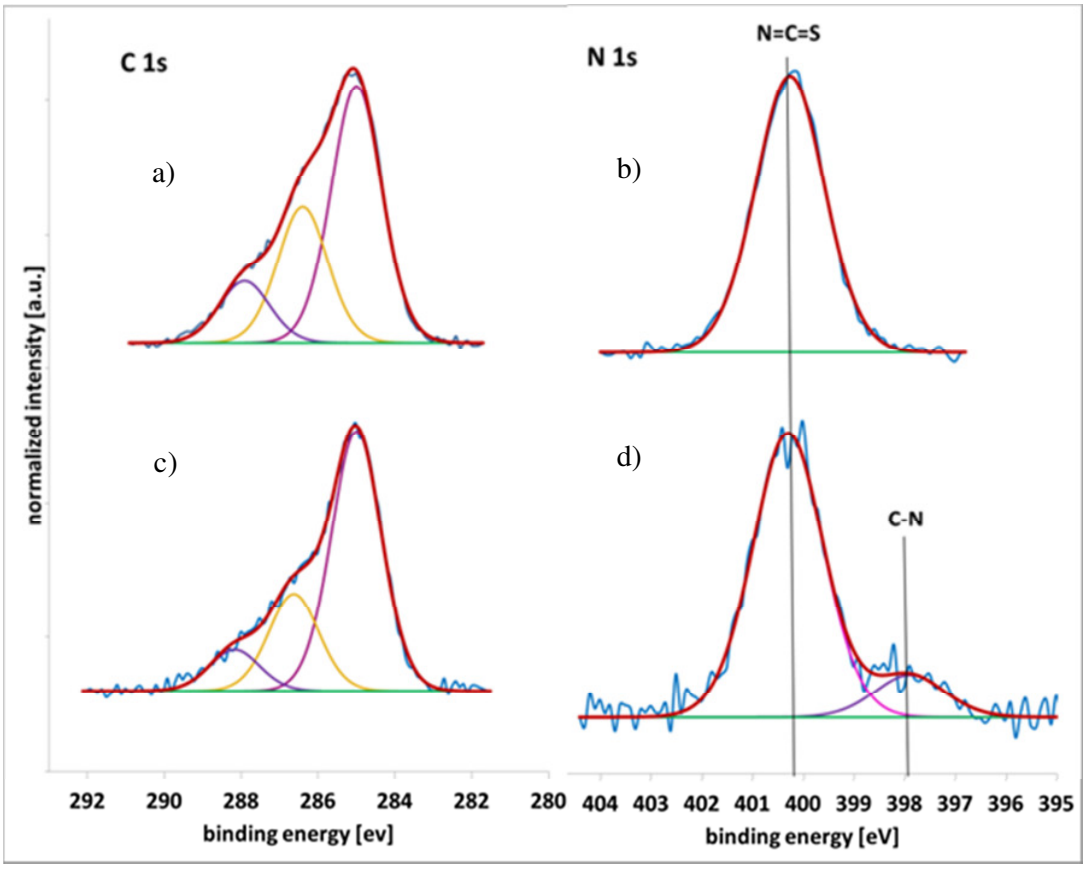

Figure 48.- XPS spectra of C 1s and N 1s comparing the custom-made available ITCPTES (a, b) versus the silane synthesized in-house ITCPTMS (c, d). For all elements no significant differences between the two silane scan be found after they were bound to the subestrate.

From the results on the XPS on the silica wafers examined, it can be concluded that, the commercial and the in-house synthesized silanes, behave very similar on the surface and in both cases the presence of the isothiocyanate group can be proved. Likewise, the silanes behave similarly when they are coupled to the oxidic substrate surface. This is also in agreement with the FTIR measurements done on the solutions before any silanization is carried out regardless of the origin of the silane.

4.2.2.4 Chemical Functionality

The isothiocyanate group reacts with nucleophilic groups such as amines and sulfhydryls, in a similar way known from the aldehydes. The most stable product of these reactions, however, is with primary amine groups [397]. Therefore, isothiocyanate compounds are almost entirely selective for the reaction with amino groups e.g. in lysine chains and N-terminal α-amines in proteins or primary amines in other molecules [397]. The reaction involves an attack of the nucleophilic species to the central electrophilic carbon of the isothiocyanate group. The resulting electron shift creates a thiourea linkage between the ITC-containing compound (in this case the silane) and the amine [398].

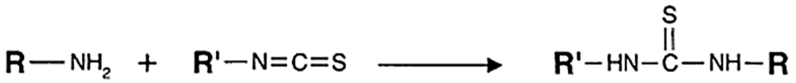

Isothiocyanates reacts best at alkaline pH values where the target amine groups are mainly unprotonated. Reaction times may vary from 4 to 24 hours at 4°C [398]. Rana and Meares [398], found that ITC-containing chelates at pH 7 could selectively modify a biomolecule exclusively at its N-terminal-α-amines while leaving the amines of lysine in the sequence unmodified. Therefore, the ITC moiety is used as a highly selective group for chemical surface modification and, as it is done in this dissertation, to immobilize DNA on a defined site. [319]. This high selectivity is used to immobilize the amino-terminated DNA-linker exclusively via the amino group at the end of the molecule, leaving the rest free for hybridization and further TMV particle assembly.

Chemical reactivity in this section will be assessed on chemically patterned substrates using microcontact printing, Dip Pen Nanolithography (DPN), and microarray spotting (for comparison with other DNA-linker fixation groups and for homogeneity assessment on glass slides).

A similar experiment to that of the aldehyde transformed substrate (see chapter 4.1.1.4) was performed in the case of the isothiocyanate functionalized substrates. Drops of the NH_2-DNA-Fluorescein solution (21 drops in total) were placed along a glass slide and evaluated. This experiment was performed to assess the relative fluorescence between the aminosilanized substrate and ITC-terminated substrate as an indicator of the chemical reactivity of the primary amine of the DNA-linker. After the fluorescence evaluation using Genepix 4000B microscanner (Molecular Devices, Germany), an increase in total intensity values (arbitrary units), when compared with the amino silanized slide, was

observed. A comparison with the amino-terminated silane and the ITC-terminated silane is shown in Figure 49. The comparison is done taking the amino terminated slide, as standard substrate from which both moieties (aldehyde and isothiocyanate) emerge. The two images inset in the graph are the actual images of the glass slides as measured in the fluorescence scanner. The color of the frame relates to the functional group evaluated in the graph.

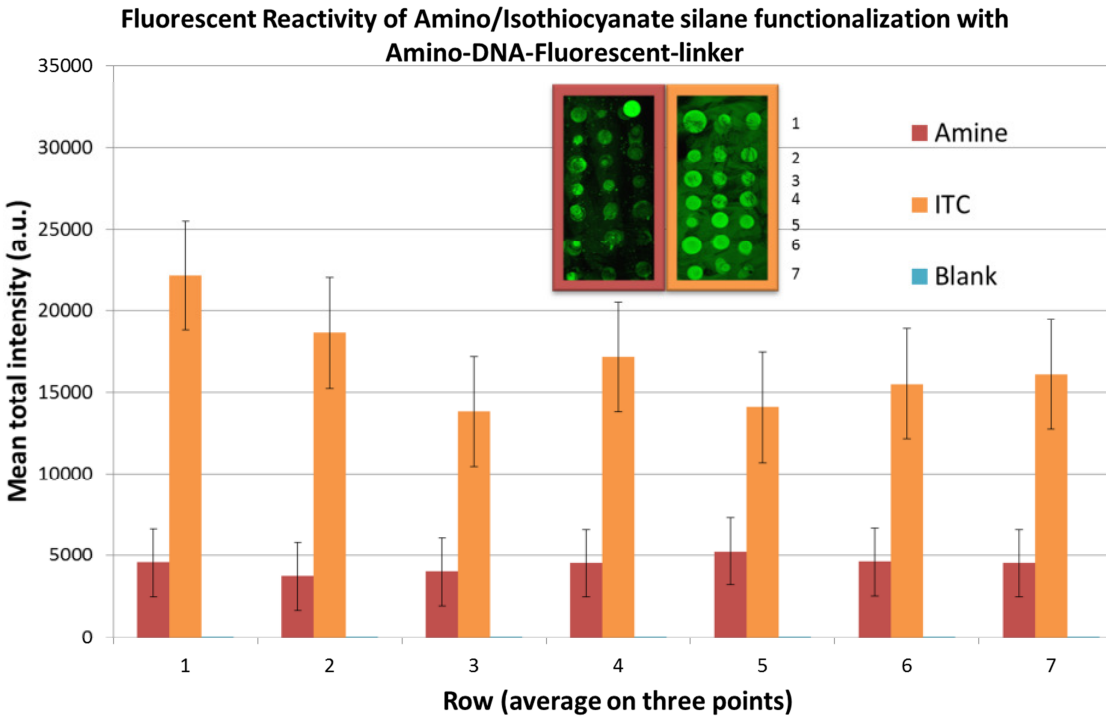

Figure 49.- Fluorescent reactivity assessment of amino/isothiocyanate terminated glass slides using DNA-amino terminated oligonucleotide as fluorophore binding molecule.

In the following pages additional reactivity assessment experiments are described. This set of experiments was designed to evaluate two aspects: the successful scaling-down on the chemical structuring techniques (through microcontact printing, microarray and DPN), and second, the homogeneous coating along bigger substrates. The reactivity of the ITCPTMS is evaluated by measuring the fluorescence signal of: i) microcontact printing with 5-aminofluorescein on isothiocyanate silanized slides, ii) microarray spotting experiments using also an aminofluorescein fluorophore iii) microarray spotting experiments using aminofluorescein for comparison with an epoxy-silanized slide, iv) DPN chemically patterned coverslips submitted to fluorescence DNA-linker to assess the reactivity in smaller scales, and v) DPN chemically patterned coverslips prepared for further particle immobilization assays, to test if the chemistry at this scale is able to

support immobilized heavier particles. An overview of the experimental techniques is explained graphically in Figure 50.

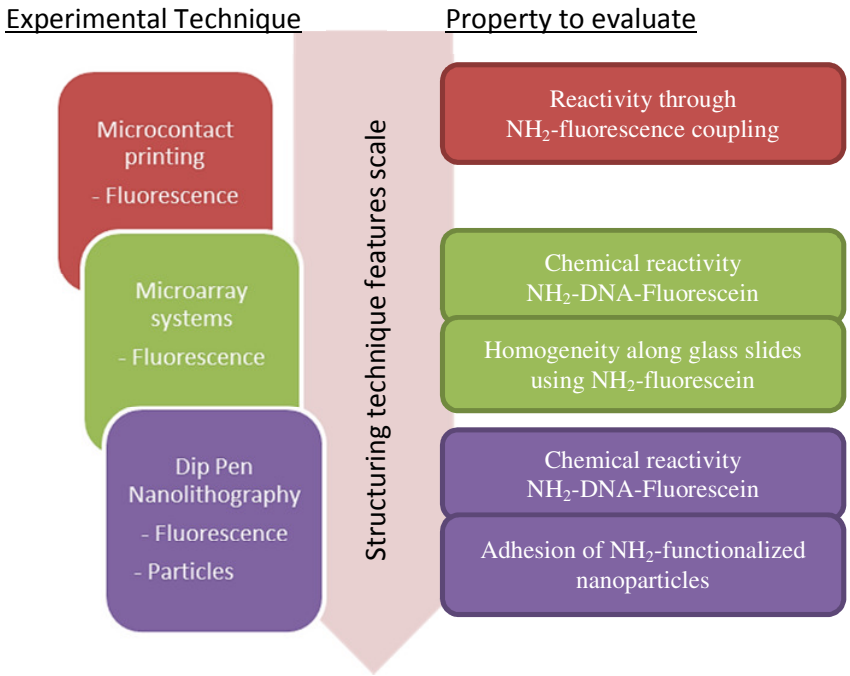

Figure 50.- Road map of experiments in section 4.2.2.4 Chemical functionality on ITC-based silanization. The experiments have been design to assess: chemical reactivity through fluorescence evaluation, homogeneity through fluorescence evaluation of microarrays on glass slides and adhesion capabilities of nanoparticles at small scales. The section approaches this assessment through scaling down the structuring technique from macrostructuring up to micro/sub-micron structuring.

4.2.2.4.1 Microcontact Printing of Aminofluorescein on ITC-functionalized Glass Slides.

Microcontact printing was performed for fluorescence assessment experiments. The ink used for this experiment was an aqueous/ethanolic (1:10) solution of aminofluorescein (1mM). The substrate was a clean glass slide functionalized with ITC-silane following the protocol in section 3.1.1. Two patterns from a gradient master were stamped: on the left (Figure 51a) a gradient in which the gaps are getting bigger while the features width is kept constant, and on the right a gradient in which the width of the features are getting bigger and the gaps are kept constant (Figure 51b). The master for the fabrication of the stamp has been kindly provided by Dr. Tamas Haraszti and his group, from the Max-Planck-Institut for Intelligent Systems (Stuttgart). The patterns are organized into 3.5 x 2.5 mm gradients with the description as the following table (Table 11) for the gradient. From the stamp, two defined gradients were used (A, B).

Table 11.- Gradient stamp dimensions for microcontact printing assessment of chemical reactivity on isothiocyanate silanized glass slides.

Field	Line width (µm)	Line spacing (µm)	Horizontal size (µm)	Vertical size (µm)
A	3	1-10; 0.5	164.5	200
B	1-10; 0.5	4	176.5	200

Figure 51 shows a fluorescence image of the fluoresceinamine ink stamped on an isothiocyanate silanized glass slide. It remarks the ability of the silane to properly react with the aminofluorescein fluorophore on the stamp. The increase in the mean fluorescence intensity values for this concentration of fluorescent molecules (1mM) demonstrated an approximately 3-4 fold increase between the stamped areas and those areas amidst which have no fluorescence molecules deposited (Figure 51e,f). The image analysis has been performed with ImageJ software. The absolute intensity results can be used for relative comparison. The analysis in this case yielded a higher fluorescence intensity on the stamped areas than on the non-stamped areas, which correlates with the selective presence of the aminofluorescein molecule on the surface.

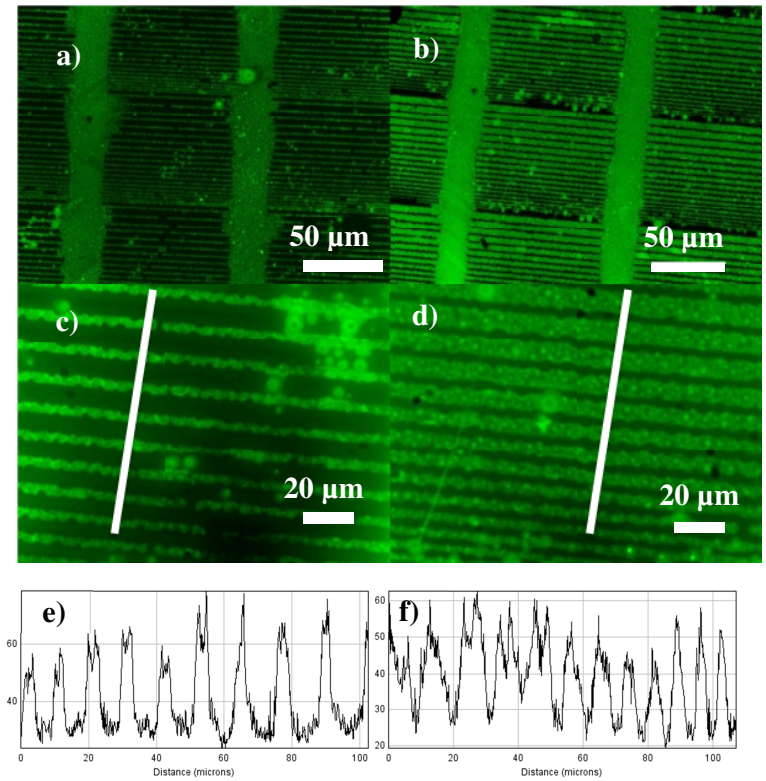

Figure 51.- Fluorescence image of microcontact printing patterns from aminofluorescein on isothiocyanate silanized glass slides. a) and c) represent stamping with the same line thickness but different spacing between them. b) and d) are stamps representing different line thickness but same spacing between them. The lines represent the places where the fluorescence intensity profile measurement was performed.

4.2.2.4.2 Isothiocyanate as a Reactive Agent for Microspotting Array Experiments.

In this section, the assessment of the chemical reactivity and the homogeneity of silanized glass slides are performed. DNA microarray analysis is widely used for studying genome data in life science. Microarray expression studies produces an enormous amount of expression and other data, which is used in return to provide key insight into function and interaction between molecules, strands or genes [399]. Microarray platforms and experimental design are produced in various formats and models and most of them are tailor-made regarding the application.

In this section, two experiments involving the evaluation of microarrays were performed:

First, in order to evaluate the reactivity of the ITC silane towards an NH_2-DNA-Fluorescein linker, the isothiocyanate group (ITCPTMS) is compared with a commercially available epoxy-terminated slide used for common experiments of DNA microarray analysis. Commercially available epoxy functionalized glass slides named Nexterion Slides (Peglab, Germany) were tested against isothiocyanate functionalized slides (thanks to Fabian Eber, Institute of Biology, Molecular biology and Plant virology section, and Prof. Dr. Hauer and Beate Rössle-Lorch from Institute of Technical Biochemistry, University of Stuttgart who kindly performed the analysis of the spotted slides) and spotted using a microarray spotter robot (Microgrid II Microarrayer Biorobotics, United States).

In a second experiment, a spotting machine at KIT (Genemachines Omnigrid 100, United States) was used to spot several ITC-silanized glass slides with a 0.01 mM NH_2-Fluorescein solution (as described in previously sections), in order to characterize the homogeneity of the ITC silanization in liquid for a defined concentration (3% volume). The experimental objective includes not only the homogeneity assessment of the coating of the ITCPTES on the glass substrates but also looks forward on providing a new experimental process scalable for use with DNA and amino containing molecules on a glass slide.

DNA Oligonucleotide-Microarray Spotting. Comparison with Epoxy Functionalized Slides.

In the first experiment, the spotting was done using an oligonucleotide holding an amine terminal group on one end and a fluorophore Cy3 molecule on the other end (Metabion, Germany). A comparison of fluorescence intensity between the ITC-terminated in-house functionalized and the epoxy-functionalized commercially available slides is performed. Two microarrays were spotted on each slide and then evaluated in a microscanner (Scan Array Express PE Applied Biosystems (Weiterstadt,Deutschland)). For spotting, different concentrations of the oligonucleotide in the spotting buffer from PegLab were used. The arrangement of the spots is random and the grid is set by the software belonging to the spotter. The arrangement with their respective concentration values are shown in Table 12. This matrix is ordered following a two-pin configuration for the spotting needle. As it can be seen in the Table 12, two spots are printed with a defined fluoresceinamine concentration followed by the next two spots with another concentration. This configuration is the same for all the slides involved in this experiment. Three slides were used in this test: 1 epoxy-coated commercially available glass slide and two isothiocyanate-coated (in-house synthesized) glass slides.

Table 12.- Oligonucleotide concentration and random arrangement for microspotting comparison between commercially available epoxy slides and isothiocyanate silanized slides.

0	2	2	3	3	4	4	5	5	6	6	7	7
4	4	4	5	5	5	6	6	6	7	7	7	1
6	7	7	7	1	1	1	2	2	2	3	3	3
2	2	3	3	3	4	4	4	5	5	5	6	6
5	5	5	6	6	6	7	7	7	1	1	1	2
7	1	1	1	2	2	2	3	3	3	4	4	4
3	3	4	4	4	5	5	5	6	6	6	7	7
6	6	6	7	7	7	1	1	1	2	2	2	3
1	2	2	2	3	3	3	4	4	4	5	5	5
4	4	5	5	5	6	6	6	7	7	7	1	1
7	7	7	1	1	1	2	2	2	3	3	3	4
2	3	3	3	4	4	4	5	5	5	6	6	6
5	5	6	6	6	7	7	7	1	1	1	2	2
1	1	1	2	2	2	3	3	3	4	4	4	5

Spot	Oligo Concentration (µM)
0	Nothing
1	0
2	0,1
3	0,5
4	1
5	5
6	10
7	20

The epoxy slide and one of the isothiocyanate slides were treated with a standard protocol for microarray oligonucleotide coupling (see Appendix A). The other isothiocyanate

functionalized slide remaining was treated according to Manning et al. [250, 251] (see Appendix A) Fluorescence intensity was evaluated following the first protocol optimized for the attachment of DNA oligonucleotides to an epoxy functional slide [400] shown in Figure 52a, an isothiocyanate functionalized slide Figure 52b.

The results show very similar results and comparable spot size between the two types of slides almost independent of the immobilization protocol followed.

The Figure 52c shows the fluorescence result for the isothiocyanate silanized slide following the protocol optimized for attachment of DNA onto glass. In all cases, the bottom array (framed in red in Figure 52 a,b,c) is taken into consideration as the top array shows on the third slide some smearing of the silane. When the concentrations of the oligonucleotide exceed 5μM in all cases a saturation signal can be seen and even if it is increased further, the fluorescence signal remains reasonably the same. Therefore a further analysis is done in the linear part of the graph in Figure 52 (inset). The results show that the ITC-functionalized slides are capable of binding the NH_2-DNA-fluorescence with nearly the same amount of fluorophore molecules. For example at a concentration of 0.5 μM of the fluorophore, the fluorescence intensity was about 19% less than the commercial slide when it was treated with the Manning protocol and if it is treated with the standard epoxy protocol, 5% less is obtained once the concentration is increased to 5 μM of the DNA-fluorescent molecule (Figure 52d graph). In the linear region the epoxy slide still shows a higher signal, but eventually it seems that the isothiocyanate slide gets closer to its values once the concentration is increased. With a little of optimization of the experimental variables (pH, temperature, concentration of the fluorophore, concentration of the ITCPTES silane on the surface, etc.) a silane for microarray oligonucleotide immobilization can be achieved with comparable results to that of the epoxy-terminated commercially available slides.

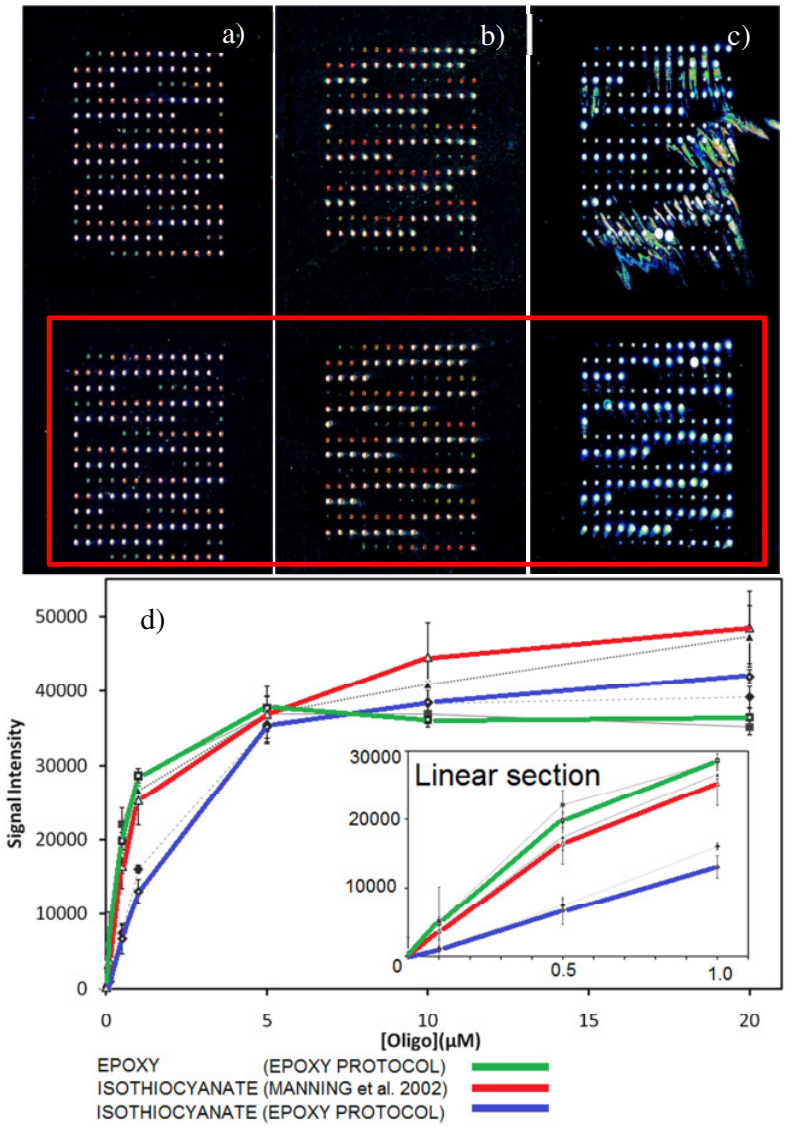

Figure 52.- Fluorescence evaluation of commercially available epoxy slides versus isothiocyanate in-house prepared silane. a) Epoxy slide treated with a standard protocol for DNA coupling, b) ITC slide treated with standard protocol as the epoxy slide and c) ITC slide treated with an optimized procedure for DNA coupling on glass slides. On the graph (d) the results from the fluorescence evaluation are plotted as signal intensity in arbitrary units versus concentration of the oligonucleotide used.

4.2.2.4.3 Assessment of Isothiocyanate Silanization Homogeneity Using the Microarray Spotter Instrumentation.

The homogeneity of the silane layer on the substrate is important for applications in fluorescence microscopy as well as in biological essays. Fluorescence experiments were performed to determine the uniformity of the coating in case of a large sample (more than 1x1 cm^2). In this experiment, several glass slides functionalized with ITC-silane according to Zeira, et al. [35] were used and coupled with NH_2-Fluorescein according to

section 2.1.1.3 of this dissertation. The fluorescein experiments showed, that although on a macroscale pattern (cm^2) the uniformity was not as expected, on a microscale (μm^2 to 1 mm^2) they confirm very good results (as shown in Figure 53).

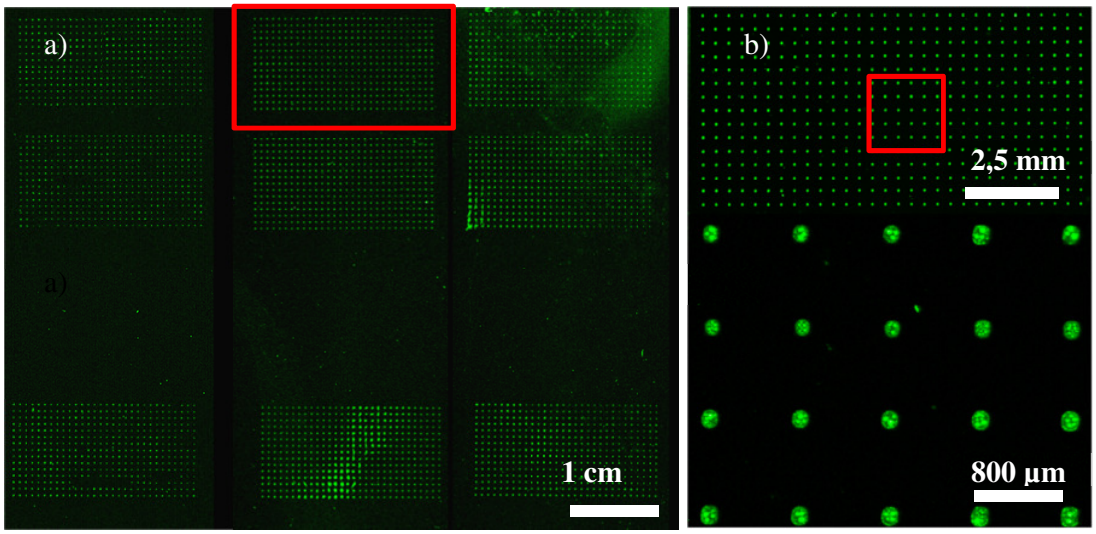

Figure 53.- Microarray homogeneity experiments. Three regions were evaluated along the longitudinal axis of three slides silanized the same way for statistical analysis. a) Slides used for the experiment, in order slide 1,2 and 3. On the right b) zoom-ins on Slide 2, on the framed areas.

This means, over the total area of a glass slide of around 5 x 3 cm, it cannot be assured that a homogeneous monolayer of the silane will form under the conditions applied (variable humidity, variable temperature, variable pressure, manufacturer variability of the substrate, undetermined concentration of the in-house synthesized silane, etc.), but if the glass slide is sectioned around 1x1 mm areas, then the coating might be proven consistent enough to couple biomolecules on at least a 1x1 mm single region. On glass with no fluorophore attached, background fluorescence due to the isothiocyanate is slightly present. Four arrays of 30x15 points per array were placed onto each slide with the same needle and from the same solution with aminofluorescein in aqueous buffer solution. The concentration of the dye is 0.01 mM in a 9.0 pH buffer (Boric acid/Potassium chloride/Sodium hydroxide). GenePix 4000B Microarray scanner (Molecular Devices) was used to scan the glass slides and assign a fluorescence intensity value, although with arbitrary units, the relative differences can be measured. The experiment has been repeated three times with three different probes for statistical analysis. An average of the spots on each row is calculated through the native software from the microscanner maker (Genepix Pro 7.0) then plotted for each region. The slides were treated simultaneously with the cleaning solutions, but silanized in three different new flasks. The silane solution was created in a single flask and then distributed in the

silanization flasks evenly. In this matter, the variability for the experiment is reduced to: different glass containers for the silanization and different glass slides (manufacturer variability of the slides). The rest of the conditions for each slide were kept equal. After the silanization is done, the slides are taken to a local spotting machine (Genemachines Omnigrid 100). Three regions can be recognized for each slide: the upper, middle and bottom region represents three different regions for microscanner spotting. Each region can be analyzed separately for each slide in order to assess the homogeneity behavior within the array. Furthermore the values can be compared against the three arrays to assess the homogeneity within the slides. Additionally the results are also normalized within the slides, so it is possible to compare different parts within the three slides. The analysis of the images in Figure 53 is carried out using the native software from the microscanner (genepix pro 7.0). The three slides were analyzed using the same gain and power of the lamp in order to be comparable and further assignment of the dots was done manually if required.

To analyze how well the fluorescence intensity is distributed along the slide, the spots were evaluated individually and their total intensity was plotted along its position in a determined column-row. When analyzing the intra variation of the slides, it can be seen along the longitudinal axis that the tendency does not extremely change either. A difference can be seen at the lower end of the slides showing a higher variance from the rest of the slide. The standard deviation is around 20-30 % of the mean value. The fluorescence intensity of the spots remains almost constant along a single slide when analyzed. A normalized plot is shown in Figure 54. Homogeneity will be assessed according to whether the fluorescence is deviated from a mean value. In this case, for each region of each sample, a mean value is calculated and all the data corresponding to that array is then normalized against that mean value. The colors in the graph represent how much they deviate from the mean value calculated. Red and green normalized values represent similar fluorescence intensities within the slide. The three arrays are placed near to each other on the plot to simulate the whole slide. On the X-axis the column position is plotted (from 1-15), and on the Y-axis the row position is plotted (from 1-30). The z-value is the normalized fluorescence intensity of the respective spot.

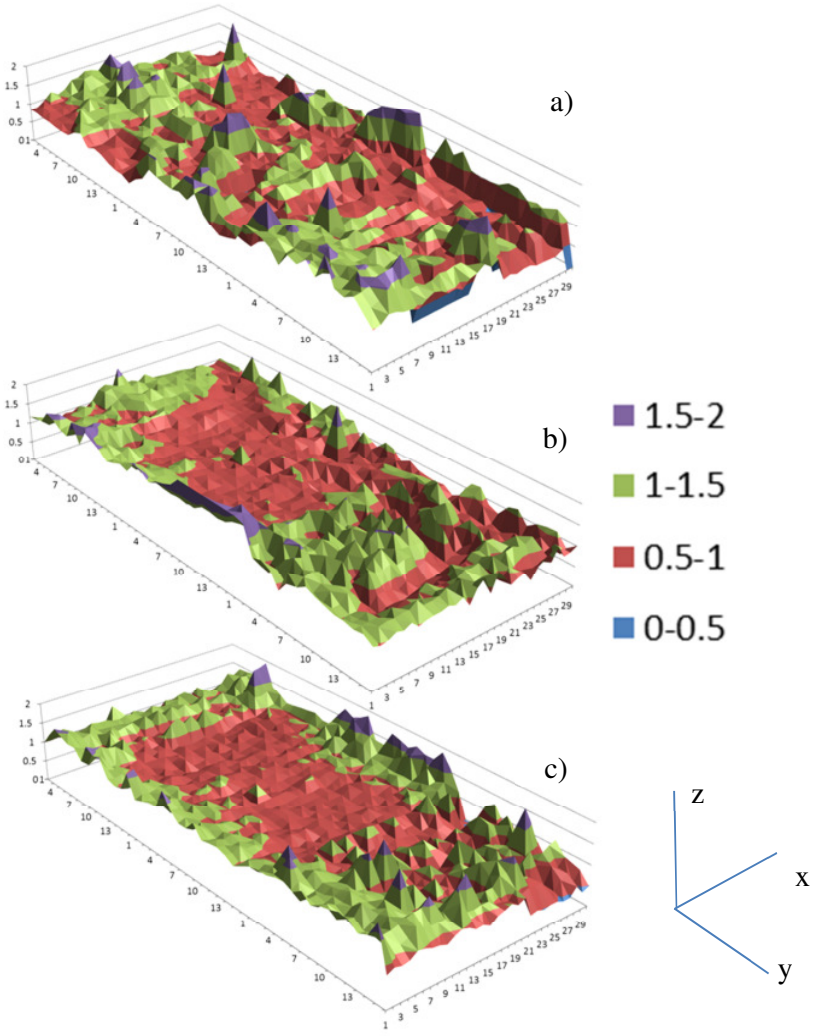

Figure 54.- Normalized surface plot of Fluorescence intensity along the slide. On the Z-axis, the fluorescence intensity, on the X-axis the column number and on the Y-axis the row number from 1 to 15 for each region of each slide. a,b and c, corresponds to slide 1,2 and 3 of Figure 56 respectively.

From the experiment it can be seen in Figure 54 that there is a homogeneous tendency within the ITC-silanized slides towards the middle region (red and green color) and this tendency is only valid when small areas are investigated (5x5 mm^2). When examined, the arrays show a slight tendency towards a higher fluorescence intensity when the position of the spot is closer to the edges (either longitudinal or transversal). The results from the three slides show that for all areas along the three slides, this behavior keeps constant along the width of the slide.

When analyzing slide 1 (Figure 54a), the fluorescence intensity values are lower and less uniform than on the other two, This observation can be appreciated better in Figure 54b&c, when comparing the first slide with the second and third one. On the third slide, a more homogeneous part tends to be found in the center of the slide, while on the first slide a higher degree of heterogeneity is found. This confirms that the silanization

procedure is variable even when maintaining the same conditions. Wieringa [401] applied amino functional silanes to glass surfaces and compared between microarray assay performances of three different silane layer thicknesses (monolayer, 2–3 layers, and multilayers) deposited using different techniques. He concluded, as other authors [42, 116, 122, 131, 136, 402], that the variability of the silane is inherent in the multiple variables involved in the silanization procedures. Additionally DNA array technology possesses many sources of technical variability that are an obstacle to obtaining high quality data sets [403-405]. In order to reduce such data discrepancy, the need for extremely homogeneous silane layers is essential. Such homogeneity can be attained through one-molecule thick layer coverage of the silane on the glass surface, although achieving complete monolayer coverage along big areas is very difficult. Thicker films can have three-dimensional aggregate structures or "islands" of multilayers and hence results in a large variability in the performance of the DNA assays. Therefore there is a chance of incomplete coverage in the case of the monolayer coatings, and poor reproducibility for multilayers coverage [403, 404].

Figure 55 shows the summary of the results from the homogeneity assessment experiments.

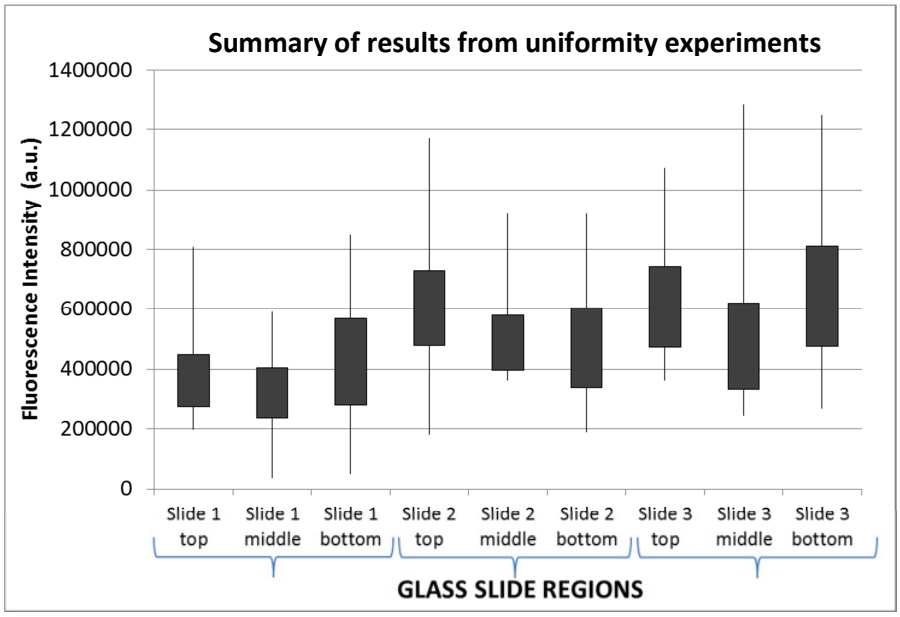

Figure 55.- Sumary of statistical analysis on fluorescence homogeneity experiments. This summarized results are taken from the plotted intensity of each dot regarding their position along the slide as shown in Figure 53.

Alongside this evaluation, it is important to define some reasons for the inhomogeneous coating from the isothiocyanate silane. The environmental factors such as humidity influencing the experiments (around 60% r.H.) can also responsible for a higher

condensation rate of the silane on the open end of the silanization glass and further inhomogeneity along the slide. A way to overcome these difficulties could be the use of a chemical vapor deposition approach and enough time to form a well-ordered silane monolayer. Exhaustive work has been already published in the search for a greater homogeneity of silane monolayers [34, 102, 113] and questions such as the extent of crosslinking among the molecules or the relative distribution of covalent bonds, hydrogen bonds and electrostatic interactions are still yet to be solved. From the experiment there can be concluded two main things: i) the slides hold variability within each other when the fluorescence evaluation is performed (due to the inhomogeneous coating of the ITCPTMS on larger areas) and ii) small areas of evaluation yields higher homogeneity than larger ones, meaning that larger areas than 25 mm^2 will give a different fluorescent intensity in average. Ambient humidity plays a very decisive role in the thickness of the silane layer as remarked by Zhu et al. [34]. Therefore, very demanding conditions must be implemented to create an extended monolayer.

4.2.2.4.4 Dip-Pen Nanolithograpy (DPN)

The chemical one-step coupling of the ITC-silane to the oxidic interface of the surface offers the opportunity to apply a Dip Pen Nanolithography (DPN) technique to create arrays of ITC-terminated spots on oxidic surfaces (specifically glass coverslips). With this method not only the size and the distance between the functionalized spots can be reduced to sub-micron dimension but also the density as well as the shape of the structures can be varied arbitrarily accordingly to the needs of the experiment [89, 210, 406, 407]. The oily texture of the silane makes it appropriate for this technique as the silane will slide through the tip very slowly allowing a better control of the size of the drops deposited on the substrate. For these experiments, the reason why the transfer of the silane was carried out onto glass coverslips is that they are better suitable for any light-fluorescence-microscopy examination afterwards as also it was the standard substrate used in the Dip pen machine.
In this section, Dip Pen Nanolithography was used to test the selectivity of highly ordered functionalized areas in order to test the ability of the technique to immobilize either particles or DNA molecules. The experimental setup for assessment of the reactivity of the ITC silane towards the amino terminated molecules was carried out (as shown in Figure 56) following two approaches: (a), fluorescence and AFM imaging of

isothiocyanate silane spotted on samples treated with 5-aminofluorescein were done and (b) a second experiment involves the introduction of amino functionalized silica nanoparticles with a diameter of approx. 50 nm, (kindly provided by Dr. Martin Silvestre, from Franzreb research group, Karlsruhe). The particles were deposited by placing a drop of solution containing the particles on top of the functional structured area and incubate it in a humid chamber for 18 hours, washed extensively and then further examined by AFM. The goal of this later experiment is to prove the specificity and reactivity towards different amino functionalized particles and the ability of the isothiocyanate group to immobilize eventually heavier and longer particles (such as TMV-like particles).

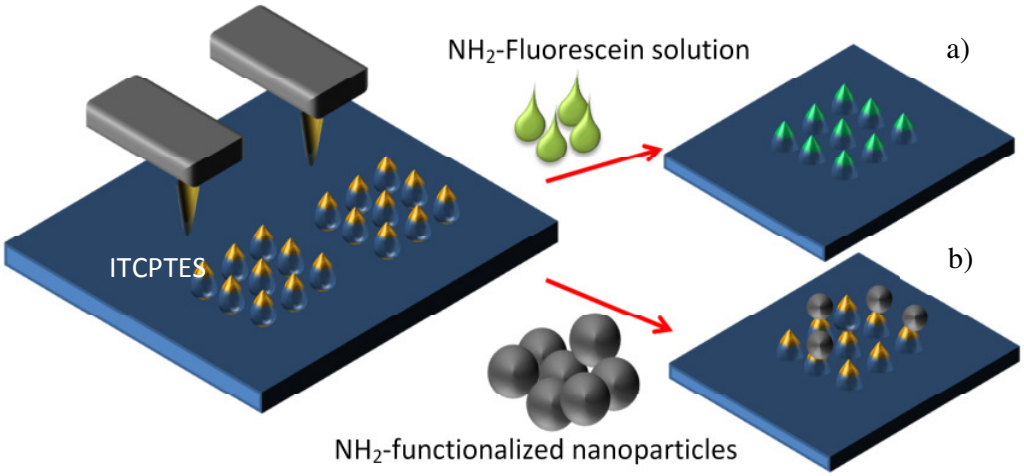

Figure 56.- Scheme for Dip Pen Nanolithography experiments. a) aminofluorescein deposition for assess of the chemical reactivity of the ITC-group, and b) aminofunctionalized nanoparticles deposition selectively on functionalized spots to address the ability of the ITCPTES to immobilize particles.

The experimental conditions are described in the protocol in section 3.1.1. Different controlled humid conditions were examined under normal optical microscopy and under AFM (20%, 30%, 40%, 50% r.H.). The result from the optical microscopy investigation of the samples after spotting with the custom-made received ITCPTES using the DPN technique before any treatment is shown in Figure 57. Fluorescence microscopy was carried out instantaneously together with AFM investigations and is described in the following chapter.

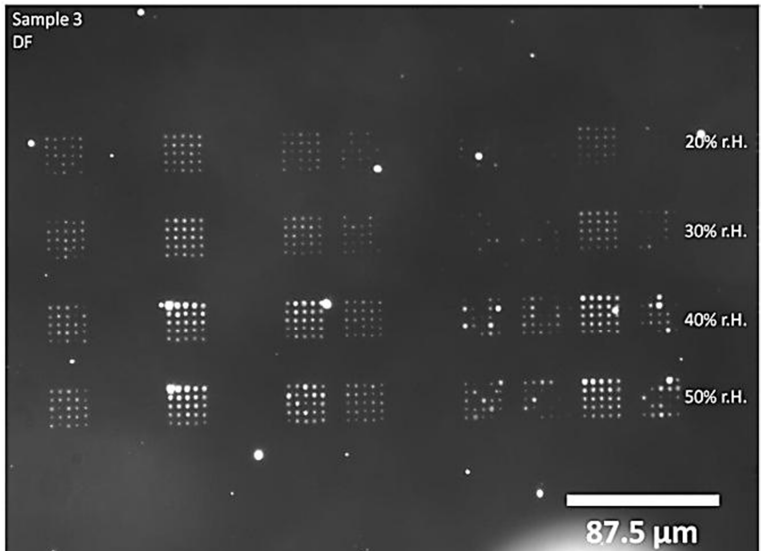

Figure 57.- Dark field light microscopy images from DPN received sample. All the samples were done following the same procedure. Upper row of spots in the sample belong to 20% r.H increasing up to 50% r.H .

Fluorescence - AFM Investigation on DPN Immobilized ITC-Silane

The deposition of the microdrops of ITCPTES takes place when the cantilever tip is in contact with the surface, and depending on the time the tip is in contact with the surface the greater the amount of silane running down from the tip due to the humidity. The alignment of the cantilevers along the chip was not perfect and therefore the distance of the tips regarding the surfaces might hold small differences which can be seen in the pattern in Figure 58 e.g. some patterns in the fluorescence image are brighter than others due to the amount of silane deposited, due to the deflection of a single cantilever on that line, due to the humidity of the chamber leading to a wider spreading of the spots, etc. From the fluorescence investigation it can be noted that the features are created in a very ordered way, and that coupling of fluoresceinamine occurs site selectively on the spotted silane. For reference, the first row is the beginning of the production of the array and each cantilever prints 5 spots before it moves forward with the next row. While the drops are getting smaller within the array production as less amount of silane remains in the tips (as shown in Figure 58b), the humidity increase (20-50% r.H.) keeps the drops growing in diameter. This can be seen on the fluorescence image (Figure 58a&b) by the increase in drop diameter when the humidity in the chamber is changed. To investigate the spots in more detail, AFM investigations were carried out. Figure 58c&d shows the results of an

AFM topographic investigation of drops with different sizes going from the top row to the bottom row on a 5x5 µm array.

The AFM height profile (Figure 58c) shows that the silane has been polymerized. The expected height for an ITC-silane monolayer is theoretically 1.5 nm. The silane spots in this experiment possess an average height of 60 nm, which corresponds to a multilayer formation (polymer interpenetrating network) because the silane is not washed away immediately after the spotting, in order to avoid any unspecific smearing of the drops all over the substrate.

Although the sample is still relatively heterogeneous regarding to spot sizes, the goal of a chemical patterning with silane on a small scale is achieved nevertheless.

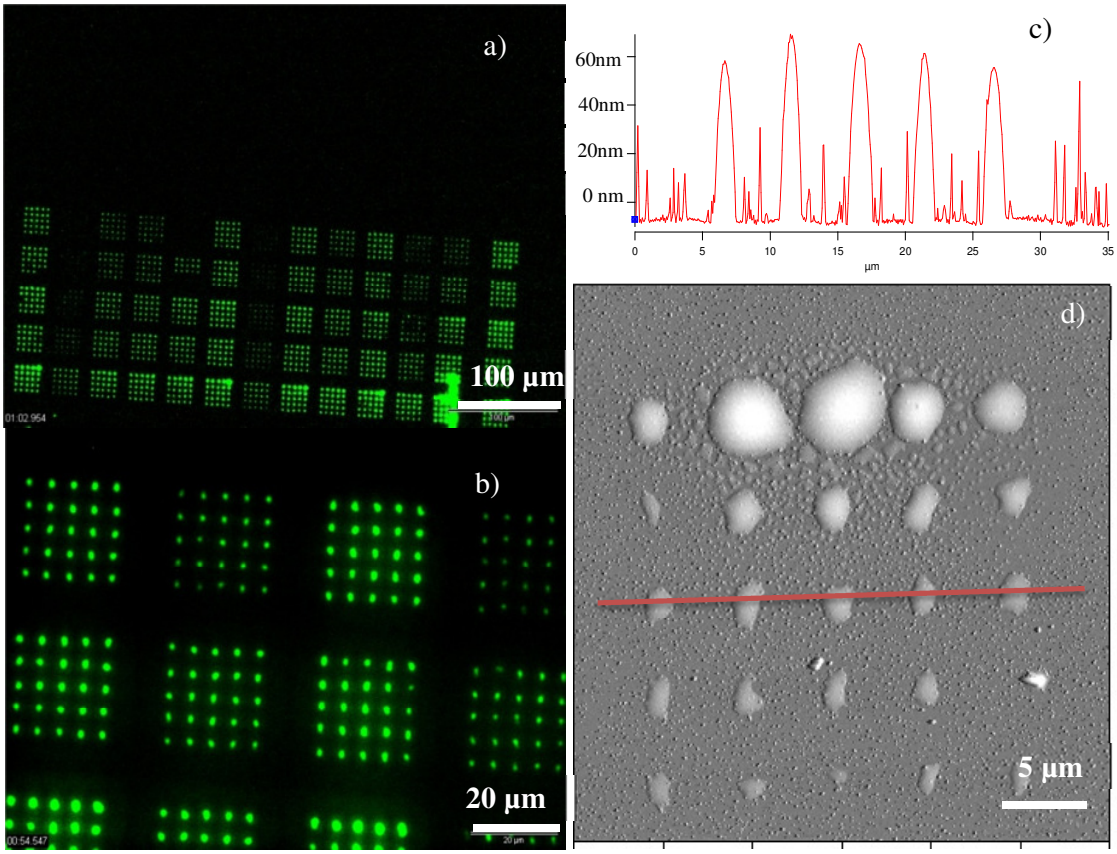

Figure 58.- a) Fluorescence image of DPN produced spot array on sample 1. b) a 10x magnification picture showing also the spotting patterns of the ITCPTES varying with the relative humidity of the chamber. AFM topographic image of a random pattern in the 50% r.H. row on sample 1. On the top (c) a profile of the middle row of the 5x5 array and bottom right (d) a topography AFM image of an aleatory patterned area.

Morphological Examination of the Aminofunctionalized Nanoparticles Immobilized by Patterning the Substrate with ITC – silane Using Dip Pen Nanolithograpy.

In the second part of the experiment the ability to couple amino functionalized silica nanoparticles and further selectively attach them into the ordered arrays is investigated. The experiment objective is to prove if the isothiocyanate silane chemistry is stable and robust enough to be able to immobilize heavier particles (~50 nm diameter) and if the immobilization is able to withstand ultrasonic rinsing and rinsing flows.

After the ITCPTES was spotted on a cover slide using DPN (Figure 57), the sample was washed with water and methanol. Then it was dipped into a solution containing iron-cored silica nanoparticles coated with 3-aminopropyltrimethoxysilane (Sigma Aldrich, Germany) with a size distribution centered at 50 nm. The coverslip was placed vertically to avoid any fixation of the particles just by gravity and subsequently adsorption of the particles in the silane polymeric matrix.

In the experiment the attachment of the nano-particles on the ITCPTES silanized spotted areas was demonstrated, but as the substrate also contained small silane residues (as shown Figure 59b) the attachment of the particles was not highly selective. In Figure 59 the results from AFM topographical examination of the pattern is shown. The pattern seems to be partially washed away by the particle solution and therefore the spots loose the circular shape and additionally the height is reduced from 60 nm to 15 nm. Nevertheless the ITCPTES spotted areas are able to allocate the particles in them. In black, the dots are better recognizable on Figure 59c-d. They seem to belong to a different material than the rest of the image. The ITC silane is also recognizable as different from the surface (Figure 59c). In summary, the amino-functionalized-nanoparticle deposition experiment on ITC silanized spots (using DPN) proved that it is possible to selectively immobilize heavier particles. This is a helpful preliminary result in order to use of this technique in the bio functionalization of surfaces by selectively immobilizing DNA-linker on DPN-spotted coverslips for the subsequent TMV self-assembly process.

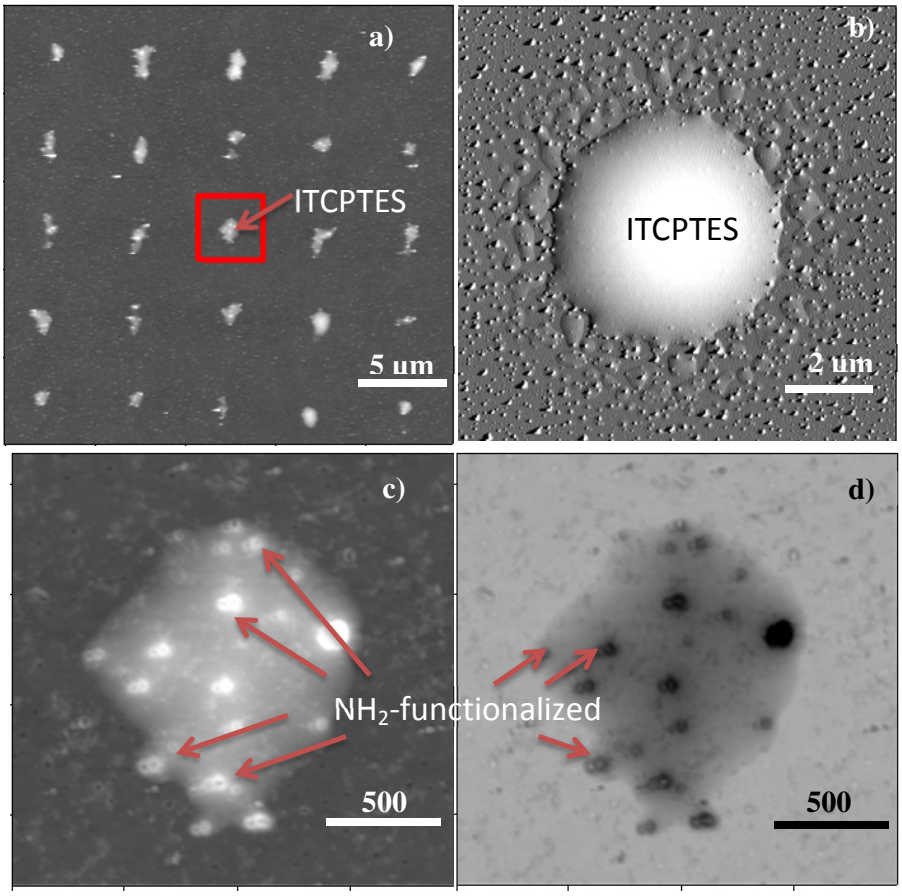

Figure 59.- AFM topografical examination on a DPN array produced with isothiocyanate silane. a) images from the sample 4 array after the washing and incubation step (ITCsilane sites on white). b) topographical image of a random single spot before any treatment and washing is performed. c , d) filtered images using the software to enhance the contrast between the particles and the substrate (in d) case the particles are shown in black). Upper row a 25x25 micron scan area was selected (a,b) and on the lower row a 3x3 micron zoom on

4.2.3 Characterization of Physical and Chemical Properties of Isothiocyanate-terminated Surfaces on Polymeric Substrates (PDMS).

To successfully transfer the silane chemistry to a polymer, it is necessary for the polymer to fulfill some important conditions: i) a polymer resistant to the solvents of the silane is required, ii) easiness to coat on a substrate or structure by casting and iii) ability to create an oxidized surface.; in this case polydimethylsiloxane (PDMS) is a very common and useful polymer which fulfill the previous requirements. The polymer is oxidized and then the isothiocyanate silane chemistry can be transferred to the surface. This transfer of the chemistry will be evaluated in the same way it has been done for the pure silica wafer substrates.

There are two ways to morphologically structure the PDMS: using spin coating, which consist in an apparatus which rotates at specific angular speeds and has the ability to effectively disperse a drop of a solvent placed on top of a sample across the surface in a very homogeneous way, and the other way is to cast a polymer by use of a master (previously created by other lithographic techniques, most commonly e-beam lithography). In this way, polydimethylsiloxane can be casted in different shapes according to the masters employed. In this work, AFM calibration grids and SERS-analytic substrates have been used as useful and well-ordered masters for different uses.

In order to achieve a proper silanization on the polymer, ultraviolet irradiation combined with an *in situ* production of ozone by two different wavelengths (184.9 and 253.7 nm) is used for the treatment (the procedure is explained in chapter 3.1.2). After the exposure to UV/O_3 the surface undergoes oxidation and radical attack as suggested by Egitto and Matienzo [172].

A low pressure mercury lamp was used to produce ozone together with the UV emission lamp. This lamp emits light in the 185 nm wavelength. Due to the strong absorption of atmospheric oxygen molecules at 185 nm, they dissociate into atomic oxygen which in turn reacts with molecular oxygen to form ozone. Both the atomic oxygen and ozone can in this way react strongly to organic substances [408]. UV light produced by the lamp and subsequently absorbed by polymers may produce free radicals, formation of excited molecules or even some ions on the surface. Eventually the oxygen species will react with the polymer (radicals, ions or molecules) releasing low molecular weight compounds, like carbon dioxide, water or other small volatiles which can desorb from the interface.

In the case of PDMS, the treatment will not remove any organosilicon compounds but an effective removal of the hydrocarbon part takes place while the silicon oxide remains on the surface. A brittle thin layer of silica is then formed and with this several oxidic species are present on the surface available for silanization [170]. In our experiments with a single substrate sample, a selective irradiation is done by covering partially the surface with a mask. For the evaluation of the topography and elastic modulus, half of the sample is then activated with UV/O_3 and silanized and the other half remains untreated. This process is depicted in Figure 60.

AFM topography analysis has been performed to investigate the topography effect of the irradiation on the polymer surface. Additionally force mapping experiments have been performed to evaluate the change in the elastic modulus from the material. Three properties have been evaluated in order to confirm the transfer of the ITCPTES to a

PDMS: (1) wettability (contact angle), (2) elementary composition (XPS) and (3) chemical reactivity (fluorescence microscopy). A final confirmation on the transfer of the ITCPTES to the oxidized PDMS will be done with the bottom-up self-assembly of tobacco mosaic virus in the next section.

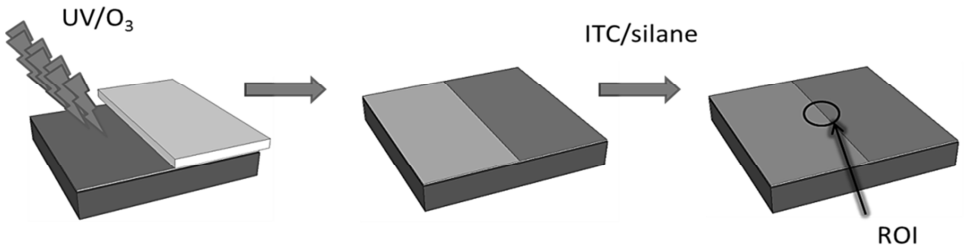

Figure 60.- Procedure of selective irradiation and further functionalization of PDMS. A non transparent mask covers partially the substrate allowing the exposed part to be oxidized and transformed into a silica like layer which in turn is isothiocyanate silanized. Afterwardss the evaluation takes place in the interface of the two regions.

The mechanisms of the thermal, photo thermal and photochemical oxidation reactions have been already systematically and thoroughly studied before [173-175, 177, 178, 180]. Generally it is suggested that the abstraction of hydrogen is the initial step. A methylene radical reacts with oxygen to give a peroxy radical and rearranges in the silanol group. A more detailed scheme of mechanisms responsible for the oxidation and further hydrophobicity recovery of the polymer on the surface are shown in the introductory chapter [162, 178, 409-416].

A plausible explanation about the mechanism and the way the PDMS is oxidized was proposed by Delman et al. [415] and it is shown on the following simplified reaction scheme.

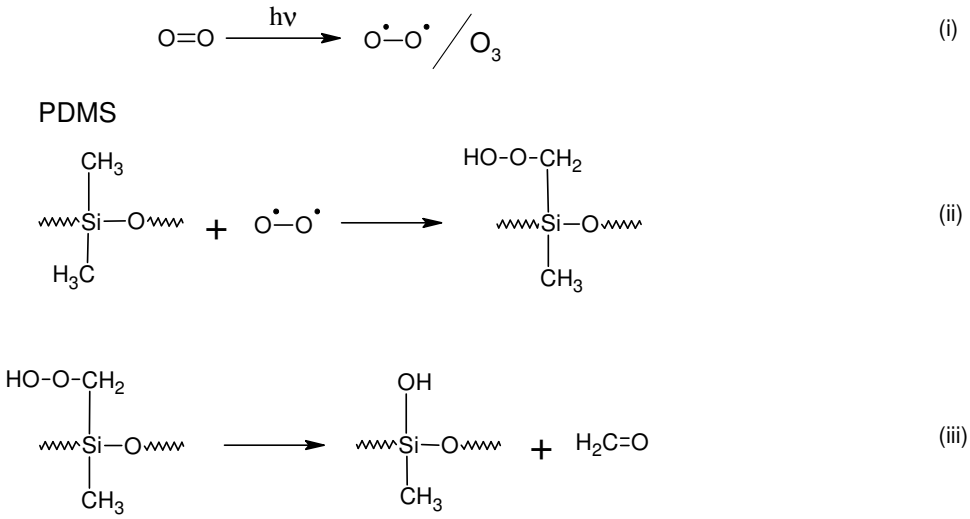

Figure 61.- Reaction scheme for the PDMS irradiation process using an UV/O_3 lamp. i) the UV light at 185 nm wavelenght transforms the oxygen in the air in reactive radical and ozone. ii) the ozone in combination with the UV attacks the methyl group of the upper layer of crosslinked PDMS leading to formation of further oxidized groups. iii) further reactions lead this oxidated species towards the formation of hydroxyl groups on the surface.

It can be assumed that other species and intermediates arise during the oxidation process (aldehydes, carboxylic acids and carbonyl groups) [187]. It can be expected that a very small percentage of the converted methyl groups will remain in these forms while the irradiation takes place. Surface oxidation by electrical discharge, plasma treatment or UV/O_3 exposure, produce a silica-like layer on the polymer. However, the silicon elastomer has the characteristic of recovery its original hydrophobicity once the treatment ceases.

4.2.3.1 Morphology and Roughness

Atomic force microscopy examination was performed on the substrate to evaluate how the surface is changed morphologically after oxidation and further silanization. The following image is an AFM topographical examination on the interface between the protected non-irradiated area (Figure 62a) and the irradiated and ITCPTES silanized area (Figure 62b). Figure 62b shows on the left a selectively irradiated half of the sample, while the other half remains untreated by covering it with a silica wafer. Figure 62a & c, a non-irradiated sample showing a wider area with a more pronounced flatness. The color scales shown in the figure are within 5 nm range. In Figure 62b & d it can be observed that the irradiation seems to affect the area in a microscopical way, modifying the surface. A small trench appears in the middle of the scan as consequence of the surface reactions taking place on the interface. Some of the features in the irradiated/silanized area remain with a circular irregular shape due to the ultrasonic treatment during silanization. This treatment creates micro jets which punch into the surface at high pressure perforating and disrupting the brittle silica-like layer [417]. Phase imaging is also performed showing a very defined shift in the phase of the irradiated area and the protected area (Figure 62d). Similarly to the non-treated substrate (Figure 62a), the portion of the substrate been protected from irradiation in the silanized sample (left area on Figure 62b), shows a higher phase shift of approximately 140°.

When the silane is applied, partial hydrophobic recovery takes place and disrupts the silica layer in addition to the condensation of the silane on the surface. This causes an increase in the roughness of the substrate (3.2 nm) as shown in Table 13 where the values are summarized. Roughness values after irradiation are comparable to those with silica. As the PDMS was casted as a replica using a clean silica wafer, it is to be expected that the flat non-treated PDMS substrate will have a roughness very close to that of the silica

wafer from which it was created (980 picometers), but after the irradiation/oxidation process, the homogeneity of the surface might increase as some of the polymer becomes crystalline and resembles the silica wafer surface (218 picometers). The roughness of the sample is comparable to the one from the silica wafer before and after silanization. An island formation is also noticeable on the substrate.

Table 13.- Roughness data for the PDMS before and after UV/O_3 treatment with further isothiocyanate silanization substrates.

Roughness Data Parameter	Pure/no treatment	UV/O_3 treated	ITC silanized
RMS:	**980 pm**	**250 pm**	**3.2 nm**
Average Deviation:	475 pm	218 pm	757 pm

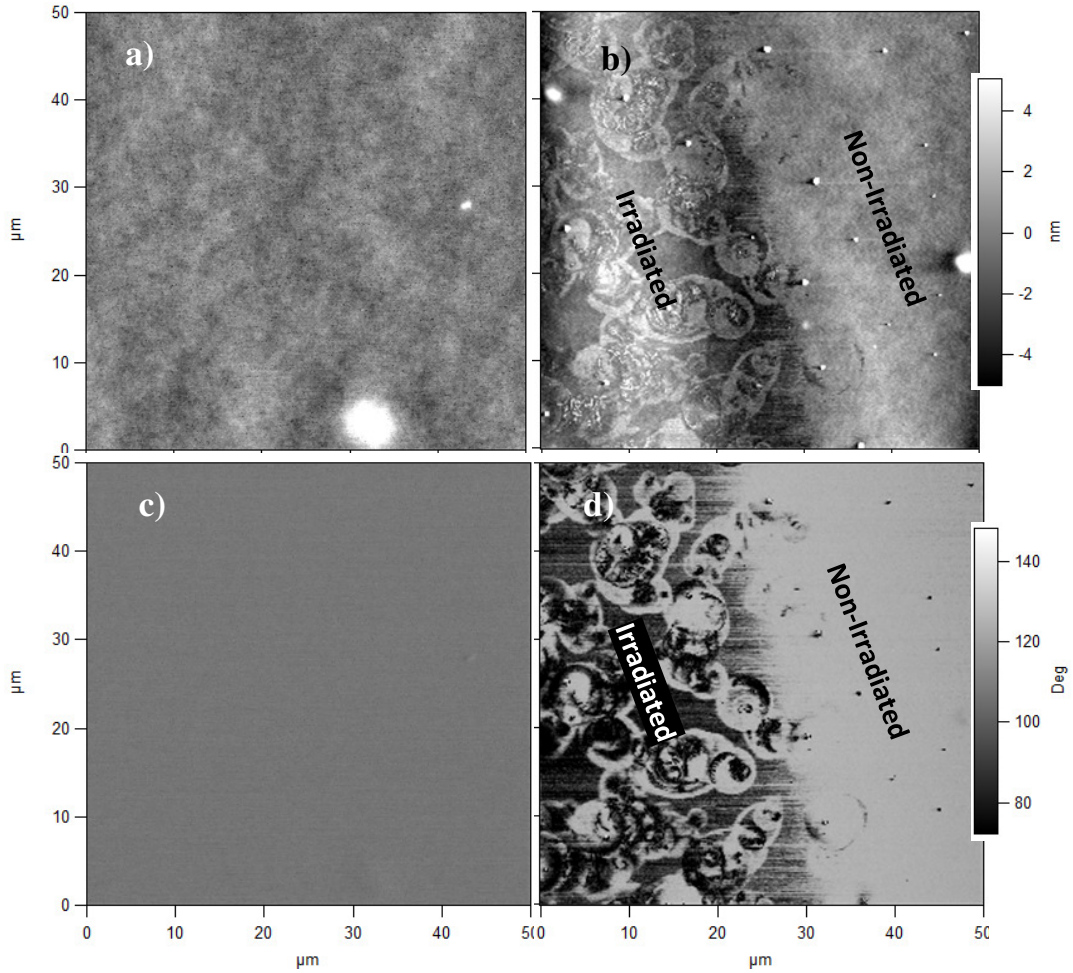

Figure 62.- AFM topography images of PDMS substrate before (a) and after the irradiation with a UV/O_3 chamber through a mask and further silanization (b). AFM phase contrast images are shown in the same layout c) for non irratiated samples and d) after irradiated and ITC-silanized substrate.

Phase imaging is very useful for this evaluation, in which the topographic analysis gives no further information. By mapping the delay response of the cantilever oscillation during the intermittent-contact scan, phase imaging can detect variations in composition, adhesion, friction, viscoelasticity, and other properties. Unfortunately phase imaging cannot identify the kind of material it is sensing (no chemical information), but it is still very useful for producing contrasting areas on heterogeneous samples. The phase shift can be thought as a delay in the oscillation as it moves up and down during a taping mode scan while in and out of contact with the sample regarding to the free oscillation of the cantilever in air. Garcia and Tamayo [418, 419] suggested that the phase in soft material is sensitive enough to map adhesion forces and viscoelastic properties. On the phase contrast image, topographic changes are not involved, and it is independent of the scan size or the features sizes. In the following Figure 63, a phase image analysis of the same experimental procedure but on a different sample is presented. On the left side, a non-irradiated area, and on the right side, an area irradiated for 6 hours (not continuously) is shown. A very pronounced shift between the treated and non-treated areas of around 20° is in agreement with Garcia and Tamayo [418, 419] observations for soft samples. The phase shift increases as the sample viscosity increases and the elastic modulus decreases. Therefore a harder material should be found on the irradiated side which shows lower phase shift (95°) than on the left side showing a higher shift (120°). This is shown in Figure 63.

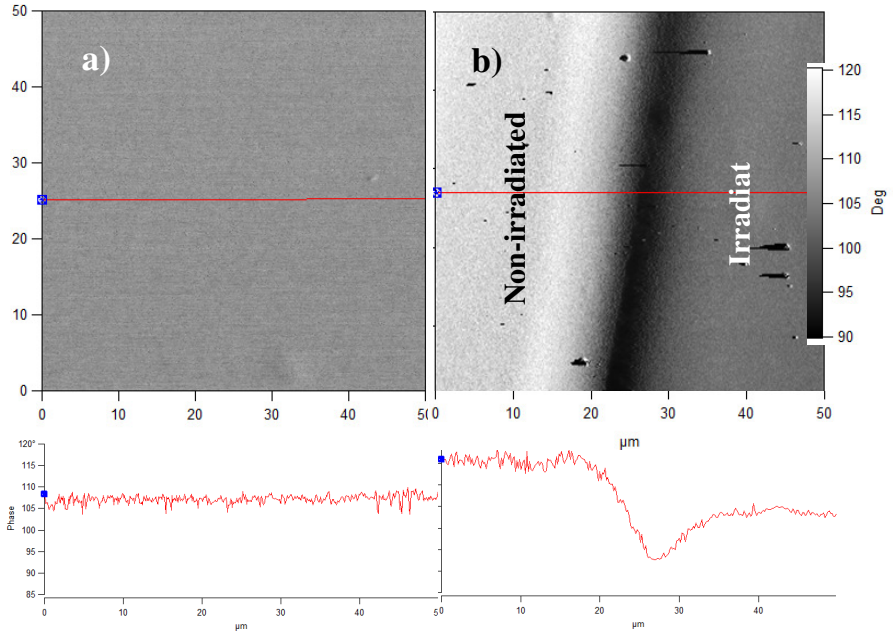

Figure 63.- AFM phase contrast image of PDMS substrate before (a) and after the irradiation with a mask (b). On the right, the picture can be divided furthermore in a irradiated area on the right and a protected area on the left.

Atomic Force Microscopy – Force Measurements

Further examination regarding the elastic properties of the material before and after irradiation was performed. Force measurements were done with the help of the AFM following the procedure from Bar et al. and Meincken et al. [420, 421]. The theory behind this characterization is extensive and has been review by many authors [422-427], therefore a very brief explanation will be given. When forces are measured in the cantilever-surface system, five regimes and effects can be recognized. While the cantilever is far away from the surface, there is no deflection affecting the cantilever and the curves therefore are a constant line both during the approach and retract of the tip. After the tip is getting in contact with the surface, repulsive and attractive forces will interact with the tip. This will cause a "snap-in" effect on the cantilever towards the surface. Afterwards, the tip is fully interacting with the surface and a constant compliance deflection is measured by the photodetector. Once the cantilever is retracting, attractive forces of the surface will cause the cantilever to deflect even at positions further from the surface, as the ones when it first snapped into. This will mostly cause a negative deflection on the cantilever and further when the force of the piezo overcomes the adhesion force of the interface, the lever will "pull-off" suddenly (Figure 64).

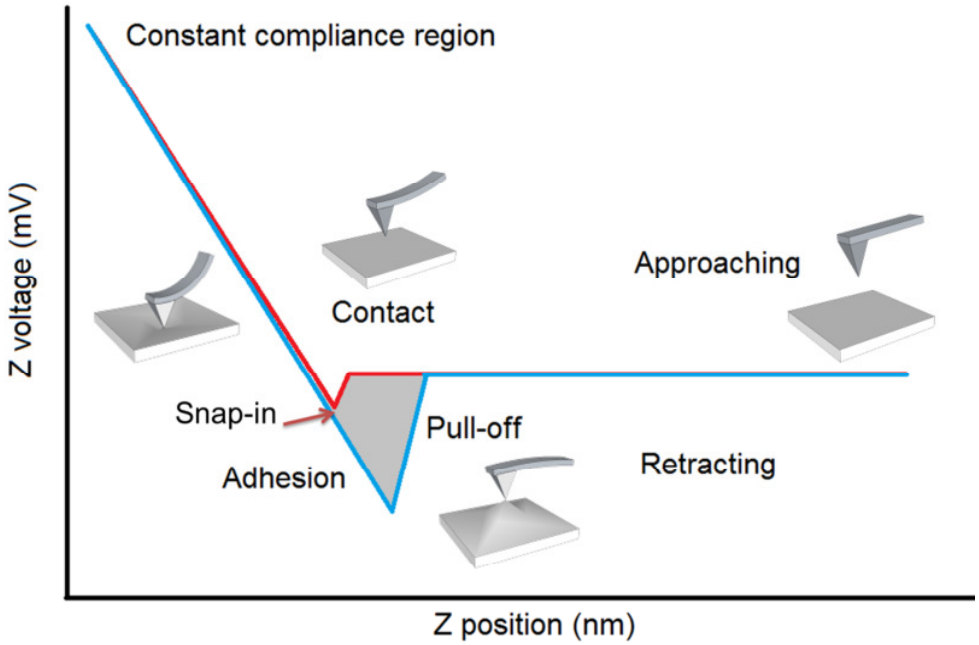

Figure 64.- Scheme of different regimes when recording an AFM force-distance curve. During the approach of the cantilever onto the substrate, attractive forces cause a snap-in into the substrate, the piezo continue the hard contact regime on the constant compliance region, and when it reaches the deflection set point, a retracting movement is started. The adhesion force between the AFM tip and the substrate cause the bending of the cantilever on the opposite direction until the force of the piezo retracting overcomes the adhesive forces.

In contact, a difference between the approach and the retraction is caused typically by plastic or elastic deformation of the substrate. Normally an elastic deformation should not lead to a hysteresis of the compliance region. In case of non-treated PDMS a hysteresis for the force-distance curve is found in the compliance region of the measurements (see Figure 65 and Figure 66), probably due to an adhesion force between the cantilever and the polymer and also the material is recovering slower than the retracting step of the measurement. Additionally, adhesion work is found on the retraction movement of the cantilever (gray area on Figure 64) bending the cantilever again with the opposite curvature.

From the experiment, the adhesion force has been calculated following the routine software of the microscope. The work of adhesion (W_a) is proportional to the force F_{ad} as the following equation suggest:

$$W_{ad} = \frac{F_{ad}^2}{2k_c} \quad (7)$$

where k_c is the spring constant of the cantilever.

The higher the work of adhesion the higher the forces of tip-substrate adhesion force. The specific parameters used for the calculation of this adhesion force experiment, work of adhesion, and further elastic modulus are shown in Table 14

Table 14.- AFM parameters used for calibration of the system in order to perform force-distance measurements.

Microscope parameter	Value	Explanation/ comment
Virtual deflection	-16.71 mV/µm	Virtual deflection is a mechanical coupling of the deflection signal with the Z movement. Mostly calculated in air.
Spring constant	9.97 nN/nm	In Hooke's law the stress is directly proportional to strain F=-kx (where k is the spring constant)
Deflection InvOLS	53.25 nm/V	Inverse optical lever sensitivity. Measurement of how much the voltage measured by a position sensitive detector varies with the displacement of the cantilever.
Trigger point	200 mV	Value at which the piezoelectric device switch directions from approaching to retracting.

The force is calculated automatically by the following formula [428] using the microscope dedicated software:

$$Force\ (nN) = spring\ constant\ (nN/nm) \cdot DeflInvOLS\ (nm/V) \cdot set\ point\ (V) \quad (8)$$

To characterize the two different areas on the surface and their differences at the same time, a force mapping was done on the boundary between the treated and non-treated areas. As expected the functionalized area produces higher adhesion forces than the non-treated area. This might be due to the transformation from the highly hydrophobic surface into a more hydrophilic surface after the irradiation which attracts more the silicon oxide tip towards it. In Figure 65 two different values of adhesion work correspondingly to the non-irradiated and the irradiated/silanized areas respectively, can be observed. As discussed before, the phase image (reference to Figure 62d or Figure 65b) gives proper information about the region which has been functionalized (left one). A force mapping is carried out by acquiring a force curve for each point in a matrix (Figure 65c). The map consists of 10000 points taken (100 lines and 100 point per line) of a single force measurement as explained before and plotted into a graph (Figure 65c). The maximum distance the cantilever travels once it is in contact with the surface – which induces the cantilever to deflect up to a certain set point- was limited via the dedicated software. The set point for a trigger point in which the cantilever should retract was 200 mV signal of the photodiode. The deflection of the cantilever reaches the set point for deflection earlier on the treated region (steeper slope) than on the untreated (gradual slope), due to the harder material posing a higher resistance on the cantilever.

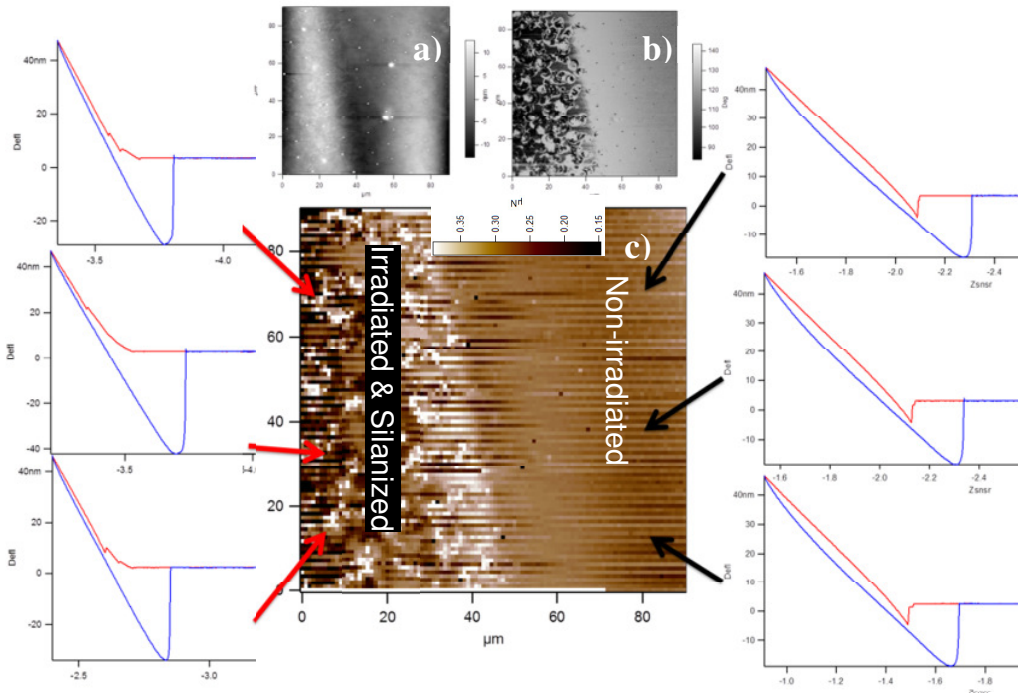

Figure 65.- Force mapping of a partially irradiated and silanized PDMS substrate. a) topographic image of the area in study, b)phase contrast image and c)force mapping image taken from the adhesion force calculated on the surface. On the left, curves taken randomly to show the force and adhesion on the cantilever after treatment. On the right, a non-treated area curves showing a higher elastic deformation

Each graph corresponds to a randomly taken single point in the force measurement map and gives information on the adhesion work of the cantilever with the surface. When this information (work of adhesion) is extracted from each point, then a plot of the adhesion forces can be done, which describes numerically the property change in the two areas (irradiated and non-irradiate). On the following graph (Figure 66), the two regions were plotted. 10 points were taken from each line at the beginning and then 10 points were taken at the end (total 1000 point per region of interest) in order to be sure that the areas are well separated between each other in the calculations. This is to exclude the transition zone between the non-irradiated and irradiated/silanized areas, and a proper evaluation can be performed. A smooth force acquisition graph was obtained from the pure untreated polymer, while that from the treated and isothiocyanate silanized area was somehow chaotic. This irregular behavior on the silane might be explained by three important factors: i) due to the hydrophobic recovery of the polymer with the time (also studied in the next section), ii) due to the lack of a complete silanization of the whole surface and iii) the pitting process taking place whenever the surface was exposed to the ultrasonic treatment involved in the silanization procedure (see chapter 3.1.1). It is important to remember that although the silica layer behaves like that of a polished wafer, it is less dense in hydroxyls than a pure silica crystal, and therefore lower attachment of silane is achievable. Although a silanization prevents the recovery of the hydrophobicity, there are regions where the silane is not effective (as we discuss previously).

As the histogram in Figure 66 shows a bimodal distribution can be seen from the data set: a first sharp amount of data corresponding to the non-treated area (light blue) showing an average adhesion force of 190 nm and second, a wider - but still normally distributed - set of data belonging to the irradiated area (orange) showing a 330 nN average adhesion force (Figure 66a). The transition between these two areas is also noticeable in the force map. This higher adhesion work/force can be explained by the formation of a water layer on top of the treated area as the silane produces a more hydrophilic surface than the non-treated PDMS. As this layer increase regarding a more hydrophilic interaction, then the cantilever feels not only the interaction with the surface itself but also with relatively higher capillary forces attaching the lever onto the surface stronger. It can be also noted, that on the compliance region of all curves, a steeper slope is found on the treated material than on the untreated region.

When the points are plotted in a single graph as shown in Figure 66b, a clear tendency can be withdrawn from the plot. The light blue curve, belonging to the non-irradiated

PDMS behaves initially linear with a very small slope. When analyzing the irradiated/ITC-silanized area, a steeper slope can be appreciated as the measurements are drawn towards the more homogeneous irradiated area (away from the non-irradiated PDMS region). A non-linearity trend at the beginning of the curve (orange) can be due to the proximity to the transitional area. A clear difference of approximately 140 nN in average can be seen between the two sets of data when the adhesion force was measured.

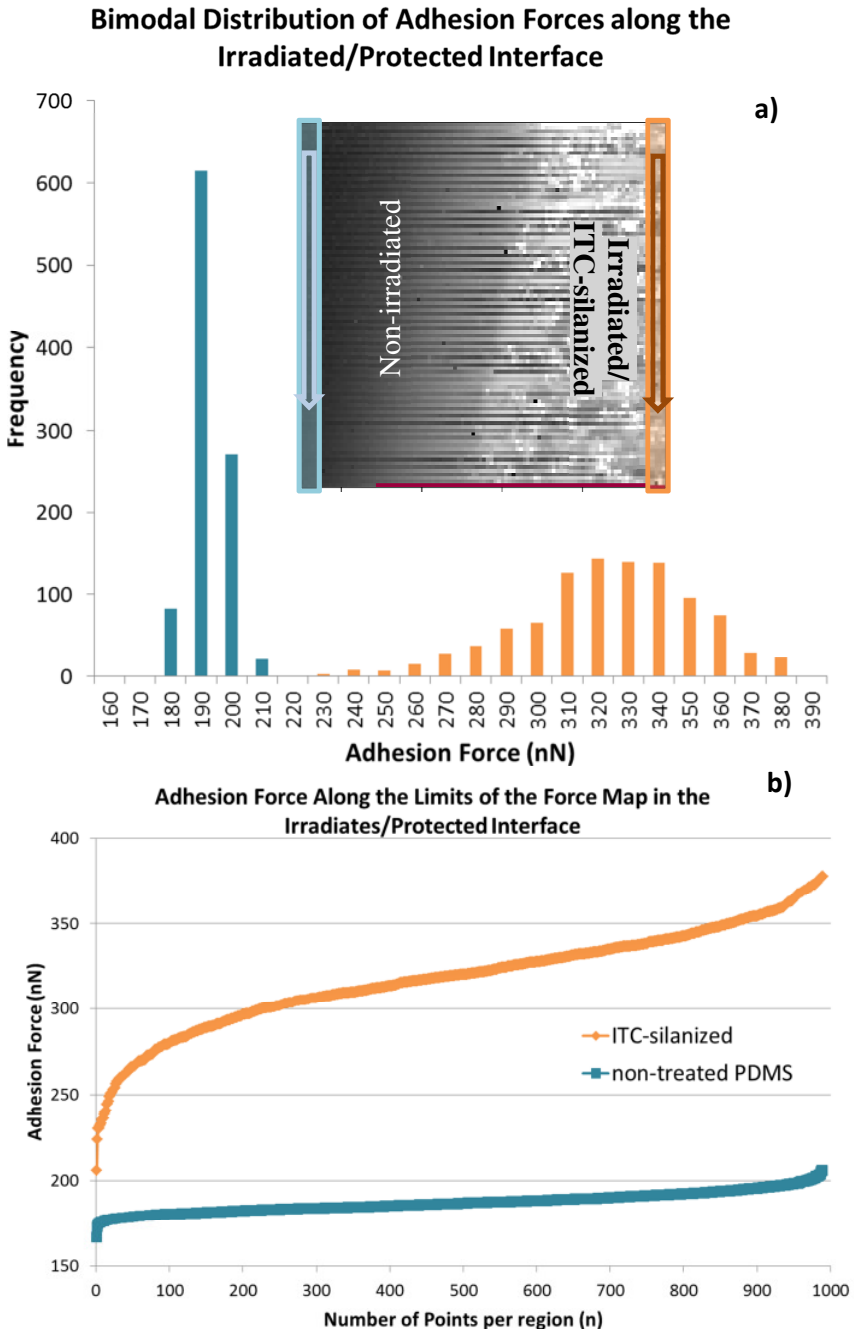

Figure 66.- Statistical analysis for two regions of the substrate. on a) a histogram show the adhesion force bi-modal distribution of the force along the sample on the silanized area and the non-treated area. b) shows the adhesion force variation along the y-axis of the measured force plot. The number of points label increase in vertical downward direction.

From this approach, the force measurements not only provide information about the adhesion forces between the surface and the cantilever tip, but also can provide some information about the elasticity of the material once the cantilever geometry is known. The stiffness of a material is measured commonly by the Young's Modulus. It is defined as the normal stress (restoring force caused due to the deformation divided by the area on which the force is applied) divided by the linear strain (ratio of the change caused by the stress to the original state of the object) when a force is applied to them [429]. In order to calculate the elastic modulus, an internal software routine following the Hertz model has been performed. According to the Hertz model [430], for indentation of a flat smooth substrate by a rigid, spherical indenter, the elastic modulus of the substrate can be obtained from indentation load–displacement curves as follows:

$$E_H = \sqrt{\frac{S^3\left(1-\nu^2\right)^2}{6RP}} \qquad (9)$$

where E_H is the elastic modulus of the substrate, ν is the Poisson's ratio of the polymer (related to the longitudinal elastic deformation produced by a simple tensile or compressive stress to the lateral deformation that happens at the same time) ($\nu \approx 0.5$ for PDMS [431]), R is the nominal radius of curvature of the indenter tip ($R \approx 10$ nm), P is the applied load, and S is the material stiffness ($S = dP / dh$) evaluated at P. The tip used was a silicon nitride conical tip NSC-35 with a 40° full cone angle. The classic Hertz's model is a hard contact model that does not take adhesive interactions into account. It can be expected a certain error from the model, but nevertheless, the important information is the relative change between the irradiated and the non-irradiated areas about 1 order of magnitude. Even though the technique has been successfully applied to estimate elastic and elastic–plastic properties of hard materials, it still requires further validation and suitable correction for soft materials to obtain accurate and reproducible results [432-436]. A better model for the calculation of the elastic modulus should be represented by the JKR equation which corrects for adhesion effects and viscoelastic materials [432, 437]. Although JKR calculations are not performed in this work (as it is out of the scope of the study) important information can be withdrawn from the experiment as there are pronounced changes in the elastic properties of the material. In Figure 67 the results from Young's modulus calculations are shown. Figure 67a shows the resulting elastic modulus map plotted when the adhesion force map is transformed using Eq. 7. The profile in Figure 67b shows the transition region between the two areas. A harder region is shown on the right of the mapping of elastic modulus and a softer region is shown on the left,

corresponding to the untreated PDMS (Figure 67b). When the two outermost borders are taken into account and the profile values plotted along the vertical axis (Figure 67c), in a similar procedure as the previous section, a clear difference between the harder region and the softer region is found. While the treated/silanized area showed a 17.7 MPa elastic modulus (comparable to those in which the PDMS has been treated with a hard coat) [438], on the non-irradiated area, a calculated young modulus of average 1.7 MPa is found. This value is in good agreement with literature, reported as 1.5 MPa for Young's modulus of the PDMS [434, 435, 438, 439]. In summary, adhesion and hardness increase in the irradiated/silanized area confirming the formation of a brittle silica-like layer when the PDMS elastomer is exposed to an UV/O_3 irradiation process. This result is also supported by the XPS evaluations done in the following section.

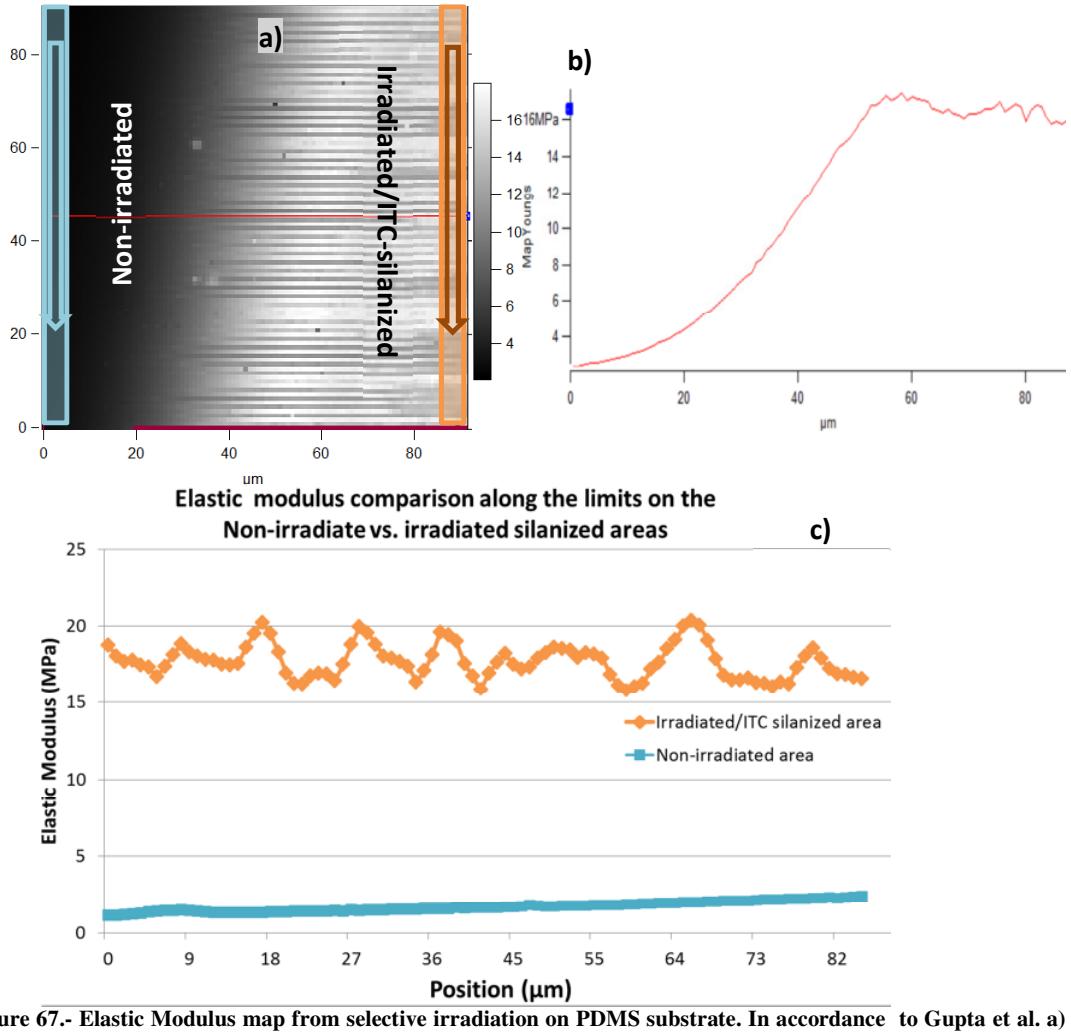

Figure 67.- Elastic Modulus map from selective irradiation on PDMS substrate. In accordance to Gupta et al. a) the right area is a softer region with a 1.6 MPa elastic modulus and on the left side a harder material with around 16 MPa elastic modulus. b) shows a profile calculation along the red line, showing the irrradiated region as a higher young modulus zone, plus the transitional region where the surface change gradually its elasticity and the soft non-irradiated area. on c) it can be seen the average plot of the elastic modulus values along the two outer borders of the image as they are the most representative for their own areas of material properties.

4.2.3.2 Wettability

In this section the change in the wettability properties on the oxidized surface of PDMS is discussed. As explained in the previous sections, a silica-like thin layer is produced when the PDMS is exposed to ultraviolet/ozone treatment [157]. This produces a decrease in the contact angle (hydrophilic behavior) as more hydroxyl groups are present on the surface due to the oxidation and eventual replacement of the methyl groups of the PDMS polymer. Several authors have studied these phenomena towards a better sealing effect in microfluidic devices, surface functionality and compatibility with aqueous solutions [207, 420, 440-442]. The irradiated surface can be schematically represented by the following Figure 68. During the irradiation, the polymer is oxidized and some longer chains are split into smaller chains which migrate towards the air-polymer interface. The smaller chains are further oxidized and their methyl groups are replaced by hydroxyl groups which in turn crosslink into an oxidic layer (silica-like). This process fluctuate nanoscopically over the complete substrate although when the surface is submitted to a macroscopical investigation, such as contact angle or fluorescence microscopy, the differences are not noticeable. As the layer of silica is just a few nanometers thick (<10 nm when the irradiation time is about 30 min) some non-crosslinked low molecular weight (LMV) chains will migrate through the cracks in the surface promoting a hydrophobicity recovery of the substrate [207].

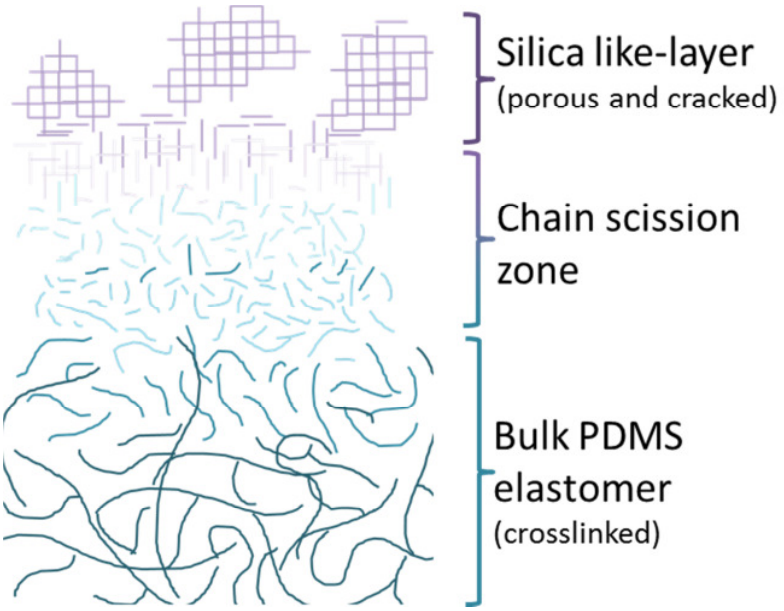

Figure 68.- Schematic representation of the PDMS surface after irradiation. It depicts the presence of different zones, from crystalline (silica-like layer) to amorphous (bulk polymer). The chain scission zone is ultimately responsible for the hydrophobicity recovery of the material with time.

Contact angle measurements were performed in a PDMS coated glass slide according to the experiments previously carried out for the silanization of glass surfaces. Millipore water droplets (9) were placed in the middle along the longitudinal axis of the slide (similar to the experimental set up carried out for the contact angle measurements on silica wafers and cleaned glass slides (see section 3.1.1.2). The contact angle of the nine points were measured as a function of time (30 min, 60 min, 90 min, 120 min, 240 min, and longer times such as 3.5 days, 7 days, 10 days and 14 days) and afterwards the angles were averaged to produce a single value which is then plotted in the graph. Figure 69 shows the follow up experiment on the hydrophobicity recovery on a PDMS coated glass slide. The coating is about 1 mm thick to avoid any interaction of the glass on the contact angle measurements and the oxidized silica-like layer is expected to be about 10 nm. After the irradiation the substrates were characterized by the sessile contact angle method. An almost linear behavior in the contact angle measured points can be observed when the substrate is evaluated in the first two hours. The results are very similar to those reported in literature [207, 440, 441, 443]. With the time, a non-linear recovery can be observed. In the inset graph on the Figure 69, a zoom in the two first hours of the recovery after irradiation is shown. The Y-axis belongs to both graphs, and the X-axis of the inset is stretched to prove the linear increase of the contact angle with increasing time.

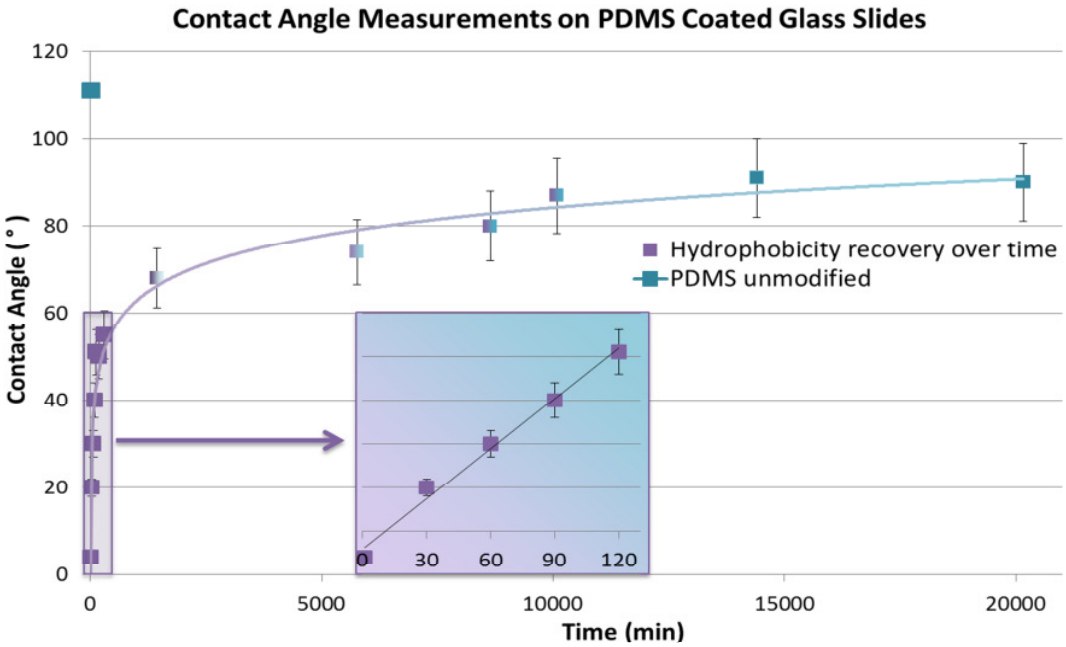

Figure 69.- Contact angle on PDMS coated glass slide irradiadet with UV-light showing the hydrophobicity recovery over time after irradiation. In the first two hours the migration of low molecular fragments is more pronounced and the increase flats over time. Inset: linear behavior from recovery in the first two hours. After that, the recovery was slowed down significantly. In the inset, the x-axis has been stretched . The y-axis is the same for both graphs.

For PDMS without any treatment, an average contact angle of 110° ± 10 was determined using the water sessile drop method which agrees with other authors who have investigated the polymer in more depth [444-446]. Irradiated PDMS after 1 hour of UV/O_3 treatment yield a contact angle below 5° (the instrument is not able to measure lower contact angles accurately). Hydrophobic recovery was already found in this shortly-irradiated sample after 30 minutes (22 ° ± 2) as suggested also in literature. The steep increase in the contact angle (and therefore the decrease in hydroxyls available) with time could be disadvantageous for the silane treatment as this one needs at least two hours for completion.

Consequently to avoid the effect of poor silanization on the PDMS, the strategy followed to countermeasure the hydrophobicity recovery was carried out as follows: after the first two hours of irradiation, a pause of 1 hour is done and later another irradiation period of two hours is performed again. This process is repeated 5 times in order to create not only a thicker silica-like thin film but also to irradiate and further oxidize the material from the LMW chains emerging to the surface (intermittent irradiation method)

In the same manner, once the sample is irradiated for the last time, the isothiocyanate silane is coupled to the newly created silica-like layer. The attachment of the isothiocyanate silane reduces the free energy of the surface hindering the hydrophobic recovery of the surface.

4.2.3.3 Elementary Composition

To prove that the SiO_2 established on top of the PDMS behaves chemically identical to the SiO_2 wafer [158, 170, 447] XPS experiments were carried out on PDMS coated surfaces before and after irradiation/silanization. The thickness of the layer of PDMS on top of the substrates was approximately 500 microns. Afterwards, selective irradiation was done in this case on the whole substrate and later silanized with 3-isothiocyanatepropyltriethoxysilane. The analysis indicated large changes in chemical composition of the sample. PDMS composition by atomic percentage before irradiation, after irradiation and after silanization is shown on Table 15. It has to be noted that the XPS cannot be completely regarded as a quantitative technique to assess the change in the elementary composition of the surface. Therefore the measurements were done on different samples in different occasions, but carefully keeping the conditions for the irradiation and silanization for all of them constant.

Table 15.- PDMS composition by atomic percentage before irradiation, after irradiation and after silanization. The representative samples are marked in different colors.

	Time of silanization	C (at.%)	O (at%)	Si(at%)
PDMS Theoretical		50	25	25
PDMS measured		41.1	29	29.9
PDMS irrad. 120 min		13.1	57.5	27.4
PDMS after ITCPTES	2 hours	21.33	48.4	25.9

The carbon atomic percentage decreases with the UV irradiation considerably. After 120 minutes under intermittent irradiation, from a starting point of 41.1%, the lowest content was around 13.15%. It can be noticed, that after the silanization, the C 1s signal increased again, up to 21.3% (on 2 h silanization time). Part of this carbon measured is due to adventitious carbon, present in any sample exposed previously to air. The reduction on the carbon content on the surface is due to the removal of the methyl groups on the surface and the partial replacement from them with hydroxyl groups as proposed by several authors [176, 440, 442, 443].

Additionally the values from oxygen and silica are found in a 1:1 (O:Si) atomic percentage proportion when measured, although the concentration is higher (29%) than that expected theoretically (25%). After irradiation the ratio between them increases up to a 2:1 (O:Si) proportion which would correspond to a composition related to silicon oxide.

Silicon 1s peak shifts from a 102.4 eV up to a value of 103.8 eV after the irradiation, corresponding very close to a measurement of SiO_2 quartz powder [448, 449] and eventually ending at a 103.5 eV after the silanization procedure.

Oxygen 1s spectra show a peak at 532.9 eV before any treatment, which shifts to a 533.3 eV after UV/O_3 treatment and have a final value at 533.0 eV after the silane reacted with the surface. This peak position corresponds very well with published data [158], before and after the treatment of irradiated PDMS with ITCPTMS. In Figure 70, the C 1s, N 1s and S 2p signals before (Figure 70d, e and f) and after silanization (Figure 70a, b and c) are shown. The presence of nitrogen and sulfur in the spectra of the silanized PDMS (Figure 70b and Figure 70c) relative to the non-treated PDMS (Figure 70e and Figure 70f, respectively) confirms the functionalization of the surface with the isothiocyanate group.

The measurements show a slight broadening of the C 1s scans of the spectra after silanization, meaning that possibly a change in the orbital environment of the atom. The

spectra have been deconvoluted [450, 451] to investigate different species in a spectrum e.g. rise of other oxidic components of carbon, such as aldehydes, carboxylic acid and carbonyl groups [452]. C 1s peak (Figure 70a) can be deconvoluted in several components: 285,0 eV (C-C, C-H), 286,7 eV (C-O, C-N), 287,8 eV (N=C=S) and 289,4 eV (O-C=O) which are in agreement to the experiments of Graf [386]. These components indicate the presence of ITCPMS but show an oxidation of the molecule, too. The S 2p doublet at 163,2 eV shows the presence of isothiocyanate whereas the doublet at 169,0 eV (Figure 70c) is also a hint at oxidation [388] but behaves similar to the S 2p doublet found for the silica wafer isothiocyanate silanization when examined.

In this case the N 1s peak (Figure 70b) can be deconvoluted into two components, one near 402,8 eV that is characteristic of protonated [453] primary amino groups, and another at 400.6 eV that can be attributed to the –N=C=S bond [386, 389]. The electrons in the isothiocyanate group might be partially delocalized between the -N=C=S group [454-457]

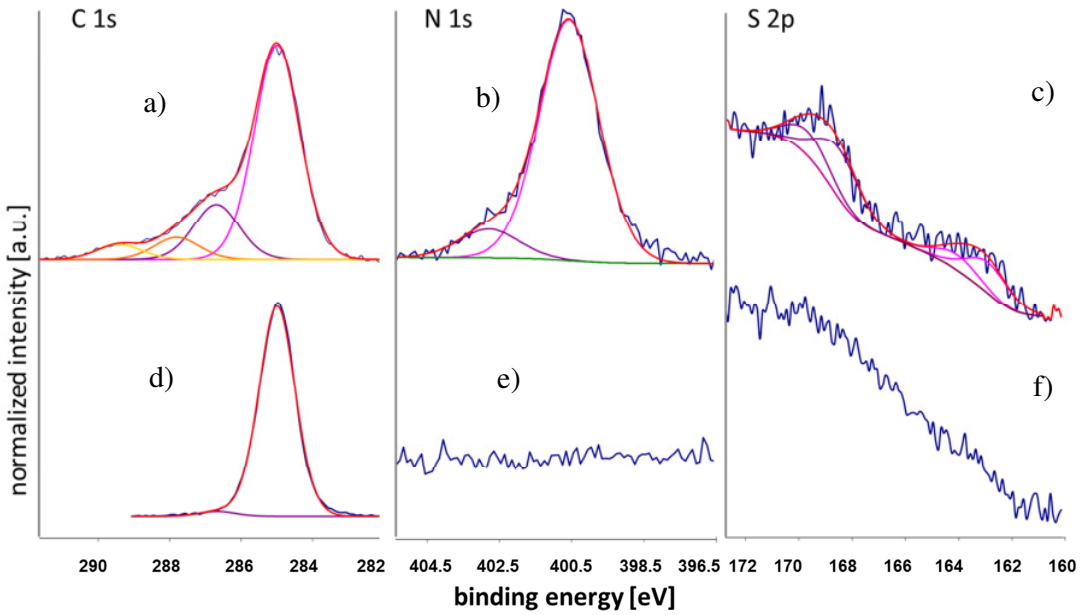

Figure 70.- X-ray photoelectron spectra of substrates ITC-functionalized PDMS (a,b,c), and non-treated PDMS (d, e, f) respectively. For all graphs, the vertical axis is expressed in arbitrary units on normalized intensity.

4.2.3.4 Chemical Functionality

Fluorescence Evaluation of PDMS Silanization

Furthermore, fluorescence microscopy was used as a fast method to check if the transfer of the chemistry onto the surface was successful. Aminofluorescein (NH_2-F) and an amino modified DNA-oligonucleotide with a fluorescent marker were used as labeling

agent. When it is coupled, a delocalization of the electrons takes place, resulting in a fluorescence intensity which is higher than in the case of non-coupled dye. This ability provides straightforward information when the coupling has been successful or not. The scheme for the experimental procedure to carry out the fluorescence assessment is shown in Figure 71. First a flat PDMS untreated surface is produced and irradiated through a mask. Afterwards the oxidized areas are silanized with ITCPTMS immediately after they are taken out from the UV/O_3 chamber. After two hours of silanization, the sample is dipped into a solution 1mM of fluoresceinamine in an aqueous buffer at pH 9.0.

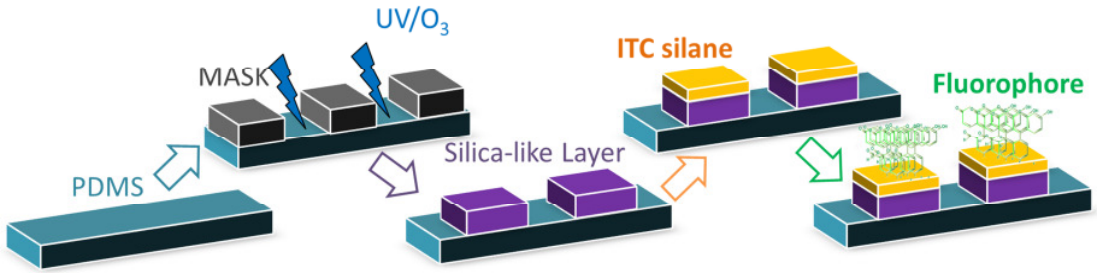

Figure 71.- Scheme of polydimethylsiloxane (PDMS) substrate treated and silanized with isothiocyanate groups, with subsequent fluoresceinamine coupling.

Two procedures for the NH_2-F coupling were used: i) The sample was dipped in an aminofluorescein solution, left for 30 minutes and then rinsed with water and buffer solution and ii) a drop of aminofluorescein was added on top of the substrate, left for 30 minutes and then rinsed thoroughly with water and buffer solution.

A secondary objective from the experiment was to assess the physisorption of the NH_2-F onto the substrate.

A selective irradiation was performed using a transmission electron microscope grid. Two experiments with different types of masks were carried out: irradiation with (1) a mixed mesh copper grid with 30-90 mesh and (2) a copper grid with 200 mesh.

After the irradiation with the mixed mesh grid, the mask was removed and the substrate was put into contact with the fluorophore by dipping it into the solution containing the aminofluorescein. These results can be seen on Figure 72 (a,b,c) which shows the difference in the fluorescent image between the irradiated/silanized PDMS and the pristine PDMS. In Figure 72a, due to the higher magnification, the spacing between the features is better resolved. This gives the impression that the areas protected by the grid are also fluorescent, but the evaluation along the picture (done with ImageJ in Figure 72d) shows that the contrast between the modified areas and the pristine PDMS in (a), (b) and

(c) is comparatively the same. In Figure 72c, there is an area showing slightly dimmed fluorescence intensity, this is due to photo bleaching on this area when using a higher magnification lens.

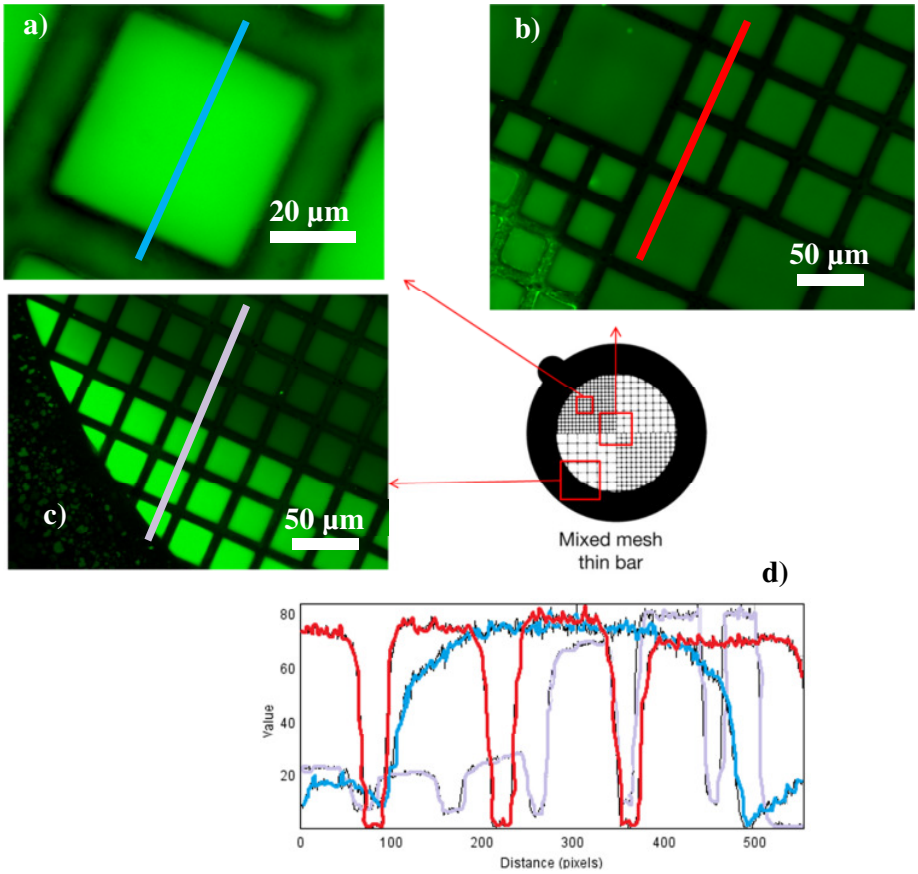

Figure 72.- Fluorescence image of aminofluorescein coupled to a PDMS substrate selecively irradiated through a TEM grid as a mask. The grid was removed before addition of the dye by completely dippimg the substrate into the flurophore solution a) 60x magnification, b) 40x magnification and c) 10x magnification. d) fluorescence intensity profile along the lines. It can be noted that although the brightness of the images are different between each other, the contrast between the functionalized and the non-functionalized remains similar.

For the second experiment (Figure 73), a drop of the fluorescein was added exclusively on the center of the pattern created by the irradiation using the 200 mesh copper grid as a mask. The purpose of this experiment was to assess the physisorption of the aminofluorescein when coupled just in certain areas (in the same way as it would be done with the DNA-linker in the forthcoming experiments in section 4.2.4). For this test, a grid of 200 mesh was used (average size per square is 60 µm x 60 µm). The grid was removed in advance, so there would not be any interaction between the grid and the non-irradiated areas which might lead to an undesired adsorption of NH_2-F on the areas in between. It can be seen that the drop (1 µl) follows partially the grid structure of the mask in the same orientation as the grid (Figure 73a,b). A contrast between the irradiated and non-irradiated

area can be seen for both areas: the non-fluorescence labeled and those wetted by the NH_2-F containing drop. Those areas which were irradiated and ITC-silanized show significantly less fluorescence (which is produced by the ITC silane) than those areas where the fluorophore was added (Figure 73c).

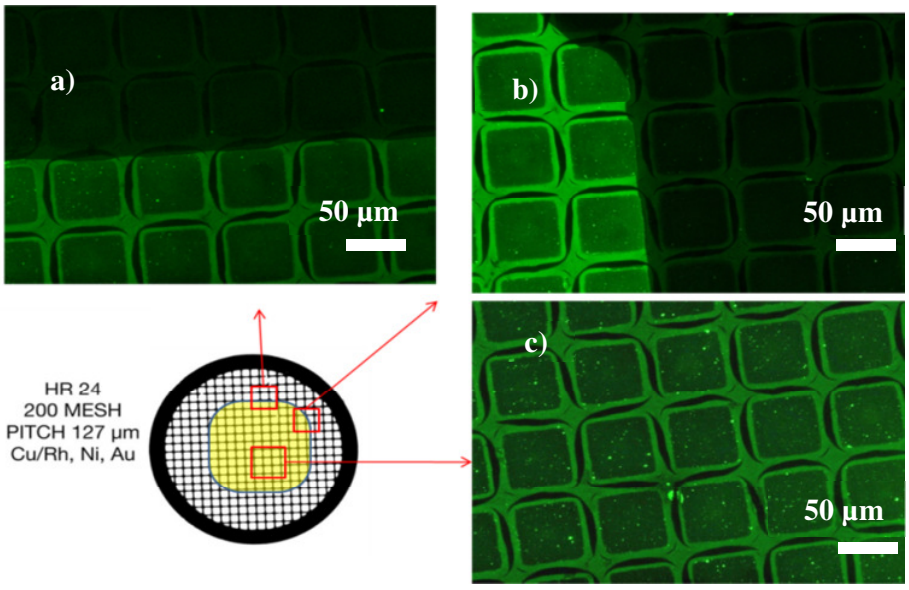

Figure 73.- Fluorescence image of PDMS irradiated through a grid and after the addition of a small drop (<1µl) of aminofluorescein to the center of the patterned area. The borders of the drop can be seen. The drop followed a square shape as the drop followed the grid pattern. a) top region of the drop, b) upper-right region and c) center region of the treated area.

In the least experiment, those patterned areas which were not in contact with the fluorophore solution can act as negative controls where no reaction on the surface took place. Additionally, where the drop was in contact with the patterned surface, there are still darker areas which were protected by the grid of irradiation. These areas set up the positive controls. Depending on the positioning of the masking grid – which has a curved side and a flat side- some irradiation penetrates partially the masking areas activating the partially protected areas in between the squares. This is more evident when the grid is placed on the curved side. This two experiments show the ability of the ITC-silane to be placed selectively and that it is subsequently used for attachment of an amino terminated fluorophore compound. The different sequences of addition of the dye or removal of the grid, point to the conclusion that the process is relatively independent of the order, but mostly dependent of the reactive pair of functional groups (ITC – NH_2).

Further experiments using the fluorescent microscopy evaluation in combination with AFM topographical examination on the same area were performed to check if the reactivity was linked with some change in the surface topography of the polymer even before the PDMS is irradiated or if it was related to some physisorptive effect of the

elastomer. In this case, a new digital video disk (DVD) was used as a master for casting the PDMS. The DVD possesses a 500 nm pitch with a 100 nm depth trench pattern when it is new. As in the previous experiments for AFM investigation of adhesion forces on the polymer (see section 4.2.3.1), the substrate was irradiated covering one half of the sample with a mask and irradiating for 1 hour. Afterwards the sample was ITC-silanized and incubated for 5 minutes in aminofluorescein. The experiment showed that the fluorescence was increased on the irradiated side, indicating the higher adsorption on the irradiated areas for the fluorophore. This is shown in more detail in Figure 74. The AFM topography doesn't show a significant difference between the irradiated/silanized and the non-irradiated PDMS surface. The phase contrast image produced from the AFM when the intermittent contact mode is used, show a well-defined transformation of the irradiated side. The phase changes by approximately 20° after irradiation (see section 4.2.3.1) are in agreement with the observation done by Tamayo et al. [418, 419]. The morphologically pre-structured polymer (PDMS) behaves in exactly the same way. If the structured features are exposed to the UV/O_3 irradiation, then the oxidation process will take place independently of the shape of the substrate. In this way, a double structuring technique can be applied: a morphological structure using a preformed master as casting model, and then a chemical activation done by the site-selective irradiation on the surface through a mask by UV/Ozone with the subsequent formation of the silica-like layer on those defined areas of the substrate.

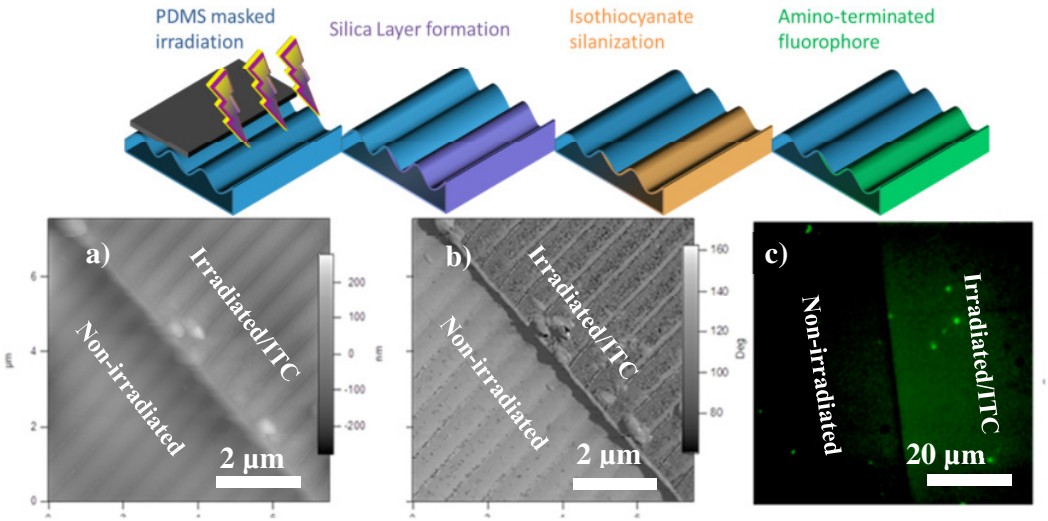

Figure 74.- AFM images (a,b) and fluorescence image (c) of structured and partly irradiated PDMS substrate. a) shows a topographic image of the two regions (indistinguishable by height), b) a phase contrast image is shown, on which the right side is a irradiated and silanized region and the left side is the non-treated area. c) fluorescence image after coupling of aminofluorescein on the silanized isothiocyanate side. The pre-structured substrate was casted from a DVD which possess typically a wavy pattern with 500 nm pitch and 100 nm depth in the trenches.

4.2.4 Application of Isothiocyanate-Based Silane Chemistry for Bottom-Up Assembly of Self-Assembled Tobacco Mosaic Virus.

In this section the use of the isothiocyanate chemistry to covalently bind Tobacco mosaic virus-like particles (TMV) in a similar way to the process done for the aldehyde terminated surfaces is presented. As discussed before isothiocyanates are well known in biochemistry for their strong coupling to amino groups in biomolecules.

In the scheme on Figure 75, the different steps involved in the modification of the substrates for biofunctionalization are shown. On a surface which is functionalized with a biological compatible isothiocyanate terminated silane a DNA linker possessing an amino terminus is bounded via covalent bond to the surface by forming a thiourea bond. RNA is then with the DNA-oligonucleotide linked by hybridization, and afterwards, by the addition of coat protein (CP), the self-assembly process is initiated, resulting finally in a TMV-like particle fixed to the substrate. As both the 5' end of the RNA and the CPs can be functionalized before the assembly process a big variety of different sequences of CPs can be prepared ("bio barcode") and – after assembly – the functionalized 5' end of the RNA can be "capped" with further molecules or functional groups.

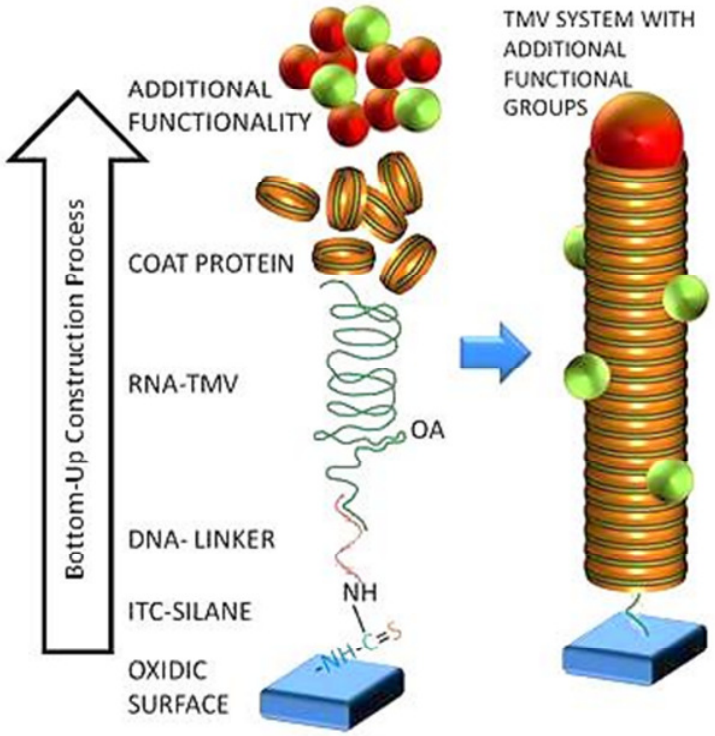

Figure 75.- Scheme of site-selective bottom-up self-assembly process of TMV-like particles on an oxidic functionalized surface. The 5' end of the viral RNA can be functionalized with additional chemicla functions

As this is one of the most important aspects of the dissertation it will be discussed in more detail throughout two experiments using different substrates. In the first part, the principle is tested by performing a self-assembly of TMV-like particles on homogeneously coated silica wafer functionalized with the isothiocyanate silane. Using Dip Pen Nanolithography as a selective simple chemical structuring technique to allocate the TMV-like rods on specific places is examined and the site selectivity is assessed on flat surfaces. In the second part, the transfer of the chemistry is done and further assembly is tested on a polymeric surface as previously explained in section 3.1.2.

4.2.4.1 Homogeneously Coated Oxidic Substrates

Three main topics were addressed to analyze the compatibility of the TMV assembly on silica substrates. It is necessary to assess the role of the ITC silane on the system, as it is the binding anchor for the TMV-like particle self-assembly driven by the RNA and DNA assembly. A first experiment evaluates the minimum time necessary for the silane to couple on the surface in order to bind properly the DNA-linker and subsequently perform the TMV-like particle assembly.

Second, once the optimized parameters for the ITC-silanization were determined, an experiment of the hybridization time required for a complete virus-like particle to assembly is carried out. In this experiment, the TMV assembly is interrupted at determined intervals and characterized by AFM.

Third, continuing with the assessment of the silane and its role on the experiment, a comparison is made between the two silanes with the same functional group: one fabricated in house (ITCPTMS) and the other custom-made from a company (ABCR, Germany) (ITCPTES). This will provide information about the role of the ITC-group and its reactivity towards the DNA-linker, while it is produced in house (fresh) or if it is custom made (aged) as well as the influence of the tail groups on the assembly of the silane and subsequently growth of the TMV on the surface (methoxy groups for in-house synthesized ITC silane and ethoxy groups for custom made ITC silane). Taking into account the information provided by the previous experiments, an optimization of the bottom-up assembly procedure is done and statistical analysis similar to that of the aldehyde-chemistry is performed.

Additionally the role of the DNA-linker is also assessed simultaneously in a simple way every time an experiment is performed. The DNA-linker possesses a complementary

strand specially coded for the RNA strand of the TMV-like particles. In the experiments described in the following, the DNA is spotted by placing a 2.5 µl drop of the solution on the center of the substrate.

Influence of Silanization Time on the Bottom-Up Self-Assembly of Viral Particles.

In the experiments described in the following the time of silanization was varied between 30 s, 120 s and 15 min respectively. DNA coupling was carried out by covering completely the surface of the ITC-silanized sample with the DNA-solution. The samples were treated keeping the time for hybridization constant (16h) and – for negative control - omitting of one of the preparation steps. Table 16 shows the overview of the 18 samples prepared. To differentiate between the samples which were silanized for different times, the index of the silanization time is used as subscripts (e.g. A_{30s}, A_{120s}, A_{15min} etc.) Three samples were prepared in the same way for each set of conditions. Sample sets A, B, D and E are negative controls. They either lack of RNA or CP treatment which is vital for the formation of TMVs as they are the two constituents of the rods. The two samples which should present in any extent the formation of particles are sample sets C and F. Both were prepared under experimental conditions suitable for a normal assembly (RNA+CP) whereby in the case of the sample set F a blocking procedure of the non-reacted, active ITC-termini after the DNA incubation took place. The layout for the experiment is shown on Table 16

Table 16.- Experimental layout to assess the proper silanization time for TMV virus assembly and further controls. A,B,D,E are negative controls as neither RNA nor CP is present in the experiment. Samples C and F have the minimum required conditions for a complete assembly on the substrate.

Silanization Time	Wafer code	Blocked	+RNA	+CP
(30s, 60s, 15min)	A	-	-	-
	B	-	+	-
	C	-	+	+
	D	+	-	-
	E	+	+	-
	F	+	+	+

From the experiments, it can be withdrawn that the silanization is vital to a proper binding of the DNA on the surface and subsequently the RNA attachment. Figure 76 summarizes the results from this set of experiments in an array of topographic AFM images. There was no visible rod found in the samples which had no RNA or CP (sample sets A, B, D,

E). Along the experimental set up, just two types of samples should render a TMV-like particle. From Table 16 it can be seen that sample sets C and F fulfill the requirements for a complete bottom up self-assembly of the particles. Indeed there were just 3 samples (C_{15min}, F_{60s} and F_{15min}) which showed virus-like particles according to the estimated length and width and they are in agreement for what would be expected from the layout of the experiment (see Table 16). In the rest of the substrates, also an increase of the surface roughness is observed. The color scale has been normalized to 30 nm and no offset in color is applied on the images. In the first rows $A_{30s,\ 120s,\ 15m}$ and $B_{30s,\ 120s,\ 15m}$ a less contaminated result of the substrate is observed. In samples $C_{30s,\ 120s,\ 15m}$ an increased deposition of impurities is observed. They come probably from the buffers, the RNA or CP solutions and cleaning solutions. In the C row (unblocked, + RNA, + CP), just in C_{15m}, small particles of protovirus can be observed. From the rows $D_{30s,\ 120s,\ 15m}$ and $E_{30s,\ 120s,\ 15m}$ no perceptible TMV-like rods or proto rods were observable but an increased deposition of impurities was noticeable. In the final row $F_{30s,\ 120s,\ 15m}$, further bottom up assembly of TMV like particles is observed. On the first sample F_{30s} it is very probable that the ITC silane layer is not properly blocked and some of impurities hinder the proper grow of TMV on the surface. Furthermore, the short silanization time doesn't allow a complete coverage of the silane on the surface. In F_{120s} particles can also be noted. Finally in F_{15m}, fully formed virus can be seen, they are around 150 nm long x 25 nm width. This gives a preliminary result for the minimal coupling time required for a proper growth and attachment of the DNA-linker and further growth of the virus-like particles. For the assessment of the images, the same AFM cantilever was used so every image could be comparable in force and interaction. In summary, the experiment show that it is necessary to provide at least a silanization time of 15 minutes in order to obtain virus-like particles. The control experiments showed that without RNA or CP, the particles cannot be assembled proving that no unspecific interaction between different components takes place.

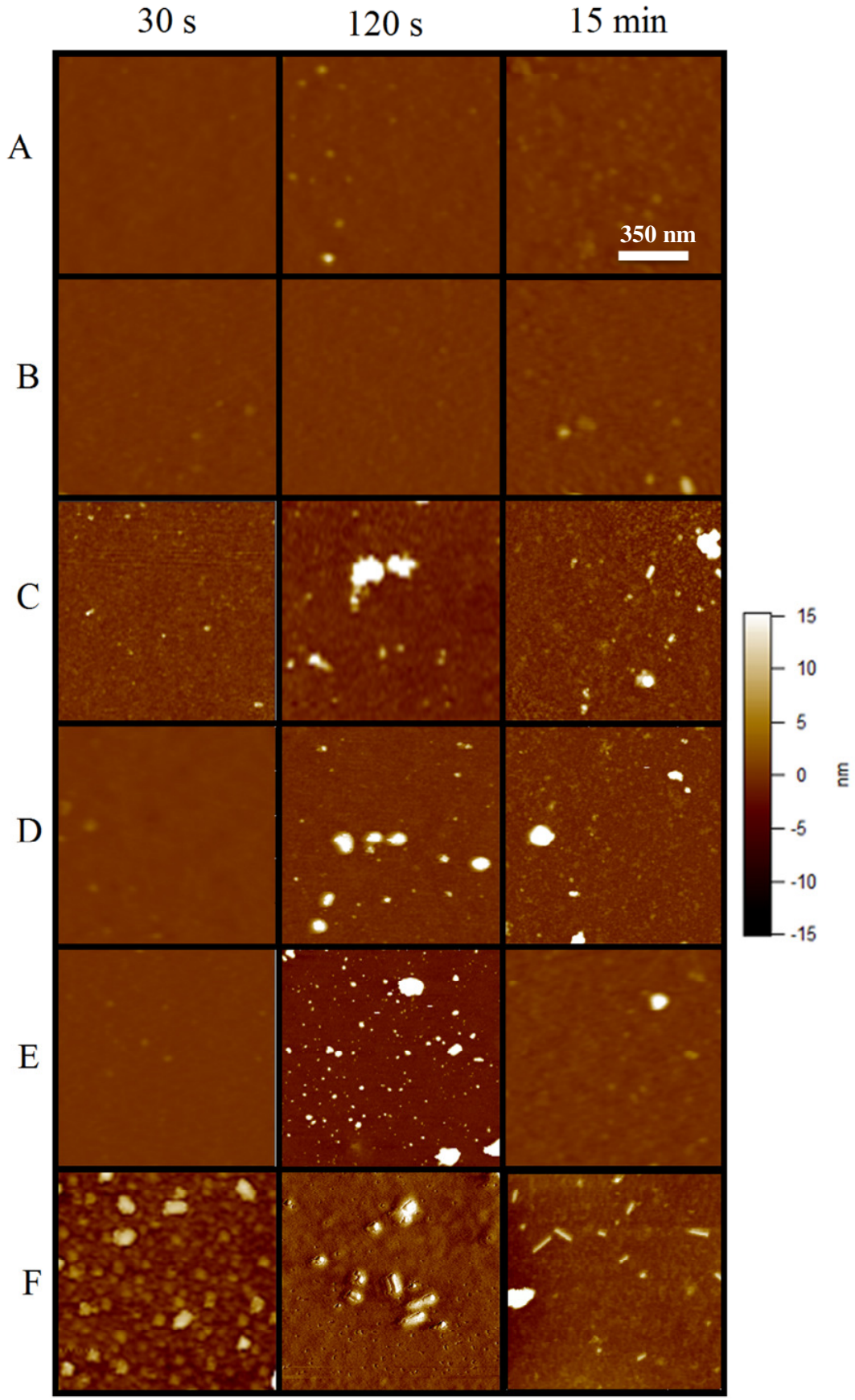

Figure 76.- AFM topographic images showing the results of experiment with different silanization times (30s, 120s, 15min) combined with different induced conditions for the formation of the TMV-like particles. For a better understanding also refer to Table 16. The scans are 3x3 μm^2.

Comparison between Different Times of Hybridization.

In this experiment, the time of hybridization was varied to assess its influence on the TMV-like particle formation. Seven different times for hybridization on the substrates were investigated: 0 min, 3 min, 10 min, 30 min, 90 min, 120 min, 270 min and 1000 min. Pre-assembled viruses grown *in vitro* with the same hybridization times in liquid were deposited on ITC-silanized wafers and left on the surface as a control experiment. After the bottom-up assembly and the deposition of the pre-assembled viral particles all samples were submitted to the same washing procedures.

Although statistical evaluation of the particle length was not performed on the samples it can be noted that after 30 minutes of incubation, some particles or proto-virus like TMVs were found in the case of the bottom-up assembly (Figure 77). After 270 min of hybridization, elongated particles with the typical diameter of the viral particle can be detected after bottom-up assembled and the preassembly. After 1000 min of hybridization most of the particles show a uniform length. This is also in agreement with Butler's[18] experiments. As discussed in his research, the specificity of the RNA presents a problem. As his work describes the self-assembly process of TMVs in solution, it is possible to compare it to the self-assembly process on the surface which is in the focus of this dissertation. According to Butler [458] the RNA nucleation on the origin-of- assembly point is fairly fast whereas the subsequently assembly of the protein and further elongation of the particles is slow. In their work they examined reassembled virus in solution with a radioactive labeled protein disk. They found that the rate of the reaction was first order regarding the disk concentration and saturates to a maximum rate of 7 subunits/second. However Richards & Williams[459] have suggested that the rate of nucleation is much slower than the first approaches. In our experiment, we compare these results with a system which self-assembles on the surface. Sterical hindrance might play an important role in the speed of the coat protein assembled on the surface. In our case we can report the first stages of nucleation happened after 10 minutes of assembly (Figure 77). Regarding the assembly, it starts centrally at the origin of assembly point (OA) of the RNA and proceeds fast (1-5 min) in one direction and slower in the other direction (about 1 h).

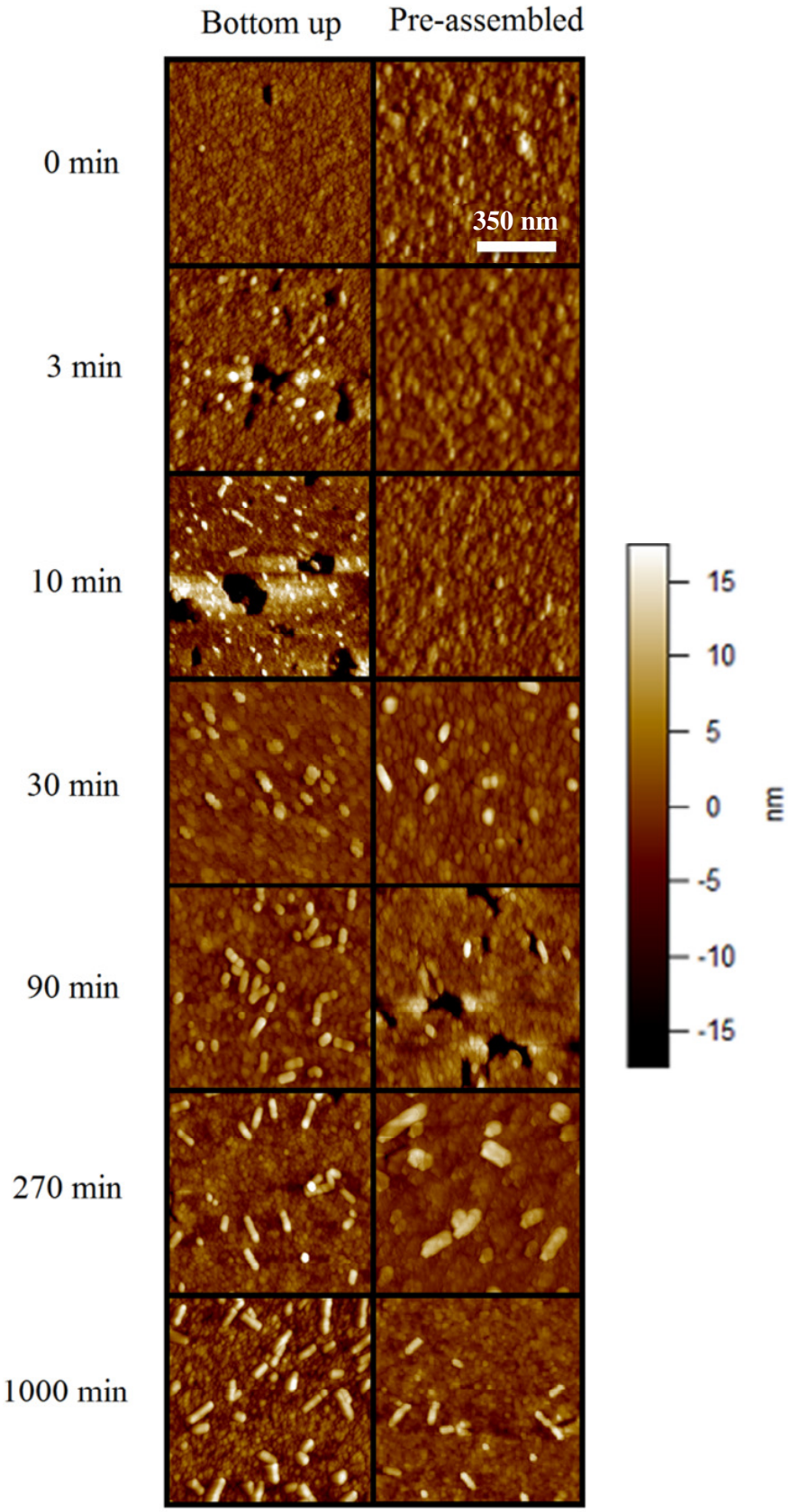

Figure 77.- AFM topographic images of an assembly-RNA time experiment. The time for hybridization and bonding of the RNA to the DNA linker is varied and tested for a bottom up approach and for a simple TMV deposition. All the images are 1x1 μm^2.

The TMV-length after complete assembly is also directed by the length of the RNA applied. Figure 78a show an *in vitro* preassembled virus particles which were deposited on the surface and bottom-up self-assembled particles, respectively. However, the preassembled virus was not able to be completely fixed on the substrate as the AFM examination showed. The virus was movable and difficult to imagine by the AFM. In the case of Figure 78, AFM images of two of the longest particles prepared by preassembled particles-experiment (a) and the bottom-up assembly (b) are shown. When comparing these two longest particles, they seem to have comparatively the same length (~150 nm) and around the same width (~30 nm). This shows that in principle bottom-up assembled virus-like particles can grow with the same length as the preassembled ones. In average a higher proportion of longer particles are found in the preassembled samples than on the bottom-up assembly. Particles found with aspect (length/width > 1), will be considered as virus-like particles in formation or completely formed. This consideration will be the basis for the statistical analysis shown in the following section.

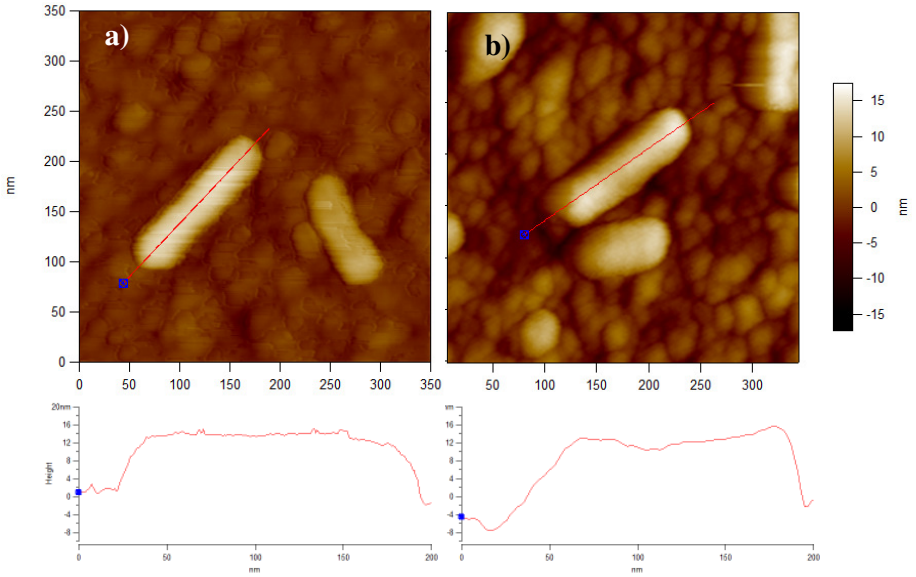

Figure 78.- AFM topographic images of TMV-particles self assembled with their respectively height profiles along the red line on each picture. a) TMV pre-assembled in solution and then deposited on the surface and b) bottom-up TMV particles self assembled directly on the surface.

Comparison between ITC silane in-house Synthesized and Custom-made Silane.

A previous characterization on the differences between the two silanes 3-isothiocyanatepropyltrimethoxysilane (ITCPTMS) or the 3-isothiocyanatepropyltriethoxysilane (ITCPTES) used in this dissertation has been performed using FT-IR (see section 4.2.1). In this section, it will be investigated whether

both silanes are proper for the self-assembling process. For all the experiments, a drop of 2.0 µl of the DNA-linker solution was deposed in the middle of the ITC-silanized wafer and incubated for 18 hours in a humid chamber to avoid any drying effects. After the incubation period, the sample was washed according to the procedure explained before (section 1A.1). Therefore, we recognize two areas in the same sample: 1) an area inside the drop of DNA, which has the complete preparation procedure and 2) an area which was not wetted by the DNA containing drop, which follows every step but the DNA addition (Figure 79). For RNA hybridization the sample was dipped in a solution of RNA, washed and finally dipped in a solution containing the CP.

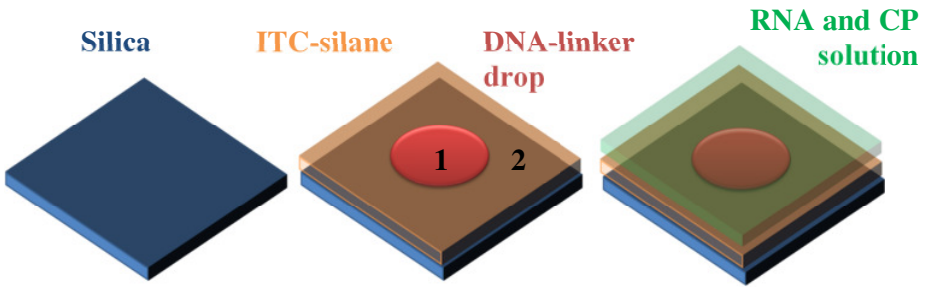

Figure 79.- Scheme showing the two areas in the same sample: 1) an area inside the drop of DNA, which has the complete preparation procedure and 2) an area which was not wetted by the DNA containing drop, which follows every step but the DNA addition. All samples were washed thoroughly after the RNA+CP addition.

Figure 80 shows two different TMV particle assemblies done with the two types of silanes described before. This means that both silanes were able to provide an anchor site to the surface for which the DNA-linker and further TMV like particle is assembled, as they both contain the isothiocyanate moiety.

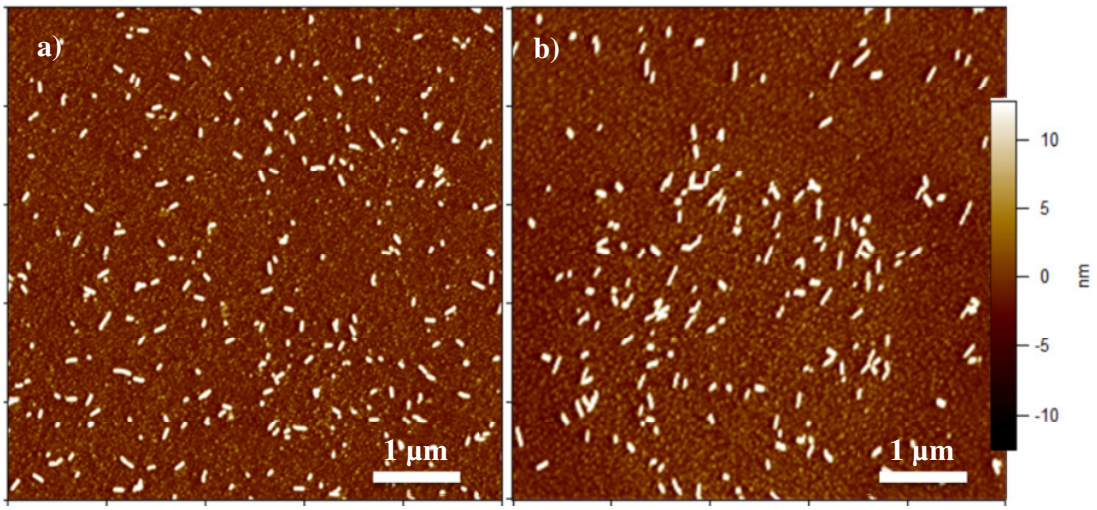

Figure 80.- AFM topographic images of TMV-like particles bottom-up assembled using an ITC-silane. the silanization took place with same experimental conditions varying only the silane molecule: a) ITCPTES and b) ITCPTMS. The latter prepared fresh while the first was bought and kept in use for one year (aged and oxidized).

After optimization of the time of silanization (as explained in the experimental section 3.1.1) and further optimization on the hybridization time (as shown previously in this section) from the biology project partner, the ITCPTMS yielded the highest particle density as it can be observed in Figure 81.

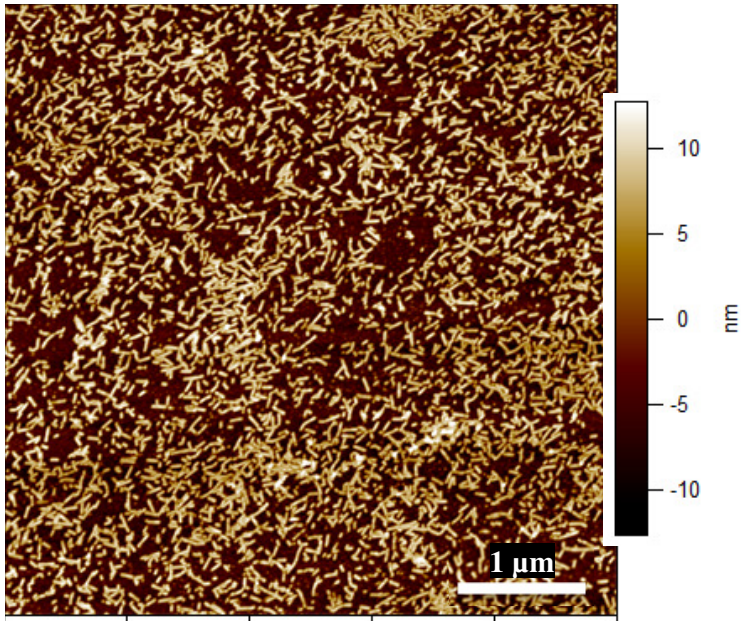

Figure 81.- AFM topographic image showing a TMV-like particles bottom-up assembly on an ITCPTMS functionalized wafer after optimization.

The ITCPTMS (in-house synthesized) silane probes were used for the statistical analysis as they provided a higher density of the virus on the surface. This higher density comes probably from the fact that the methoxy groups are more reactive towards the surface and therefore a higher density of the silane can be obtained. Figure 82 shows the AFM topography image of TMV-like particles assembled on a silicon substrate, which was subjected to the complete preparation procedure (i.e. ITC-functionalization → coupling of DNA-Linker → RNA coupling → adding coat protein). In AFM topography images the height of the features is visualized by their brightness. AFM topographic examination on non-structured silica wafers after optimization of some parameters (hybridization time, silanization time) is shown in Figure 82a. The TMV-like particle length distribution shown in Figure 82b give an idea about different lengths (corresponding to different stages of the assembly) found with the average length of 85 nm, holding a standard deviation of 30 nm. The TMV-like particles were found exclusively on those chips that were subjected to the complete assembly process. As expected, no TMV-like particles were found in the control experiments on silica wafers.

The determination of the length distribution of the TMV-like particles on the surface was carried out using the proprietary software from the AFM as well as ImageJ software for particle length calculations. Only those TMV-particles with a height profile of approximately 12 nm were taken into account as the particles were expected to have a 18 nm radius. The reason for the flattening effect on the TMV-like particles laying on the surface horizontally is due to the higher force exerted by the tip on the particle in order to obtain proper topographical images. The average length expected was between 100 and 150 nm due to the RNA used for the experiments. Approximately forty percent have lengths between 70 and 90 nm, 20% between 100 -120 nm, and 12% between 130-150 nm. Very few were found to be longer than 160 nm (3%). The discrepancy between the expected particle length (100-150 nm) and the observed lengths can be explained e.g by RNA degradation, blocked origin of assembly, blocked accessible assembly sites along the RNA. The 20% of those particles with lengths between 40-60 nm can be considered as proto particles not completely formed.

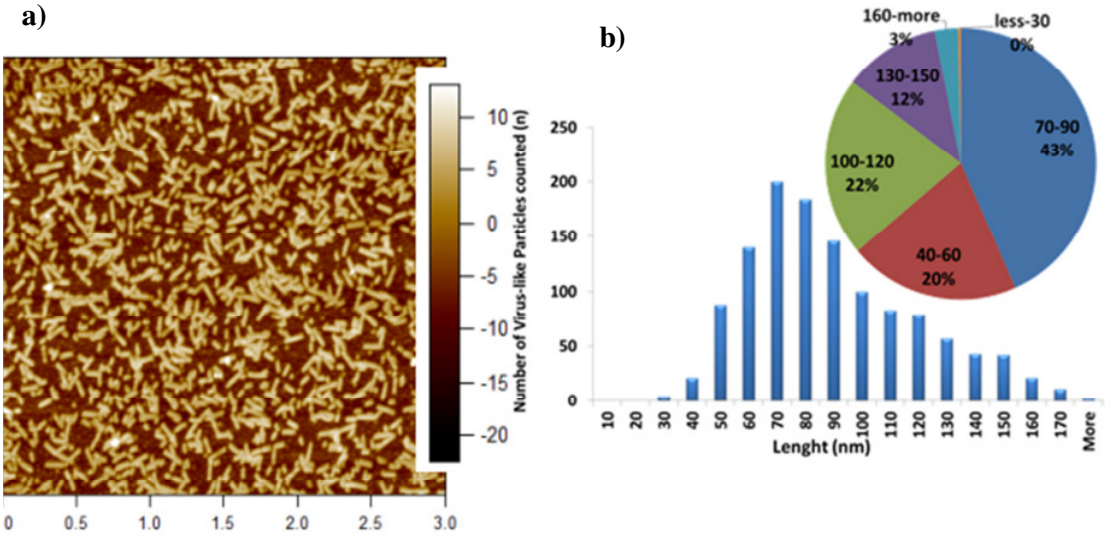

Figure 82.- Self-assembly of TMV-like nanorod structures on ITC-terminated silicon substrates. Representative AFM topography of a substrate (a) coated with self-assembled TMV-like particle after all preparation steps, and (b) statistical analysis of the particle length based on (a).

The samples for the negative controls were silanized in the same batch as the other positive control samples.

There were three different negative control experiments carried out: (1) the first control experiment was done omitting the primer-DNA assembly but carrying out the treatment with the RNA and with CP. As a result, no visible rods could be detected on the substrate where the DNA was not spotted. The spotting took place only on the center of the

substrate, and the Figure 83a corresponds to an area outside of the DNA-linker drop. Thus the unspecific physisorption of RNA on the surface can be excluded (outside the drop of DNA linker area). (2) the second control experiment on the feasibility of the virus to assemble in solution (shown in Figure 83c as TEM image) was performed by mixing the same RNA and CP as those used for the bottom-up assembly on the surface and then spot them onto a previously silanized wafer (Figure 83b). As a result TMV-like particles were found on the carbon coated copper grid in the TEM (Figure 83c), which shows that the pre-assembly was successful, however, on the surface of the silanized Si wafer, no pre-assembled TMV particles could be recognized by AFM (Figure 83b) due to low unspecific interaction between the CPs of the virus particles and the supporting substrate. The first two control experiments exclude physisorption as responsible for the coupling of the virus on the surface. Furthermore, (3) in third control experiment the step of RNA coupling and further CP addition was skipped during sample preparation, as a result no TMV-like rods were found, which shows that without RNA + CP, self-assembly does not occur (either by just the CP assembly without RNA under very specific conditions of pH as shown by Butler and Durham [460-462]) and no cross contamination between samples takes place either at any stage or procedure (Figure 83d).

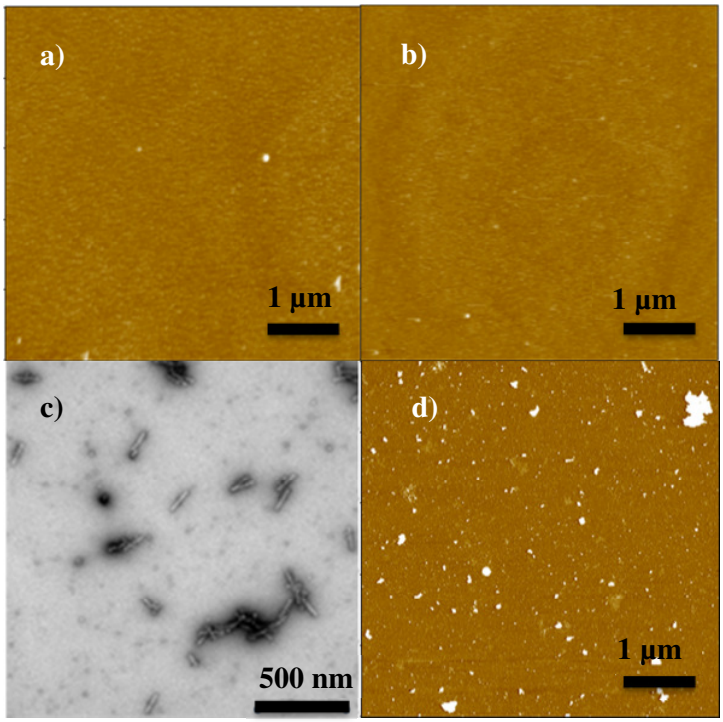

Figure 83.- Control experiments for bottom up assembly of TMV-like particles on a ITC functionalized silica wafer. a) AFM topographic image showing result from control experiment outside the drop, b) AFM topographic image showing the result of preassembled virus spotted on the functionalized silica wafer but washed away thoroughly, c) Transmission Electron microscope image of self-assembled virus in solution the scale bar is 500 nm d) AFM image showing the control experiment inside the drop without RNA and CP. All the AFM images are 5x5 µm^2

The TMV-like particles resulting from the self-assembly process on the surface show a characteristic feature: their length/width ratio is different than those assembled in liquid. The average length of the particles was calculated around 120 nm for those RNA with 3000 base pairs.

4.2.4.2 Chemically Patterned SAMs on Oxidic Substrates

The chemical one-step coupling of the ITC-silane to the oxidic interface of the surface offers the opportunity to apply Dip Pen Nanolithography (DPN) to create arrays of ITC-terminated spots on glass coverslips. With this method not only the size and the distance between the functionalized spots can be reduced to sub-micron dimension but also the density as well as the shape of the structures can be varied arbitrarily (for further reading please look [89, 210, 406, 407]). As the TMV-like particles are confined into an even smaller functional area the re-assessment of features by AFM is easier on the spotted sites than on non-structured substrates. Figure 84 shows AFM images of a 5 x 5 spots-array (41a,41c,41e) of ITC functionalized spots created by DPN and a zoom on a random spot over that array (Figure 84b, Figure 84d, Figure 84f). Tobacco mosaic virus particles assembled on the surface of patterned specific isothiocyanate silane spots on glass cover slides. Preliminary assessment of the substrate was done with a complementary amino fluorescein experiment (see section 4.2.2.4) in order to ensure the distribution, order and reactivity of the silane towards an amino group. The experiment showed indeed specificity with a clear preference for the silanized areas. The spots shown in Figure 84a and Figure 84b have an average height of 25 nm. This is significantly higher than it would be expected from a monolayer of the ITC-silane on the surface. However, in contrast to the preparation of the ITC-terminated Si wafer which was described before, the deposition of the small droplets of the ITC-silane on the glass by the DPN method in air with a relative humidity of 30% results in a polymerization of all deposed molecules, as no washing or rinsing is carried out to remove the excess of ITC-silane from the spotted areas and thus an ITC-silane multilayer is formed. The polymerization of silanes under high humidity is well known in literature [36].

After the coupling of DNA linker (Figure 84b), the samples were washed thoroughly. Hybridization of RNA strands and induction of assembly by the addition of TMV CP was performed and a significant decrease in height of the spotted areas from 25 nm to a 10 nm plateau could be observed. This is probably due to the removal of parts of the

polymerized non-covalently bound material by several washing steps during RNA immobilization and the assembly of the nucleoprotein tubes. A density decreasing of grown TMV-like particles can be observed in Figure 84f going from the rim of the spot to its center. This can also be appreciated with a higher magnification on the Figure 85a. From the experiments with Si-wafers and UV-irradiated PDMS we found (1) that the coupling of the RNA to the DNA is selective and (2) that no unspecific adsorption of the RNA on the silanized surface can be observed without DNA (Figure 85b). Therefore the appearance of TMV-like particles on the spotted areas proves that a site selective immobilization of the DNA took place even under the observed polymerized silane. The density gradient of the particles can thus be explained by a diffusion of the DNA containing solution underneath the polymerized silane, which is just loosely bound to the substrate and is washed away during the further preparation steps of TMV nanoparticle preparation. The DNA is immobilized by those ITC-terminated silane molecules which are covalently bound to the glass substrate and is not removed during the washing procedures.

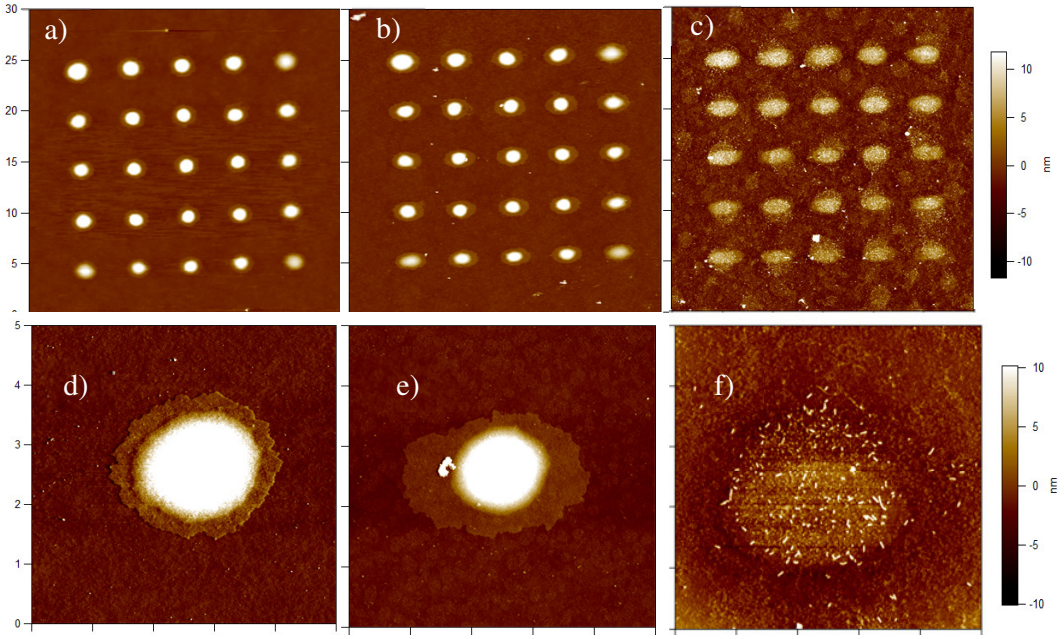

Figure 84.- AFM topographic images of DPN functionalized substrate showing a high specific selectivity for virus particles. On the upper row, scan areas of 30x30 microns (a,b,c) and on the lower row scan areas of 5x5 microns (d,e,f). ITCPTMS dots were deposited (a,d) on glass coverslip, then a DNA-linker drop covering the whole array at the same time was placed on top (b,e) and a final step of RNA coupling and CP addition (c,f) in order to obtain the virus-like particles as shown.

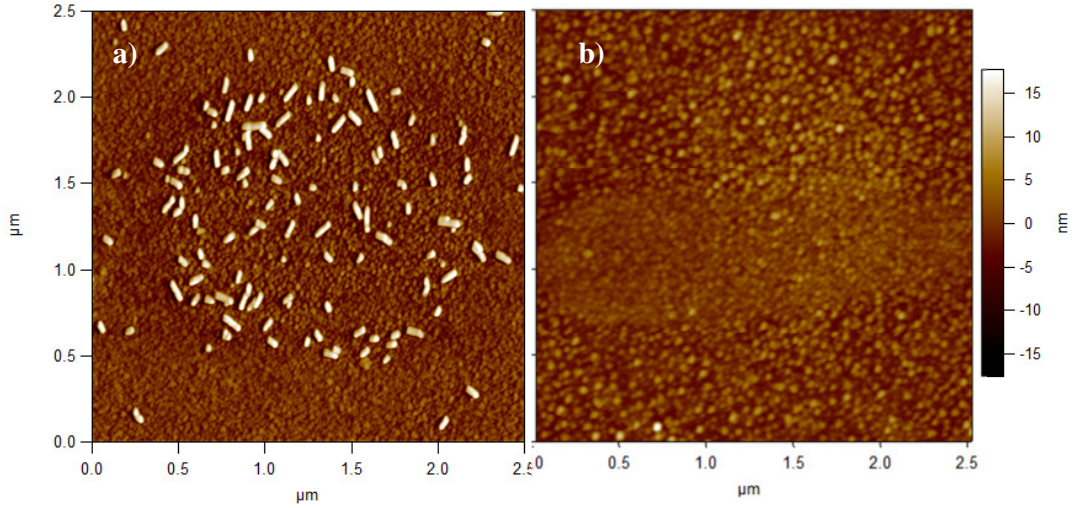

Figure 85.- AFM images showing a topographic examination on two different substrates treated with the same ITCPTMS using DPN. a) Complete process done as explained above (silanization-DNA ligand attachament- RNA hibridization- CP addition - BU assembly). b) Substrate with preassembled virus deposited on the surface and then washed out the same way the final washing step for the self assembled virus is performed.

A comparative statistical analysis was performed in the same way as the analysis performed for the PDMS and flat silica wafer substrates. The length distribution remained relatively similar to those before. A broader length distribution was found around 100-120 nm while TMV particles longer than 150 nm were not so common. In Figure 86b the statistical analysis of the length distribution of the TMV-like particles assembled on a glass cover slip (Figure 86a) is shown. Approximately 35% of the evaluated TMV particles had lengths between 70 and 90 nm, 36% between 100 and 120 nm, and 19% between 130 and 150 nm. Very few were found to be longer than 160 nm (5%).

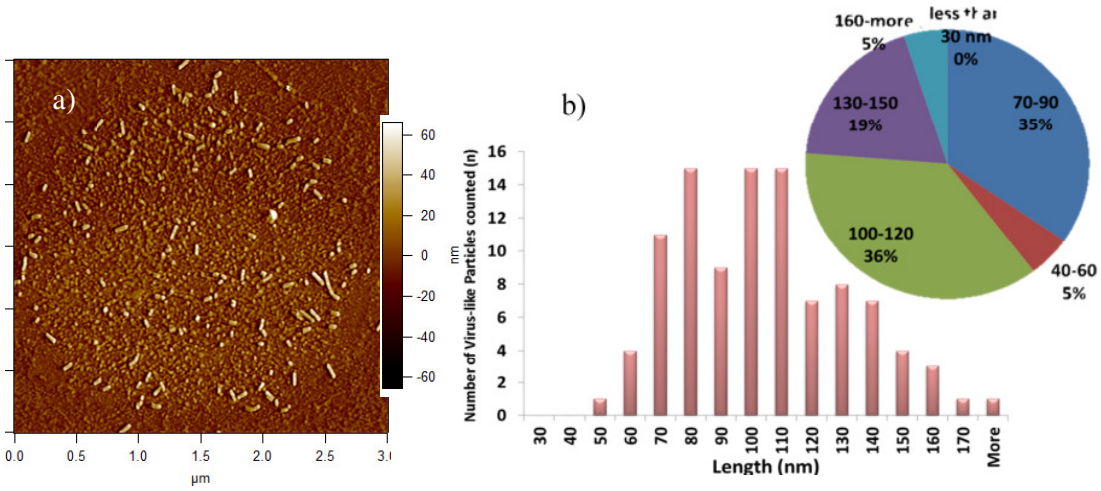

Figure 86.- Bottom up assembly of TMV-like particles on a ITC functionalized Dip Pen Nanolithography estructured silica wafer. a) 3x3 µm scan area, b) statistical analysis on picture.

4.2.4.3 Chemically Patterned SAMs on Polymeric Substrates

Besides the functionalization of silica surfaces we examined the site selective coupling of the ITCPTMS onto oxidized PDMS based substrates. The PPDMS contains silica atoms and methyl terminated bonds. The presence of oxygen in the polymer matrix, but especially in the air allows us to oxidize the upper layer of the polymeric bulk by using an Ultraviolet and Ozone generator lamp as mention in section 2.1.3.2. We use this technique to produce a selectively oxidized silica-like substrate by irradiating the PDMS substrates with UV/O_3 through masks as described in the scheme of Figure 87.

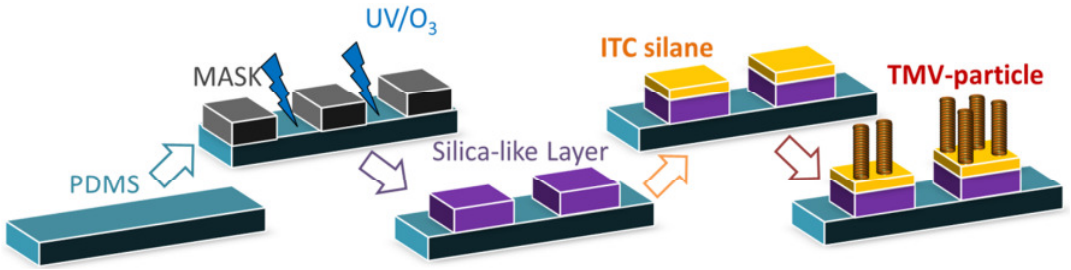

Figure 87.-Scheme of polydimethylsiloxane (PDMS) substrate treated and silanized with isothiocyanate groups, with subsequent TMV assembly.

After the complete procedure of TMV bottom-up assembly was carried out (silanization-DNA coupling- RNA coupling- CP) two regions were then visible: (1) squares in which the conversion from PDMS to the Silica-like surface took place and (2) the bars in which the mask hindered the process of oxidation leaving the polymer unchanged (Figure 88a). Due to the positioning of the mask, which has a flat side and a slightly curved side, if the mask has been placed on the curved side, then features like the rim around the most irradiated areas are found and some material has been also transformed. This can be seen in Figure 88b as a fainted area surrounding the irradiated and silanized part. While the rest of the PDMS substrate remains untreated (Figure 88d) on the silanized areas the bottom up assembly process takes place, as shown in the zoom-in image of the irradiated/silanized area in Figure 88c. Completely formed virus can be found on the square parts of the irradiated and chemically modified PDMS patterns of the polymer (Figure 88e) and they show a broader length distribution than those on the silica wafer without any structuring. By some means the polymer shows also a higher porosity level than before the treatment with the silane and further assembly.

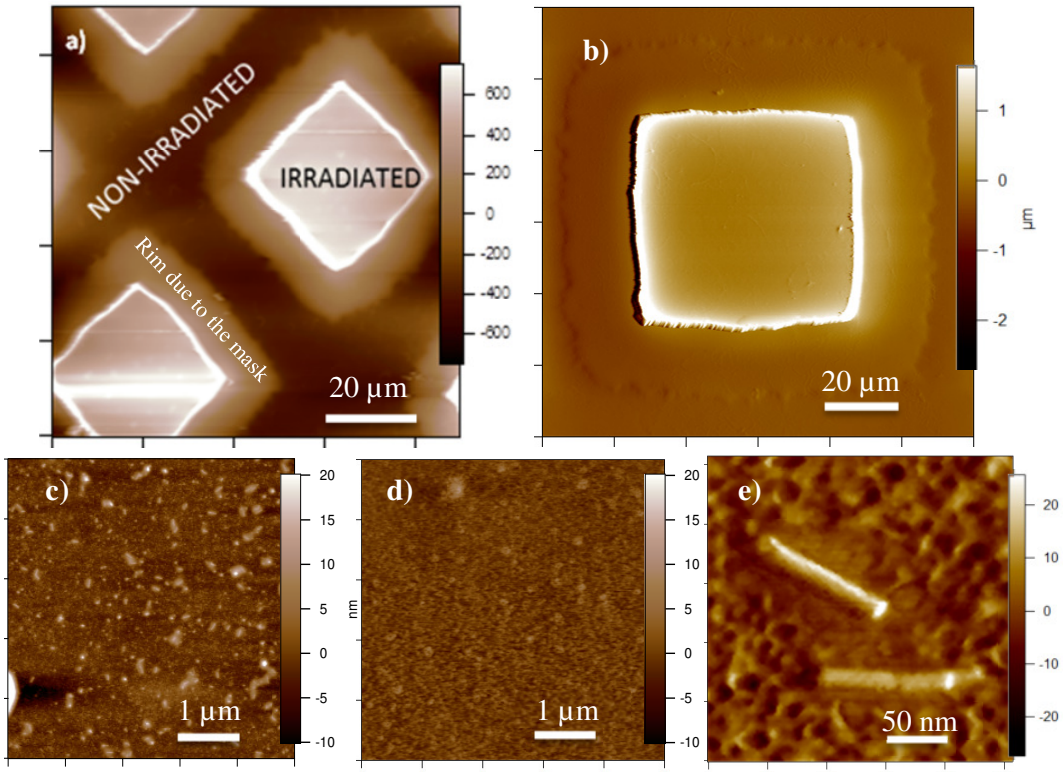

Figure 88.- AFM images showing the results from bottom up assembly of TMV-like particles on a site selective ITC functionalized PDMS substrate. a) 90x90 µm scan area with the irradiated and protected areas, b) 60x60 µm scan area with the irradiated area and the rim around due to the positioning of the grid c) zoom in on the irradiated area showing TMV-like particles d) zoom scan on the non-irradiated parts of the polymer where no particle can be found and e) a 250x250 nm zoom showing TMV-particles grown on the treated regions as elongated rods.

The average lengths of the rods are in agreement with those, which were assembled on pure silica wafer. The histogram in Figure 89a shows the results of the determination of particle length over the 25 μm^2 area of Figure 88c. It can be noticed that the average length of the TMV-like particles are around 87 nm with a standard deviation of 34 nm. Although the mean and standard deviation are in agreement with the results from the silica wafer experiments, a distribution with a more pronounced skewness towards longer particles was found.

The TMV-like particles self-assembled exclusively on those surface areas which were irradiated and silanized. This indicates a highly selective coupling of the virus RNA on the respective areas. The increased roughness (RMS= 3.196 nm) of these PDMS areas after been silanized by the ITCPTES as shown in Table 14, compared to those of the silanized Si wafers depicted in Table 9 (RMS = 1.867 nm) might be due to the described hydrophobicity recovery of the polymer during the initial time period of the irradiation process. In Figure 89b the statistical analysis of the length distribution of the TMV-like particles is shown. About 27% of the evaluated TMV particles had lengths between 40

and 60 nm, 34% between 70 and 90 nm, 18% between 100 and 120 nm and 17% between 130 and 150 nm. Very few were found to be longer than 160 nm (4%). It can be concluded that only in the case of the non-structured Si wafer (Figure 82) a pronounced maximum in the length distribution of the TMV-like particles can be detected. This discrepancy can be due to different reasons as e.g. the unspecific interaction between the free RNA strand with the surface or sterical hindrance during the formation of the protein coat and the fact that once the RNA is prepared, it is shorten significantly up to 2884 nucleotides corresponding to a theoretical value of 135 nm in length. The high density of TMV-like particles obtained with silicon surfaces could not be reproduced on PDMS.

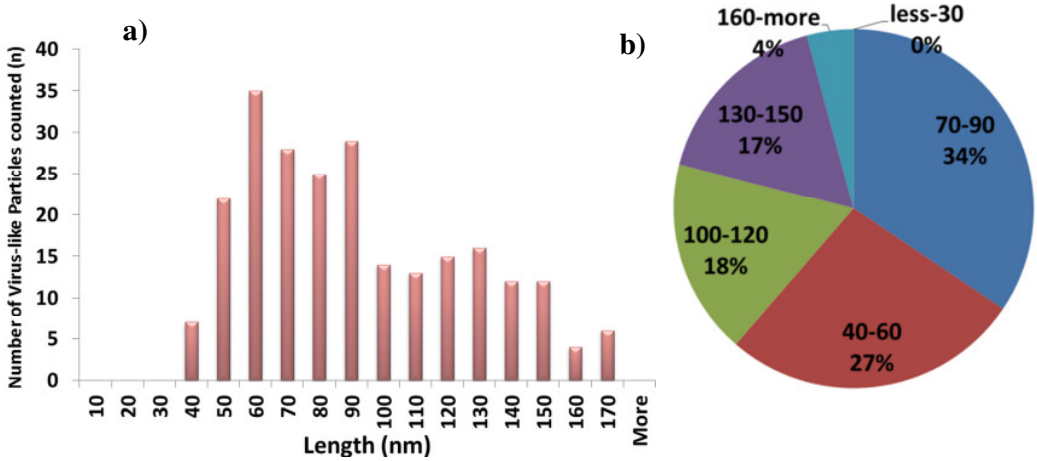

Figure 89.- Descriptive statistical analysis of TMV-like particle lenghts grown on PDMS selectively irradiated substrates. a) histogram showing the amount of particles found corresponding to their lengths taken from two different treated regions. b) distribution of the particle length by percentage.

5 Conclusions

5.1 General Conclusions

Within this work a new chemical approach based on isothiocyanate-terminated silanes is introduced as an alternative to the aldehyde based surface chemistry for the preparation of structured and non-structured substrates of different materials (glass, silicon and polymer) which are optimized for the site-selective bottom-up assembly of tobacco mosaic virus (TMV-) like particles. To reach this goal first the ITC-terminated silane was synthesized and coupled to different substrates. Beside glass and Si wafers with a native oxide layer also the polymer polydimethylsiloxane (PDMS) was used as substrate material, whereby PDMS was irradiated with UV-light to create an oxidic layer on top of the polymer, which – in turn – can be treated then as an oxidic substrate as well. In all cases first non-structured substrates were prepared, chemically modified and characterized intensively by surface-analytical methods as XPS, IRRAS, contact angle measurement or fluorescence microscopy. In a further step the coupling strategies were combined with different structuring techniques as micro contact printing (μCP), Dip Pen Nanolithography (DPN) and UV-light irradiation to prepare surface patterns, which were then chemically terminated with the ITC-silane. To test the applicability of the substrates for bottom-up assembly of TMV-like particles, a DNA-linker was immobilized on the ITC-functionalized areas followed by the RNA coupled to the DNA via hybridization. After the coat proteins were added, the assembled virus particles could be observed on the substrate. This proves for the first time that the ITC-based chemistry developed in this work can be used for the bottom-up assembly of virus-like particles.

All the results are summarized in more detail in the following: In a first step the conversion of 3-aminopropyltrimethoxysilane in solution to 3-isothiocyanatepropyltrimethoxysilane has been examined using infrared spectroscopy. The appearance of the broad band centered around 2100 cm^{-1} after the reaction has taken place, confirms the strong double bond stretching between the –N=C=S group. By the use of Raman spectroscopy the reactants could be traced (consumption of carbon disulfide over time) which confirms the successful transformation of the amine towards the isothiocyanate group.

The coupling of the synthesized ITC-silane to oxidic substrates as glass, Si wafers and UV-irradiated PDMS has been studied using X-ray photo electron spectroscopy (XPS). The results confirm the presence of the ITC group on the surface in all cases. XPS was also used to determine the amount of hydroxyl groups on the surface by measuring the amount of oxygen

atoms present in the substrates. The fact that PDMS after the irradiation procedure showed a higher amount of oxygen on the surface than the same substrate after the additional treatment with the ITC-silane is a hint that the covalent coupling of the silane to the surface has been successful.

The presence of the isothiocyanate termination on the surface was examined – beside by XPS – also indirectly by fluorescence microscopy using an amino terminated DNA-oligomer holding a fluorescence molecule on the other end. These experiments were used also to compare a commercially acquired epoxy functionalized slide versus an isothiocyanate silanized in house slide. The results showed that the chemical reactivity of ITC-silanized slides is comparable. Further experiments were performed using the NH_2-terminated fluorescein-labeled DNA molecule (NH_2-DNA-Fluorecein) which was spotted by hand and evaluating the amino, aldehyde and isothiocyanate functional groups when they are coupled to glass slides. These experiments showed that under the same experimental conditions, the ITC-terminated substrates show a higher total fluorescence intensity compared to that from the amino- and aldehyde-terminated surfaces. The results are summarized and shown in Figure 90. The aldehyde chemistry, although successful, turned out being less prone to bind amino terminated oligonucleotides containing a fluorescent molecule. The measured fluorescence intensity of the NH_2-DNA-Fluorescein after coupling, increased in the following order: non-functionalized slide < aminoterminated slide < aldehyde terminated slide < ITC-coated slide.

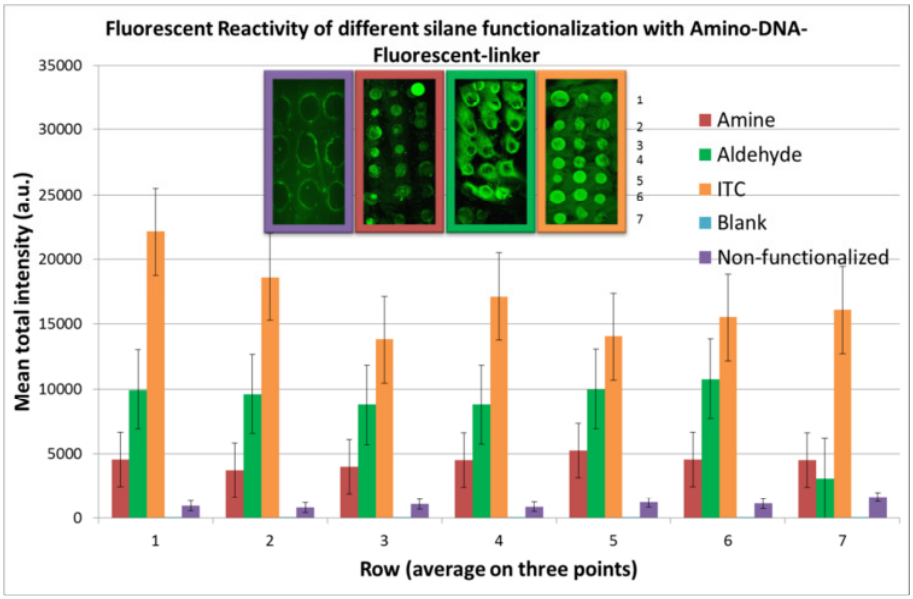

Figure 90.- Fluorescent reactivity evaluation on glass slides silanized with: i) aminopropyltrimethoxysilane, ii) aminopropyltrimethoxysilane + aldehyde coupling and iii) isothiocyanatepropyltrimethoxysilane. An additional control was done with a non-functionalized silane for background assesment.

Atomic force microscope was used to characterize the morphology of the surface before and after the silanization. Physical changes monitored by the AFM appear to follow qualitatively with chemical changes reasonably well for all the silanes in study. For the isothiocyanate silane, when a 5x5 μm^2 area is studied, although no extreme changes could be seen, the total quadratic mean of the surface roughness (RMS) increased from a 0.2 nm before silanization up to 1.9 nm after the silanization was performed. The samples indeed showed a rougher surface after treatment, but an important observation from this AFM images is the formation of small islands of the silane across the complete surface. The increase in roughness was common for all the substrates independent of the original surface (smooth silica wafer, glass or polymer).

In order to create dense arrays of TMV-like particles in defined patches highly reproducible, we describe new routes for the site-selective bottom-up assembly of TMVs.

The novel aspects are (1) the application of an isothiocyanate (ITC) based chemistry to immobilize the viral RNA, which allows the preparation of a high surface density of self-assembled TMV, (2) the combination of the ITC chemistry with UV-lithography and Dip Pen Nanolithography, which allows the exact control of shape and size of the assembling sites on the substrates, (3) the transfer of the ITC-based chemistry to PDMS, which is a polymeric standard material of micro fluidic devices for applications in the fields of lab-on-a-chip technology and (4) the use of DNA/RNA hybridization for immobilization of assembly-directing RNA.

From the experiments it can be concluded that the new approach to realize bottom-up self-assembly of TMV-like particles on oxidic interfaces based on the formation of thiourea bond between an ITC-terminated substrate and an amino functionalized linker DNA is successful and can be carried out site selectively on both Si wafers with a native oxide layer and on UV irradiated polydimethylsiloxane (PDMS). In addition we could show that the combination of the ITC-based chemistry with two different structuring techniques - the Dip Pen Nanolithography and the photo oxidation of PDMS - results in a site-selective growth of TMV-like particles. Compared to the method described in Müller et al.[72] the coupling of the aminated DNA linker via the ITC terminated silanes resulted in a reproducible high density of the grown TMV-like particles while the geometry of the coupling sites can be varied in size and shape in a well-defined manner in the case of Dip Pen Nanolithography (DPN) and UV-lithography of the PDMS material [73]. A graphical summary of results from the TMV bottom-up site selective assembly is shown in Figure 91.

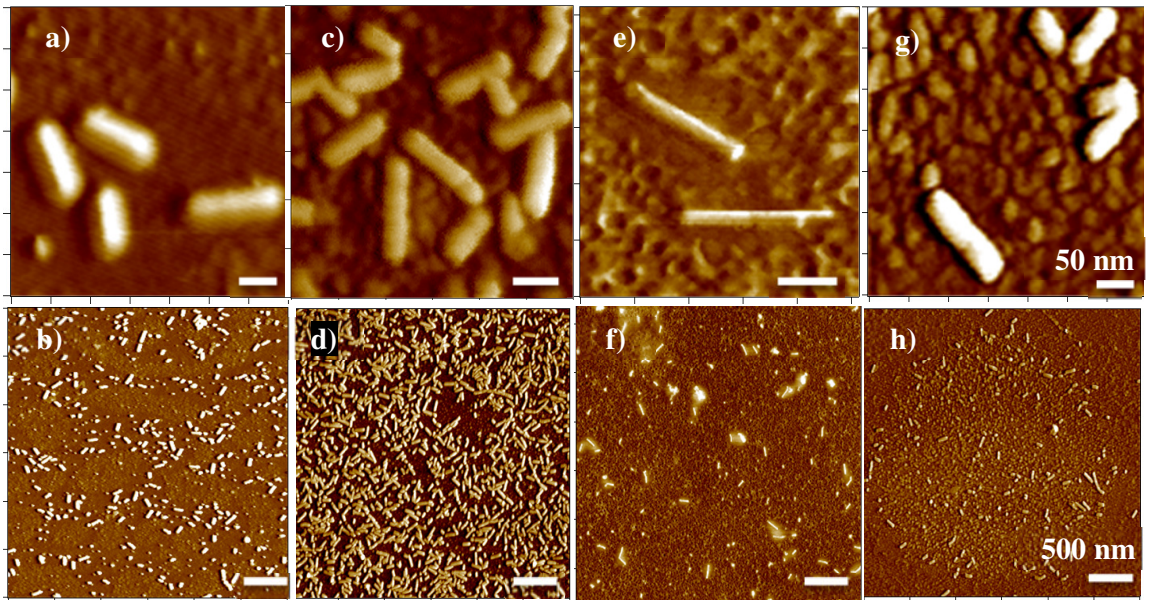

Figure 91.- AFM topographic images, shown as a summary of the silanized substrates submitted to the TMV-like particles bottom up assembly . a-b) aldehyde functional substrate on silica wafer with a PMMA masking for selective attachment. c-d) isothiocyanate functionalized silica wafer with no structuring. e-f) isothiocyanate silanized PDMS substrate using a chemical selective structuring irradiation technique. g-h) isothiocyanate silanized glass slide using a chemical structuring *via* dip pen nanolithograpy for selective deposition of the silane. The scales in the a,c,e,g images is 50 nm while in the b,d,f,h images is 500 nm.

5.2 Outlook

The assembly of TMV-like particles on the substrates proved a new methodology how versatile components can be of use for materials and/or surfaces prepared for miniaturized devices or high-throughput multifunctional systems. The accessibility of this biotemplates to be merged with other techniques (lab-on-a-chip, biosensors, etc.) makes the systems relevant for improving and building on top of the knowledge provided by this thesis in order to deliver a more controllable and spatially selective bottom-up integration of biological moieties.

As one of the main intentions of this work was to prove that a site-selective growth of the TMV-like particles can be realized by combining the bottom-up self-assembly with top-down structuring methods, more experiments will be necessary to find out why the different substrate materials and structuring techniques result in different particle densities and/or length distributions. The approach of transferring the ITC-based chemistry for TMV particle growth to the PDMS material which is used in the preparation e.g. of micro fluidic devices opens the access to many applications in the field of lab-on-a-chip techniques, where TMV-like particles will be developed to form upright standing carriers e.g. of enzymes for analytical purpose. One approach in this direction is project A6 of the “Kompetenznetz für

Funktionelle Nanostrukturen (KFN)" of the "Baden-Württemberg-Stiftung". The results presented in this thesis have been essential for granting this follow-up project.

Beside this idea to imbed the TMV-like particles into a technical environment, there are also challenges focusing on the chemistry of the coat proteins of the nanoparticles: Further goals might include, but not exclusively: a) genetically modified virus coat protein with different functional groups which can be arranged in a selected order along the longitudinal axis of the virus-like particle providing in this way optimal availability for bioconjugation of other molecules such as high-affinity peptides, enzymes or antibodies. This adaptable order in the functionality assembly can serve as a "bar-coding" system for other biointegrative strategies. As mention before, the biochemically accessibility of the TMV-like particles could eventually be improved by bringing the particles to stand up perpendicular to the surface. This would provide a lower sterical hindrance and eventually a higher density gradient of the particles and therefore a higher biosensoring capability of the surface.

Similar strategies for microstructuring the morphology of the substrates (polymer blends, breath figures, gold/silica etching processes, casting and molding of elastomers, etc.) and chemically nanostructuring the surfaces (DPN, AFM-grafting, AFM-shaving, etc.) can be implemented. Further polymer systems (polystyrene, polymethylmethacrylate, polypropylene etc.) could be eventually tested to check whether these systems can provide with site-selective coupling capabilities.

6 REFERENCES

1. Gao, J., H. Gu, and B. Xu, *Multifunctional Magnetic Nanoparticles: Design, Synthesis, and Biomedical Applications.* Accounts of Chemical Research, 2009. **42**(8): p. 1097-1107.
2. Fischlechner, M. and E. Donath, *Viruses as Building Blocks for Materials and Devices.* Angewandte Chemie International Edition, 2007. **46**(18): p. 3184-3193.
3. Favret, E.A. and N.O. Fuentes, *Functional properties of bio-inspired surfaces: characterization and technological applications*2009: World Scientific.
4. Clare, D.K. and E.V. Orlova, *4.6 Å Cryo-EM reconstruction of tobacco mosaic virus from images recorded at 300 keV on a 4k CCD camera.* Journal of Structural Biology, 2010. **171**(3): p. 303-308.
5. Kadri, A., et al., *Engineered Tobacco mosaic virus mutants with distinct physical characteristics in planta and enhanced metallization properties.* Virus Research, 2011. **157**(1): p. 35-46.
6. Dawson, W.O., P. Bubrick, and G.L. Grantham, *Modifications of the Tobacco Mosaic Virus Coat Protein Gene Affecting Replication, Movement, and Symptomatology.* Phytopathology, 1988. **78**(6): p. 783-789.
7. Mueller, A., et al., *In vitro assembly of Tobacco mosaic virus coat protein variants derived from fission yeast expression clones or plants.* Journal of Virological Methods, 2010. **166**(1–2): p. 77-85.
8. Dujardin, E., et al., *Organization of Metallic Nanoparticles Using Tobacco Mosaic Virus Templates.* Nano Letters, 2003. **3**(3): p. 413-417.
9. Górzny, M.Ł., A.S. Walton, and S.D. Evans, *Synthesis of High-Surface-Area Platinum Nanotubes Using a Viral Template.* Advanced Functional Materials, 2010. **20**(8): p. 1295-1300.
10. Chen, X., et al., *Virus-Enabled Silicon Anode for Lithium-Ion Batteries.* ACS Nano, 2010. **4**(9): p. 5366-5372.
11. Royston, E., et al., *Self-Assembly of Virus-Structured High Surface Area Nanomaterials and Their Application as Battery Electrodes.* Langmuir, 2007. **24**(3): p. 906-912.
12. Wu, Z., et al., *Enhancing the Magnetoviscosity of Ferrofluids by the Addition of Biological Nanotubes.* ACS Nano, 2010. **4**(8): p. 4531-4538.
13. Tseng, R.J., et al., *Digital memory device based on tobacco mosaic virus conjugated with nanoparticles.* Nature nanotechnology, 2006. **1**(1): p. 72-7.
14. Adams, M., J. Antoniw, and J. Kreuze, *Virgaviridae: a new family of rod-shaped plant viruses.* Archives of Virology, 2009. **154**(12): p. 1967-1972.
15. Klug, A., *The tobacco mosaic virus particle: structure and assembly.* Philosophical Transactions of the Royal Society of London. Series B: Biological Sciences, 1999. **354**(1383): p. 531-535.
16. Lebeurier, G., A. Nicolaieff, and K.E. Richards, *Inside-Out Model for Self-Assembly of Tobacco Mosaic Virus.* Proceedings of the National Academy of Sciences of the United States of America, 1977. **74**(1): p. 149-153.
17. Butler, P.J. and G.P. Lomonossoff, *RNA-protein interactions in the assembly of tobacco mosaic virus.* Biophysical Journal, 1980. **32**(1): p. 295-312.
18. Butler, P.J.G., *Self–assembly of tobacco mosaic virus: the role of an intermediate aggregate in generating both specificity and speed.* Philosophical Transactions of the Royal Society of London. Series B: Biological Sciences, 1999. **354**(1383): p. 537-550.
19. Whitesides, G.M. and B. Grzybowski, *Self-Assembly at All Scales.* Science, 2002. **295**(5564): p. 2418-2421.
20. Ariga, K., J. Hill, and H. Endo, *Developments in Molecular Recognition and Sensing at Interfaces.* International Journal of Molecular Sciences, 2007. **8**(8): p. 864-883.
21. Kim, D. and D. Kang, *Molecular Recognition and Specific Interactions for Biosensing Applications.* Sensors, 2008. **8**(10): p. 6605-6641.
22. Jelinek, R., *Cellular and Biomolecular Recognition: Synthetic and Non-Biological Molecules*2009: Wiley-VCH.
23. Sugimura, H., et al., *Photolithography based on organosilane self-assembled monolayer resist.* Electrochimica Acta, 2001. **47**(1–2): p. 103-107.
24. Anderson, M.E., et al., *Combining Conventional Lithography with Molecular Self-Assembly for Chemical Patterning.* Advanced Materials, 2006. **18**(24): p. 3258-3260.
25. Lercel, M.J., et al., *Electron beam lithography with monolayers of alkylthiols and alkylsiloxanes.* Journal of Vacuum Science & Technology B: Microelectronics and Nanometer Structures, 1994. **12**(6): p. 3663-3667.
26. Gooding, J.J., et al., *Self-Assembled Monolayers into the 21st Century: Recent Advances and Applications.* Electroanalysis, 2003. **15**(2): p. 81-96.
27. Gooding, J.J. and D.B. Hibbert, *The application of alkanethiol self-assembled monolayers to enzyme electrodes.* TrAC Trends in Analytical Chemistry, 1999. **18**(8): p. 525-533.
28. Fibbioli, M., et al., *Redox-active self-assembled monolayers as novel solid contacts for ion-selective electrodes.* Chemical Communications, 2000(5): p. 339-340.
29. Deng, H., et al., *Corrosion prevention of iron with novel organic inhibitor of hydroxamic acid and UV irradiation.* Electrochimica Acta, 2008. **53**(6): p. 2972-2983.
30. Hintze, P.E. and L.M. Calle, *Electrochemical properties and corrosion protection of organosilane self-assembled monolayers on aluminum 2024-T3.* Electrochimica Acta, 2006. **51**(8–9): p. 1761-1766.
31. Mathiyarasu, J., S.S. Pathak, and V. Yegnaraman, *Review on Corrosion prevention of Copper using ultrathin organic monolayers*, in *Corrosion Reviews*2006. p. 307.
32. Wang, M., et al., *Self-Assembled Silane Monolayers: Fabrication with Nanoscale Uniformity.* Langmuir, 2005. **21**(5): p. 1848-1857.
33. Zhuravlev, L.T., *Concentration of hydroxyl groups on the surface of amorphous silicas.* Langmuir, 1987. **3**(3): p. 316-318.
34. Zhu, M., M.Z. Lerum, and W. Chen, *How To Prepare Reproducible, Homogeneous, and Hydrolytically Stable Aminosilane-Derived Layers on Silica.* Langmuir, 2011. **28**(1): p. 416-423.
35. Zeira, A., et al., *Contact Electrochemical Replication of Hydrophilic−Hydrophobic Monolayer Patterns.* ACS Nano, 2008. **2**(12): p. 2554-2568.

36. YANG, L., ET AL., *FILM FORMING KINETICS AND REACTION MECHANISM OF Γ-GLYCIDOXYPROPYLTRIMETHOXYSILANE ON LOW CARBON STEEL SURFACES.* APPLIED SURFACE SCIENCE, 2010. **256**(22): P. 6787-6794.
37. WADDELL, T.G., D.E. LEYDEN, AND M.T. DEBELLO, *THE NATURE OF ORGANOSILANE TO SILICA-SURFACE BONDING.* JOURNAL OF THE AMERICAN CHEMICAL SOCIETY, 1981. **103**(18): P. 5303-5307.
38. VANDENBERG, E.T., ET AL., *STRUCTURE OF 3-AMINOPROPYL TRIETHOXY SILANE ON SILICON OXIDE.* JOURNAL OF COLLOID AND INTERFACE SCIENCE, 1991. **147**(1): P. 103-118.
39. VALLANT, T., ET AL., *INVESTIGATION OF THE FORMATION AND STRUCTURE OF SELF-ASSEMBLED ALKYLSILOXANE MONOLAYERS ON SILICON USING IN SITU ATTENUATED TOTAL REFLECTION INFRARED SPECTROSCOPY.* LANGMUIR, 1999. **15**(16): P. 5339-5346.
40. VALLANT, T., ET AL., *FORMATION OF SELF-ASSEMBLED OCTADECYLSILOXANE MONOLAYERS ON MICA AND SILICON SURFACES STUDIED BY ATOMIC FORCE MICROSCOPY AND INFRARED SPECTROSCOPY.* THE JOURNAL OF PHYSICAL CHEMISTRY B, 1998. **102**(37): P. 7190-7197.
41. SAGIV, J., *ORGANIZED MONOLAYERS BY ADSORPTION. 1. FORMATION AND STRUCTURE OF OLEOPHOBIC MIXED MONOLAYERS ON SOLID SURFACES.* JOURNAL OF THE AMERICAN CHEMICAL SOCIETY, 1980. **102**(1): P. 92-98.
42. SILBERZAN, P., ET AL., *SILANATION OF SILICA SURFACES. A NEW METHOD OF CONSTRUCTING PURE OR MIXED MONOLAYERS.* LANGMUIR, 1991. **7**(8): P. 1647-1651.
43. BRANDRISS, S. AND S. MARGEL, *SYNTHESIS AND CHARACTERIZATION OF SELF-ASSEMBLED HYDROPHOBIC MONOLAYER COATINGS ON SILICA COLLOIDS.* LANGMUIR, 1993. **9**(5): P. 1232-1240.
44. TILLMAN, N., ET AL., *INCORPORATION OF PHENOXY GROUPS IN SELF-ASSEMBLED MONOLAYERS OF TRICHLOROSILANE DERIVATIVES. EFFECTS ON FILM THICKNESS, WETTABILITY, AND MOLECULAR ORIENTATION.* JOURNAL OF THE AMERICAN CHEMICAL SOCIETY, 1988. **110**(18): P. 6136-6144.
45. GUN, J., R. ISCOVICI, AND J. SAGIV, *ON THE FORMATION AND STRUCTURE OF SELF-ASSEMBLING MONOLAYERS: II. A COMPARATIVE STUDY OF LANGMUIR—BLODGETT AND ADSORBED FILMS USING ELLIPSOMETRY AND IR REFLECTION—ABSORPTION SPECTROSCOPY.* JOURNAL OF COLLOID AND INTERFACE SCIENCE, 1984. **101**(1): P. 201-213.
46. YASSERI, A.A., N.P. KOBAYASHI, AND T.I. KAMINS, *FORMATION AND CHARACTERIZATION OF LONG-CHAINED ALKYLSILOXANE SELF-ASSEMBLED MONOLAYERS ON ATOMIC-LAYER-DEPOSITED ALUMINUM OXIDE SURFACES.* APPLIED PHYSICS A: MATERIALS SCIENCE & PROCESSING, 2006. **84**(1): P. 1-5.
47. ROZENFELD, O., ET AL., *SELF-ASSEMBLED MONOLAYER COATINGS ON AMORPHOUS IRON.* LANGMUIR, 1994. **10**(11): P. 3919-3921.
48. ULMAN, A. AND N. TILLMAN, *SELF-ASSEMBLING DOUBLE LAYERS ON GOLD SURFACES: THE MERGING OF TWO CHEMISTRIES.* LANGMUIR, 1989. **5**(6): P. 1418-1420.
49. LAIBINIS, P.E. AND G.M. WHITESIDES, *Ω-TERMINATED ALKANETHIOLATE MONOLAYERS ON SURFACES OF COPPER, SILVER, AND GOLD HAVE SIMILAR WETTABILITIES.* JOURNAL OF THE AMERICAN CHEMICAL SOCIETY, 1992. **114**(6): P. 1990-1995.
50. LAIBINIS, P.E., ET AL., *COMPARISON OF THE STRUCTURES AND WETTING PROPERTIES OF SELF-ASSEMBLED MONOLAYERS OF N-ALKANETHIOLS ON THE COINAGE METAL SURFACES, COPPER, SILVER, AND GOLD.* JOURNAL OF THE AMERICAN CHEMICAL SOCIETY, 1991. **113**(19): P. 7152-7167.
51. XIA, Y., ET AL., *A SELECTIVE ETCHING SOLUTION FOR USE WITH PATTERNED SELF-ASSEMBLED MONOLAYERS OF ALKANETHIOLATES ON GOLD.* CHEMISTRY OF MATERIALS, 1995. **7**(12): P. 2332-2337.
52. WHITESIDES, G.M., ET AL., *SOFT LITHOGRAPHY IN BIOLOGY AND BIOCHEMISTRY.* ANNUAL REVIEW OF BIOMEDICAL ENGINEERING, 2001. **3**(1): P. 335-373.
53. VERICAT, C., ET AL., *SELF-ASSEMBLED MONOLAYERS OF THIOLS AND DITHIOLS ON GOLD: NEW CHALLENGES FOR A WELL-KNOWN SYSTEM.* CHEMICAL SOCIETY REVIEWS, 2010. **39**(5): P. 1805-1834.
54. LIU, S., R. MAOZ, AND J. SAGIV, *PLANNED NANOSTRUCTURES OF COLLOIDAL GOLD VIA SELF-ASSEMBLY ON HIERARCHICALLY ASSEMBLED ORGANIC BILAYER TEMPLATE PATTERNS WITH IN-SITU GENERATED TERMINAL AMINO FUNCTIONALITY.* NANO LETTERS, 2004. **4**(5): P. 845-851.
55. BIEBUYCK, H.A. AND G.M. WHITESIDES, *AUTOPHOBIC PINNING OF DROPS OF ALKANETHIOLS ON GOLD.* LANGMUIR, 1994. **10**(12): P. 4581-4587.
56. BAIN, C.D., ET AL., *FORMATION OF MONOLAYER FILMS BY THE SPONTANEOUS ASSEMBLY OF ORGANIC THIOLS FROM SOLUTION ONTO GOLD.* JOURNAL OF THE AMERICAN CHEMICAL SOCIETY, 1989. **111**(1): P. 321-335.
57. LAIBINIS, P.E. AND G.M. WHITESIDES, *SELF-ASSEMBLED MONOLAYERS OF N-ALKANETHIOLATES ON COPPER ARE BARRIER FILMS THAT PROTECT THE METAL AGAINST OXIDATION BY AIR.* JOURNAL OF THE AMERICAN CHEMICAL SOCIETY, 1992. **114**(23): P. 9022-9028.
58. MAO, C., A. LIU, AND B. CAO, *VIRUS-BASED CHEMICAL AND BIOLOGICAL SENSING.* ANGEWANDTE CHEMIE INTERNATIONAL EDITION, 2009. **48**(37): P. 6790-6810.
59. WILLNER, I., ET AL., *ELECTRICAL WIRING OF GLUCOSE OXIDASE BY RECONSTITUTION OF FAD-MODIFIED MONOLAYERS ASSEMBLED ONTO AU-ELECTRODES.* JOURNAL OF THE AMERICAN CHEMICAL SOCIETY, 1996. **118**(42): P. 10321-10322.
60. GERASOPOULOS, K., ET AL., *BIOFABRICATION METHODS FOR THE PATTERNED ASSEMBLY AND SYNTHESIS OF VIRAL NANOTEMPLATES.* NANOTECHNOLOGY, 2010. **21**(5): P. 055304.
61. KELLEY, S.O., ET AL., *LONG-RANGE ELECTRON TRANSFER THROUGH DNA FILMS.* ANGEWANDTE CHEMIE INTERNATIONAL EDITION, 1999. **38**(7): P. 941-945.
62. HOLMLIN, R.E., P.J. DANDLIKER, AND J.K. BARTON, *CHARGE TRANSFER THROUGH THE DNA BASE STACK.* ANGEWANDTE CHEMIE INTERNATIONAL EDITION IN ENGLISH, 1997. **36**(24): P. 2714-2730.
63. WILHELM, T. AND G. WITTSTOCK, *ANALYSE VON WECHSELWIRKUNGEN IN GEMUSTERTEN MULTIENZYMSCHICHTEN MIT ELEKTROCHEMISCHER RASTERMIKROSKOPIE.* ANGEWANDTE CHEMIE, 2003. **115**(20): P. 2350-2353.
64. LIPSHUTZ, R.J., ET AL., *USING OLIGONUCLEOTIDE PROBE ARRAYS TO ACCESS GENETIC DIVERSITY.* BIOTECHNIQUES, 1995. **19**(3): P. 442-447.
65. GUO, Z., ET AL., *DIRECT FLUORESCENCE ANALYSIS OF GENETIC POLYMORPHISMS BY HYBRIDIZATION WITH OLIGONUCLEOTIDE ARRAYS ON GLASS SUPPORTS.* NUCLEIC ACIDS RESEARCH, 1994. **22**(24): P. 5456-5465.
66. PEASE, A.C., ET AL., *LIGHT-GENERATED OLIGONUCLEOTIDE ARRAYS FOR RAPID DNA SEQUENCE ANALYSIS.* PROCEEDINGS OF THE NATIONAL ACADEMY OF SCIENCES, 1994. **91**(11): P. 5022-5026.
67. CHIU, C.-S., ET AL., *IMMOBILIZATION OF DNA-AU NANOPARTICLES ON AMINOSILANE-FUNCTIONALIZED ALUMINUM NITRIDE EPITAXIAL FILMS FOR SURFACE ACOUSTIC WAVE SENSING.* APPLIED PHYSICS LETTERS, 2008. **93**(16): P. 163106.
68. CHRISEY, L.A., G.U. LEE, AND C.E. O'FERRALL, *COVALENT ATTACHMENT OF SYNTHETIC DNA TO SELF-ASSEMBLED MONOLAYER FILMS.* NUCLEIC ACIDS RESEARCH, 1996. **24**(15): P. 3031-3039.
69. SCHÜLER, T., ET AL., *UV CROSS-LINKING OF UNMODIFIED DNA ON GLASS SURFACES.* ANALYTICAL AND BIOANALYTICAL CHEMISTRY, 2009. **395**(4): P. 1097-1105.

70. LAMTURE, J.B., ET AL., *DIRECT DETECTION OF NUCLEIC ACID HYBRIDIZATION ON THE SURFACE OF A CHARGE COUPLED DEVICE.* NUCLEIC ACIDS RESEARCH, 1994. **22**(11): P. 2121-2125.
71. CHRISEY, L.A., ET AL., *FABRICATION OF PATTERNED DNA SURFACES.* NUCLEIC ACIDS RESEARCH, 1996. **24**(15): P. 3040-3047.
72. MUELLER, A., ET AL., *INDUCIBLE SITE-SELECTIVE BOTTOM-UP ASSEMBLY OF VIRUS-DERIVED NANOTUBE ARRAYS ON RNA-EQUIPPED WAFERS.* ACS NANO, 2011. **5**(6): P. 4512-4520.
73. AZUCENA, C., ET AL., *NEW APPROACHES FOR BOTTOM-UP ASSEMBLY OF TOBACCO MOSAIC VIRUS-DERIVED NUCLEOPROTEIN TUBES ON DEFINED PATTERNS ON SILICA- AND POLYMER-BASED SUBSTRATES.* LANGMUIR 28 (42), 14867-14877, 2012.
74. SHAW, W.H.R. AND D.G. WALKER, *KINETIC STUDIES OF THIOUREA DERIVATIVES. IV. THE METHYLATED THIOUREAS. CONCLUSIONS1.* JOURNAL OF THE AMERICAN CHEMICAL SOCIETY, 1958. **80**(20): P. 5337-5342.
75. ULMAN, A., *FORMATION AND STRUCTURE OF SELF-ASSEMBLED MONOLAYERS.* CHEMICAL REVIEWS, 1996. **96**(4): P. 1533-1554.
76. WANG, H., ET AL., *EFFECT OF SILANE GRAFTING ON THE MICROSTRUCTURE OF HIGH-DENSITY POLYETHYLENE/ORGANICALLY MODIFIED MONTMORILLONITE NANOCOMPOSITES.* POLYMER INTERNATIONAL, 2008. **57**(1): P. 50-56.
77. FLIKWEERT, A.J., ET AL., *MICROCRYSTALLINE THIN-FILM SOLAR CELL DEPOSITION ON MOVING SUBSTRATES USING A LINEAR VHF-PECVD REACTOR AND A CROSS-FLOW GEOMETRY.* JOURNAL OF PHYSICS D: APPLIED PHYSICS, 2012. **45**(1): P. 015101.
78. WANG, X., ET AL., *SYNTHESES, PROPERTIES AND ELECTROCHEMICAL ACTIVITY OF CARBON MICROTUBES MODIFIED WITH AMINO GROUPS.* ADVANCED FUNCTIONAL MATERIALS, 2008. **18**(12): P. 1809-1823.
79. BRIAND, E., ET AL., *CHEMICAL MODIFICATIONS OF AU/SIO2 TEMPLATE SUBSTRATES FOR PATTERNED BIOFUNCTIONAL SURFACES.* LANGMUIR, 2010. **27**(2): P. 678-685.
80. GHOSH, M., ET AL., *MULTIFUNCTIONAL SURFACES WITH DISCRETE FUNCTIONALIZED REGIONS FOR BIOLOGICAL APPLICATIONS.* LANGMUIR, 2008. **24**(15): P. 8134-8142.
81. KIM, J., ET AL., *FORMATION, STRUCTURE, AND REACTIVITY OF AMINO-TERMINATED ORGANIC FILMS ON SILICON SUBSTRATES.* JOURNAL OF COLLOID AND INTERFACE SCIENCE, 2009. **329**(1): P. 114-119.
82. TINGAUT, P., ET AL., *FUNCTIONALISATION OF WOOD BY REACTION WITH 3-ISOCYANATOPROPYLTRIETHOXYSILANE: GRAFTING AND HYDROLYSIS OF THE TRIETHOXYSILANE END GROUPS*, IN *HOLZFORSCHUNG*2005. P. 397.
83. ARKLES, B., *TAILORING SURFACES WITH SILANES*, 1977, CHEMTECH P. 766-778.
84. LEX, A., ET AL., *SYNTHESIS OF A PHOTOSENSITIVE THIOCYANATE-FUNCTIONALIZED TRIALKOXYSILANE AND ITS APPLICATION IN PATTERNED SURFACE MODIFICATIONS.* CHEMISTRY OF MATERIALS, 2008. **20**(5): P. 2009-2015.
85. SAPRIGIN, A.V., ET AL., *SPECTROSCOPIC QUANTIFICATION OF COVALENTLY IMMOBILIZED OLIGONUCLEOTIDES.* SURFACE AND INTERFACE ANALYSIS, 2005. **37**(1): P. 24-32.
86. CHARLES, P.T., ET AL., *FABRICATION AND SURFACE CHARACTERIZATION OF DNA MICROARRAYS USING AMINE- AND THIOL-TERMINATED OLIGONUCLEOTIDE PROBES†.* LANGMUIR, 2002. **19**(5): P. 1586-1591.
87. TANG, Y., ET AL., *COUPLING PROTEINS TO AMINE-TERMINATED MAGNETIC PARTICLES ACTIVATED WITH 1,4-PHENYLENE DIISOTHIOCYANATE.* CHINESE JOURNAL OF CHEMISTRY, 2010. **28**(4): P. 627-632.
88. KALININA, S., ET AL., *ISOTHIOCYANATE-FUNCTIONALIZED RGD PEPTIDES FOR TAILORING CELL-ADHESIVE SURFACE PATTERNS.* BIOMATERIALS, 2008. **29**(20): P. 3004-3013.
89. PINER, R.D., ET AL., *"DIP-PEN" NANOLITHOGRAPHY.* SCIENCE, 1999. **283**(5402): P. 661-663.
90. WALHEIM, S., ET AL., *STRUCTURE FORMATION VIA POLYMER DEMIXING IN SPIN-CAST FILMS.* MACROMOLECULES, 1997. **30**(17): P. 4995-5003.
91. ZISMAN, W.A., W.C. BIGELOW, AND D.L. PICKETT, *OLEOPHOBIC MONOLAYERS. 1. FILMS ADSORBED FROM SOLUTIONS IN NON-POLAR LIQUIDS.* JOURNAL OF COLLOID SCIENCE, 1946. **1**(6): P. 513-538.
92. NUZZO, R.G. AND D.L. ALLARA, *ADSORPTION OF BIFUNCTIONAL ORGANIC DISULFIDES ON GOLD SURFACES.* JOURNAL OF THE AMERICAN CHEMICAL SOCIETY, 1983. **105**(13): P. 4481-4483.
93. MAOZ, R. AND J. SAGIV, *ON THE FORMATION AND STRUCTURE OF SELF-ASSEMBLING MONOLAYERS. I. A COMPARATIVE ATR-WETTABILITY STUDY OF LANGMUIR—BLODGETT AND ADSORBED FILMS ON FLAT SUBSTRATES AND GLASS MICROBEADS.* JOURNAL OF COLLOID AND INTERFACE SCIENCE, 1984. **100**(2): P. 465-496.
94. SCHWARTZ, D.K., *MECHANISMS AND KINETICS OF SELF-ASSEMBLED MONOLAYER FORMATION.* ANNUAL REVIEW OF PHYSICAL CHEMISTRY, 2001. **52**(1): P. 107-137.
95. CHAUDHURY, M.K., T.M. GENTLE, AND E.P. PLUEDDEMANN, *ADHESION MECHANISM OF POLYVINYL CHLORIDE TO SILANE PRIMED METAL SURFACES.* JOURNAL OF ADHESION SCIENCE AND TECHNOLOGY, 1987. **1**(1): P. 29-38.
96. ROTH, C.A., *SILYLATION OF ORGANIC CHEMICALS.* PRODUCT R&D, 1972. **11**(2): P. 134-139.
97. CHECHIK, V. AND C.J.M. STIRLING, *GOLD–THIOL SELF-ASSEMBLED MONOLAYERS*, IN *PATAI'S CHEMISTRY OF FUNCTIONAL GROUPS*2009, JOHN WILEY & SONS, LTD.
98. BOECKL, M. AND D. GRAHAM, *SELF-ASSEMBLED MONOLAYERS: ADVANTAGES OF PURE ALKANETHIOLS.* MATERIAL MATTERS, 2006. **1.2**(3).
99. LOVE, J.C., ET AL., *SELF-ASSEMBLED MONOLAYERS OF THIOLATES ON METALS AS A FORM OF NANOTECHNOLOGY.* CHEMICAL REVIEWS, 2005. **105**(4): P. 1103-1170.
100. COLLET, J., ET AL., *LOW-VOLTAGE, 30 NM CHANNEL LENGTH, ORGANIC TRANSISTORS WITH A SELF-ASSEMBLED MONOLAYER AS GATE INSULATING FILMS.* APPLIED PHYSICS LETTERS, 2000. **76**(14): P. 1941-1943.
101. CIAMPI, S., J.B. HARPER, AND J.J. GOODING, *WET CHEMICAL ROUTES TO THE ASSEMBLY OF ORGANIC MONOLAYERS ON SILICON SURFACES VIA THE FORMATION OF SI-C BONDS: SURFACE PREPARATION, PASSIVATION AND FUNCTIONALIZATION.* CHEMICAL SOCIETY REVIEWS, 2010. **39**(6): P. 2158-2183.
102. BRZOSKA, J.B., I.B. AZOUZ, AND F. RONDELEZ, *SILANIZATION OF SOLID SUBSTRATES: A STEP TOWARD REPRODUCIBILITY.* LANGMUIR, 1994. **10**(11): P. 4367-4373.
103. PAKSTIS, L.M., ET AL., *EVALUATION OF POLYDIMETHYLSILOXANE MODIFICATION METHODS FOR CELL RESPONSE.* JOURNAL OF BIOMEDICAL MATERIALS RESEARCH PART A, 2010. **92A**(2): P. 604-614.
104. BOUKHERROUB, R., ET AL., *NEW SYNTHETIC ROUTES TO ALKYL MONOLAYERS ON THE SI(111) SURFACE1.* LANGMUIR, 1999. **15**(11): P. 3831-3835.
105. SUZUKI, N. AND H. ISHIDA, *A REVIEW ON THE STRUCTURE AND CHARACTERIZATION TECHNIQUES OF SILANE/MATRIX INTERPHASES.* MACROMOLECULAR SYMPOSIA, 1996. **108**(1): P. 19-53.
106. HAENSCH, C., S. HOEPPENER, AND U.S. SCHUBERT, *CHEMICAL MODIFICATION OF SELF-ASSEMBLED SILANE BASED MONOLAYERS BY SURFACE REACTIONS.* CHEMICAL SOCIETY REVIEWS, 2010. **39**(6): P. 2323-2334.
107. GOODING, J.J. AND S. CIAMPI, *THE MOLECULAR LEVEL MODIFICATION OF SURFACES: FROM SELF-ASSEMBLED MONOLAYERS TO COMPLEX MOLECULAR ASSEMBLIES.* CHEMICAL SOCIETY REVIEWS, 2011. **40**(5): P. 2704-2718.

108. CONTRIBUTORS, W. *SILANES*. 2012 13 OCTOBER 2011]; AVAILABLE FROM: HTTP://EN.WIKIPEDIA.ORG/W/INDEX.PHP?TITLE=SILANES&OLDID=455451658.
109. MITTAL, K.L., *SILANES AND OTHER COUPLING AGENTS*2000: VSP.
110. OLMOS, D., ET AL., *HYDROLYTIC DAMAGE STUDY OF THE SILANE COUPLING REGION IN COATED SILICA MICROFIBRES: PH AND COATING TYPE EFFECTS.* JOURNAL OF MATERIALS PROCESSING TECHNOLOGY, 2003. **143–144**(0): P. 82-86.
111. PLUEDDEMANN, E.P., *SILANE COUPLING AGENTS*, IN *PLENUM PRESS*1991: NEW YORK AND LONDON.
112. KANG, H.J. AND F.D. BLUM, *STRUCTURE AND DYNAMICS OF AMINO FUNCTIONAL SILANES ADSORBED ON SILICA SURFACES.* THE JOURNAL OF PHYSICAL CHEMISTRY, 1991. **95**(23): P. 9391-9396.
113. HOWARTER, J.A. AND J.P. YOUNGBLOOD, *OPTIMIZATION OF SILICA SILANIZATION BY 3-AMINOPROPYLTRIETHOXYSILANE.* LANGMUIR, 2006. **22**(26): P. 11142-11147.
114. KALLURY, K.M.R., P.M. MACDONALD, AND M. THOMPSON, *EFFECT OF SURFACE WATER AND BASE CATALYSIS ON THE SILANIZATION OF SILICA BY (AMINOPROPYL)ALKOXYSILANES STUDIED BY X-RAY PHOTOELECTRON SPECTROSCOPY AND 13C CROSS-POLARIZATION/MAGIC ANGLE SPINNING NUCLEAR MAGNETIC RESONANCE.* LANGMUIR, 1994. **10**(2): P. 492-499.
115. METWALLI, E., ET AL., *SURFACE CHARACTERIZATIONS OF MONO-, DI-, AND TRI-AMINOSILANE TREATED GLASS SUBSTRATES.* JOURNAL OF COLLOID AND INTERFACE SCIENCE, 2006. **298**(2): P. 825-831.
116. ASENATH SMITH, E. AND W. CHEN, *HOW TO PREVENT THE LOSS OF SURFACE FUNCTIONALITY DERIVED FROM AMINOSILANES.* LANGMUIR, 2008. **24**(21): P. 12405-12409.
117. ANGST, D.L. AND G.W. SIMMONS, *MOISTURE ABSORPTION CHARACTERISTICS OF ORGANOSILOXANE SELF-ASSEMBLED MONOLAYERS.* LANGMUIR, 1991. **7**(10): P. 2236-2242.
118. GLASER, A., ET AL., *INVESTIGATION OF THE ROLE OF THE INTERPLAY BETWEEN WATER AND TEMPERATURE ON THE GROWTH OF ALKYLSILOXANE SUBMONOLAYERS ON SILICON.* LANGMUIR, 2004. **20**(13): P. 5599-5604.
119. PARIKH, A.N., ET AL., *CORRELATION OF MOLECULAR ORGANIZATION AND SUBSTRATE WETTABILITY IN THE SELF-ASSEMBLY OF N-ALKYLSILOXANE MONOLAYERS.* THE JOURNAL OF PHYSICAL CHEMISTRY, 1995. **99**(24): P. 9996-10008.
120. FOISNER, J., ET AL., *ATOMIC FORCE MICROSCOPY INVESTIGATION OF THE GROWTH OF DIFFERENT ALKYLSILOXANE MONOLAYERS FROM HIGHLY CONCENTRATED SOLUTIONS.* LANGMUIR, 2003. **19**(9): P. 3741-3746.
121. BRUNNER, H., ET AL., *SUBSTRATE EFFECTS ON THE FORMATION OF ALKYLSILOXANE MONOLAYERS.* LANGMUIR, 1999. **15**(6): P. 1899-1901.
122. ROZLOSNIK, N., M.C. GERSTENBERG, AND N.B. LARSEN, *EFFECT OF SOLVENTS AND CONCENTRATION ON THE FORMATION OF A SELF-ASSEMBLED MONOLAYER OF OCTADECYLSILOXANE ON SILICON (001).* LANGMUIR, 2003. **19**(4): P. 1182-1188.
123. LEITNER, T., ET AL., *INVESTIGATIONS OF THE GROWTH OF SELF-ASSEMBLED OCTADECYLSILOXANE MONOLAYERS WITH ATOMIC FORCE MICROSCOPY.* MICROCHIMICA ACTA, 2000. **133**(1): P. 331-336.
124. ALLARA, D.L., A.N. PARIKH, AND F. RONDELEZ, *EVIDENCE FOR A UNIQUE CHAIN ORGANIZATION IN LONG CHAIN SILANE MONOLAYERS DEPOSITED ON TWO WIDELY DIFFERENT SOLID SUBSTRATES.* LANGMUIR, 1995. **11**(7): P. 2357-2360.
125. FINKLEA, H.O., ET AL., *FORMATION OF AN ORGANIZED MONOLAYER BY SOLUTION ADSORPTION OF OCTADECYLTRICHLOROSILANE ON GOLD: ELECTROCHEMICAL PROPERTIES AND STRUCTURAL CHARACTERIZATION.* LANGMUIR, 1986. **2**(2): P. 239-244.
126. SCHREIBER, F., *STRUCTURE AND GROWTH OF SELF-ASSEMBLING MONOLAYERS.* PROGRESS IN SURFACE SCIENCE, 2000. **65**(5–8): P. 151-257.
127. SHLYAKHTENKO, L.S., ET AL., *ATOMIC FORCE MICROSCOPY IMAGING OF DNA COVALENTLY IMMOBILIZED ON A FUNCTIONALIZED MICA SUBSTRATE.* BIOPHYSICAL JOURNAL, 1999. **77**(1): P. 568-576.
128. ALMEIDA, A.T., M.C. SALVADORI, AND D.F.S. PETRI, *ENOLASE ADSORPTION ONTO HYDROPHOBIC AND HYDROPHILIC SOLID SUBSTRATES.* LANGMUIR, 2002. **18**(18): P. 6914-6920.
129. SUGIMURA, H. AND N. NAKAGIRI, *NANOSCOPIC SURFACE ARCHITECTURE BASED ON SCANNING PROBE ELECTROCHEMISTRY AND MOLECULAR SELF-ASSEMBLY.* JOURNAL OF THE AMERICAN CHEMICAL SOCIETY, 1997. **119**(39): P. 9226-9229.
130. SHIM, H.Y., ET AL., *MICROPATTERNING OF DIACETYLENIC LIPOSOMES ON GLASS SURFACES.* MATERIALS SCIENCE AND ENGINEERING: C, 2004. **24**(1–2): P. 157-161.
131. ARKLES, B., ET AL., *FACTORS CONTRIBUTING TO THE STABILITY OF ALKOXYSILANES IN AQUEOUS SOLUTION.* JOURNAL OF ADHESION SCIENCE AND TECHNOLOGY, 1992. **6**(1): P. 193-206.
132. BLITZ, J.P., R.S. SHREEDHARA MURTHY, AND D.E. LEYDEN, *THE ROLE OF AMINE STRUCTURE ON CATALYTIC ACTIVITY FOR SILYLATION REACTIONS WITH CAB-O-SIL.* JOURNAL OF COLLOID AND INTERFACE SCIENCE, 1988. **126**(2): P. 387-392.
133. BLITZ, J.P., R.S.S. MURTHY, AND D.E. LEYDEN, *AMMONIA-CATALYZED SILYLATION REACTIONS OF CAB-O-SIL WITH METHOXYMETHYLSILANES.* JOURNAL OF THE AMERICAN CHEMICAL SOCIETY, 1987. **109**(23): P. 7141-7145.
134. TRIPP, C.P., P. KAZMAIER, AND M.L. HAIR, *A LOW FREQUENCY INFRARED AND AB INITIO STUDY OF THE REACTION OF TRICHLOROSILANE WITH SILICA.* LANGMUIR, 1996. **12**(26): P. 6404-6406.
135. TRIPP, C.P. AND M.L. HAIR, *CHEMICAL ATTACHMENT OF CHLOROSILANES TO SILICA: A TWO-STEP AMINE-PROMOTED REACTION.* THE JOURNAL OF PHYSICAL CHEMISTRY, 1993. **97**(21): P. 5693-5698.
136. KANAN, S.M., W.T.Y. TZE, AND C.P. TRIPP, *METHOD TO DOUBLE THE SURFACE CONCENTRATION AND CONTROL THE ORIENTATION OF ADSORBED (3-AMINOPROPYL)DIMETHYLETHOXYSILANE ON SILICA POWDERS AND GLASS SLIDES.* LANGMUIR, 2002. **18**(17): P. 6623-6627.
137. FENG, J., ET AL., *CO-PATTERNING CHITOSAN AND BOVINE SERUM ALBUMIN ON AN ALDEHYDE-ENRICHED GLASS SUBSTRATE BY MICROCONTACT PRINTING.* THIN SOLID FILMS, 2004. **460**(1–2): P. 286-290.
138. KALUZA, L., *ÜBER EINE NEUE DARSTELLUNGSMETHODE VON SENFÖLEN.* MONATSHEFTE FÜR CHEMIE 1909. **30**: P. 717.
139. HODGKINS, J.E. AND W.P. REEVES, *THE MODIFIED KALUZA SYNTHESIS. III. THE SYNTHESIS OF SOME AROMATIC ISOTHIOCYANATES.* THE JOURNAL OF ORGANIC CHEMISTRY, 1964. **29**(10): P. 3098-3099.
140. HODGKINS, J.E., W.P. REEVES, AND Y.-T.G. LIU, *THE MODIFIED KALUZA SYNTHESIS. II.1 KINETICS AND MECHANISM.* JOURNAL OF THE AMERICAN CHEMICAL SOCIETY, 1961. **83**(11): P. 2532-2536.
141. HODGKINS, J.E. AND M.G. ETTLINGER, *THE SYNTHESIS OF ISOTHIOCYANATES FROM AMINES.* THE JOURNAL OF ORGANIC CHEMISTRY, 1956. **21**(4): P. 404-405.
142. COULL, J.M., ET AL., *FUNCTIONALIZED MEMBRANE SUPPORTS FOR COVALENT PROTEIN MICROSEQUENCE ANALYSIS.* ANALYTICAL BIOCHEMISTRY, 1991. **194**(1): P. 110-120.
143. HWANG, E.-S. AND G.H. KIM, *ALLYL ISOTHIOCYANATE INFLUENCES CELL ADHESION, MIGRATION AND METALLOPROTEINASE GENE EXPRESSION IN SK-HEP1 CELLS.* EXPERIMENTAL BIOLOGY AND MEDICINE, 2009. **234**(1): P. 105-111.
144. DUFFY, D.C., ET AL., *RAPID PROTOTYPING OF MICROFLUIDIC SYSTEMS IN POLY(DIMETHYLSILOXANE).* ANALYTICAL CHEMISTRY, 1998. **70**(23): P. 4974-4984.
145. EFFENHAUSER, C.S., ET AL., *INTEGRATED CAPILLARY ELECTROPHORESIS ON FLEXIBLE SILICONE MICRODEVICES: ANALYSIS OF DNA RESTRICTION FRAGMENTS AND DETECTION OF SINGLE DNA MOLECULES ON MICROCHIPS.* ANALYTICAL CHEMISTRY, 1997. **69**(17): P. 3451-3457.

146. McDonald, J.C. and G.M. Whitesides, *Poly(dimethylsiloxane) as a Material for Fabricating Microfluidic Devices.* Accounts of Chemical Research, 2002. **35**(7): p. 491-499.
147. Li, H.-F., et al., *A polymeric master replication technology for mass fabrication of poly(dimethylsiloxane) microfluidic devices.* ELECTROPHORESIS, 2005. **26**(9): p. 1825-1833.
148. Wilson, C.G., *A Decade of Step and Flash Imprint Lithography.* Journal of Photopolymer Science and Technology, 2009. **22**(2): p. 147-153.
149. Pease, R.F. and S.Y. Chou, *Lithography and Other Patterning Techniques for Future Electronics.* Proceedings of the IEEE, 2008. **96**(2): p. 248-270.
150. Ratner, B.D., *Biomaterials Science: An Introduction to Materials in Medicine*2004: Elsevier Academic Press.
151. Xia, Y. and G.M. Whitesides, *Soft Lithography.* Annual Review of Materials Science, 1998. **28**(1): p. 153-184.
152. Kumar, A. and G.M. Whitesides, *Features of gold having micrometer to centimeter dimensions can be formed through a combination of stamping with an elastomeric stamp and an alkanethiol ``ink'' followed by chemical etching.* Applied Physics Letters, 1993. **63**(14): p. 2002-2004.
153. Singhvi, R., et al., *Engineering cell shape and function.* Science, 1994. **264**(5159): p. 696-698.
154. Chambon, F. and H.H. Winter, *Linear Viscoelasticity at the Gel Point of a Crosslinking PDMS with Imbalanced Stoichiometry.* Journal of Rheology, 1987. **31**(8): p. 683-697.
155. Chaudhury, M.K. and G.M. Whitesides, *Direct measurement of interfacial interactions between semispherical lenses and flat sheets of poly(dimethylsiloxane) and their chemical derivatives.* Langmuir, 1991. **7**(5): p. 1013-1025.
156. Xue, C.-Y., et al., *UV-Defined Flat PDMS Stamps Suitable for Microcontact Printing.* Langmuir, 2009. **26**(5): p. 3739-3743.
157. Waddell, E.A., et al., *Surface modification of Sylgard 184 polydimethylsiloxane by 254 nm excimer radiation and characterization by contact angle goniometry, infrared spectroscopy, atomic force and scanning electron microscopy.* Applied Surface Science, 2008. **254**(17): p. 5314-5318.
158. Schnyder, B., et al., *UV-irradiation induced modification of PDMS films investigated by XPS and spectroscopic ellipsometry.* Surface Science, 2003. **532–535**(0): p. 1067-1071.
159. Sadhu, V.B., et al., *Surface Modification of Elastomeric Stamps for Microcontact Printing of Polar Inks.* Langmuir, 2007. **23**(12): p. 6850-6855.
160. Ouyang, M., et al., *Conversion of Some Siloxane Polymers to Silicon Oxide by UV/Ozone Photochemical Processes.* Chemistry of Materials, 2000. **12**(6): p. 1591-1596.
161. Oláh, A., H. Hillborg, and G.J. Vancso, *Hydrophobic recovery of UV/ozone treated poly(dimethylsiloxane): adhesion studies by contact mechanics and mechanism of surface modification.* Applied Surface Science, 2005. **239**(3–4): p. 410-423.
162. Nielsen, J.M., *Degradation of Methyl Silicone Fluids Under Nitrogen Atmosphere at 370 °C.* J. Appl. Polym. Sci., Appl. Polym. Symp., 1979. **35**: p. 223-224.
163. Song, H., J.D. Tice, and R.F. Ismagilov, *A Microfluidic System for Controlling Reaction Networks in Time.* Angewandte Chemie International Edition, 2003. **42**(7): p. 768-772.
164. Shyichuk, A.V. and J.R. White, *Analysis of chain-scission and crosslinking rates in the photo-oxidation of polystyrene.* Journal of Applied Polymer Science, 2000. **77**(13): p. 3015-3023.
165. Nowakowska, M., J. Kowal, and B. Waligora, *Photo-oxidation of polystyrene film: 2. Photo-oxidation of polystyrene film with light absorbed by the polystyrene-oxygen complex.* Polymer, 1978. **19**(11): p. 1317-1319.
166. Hozumi, A., H. Inagaki, and T. Kameyama, *The hydrophilization of polystyrene substrates by 172-nm vacuum ultraviolet light.* Journal of Colloid and Interface Science, 2004. **278**(2): p. 383-392.
167. Gejo, J.L., et al., *Vacuum-ultraviolet photochemically initiated modification of polystyrene surfaces: morphological changes and mechanistic investigations.* Photochemical & Photobiological Sciences, 2006. **5**(10): p. 948-954.
168. Geuskens, G., et al., *Photo-oxidation of polymers—II: The sensitized decomposition of hydroperoxides as the main path for initiation of the photo-oxidation of polystyrene irradiated at 253.7 nm.* European Polymer Journal, 1978. **14**(4): p. 299-303.
169. Grassie, N. and N.A. Weir, *The photooxidation of polymers. II. Photolysis of polystyrene.* Journal of Applied Polymer Science, 1965. **9**(3): p. 975-986.
170. Efimenko, K., W.E. Wallace, and J. Genzer, *Surface Modification of Sylgard-184 Poly(dimethyl siloxane) Networks by Ultraviolet and Ultraviolet/Ozone Treatment.* Journal of Colloid and Interface Science, 2002. **254**(2): p. 306-315.
171. Matienzo, L. and F. Egitto, *Transformation of poly(dimethylsiloxane) into thin surface films of SiO_2: by UV/ozone treatment. Part II: segregation and modification of doped polymer blends.* Journal of Materials Science, 2006. **41**(19): p. 6374-6384.
172. Egitto, F. and L. Matienzo, *Transformation of Poly(dimethylsiloxane) into thin surface films of SiO_2: by UV/Ozone treatment. Part I: Factors affecting modification.* Journal of Materials Science, 2006. **41**(19): p. 6362-6373.
173. Morvan, J., et al., *Infrared investigation of the role of ozone oxidation in the adhesion of polydimethylsiloxane films.* Journal of Colloid and Interface Science, 1984. **97**(1): p. 149-156.
174. Lee, L.-H., *Enhancement of Surface Wettability of Abhesive Silicone Rubber by Oxidation.* The Journal of Adhesion, 1972. **4**(1): p. 39-49.
175. Kim, H. and M.W. Urban, *Effect of Discharge Gases on Microwave Plasma Reactions of Imidazole on Poly(dimethylsiloxane) Surfaces: Quantitative ATR FT-IR Spectroscopic Analysis.* Langmuir, 1999. **15**(10): p. 3499-3505.
176. Kim, H. and M.W. Urban, *Reaction Sites on Poly(dimethylsiloxane) Elastomer Surfaces in Microwave Plasma Reactions with Gaseous Imidazole: A Spectroscopic Study.* Langmuir, 1996. **12**(4): p. 1047-1050.
177. Khorasani, M.T., H. Mirzadeh, and P.G. Sammes, *Laser induced surface modification of polydimethylsiloxane as a super-hydrophobic material.* Radiation Physics and Chemistry, 1996. **47**(6): p. 881-888.
178. Hollahan, J.R. and G.L. Carlson, *Hydroxylation of polymethylsiloxane surfaces by oxidizing plasmas.* Journal of Applied Polymer Science, 1970. **14**(10): p. 2499-2508.
179. Gaboury Scott, R. and W. Urban Marek, *Analysis of Gas?Plasma-Modified Poly(dimethylsiloxane) Elastomer Surfaces*, in *Structure-Property Relations in Polymers*1993, American Chemical Society. p. 777-790.

180. BALYKOVA, T.N. AND V.V. RODE, *PROGRESS IN THE STUDY OF THE DEGRADATION AND STABILISATION OF SILOXANE POLYMERS.* RUSSIAN CHEMICAL REVIEWS, 1969. **38**(4): P. 306.
181. GENZER, J. AND K. EFIMENKO, *CREATING LONG-LIVED SUPERHYDROPHOBIC POLYMER SURFACES THROUGH MECHANICALLY ASSEMBLED MONOLAYERS.* SCIENCE, 2000. **290**(5499): P. 2130-2133.
182. CHAUDHURY, M.K., *SURFACE FREE ENERGIES OF ALKYLSILOXANE MONOLAYERS SUPPORTED ON ELASTOMERIC POLYDIMETHYLSILOXANES.* JOURNAL OF ADHESION SCIENCE AND TECHNOLOGY, 1993. **7**(6): P. 669-675.
183. MANOJ K, C., *SELF-ASSEMBLED MONOLAYERS ON POLYMER SURFACES.* BIOSENSORS AND BIOELECTRONICS, 1995. **10**(9–10): P. 785-788.
184. FERGUSON, G.S., ET AL., *MONOLAYERS ON DISORDERED SUBSTRATES: SELF-ASSEMBLY OF ALKYLTRICHLOROSILANES ON SURFACE-MODIFIED POLYETHYLENE AND POLY(DIMETHYLSILOXANE).* MACROMOLECULES, 1993. **26**(22): P. 5870-5875.
185. KIM, J., M.K. CHAUDHURY, AND M.J. OWEN, *MODELING HYDROPHOBIC RECOVERY OF ELECTRICALLY DISCHARGED POLYDIMETHYLSILOXANE ELASTOMERS.* JOURNAL OF COLLOID AND INTERFACE SCIENCE, 2006. **293**(2): P. 364-375.
186. LÖTTERS, J.C., ET AL., *THE MECHANICAL PROPERTIES OF THE RUBBER ELASTIC POLYMER POLYDIMETHYLSILOXANE FOR SENSOR APPLICATIONS.* JOURNAL OF MICROMECHANICS AND MICROENGINEERING, 1997. **7**(3): P. 145.
187. GRAUBNER, V.M., ET AL., *PHOTOCHEMICAL MODIFICATION OF CROSS-LINKED POLY(DIMETHYLSILOXANE) BY IRRADIATION AT 172 NM.* MACROMOLECULES, 2004. **37**(16): P. 5936-5943.
188. GRAUBNER, V.M., ET AL., *INCUBATION AND ABLATION BEHAVIOR OF POLY(DIMETHYLSILOXANE) FOR 266 NM IRRADIATION.* APPLIED SURFACE SCIENCE, 2002. **197-198**: P. 786-790.
189. TÓTH, A., ET AL., *OXIDATIVE DAMAGE AND RECOVERY OF SILICONE RUBBER SURFACES. I. X-RAY PHOTOELECTRON SPECTROSCOPIC STUDY.* JOURNAL OF APPLIED POLYMER SCIENCE, 1994. **52**(9): P. 1293-1307.
190. MORRA, M., ET AL., *ON THE AGING OF OXYGEN PLASMA-TREATED POLYDIMETHYLSILOXANE SURFACES.* JOURNAL OF COLLOID AND INTERFACE SCIENCE, 1990. **137**(1): P. 11-24.
191. OWEN, M.J. AND P.J. SMITH, *PLASMA TREATMENT OF POLYDIMETHYLSILOXANE.* JOURNAL OF ADHESION SCIENCE AND TECHNOLOGY, 1994. **8**(10): P. 1063-1075.
192. SMITH, P.J., ET AL. *SURFACE STUDIES OF CORONA-TREATED SILICONE RUBBER HIGH-VOLTAGE INSULATION.* IN *ELECTRICAL INSULATION AND DIELECTRIC PHENOMENA, 1992. ANNUAL REPORT. CONFERENCE ON.* 1992.
193. HILLBORG, H. AND U.W. GEDDE, *HYDROPHOBICITY RECOVERY OF POLYDIMETHYLSILOXANE AFTER EXPOSURE TO CORONA DISCHARGES.* POLYMER, 1998. **39**(10): P. 1991-1998.
194. GORUR, R.S., ET AL., *AGING IN SILICONE RUBBER USED FOR OUTDOOR INSULATION.* POWER DELIVERY, IEEE TRANSACTIONS ON, 1992. **7**(2): P. 525-538.
195. CHANG, J.W. AND R.S. GORUR, *SURFACE RECOVERY OF SILICONE RUBBER USED FOR HV OUTDOOR INSULATION.* DIELECTRICS AND ELECTRICAL INSULATION, IEEE TRANSACTIONS ON, 1994. **1**(6): P. 1039-1046.
196. KIM, S.-H., ET AL., *CHEMICAL CHANGES AT THE SURFACE OF RTV SILICONE RUBBER COATINGS ON INSULATORS DURING DRY-BAND ARCING.* IEEE TRANSACTIONS ON DIELECTRICS AND ELECTRICAL INSULATION, 1994. **1**(1): P. 106-123.
197. HUI, D. AND R. HACKAM, *ELECTRICAL PERFORMANCE OF RTV SILICONE RUBBER COATING OF DIFFERENT THICKNESSES ON PORCELAIN.* POWER DELIVERY, IEEE TRANSACTIONS ON, 1997. **12**(2): P. 857-866.
198. DE LA O, A., R.S. GORUR, AND J.T. BURNHAM, *ELECTRICAL PERFORMANCE OF NON-CERAMIC INSULATORS IN ARTIFICIAL CONTAMINATION TESTS. ROLE OF RESTING TIME.* DIELECTRICS AND ELECTRICAL INSULATION, IEEE TRANSACTIONS ON, 1996. **3**(6): P. 827-835.
199. DENG, H. AND R. HACKAM, *LOW-MOLECULAR WEIGHT SILICONE FLUID IN RTV SILICONE RUBBER COATINGS.* IEEE TRANSACTIONS ON DIELECTRICS AND ELECTRICAL INSULATION, 1999. **6**(1): P. 84-94.
200. KIM, S.H., E.A. CHERNEY, AND R. HACKAM, *SUPPRESSION MECHANISM OF LEAKAGE CURRENT ON RTV COATED PORCELAIN AND SILICONE RUBBER INSULATORS.* POWER DELIVERY, IEEE TRANSACTIONS ON, 1991. **6**(4): P. 1549-1556.
201. KARADY, G.G., M. SHAH, AND R.L. BROWN, *FLASHOVER MECHANISM OF SILICONE RUBBER INSULATORS USED FOR OUTDOOR INSULATION-I.* POWER DELIVERY, IEEE TRANSACTIONS ON, 1995. **10**(4): P. 1965-1971.
202. HOMMA, H., ET AL., *DIFFUSION OF LOW MOLECULAR WEIGHT SILOXANE FROM BULK TO SURFACE.* DIELECTRICS AND ELECTRICAL INSULATION, IEEE TRANSACTIONS ON, 1999. **6**(3): P. 370-375.
203. WANKOWICZ, J.G., S.M. GUBANSKI, AND W.D. LAMPE, *LOSS AND RECOVERY OF HYDROPHOBICITY ON RTV COATING SURFACES.* DIELECTRICS AND ELECTRICAL INSULATION, IEEE TRANSACTIONS ON, 1994. **1**(4): P. 604-614.
204. VLASTOS, A.E. AND S.M. GUBANSKI, *SURFACE STRUCTURAL CHANGES OF NATURALLY AGED SILICONE AND EPDM COMPOSITE INSULATORS.* POWER DELIVERY, IEEE TRANSACTIONS ON, 1991. **6**(2): P. 888-900.
205. BLACKMORE, P. AND D. BIRTWHISTLE, *SURFACE DISCHARGES ON POLYMERIC INSULATOR SHED SURFACES.* DIELECTRICS AND ELECTRICAL INSULATION, IEEE TRANSACTIONS ON, 1997. **4**(2): P. 210-217.
206. KIM, J., M.K. CHAUDHURY, AND M.J. OWEN, *HYDROPHOBICITY LOSS AND RECOVERY OF SILICONE HV INSULATION.* DIELECTRICS AND ELECTRICAL INSULATION, IEEE TRANSACTIONS ON, 1999. **6**(5): P. 695-702.
207. KIM, J., M.K. CHAUDHURY, AND M.J. OWEN, *HYDROPHOBIC RECOVERY OF POLYDIMETHYLSILOXANE ELASTOMER EXPOSED TO PARTIAL ELECTRICAL DISCHARGE.* JOURNAL OF COLLOID AND INTERFACE SCIENCE, 2000. **226**(2): P. 231-236.
208. BOLTAU, M., ET AL., *SURFACE-INDUCED STRUCTURE FORMATION OF POLYMER BLENDS ON PATTERNED SUBSTRATES.* NATURE, 1998. **391**(6670): P. 877-879.
209. EIGLER, D.M. AND E.K. SCHWEIZER, *POSITIONING SINGLE ATOMS WITH A SCANNING TUNNELLING MICROSCOPE.* NATURE, 1990. **344**(6266): P. 524-526.
210. SALAITA, K., Y. WANG, AND C.A. MIRKIN, *APPLICATIONS OF DIP-PEN NANOLITHOGRAPHY.* NAT NANO, 2007. **2**(3): P. 145-155.
211. LEE, K.-B., J.-H. LIM, AND C.A. MIRKIN, *PROTEIN NANOSTRUCTURES FORMED VIA DIRECT-WRITE DIP-PEN NANOLITHOGRAPHY.* JOURNAL OF THE AMERICAN CHEMICAL SOCIETY, 2003. **125**(19): P. 5588-5589.
212. FODOR, S.P.A., *DNA SEQUENCING: MASSIVELY PARALLEL GENOMICS.* SCIENCE, 1997. **277**(5324): P. 393-395.
213. BIER, F. AND F. KLEINJUNG, *FEATURE-SIZE LIMITATIONS OF MICROARRAY TECHNOLOGY - A CRITICAL REVIEW.* FRESENIUS' JOURNAL OF ANALYTICAL CHEMISTRY, 2001. **371**(2): P. 151-156.
214. SOTO, C.M. AND B.R. RATNA, *VIRUS HYBRIDS AS NANOMATERIALS FOR BIOTECHNOLOGY.* CURRENT OPINION IN BIOTECHNOLOGY, 2010. **21**(4): P. 426-438.
215. YOUNG, M., ET AL., *PLANT VIRUSES AS BIOTEMPLATES FOR MATERIALS AND THEIR USE IN NANOTECHNOLOGY.* ANNUAL REVIEW OF PHYTOPATHOLOGY, 2008. **46**(1): P. 361-384.
216. LI, K., ET AL., *VIRUSES AND THEIR POTENTIAL IN BIOIMAGING AND BIOSENSING APPLICATIONS.* ANALYST, 2010. **135**(1).
217. WU, Z., ET AL., *PREPARATION AND MAGNETOVISCOSITY OF NANOTUBE FERROFLUIDS BY VIRAL SCAFFOLDING AND ALD ON POROUS TEMPLATES.* PHYSICA STATUS SOLIDI (B), 2010. **247**(10): P. 2412-2423.

218. ABU-SALAH, K.M., A.A. ANSARI, AND S.A. ALROKAYAN, *DNA-BASED APPLICATIONS IN NANOBIOTECHNOLOGY.* JOURNAL OF BIOMEDICINE AND BIOTECHNOLOGY, 2010. **2010**.
219. NAM, K.T., ET AL., *VIRUS-ENABLED SYNTHESIS AND ASSEMBLY OF NANOWIRES FOR LITHIUM ION BATTERY ELECTRODES.* SCIENCE, 2006. **312**(5775): P. 885-888.
220. LEE, Y.J., ET AL., *FABRICATING GENETICALLY ENGINEERED HIGH-POWER LITHIUM-ION BATTERIES USING MULTIPLE VIRUS GENES.* SCIENCE, 2009. **324**(5930): P. 1051-1055.
221. DEDEO, M.T., ET AL., *NANOSCALE PROTEIN ASSEMBLIES FROM A CIRCULAR PERMUTANT OF THE TOBACCO MOSAIC VIRUS.* NANO LETTERS, 2009. **10**(1): P. 181-186.
222. BUTLER, P.J.G., A.C.H. DURHAM, AND A. KLUG, *STRUCTURES AND ROLES OF THE POLYMORPHIC FORMS OF TOBACCO MOSAIC VIRUS PROTEIN: IV. CONTROL OF MODE OF AGGREGATION OF TOBACCO MOSAIC VIRUS PROTEIN BY PROTON BINDING.* JOURNAL OF MOLECULAR BIOLOGY, 1972. **72**(1): P. 1-18.
223. BLOOMER, A.C., ET AL., *PROTEIN DISK OF TOBACCO MOSAIC VIRUS AT 2.8 [ANGST] RESOLUTION SHOWING THE INTERACTIONS WITHIN AND BETWEEN SUBUNITS.* NATURE, 1978. **276**(5686): P. 362-368.
224. FRAENKEL-CONRAT, H. AND R.C. WILLIAMS, *RECONSTITUTION OF ACTIVE TOBACCO MOSAIC VIRUS FROM ITS INACTIVE PROTEIN AND NUCLEIC ACID COMPONENTS.* PROCEEDINGS OF THE NATIONAL ACADEMY OF SCIENCES, 1955. **41**(10): P. 690-698.
225. PELESKO, J.A., *SELF ASSEMBLY: THE SCIENCE OF THINGS THAT PUT THEMSELVES TOGETHER*2007: CHAPMAN & HALL/CRC.
226. LAUFFER, M.A., *ENTROPY-DRIVEN PROCESSES IN BIOLOGY: POLYMERIZATION OF TOBACCO MOSAIC VIRUS PROTEIN AND SIMILAR REACTIONS*. MOLECULAR BIOLOGY, BIOCHEMISTRY, AND BIOPHYSICS1975, SPRINGER-VERLAG: NEW YORK.
227. DOMINGO, G.J., S. ORRU, AND R.N. PERHAM, *MULTIPLE DISPLAY OF PEPTIDES AND PROTEINS ON A MACROMOLECULAR SCAFFOLD DERIVED FROM A MULTIENZYME COMPLEX.* JOURNAL OF MOLECULAR BIOLOGY, 2001. **305**(2): P. 259-267.
228. KOVACS, E.W., ET AL., *DUAL-SURFACE-MODIFIED BACTERIOPHAGE MS2 AS AN IDEAL SCAFFOLD FOR A VIRAL CAPSID-BASED DRUG DELIVERY SYSTEM.* BIOCONJUGATE CHEMISTRY, 2007. **18**(4): P. 1140-1147.
229. SEEBECK, F.P., ET AL., *A SIMPLE TAGGING SYSTEM FOR PROTEIN ENCAPSULATION.* JOURNAL OF THE AMERICAN CHEMICAL SOCIETY, 2006. **128**(14): P. 4516-4517.
230. BUTLER, P.J., *STRUCTURES AND ROLES OF THE POLYMORPHIC FORMS OF TOBACCO MOSAIC VIRUS PROTEIN: VI. ASSEMBLY OF THE NUCLEOPROTEIN RODS OF TOBACCO MOSAIC VIRUS FROM THE PROTEIN DISKS AND RNA.* JOURNAL OF MOLECULAR BIOLOGY, 1972. **72**(1): P. 25-35.
231. DAVID, Z., *THE NUCLEOTIDE SEQUENCE AT THE ORIGIN FOR ASSEMBLY ON TOBACCO MOSAIC VIRUS RNA.* CELL, 1977. **11**(3): P. 463-482.
232. BHYRAVBHATLA, B., S.J. WATOWICH, AND D.L.D. CASPAR, *REFINED ATOMIC MODEL OF THE FOUR-LAYER AGGREGATE OF THE TOBACCO MOSAIC VIRUS COAT PROTEIN AT 2.4-Å RESOLUTION.* BIOPHYSICAL JOURNAL, 1998. **74**(1): P. 604-615.
233. YOSHIMI, O., *MOLECULAR ASSEMBLY OF TOBACCO MOSAIC VIRUS IN VITRO.* ADVANCES IN BIOPHYSICS, 1986. **22**(0): P. 95-149.
234. GOELET, P., ET AL., *NUCLEOTIDE SEQUENCE OF TOBACCO MOSAIC VIRUS RNA.* PROCEEDINGS OF THE NATIONAL ACADEMY OF SCIENCES OF THE UNITED STATES OF AMERICA, 1982. **79**(19): P. 5818-5822.
235. KIM, K.-S., ET AL., *EFFECTS OF ORGANIC CONTAMINANTS DURING METAL OXIDE SEMICONDUCTOR PROCESSES.* JOURNAL OF THE ELECTROCHEMICAL SOCIETY, 2008. **155**(6): P. H426-H431.
236. VOSSEN, J.L. AND W. KERN, *THIN FILM PROCESSES*1978: ACADEMIC PRESS.
237. OVERBERGER, C.G. AND H.A. FRIEDMAN, *THIOUREAS AND ISOTHIURONIUM SALTS. MONOMERIC DERIVATIVES.* THE JOURNAL OF ORGANIC CHEMISTRY, 1965. **30**(6): P. 1926-1929.
238. DAINS, F.B., BREWSTER, R. Q. AND OLANDER, C. P. , *PHENYL ISOTHIOCYANATE.* . ORGANIC SYNTHESES, COLL., 1941. **1**: P. 447.
239. JOCHIMS, J.C. AND A. SEELIGER, *EINE NEUE SYNTHESE ALIPHATISCHER ISOTHIOCYANATE.* ANGEWANDTE CHEMIE, 1967. **79**(3): P. 151-151.
240. HALLER, I., *COVALENTLY ATTACHED ORGANIC MONOLAYERS ON SEMICONDUCTOR SURFACES.* JOURNAL OF THE AMERICAN CHEMICAL SOCIETY, 1978. **100**(26): P. 8050-8055.
241. BEIER, M. AND J.D. HOHEISEL, *VERSATILE DERIVATISATION OF SOLID SUPPORT MEDIA FOR COVALENT BONDING ON DNA-MICROCHIPS.* NUCLEIC ACIDS RESEARCH, 1999. **27**(9): P. 1970-1977.
242. KIM, H.J., ET AL., *DETECTION OF CUII BY A CHEMODOSIMETER-FUNCTIONALIZED MONOLAYER ON MESOPOROUS SILICA.* ADVANCED MATERIALS, 2008. **20**(17): P. 3229-3234.
243. DELAMARCHE, E., ET AL., *IMMOBILIZATION OF ANTIBODIES ON A PHOTOACTIVE SELF-ASSEMBLED MONOLAYER ON GOLD.* LANGMUIR, 1996. **12**(8): P. 1997-2006.
244. BUINING, P.A., ET AL., *PREPARATION OF FUNCTIONAL SILANE-STABILIZED GOLD COLLOIDS IN THE (SUB)NANOMETER SIZE RANGE.* LANGMUIR, 1997. **13**(15): P. 3921-3926.
245. HOOK, D.J., ET AL., *SILANIZATION OF RADIO FREQUENCY GLOW DISCHARGE MODIFIED EXPANDED POLY(TETRAFLUOROETHYLENE) USING (AMINOPROPYL)TRIETHOXYSILANE.* LANGMUIR, 1991. **7**(1): P. 142-151.
246. NASHAT, A.H., M. MORONNE, AND M. FERRARI, *DETECTION OF FUNCTIONAL GROUPS AND ANTIBODIES ON MICROFABRICATED SURFACES BY CONFOCAL MICROSCOPY.* BIOTECHNOLOGY AND BIOENGINEERING, 1998. **60**(2): P. 137-146.
247. KALUZA, L., *ÜBER EINE NEUE DARSTELLUNGSMETHODE VON SENFÖLEN.* MONATSHEFTE FÜR CHEMIE / CHEMICAL MONTHLY, 1912. **33**(4): P. 363-371.
248. YAMAMOTO, T., ET AL., *SYNTHESIS OF ALKYL ISOTHIOCYANATES FROM PRIMARY ALKYL AMINES USING DICYANADIAMIDE AS A DEHYDROSULFURIZING AGENT.* ORGANIC PREPARATIONS AND PROCEDURES INTERNATIONAL, 1994. **26**(5): P. 555-557.
249. YAMAMOTO, T., ET AL., *ONE-POT SYNTHESIS OF ISOTHIOCYANATES FROM PRIMARY AMINES SYTHESIS USING CYANAMIDE.* ORGANIC PREPARATIONS AND PROCEDURES INTERNATIONAL, 1992. **24**(3): P. 346-349.
250. MANNING, M. AND G. REDMOND, *FORMATION AND CHARACTERIZATION OF DNA MICROARRAYS AT SILICON NITRIDE SUBSTRATES.* LANGMUIR, 2004. **21**(1): P. 395-402.
251. MANNING, M., ET AL., *A VERSATILE MULTI-PLATFORM BIOCHIP SURFACE ATTACHMENT CHEMISTRY.* MATERIALS SCIENCE AND ENGINEERING: C, 2003. **23**(3): P. 347-351.
252. WEI-CHENG, L., C.C.-C. A., AND H. KUO-CHENG, *DESIGN AND FABRICATION OF SOFT ZOOM LENS*. VOL. 7061. 2008, BELLINGHAM, WA, ETATS-UNIS: SOCIETY OF PHOTO-OPTICAL INSTRUMENTATION ENGINEERS. VARIOUS PAGINGS.
253. ANDERSON, J.R., ET AL., *FABRICATION OF TOPOLOGICALLY COMPLEX THREE-DIMENSIONAL MICROFLUIDIC SYSTEMS IN PDMS BY RAPID PROTOTYPING.* ANALYTICAL CHEMISTRY, 2000. **72**(14): P. 3158-3164.
254. TON-THAT, C., ET AL., *XPS AND AFM SURFACE STUDIES OF SOLVENT-CAST PS/PMMA BLENDS.* POLYMER, 2001. **42**(3): P. 1121-1129.
255. JOURLIN-CASTELLI, C., *TRANSCRIPTOME ANALYSIS BY MICROARRAYS*, IN *PROKARYOTIC GENOMICS*, M. BLOT, EDITOR 2003, BIRKHÄUSER VERLAG: BASEL ; BOSTON. P. 145-156.

256. MANNING, M., ET AL., *A VERSATILE MULTI-PLATFORM BIOCHIP SURFACE ATTACHMENT CHEMISTRY.* MATERIALS SCIENCE & ENGINEERING C, 2003. **23**(3): P. 347-351.
257. NOY, A., D.V. VEZENOV, AND C.M. LIEBER, *CHEMICAL FORCE MICROSCOPY.* ANNUAL REVIEW OF MATERIALS SCIENCE, 1997. **27**(1): P. 381-421.
258. HANSMA, H.G. AND J.H. HOH, *BIOMOLECULAR IMAGING WITH THE ATOMIC FORCE MICROSCOPE.* ANNUAL REVIEW OF BIOPHYSICS AND BIOMOLECULAR STRUCTURE, 1994. **23**(1): P. 115-140.
259. MARTIN, Y., C.C. WILLIAMS, AND H.K. WICKRAMASINGHE, *ATOMIC FORCE MICROSCOPE--FORCE MAPPING AND PROFILING ON A SUB 100-[A-RING] SCALE.* JOURNAL OF APPLIED PHYSICS, 1987. **61**(10): P. 4723-4729.
260. GERBER, C., ET AL., *SCANNING TUNNELING MICROSCOPE COMBINED WITH A SCANNING ELECTRON MICROSCOPE.* REVIEW OF SCIENTIFIC INSTRUMENTS, 1986. **57**(2): P. 221-224.
261. DEMUTH, J.E., ET AL., *A SIMPLIFIED SCANNING TUNNELING MICROSCOPE FOR SURFACE SCIENCE STUDIES.* JOURNAL OF VACUUM SCIENCE & TECHNOLOGY A: VACUUM, SURFACES, AND FILMS, 1986. **4**(3): P. 1320-1323.
262. AMER, N.M., A. SKUMANICH, AND D. RIPPLE, *PHOTOTHERMAL MODULATION OF THE GAP DISTANCE IN SCANNING TUNNELING MICROSCOPY.* APPLIED PHYSICS LETTERS, 1986. **49**(3): P. 137-139.
263. AMATO, I., *CANDID CAMERAS FOR THE NANOWORLD.* SCIENCE, 1997. **276**(5321): P. 1982-1985.
264. GIESSIBL, F.J., *ADVANCES IN ATOMIC FORCE MICROSCOPY.* REVIEWS OF MODERN PHYSICS, 2003. **75**(3): P. 949-983.
265. JOHNSTON, E.E. AND B.D. RATNER, *SURFACE CHARACTERIZATION OF PLASMA DEPOSITED ORGANIC THIN FILMS.* JOURNAL OF ELECTRON SPECTROSCOPY AND RELATED PHENOMENA, 1996. **81**(3): P. 303-317.
266. MEYER, E., ET AL., *STRUCTURE AND DYNAMICS OF SOLID SURFACES OBSERVED BY ATOMIC FORCE MICROSCOPY.* ULTRAMICROSCOPY, 1992. **42–44, PART 1**(0): P. 274-280.
267. GARCÍA, R. AND A. SAN PAULO, *ATTRACTIVE AND REPULSIVE TIP-SAMPLE INTERACTION REGIMES IN TAPPING-MODE ATOMIC FORCE MICROSCOPY.* PHYSICAL REVIEW B, 1999. **60**(7): P. 4961-4967.
268. C.S, F., *X-RAY PHOTOELECTRON SPECTROSCOPY: PROGRESS AND PERSPECTIVES.* JOURNAL OF ELECTRON SPECTROSCOPY AND RELATED PHENOMENA, 2010. **178–179**(0): P. 2-32.
269. TURNER, N.H., *SURFACE ANALYSIS: X-RAY PHOTOELECTRON SPECTROSCOPY AND AUGER ELECTRON SPECTROSCOPY.* ANALYTICAL CHEMISTRY, 1986. **58**(5): P. 153R-165R.
270. TURNER, D.W., *PHOTOELECTRON SPECTROSCOPY.* ANNUAL REVIEW OF PHYSICAL CHEMISTRY, 1970. **21**(1): P. 107-128.
271. CARLSON, T.A., *PHOTOELECTRON SPECTROSCOPY.* ANNUAL REVIEW OF PHYSICAL CHEMISTRY, 1975. **26**(1): P. 211-234.
272. SOLOMON, E.I., ET AL., *VARIABLE ENERGY PHOTOELECTRON SPECTROSCOPY: ELECTRONIC STRUCTURE AND ELECTRONIC RELAXATION.* COORDINATION CHEMISTRY REVIEWS, 2005. **249**(1–2): P. 229-253.
273. OURA, K., ET AL., *SURFACE SCIENCE: AN INTRODUCTION*2003, BERLIN: SPRINGER VERLAG.
274. PARRY, K.L., ET AL., *ARXPS CHARACTERISATION OF PLASMA POLYMERISED SURFACE CHEMICAL GRADIENTS.* SURFACE AND INTERFACE ANALYSIS, 2006. **38**(11): P. 1497-1504.
275. J.H, S., *HARTREE-SLATER SUBSHELL PHOTOIONIZATION CROSS-SECTIONS AT 1254 AND 1487 EV.* JOURNAL OF ELECTRON SPECTROSCOPY AND RELATED PHENOMENA, 1976. **8**(2): P. 129-137.
276. COOK, B.W. AND K. JONES, *A PROGRAMMED INTRODUCTION TO INFRARED SPECTROSCOPY*1972: HEYDEN.
277. STEWART, J.E., *INFRARED SPECTROSCOPY: EXPERIMENTAL METHODS AND TECHNIQUES*1970: M. DEKKER.
278. SMITH, B.C., *FUNDAMENTALS OF FOURIER TRANSFORM INFRARED SPECTROSCOPY*. 2 ED2009: TAYLOR AND FRANCIS. 193.
279. SCHRADER, B., *INFRARED AND RAMAN SPECTROSCOPY*2008: JOHN WILEY & SONS.
280. CHASE, D.B. AND J.F. RABOLT, *FOURIER TRANSFORM RAMAN SPECTROSCOPY: FROM CONCEPT TO EXPERIMENT*1994: ACADEMIC PRESS.
281. GRIFFITHS, P.R. AND J.A.D. HASETH, *FOURIER TRANSFORM INFRARED SPECTROMETRY*2007: JOHN WILEY & SONS.
282. DAVID E, B., *CHARACTERIZATION OF THE SOLID-STATE: SPECTROSCOPIC TECHNIQUES.* ADVANCED DRUG DELIVERY REVIEWS, 2001. **48**(1): P. 43-65.
283. HIBBEN, J.H., *RAMAN SPECTRA IN ORGANIC CHEMISTRY.* CHEMICAL REVIEWS, 1936. **18**(1): P. 1-232.
284. BOHETS, H. AND B.J. VAN DER VEKEN, *RAMAN AND INFRARED SPECTRA, CONFORMATIONAL STABILITY, VIBRATIONAL ASSIGNMENT AND AB INITIO CALCULATIONS FOR ETHYL CHLOROFORMATE.* JOURNAL OF RAMAN SPECTROSCOPY, 1995. **26**(8-9): P. 821-834.
285. HIRSCHFELD, T. AND B. CHASE, *FT-RAMAN SPECTROSCOPY: DEVELOPMENT AND JUSTIFICATION.* APPL. SPECTROSC., 1986. **40**(2): P. 133-137.
286. XIE, Q. AND F. MCCOURT, *NANOTECHNOLOGY ENGINEERING NE 226 LAB MANUAL*, 2007, UNIVERSITY OF WATERLOO: WATERLOO. P. 28-34.
287. YOUNG, T., *AN ESSAY ON THE COHESION OF FLUIDS.* PHILOSOPHICAL TRANSACTIONS OF THE ROYAL SOCIETY OF LONDON, 1805. **95**: P. 65-87.
288. SHAFRIN ELAINE, G. AND A. ZISMAN WILLIAM, *UPPER LIMITS TO THE CONTACT ANGLES OF LIQUIDS ON SOLIDS*, IN *CONTACT ANGLE, WETTABILITY, AND ADHESION*1964, AMERICAN CHEMICAL SOCIETY. P. 145-157.
289. MELROSE J, C., *EVIDENCE FOR SOLID-FLUID INTERFACIAL TENSIONS FROM CONTACT ANGLES*, IN *CONTACT ANGLE, WETTABILITY, AND ADHESION*1964, AMERICAN CHEMICAL SOCIETY. P. 158-179.
290. WENZEL, R.N., *RESISTANCE OF SOLID SURFACES TO WETTING BY WATER.* INDUSTRIAL & ENGINEERING CHEMISTRY, 1936. **28**(8): P. 988-994.
291. MITTAL, K.L., *CONTACT ANGLE, WETTABILITY AND ADHESION*2009: BRILL ACADEMIC PUB.
292. FOWKES, F.M., *ATTRACTIVE FORCES AT INTERFACES.* INDUSTRIAL & ENGINEERING CHEMISTRY, 1964. **56**(12): P. 40-52.
293. ROTENBERG, Y., L. BORUVKA, AND A.W. NEUMANN, *DETERMINATION OF SURFACE-TENSION AND CONTACT-ANGLE FROM THE SHAPES OF AXISYMMETRIC FLUID INTERFACES.* JOURNAL OF COLLOID AND INTERFACE SCIENCE, 1983. **93**(1): P. 169-183.
294. KOOPAL, L.K., *WETTING OF SOLID SURFACES: FUNDAMENTALS AND CHARGE EFFECTS.* ADVANCES IN COLLOID AND INTERFACE SCIENCE, 2012. **179-182**: P. 29-42.
295. STAROV, V.M., ET AL., *SPREADING OF LIQUID DROPS OVER POROUS SUBSTRATES.* ADVANCES IN COLLOID AND INTERFACE SCIENCE, 2003. **104**(1–3): P. 123-158.
296. SPERLING, L.H., *INTERPENETRATING POLYMER NETWORKS: AN OVERVIEW*, IN *INTERPENETRATING POLYMER NETWORKS*1994, AMERICAN CHEMICAL SOCIETY. P. 3-38.
297. ZAMMATTEO, N., ET AL., *COMPARISON BETWEEN DIFFERENT STRATEGIES OF COVALENT ATTACHMENT OF DNA TO GLASS SURFACES TO BUILD DNA MICROARRAYS.* ANALYTICAL BIOCHEMISTRY, 2000. **280**(1): P. 143-150.
298. LASZLO HEVESI, L.J., JOSÉ REMACLE, *METHOD FOR OBTAINING A SURFACE ACTIVATION OF A SOLID SUPPORT FOR BUILDING BIOCHIP MICROARRAYS.*, 2002: UNITED STATED.

299. YERSHOV, G., ET AL., *DNA ANALYSIS AND DIAGNOSTICS ON OLIGONUCLEOTIDE MICROCHIPS.* PROCEEDINGS OF THE NATIONAL ACADEMY OF SCIENCES, 1996. **93**(10): P. 4913-4918.
300. YAO, T., *A CHEMICALLY-MODIFIED ENZYME MEMBRANE ELECTRODE AS AN AMPEROMETRIC GLUCOSE SENSOR.* ANALYTICA CHIMICA ACTA, 1983. **148**(0): P. 27-33.
301. HABEEB, A.F.S.A. AND R. HIRAMOTO, *REACTION OF PROTEINS WITH GLUTARALDEHYDE.* ARCHIVES OF BIOCHEMISTRY AND BIOPHYSICS, 1968. **126**(1): P. 16-26.
302. BOWES, J.H. AND C.W. CATER, *THE INTERACTION OF ALDEHYDES WITH COLLAGEN.* BIOCHIMICA ET BIOPHYSICA ACTA (BBA) - PROTEIN STRUCTURE, 1968. **168**(2): P. 341-352.
303. HOPWOOD, D., C. ALLEN, AND M. MCCABE, *THE REACTIONS BETWEEN GLUTARALDEHYDE AND VARIOUS PROTEINS. AN INVESTIGATION OF THEIR KINETICS.* THE HISTOCHEMICAL JOURNAL, 1970. **2**(2): P. 137-150.
304. ALEXA, G., D. CHISALITA, AND G. CHIRITA, *REACTION OF DIALDEHYDE WITH FUNCTIONAL GROUPS IN COLLAGEN.* REV. TECH. IND. CUIR. , 1971. **63**: P. 5-14.
305. OKUDA, K., ET AL., *REACTION OF GLUTARALDEHYDE WITH AMINO AND THIOL COMPOUNDS.* JOURNAL OF FERMENTATION AND BIOENGINEERING, 1991. **71**(2): P. 100-105.
306. KAWAHARA, J.-I., ET AL., *THE STRUCTURE OF GLUTARALDEHYDE IN AQUEOUS SOLUTION DETERMINED BY ULTRAVIOLET ABSORPTION AND LIGHT SCATTERING.* ANALYTICAL BIOCHEMISTRY, 1992. **201**(1): P. 94-98.
307. TASHIMA, T., ET AL., *STRUCTURE OF A NEW OLIGOMER OF GLUTARALDEHYDE PRODUCED BY ALDOL CONDENSATION REACTION.* THE JOURNAL OF ORGANIC CHEMISTRY, 1991. **56**(2): P. 694-697.
308. TASHIMA, T., ET AL., *ISOLATION AND IDENTIFICATION OF NEW OLIGOMERS IN AQUEOUS SOLUTION OF GLUTARALDEHYDE(ANALYTICAL,CHEMICAL).* CHEMICAL & PHARMACEUTICAL BULLETIN, 1987. **35**(10): P. 4169-4180.
309. MARGEL, S. AND A. REMBAUM, *SYNTHESIS AND CHARACTERIZATION OF POLY(GLUTARALDEHYDE). A POTENTIAL REAGENT FOR PROTEIN IMMOBILIZATION AND CELL SEPARATION.* MACROMOLECULES, 1980. **13**(1): P. 19-24.
310. REMBAUM, A., S. MARGEL, AND J. LEVY, *POLYGLUTARALDEHYDE: A NEW REAGENT FOR COUPLING PROTEINS TO MICROSPHERES AND FOR LABELING CELL-SURFACE RECEPTORS.* JOURNAL OF IMMUNOLOGICAL METHODS, 1978. **24**(3–4): P. 239-250.
311. MONSAN, P., G. PUZO, AND H. MAZARGUIL, *ÉTUDE DU MÉCANISME D'ÉTABLISSEMENT DES LIAISONS GLUTARALDÉHYDE-PROTÉINES.* BIOCHIMIE, 1976. **57**(11–12): P. 1281-1292.
312. ASO, C. AND Y. AITO, *STUDIES ON THE POLYMERIZATION OF BIFUNCTIONAL MONOMERS. II. POLYMERIZATION OF GLUTARALDEHYDE.* DIE MAKROMOLEKULARE CHEMIE, 1962. **58**(1): P. 195-203.
313. KORN, A.H., S.H. FEAIRHELLER, AND E.M. FILACHOINE, *GLUTARALDEHYDE: NATURE OF THE REAGENT.* JOURNAL OF MOLECULAR BIOLOGY, 1972. **65**(3): P. 525-529.
314. HARDY, P.M., A.C. NICHOLLS, AND H.N. RYDON, *THE NATURE OF THE CROSS-LINKING OF PROTEINS BY GLUTARALDEHYDE. PART I. INTERACTION OF GLUTARALDEHYDE WITH THE AMINO-GROUPS OF 6-AMINOHEXANOIC ACID AND OF [SMALL ALPHA]-N-ACETYL-LYSINE.* JOURNAL OF THE CHEMICAL SOCIETY, PERKIN TRANSACTIONS 1, 1976(9): P. 958-962.
315. SONG, J., ET AL., *FUNCTIONAL GLASS SLIDES FOR IN VITRO EVALUATION OF INTERACTIONS BETWEEN OSTEOSARCOMA TE85 CELLS AND MINERAL-BINDING LIGANDS.* JOURNAL OF MATERIALS CHEMISTRY, 2004. **14**(17): P. 2643-2648.
316. HARDY, P.M., A.C. NICHOLLS, AND H.N. RYDON, *THE NATURE OF GLUTARALDEHYDE IN AQUEOUS SOLUTION.* JOURNAL OF THE CHEMICAL SOCIETY D: CHEMICAL COMMUNICATIONS, 1969(10): P. 565-566.
317. CAREY, F.A. AND R.J. SUNDBERG, *ADVANCED ORGANIC CHEMISTRY: REACTIONS AND SYNTHESIS*2007: SPRINGER.
318. BROWN, W.H., ET AL., *ORGANIC CHEMISTRY, ENHANCED EDITION*2010: CENGAGE LEARNING.
319. HERMANSON, G.T., *BIOCONJUGATE TECHNIQUES*2008: ACADEMIC PRESS.
320. XING, Y. AND E. BORGUET, *SPECIFICITY AND SENSITIVITY OF FLUORESCENCE LABELING OF SURFACE SPECIES.* LANGMUIR, 2006. **23**(2): P. 684-688.
321. FERRARI, M., R. BASHIR, AND S. WERELEY, *BIOMEMS AND BIOMEDICAL NANOTECHNOLOGY: BIOMOLECULAR SENSING, PROCESSING AND ANALYSIS*2006: SPRINGER.
322. CASS, A.E.G., T. CASS, AND F.S. LIGLER, *IMMOBILIZED BIOMOLECULES IN ANALYSIS: A PRACTICAL APPROACH*1998: OXFORD UNIVERSITY PRESS.
323. BERLINGER, A., ET AL., *INFLUENCE OF SULPHONATION ON POLYMER AND POLYMER BLEND SURFACES STUDIED BY ATOMIC FORCE MICROSCOPY.* SURFACE AND INTERFACE ANALYSIS, 2001. **32**(1): P. 144-147.
324. GLIEMANN, H., ET AL., *NANOSTRUCTURE FORMATION IN POLYMER THIN FILMS INFLUENCED BY HUMIDITY.* SURFACE AND INTERFACE ANALYSIS, 2007. **39**(1): P. 1-8.
325. TANAKA, K., A. TAKAHARA, AND T. KAJIYAMA, *FILM THICKNESS DEPENDENCE OF THE SURFACE STRUCTURE OF IMMISCIBLE POLYSTYRENE/POLY(METHYL METHACRYLATE) BLENDS.* MACROMOLECULES, 1996. **29**(9): P. 3232-3239.
326. CUI, L., ET AL., *SOLVENT AND POLYMER CONCENTRATION EFFECTS ON THE SURFACE MORPHOLOGY EVOLUTION OF IMMISCIBLE POLYSTYRENE/POLY(METHYL METHACRYLATE) BLENDS.* THIN SOLID FILMS, 2006. **515**(4): P. 2038-2048.
327. BENDAHMANE, M., ET AL., *DISPLAY OF EPITOPES ON THE SURFACE OF TOBACCO MOSAIC VIRUS: IMPACT OF CHARGE AND ISOELECTRIC POINT OF THE EPITOPE ON VIRUS-HOST INTERACTIONS.* JOURNAL OF MOLECULAR BIOLOGY, 1999. **290**(1): P. 9-20.
328. SUCI, P.A., ET AL., *INFLUENCE OF ELECTROSTATIC INTERACTIONS ON THE SURFACE ADSORPTION OF A VIRAL PROTEIN CAGE.* LANGMUIR, 2005. **21**(19): P. 8686-8693.
329. YI, H., G.W. RUBLOFF, AND J.N. CULVER, *TMV MICROARRAYS: HYBRIDIZATION-BASED ASSEMBLY OF DNA-PROGRAMMED VIRAL NANOTEMPLATES.* LANGMUIR, 2007. **23**(5): P. 2663-2667.
330. TAN, W.S., ET AL., *HIERARCHICAL ASSEMBLY OF VIRAL NANOTEMPLATES WITH ENCODED MICROPARTICLES VIA NUCLEIC ACID HYBRIDIZATION.* LANGMUIR, 2008. **24**(21): P. 12483-12488.
331. STEINMETZ, N.F., ET AL., *ASSEMBLY OF MULTILAYER ARRAYS OF VIRAL NANOPARTICLES VIA BIOSPECIFIC RECOGNITION: A QUARTZ CRYSTAL MICROBALANCE WITH DISSIPATION MONITORING STUDY.* BIOMACROMOLECULES, 2008. **9**(2): P. 456-462.
332. YOO, P.J., ET AL., *SPONTANEOUS ASSEMBLY OF VIRUSES ON MULTILAYERED POLYMER SURFACES.* NAT MATER, 2006. **5**(3): P. 234-240.
333. CHEUNG, C.L., ET AL., *FABRICATION OF ASSEMBLED VIRUS NANOSTRUCTURES ON TEMPLATES OF CHEMOSELECTIVE LINKERS FORMED BY SCANNING PROBE NANOLITHOGRAPHY.* JOURNAL OF THE AMERICAN CHEMICAL SOCIETY, 2003. **125**(23): P. 6848-6849.
334. BALCI, S., ET AL., *PRINTING AND ALIGNING MESOSCALE PATTERNS OF TOBACCO MOSAIC VIRUS ON SURFACES.* ADVANCED MATERIALS, 2008. **20**(11): P. 2195-2200.
335. YI, H., ET AL., *PATTERNED ASSEMBLY OF GENETICALLY MODIFIED VIRAL NANOTEMPLATES VIA NUCLEIC ACID HYBRIDIZATION.* NANO LETTERS, 2005. **5**(10): P. 1931-1936.
336. CHEN, I.J., E.C. ECKSTEIN, AND E. LINDNER, *COMPUTATION OF TRANSIENT FLOW RATES IN PASSIVE PUMPING MICRO-FLUIDIC SYSTEMS.* LAB ON A CHIP, 2009. **9**(1): P. 107-114.

337. GOSSETT, D., ET AL., *LABEL-FREE CELL SEPARATION AND SORTING IN MICROFLUIDIC SYSTEMS.* ANALYTICAL & BIOANALYTICAL CHEMISTRY, 2010. **397**(8): P. 3249-3267.
338. LIU, K.-K., ET AL., *MICROFLUIDIC SYSTEMS FOR BIOSENSING.* SENSORS, 2010. **10**(7): P. 6623-6661.
339. ROMANOWSKI, F. AND H. KLENK, *THIOCYANATES AND ISOTHIOCYANATES, ORGANIC*, IN *ULLMANN'S ENCYCLOPEDIA OF INDUSTRIAL CHEMISTRY*2000, WILEY-VCH VERLAG GMBH & CO. KGAA.
340. HECHT, S.S., *INHIBITION OF CARCINOGENESIS BY ISOTHIOCYANATES.* DRUG METABOLISM REVIEWS, 2000. **32**(3-4): P. 395-411.
341. ZHANG, Y., J. LI, AND L. TANG, *CANCER-PREVENTIVE ISOTHIOCYANATES: DICHOTOMOUS MODULATORS OF OXIDATIVE STRESS.* FREE RADICAL BIOLOGY AND MEDICINE, 2005. **38**(1): P. 70-77.
342. M. BOEGER, J.D., CIBA-GEIGY, EDITOR 1985.
343. B. S. DRACH, E.P.S., A. V. KIRSANOV, ZH. ORG. KHIM, 1872. **8**.
344. KHARASCH, M.S., E.M. MAY, AND F.R. MAYO, *THE ADDITION OF THIOCYANIC ACID TO OLEFINIC DOUBLE BONDS.* JOURNAL OF THE AMERICAN CHEMICAL SOCIETY, 1937. **59**(8): P. 1580-1580.
345. WONG, R. AND S.J. DOLMAN, *ISOTHIOCYANATES FROM TOSYL CHLORIDE MEDIATED DECOMPOSITION OF IN SITU GENERATED DITHIOCARBAMIC ACID SALTS.* THE JOURNAL OF ORGANIC CHEMISTRY, 2007. **72**(10): P. 3969-3971.
346. BEARD, C.I. AND B.P. DAILEY, *THE STRUCTURE AND DIPOLE MOMENT OF ISOTHIOCYANIC ACID.* THE JOURNAL OF CHEMICAL PHYSICS, 1950. **18**(11): P. 1437-1441.
347. KNISELEY, R.N., R.P. HIRSCHMANN, AND V.A. FASSEL, *THE INFRARED SPECTRA OF ALKYL ISOTHIOCYANATES.* SPECTROCHIMICA ACTA PART A: MOLECULAR SPECTROSCOPY, 1967. **23**(1): P. 109-127.
348. BADGER, R.M., *NOTE ON THE SPECTRA OF THE DISUBSTITUTED ACETYLENES AND OF THE MUSTARD OILS.* THE JOURNAL OF CHEMICAL PHYSICS, 1937. **5**(3): P. 178-180.
349. WHITE, L.D. AND C.P. TRIPP, *REACTION OF (3-AMINOPROPYL)DIMETHYLETHOXYSILANE WITH AMINE CATALYSTS ON SILICA SURFACES.* JOURNAL OF COLLOID AND INTERFACE SCIENCE, 2000. **232**(2): P. 400-407.
350. PEÑA-ALONSO, R., ET AL., *STUDY OF THE HYDROLYSIS AND CONDENSATION OF Γ-AMINOPROPYLTRIETHOXYSILANE BY FT-IR SPECTROSCOPY.* JOURNAL OF MATERIALS SCIENCE, 2007. **42**(2): P. 595-603.
351. ISHIDA, H. AND J.L. KOENIG, *EFFECT OF HYDROLYSIS AND DRYING ON THE SILOXANE BONDS OF A SILANE COUPLING AGENT DEPOSITED ON E-GLASS FIBERS.* JOURNAL OF POLYMER SCIENCE: POLYMER PHYSICS EDITION, 1980. **18**(2): P. 233-237.
352. CHIANG, C.-H., H. ISHIDA, AND J.L. KOENIG, *THE STRUCTURE OF Γ-AMINOPROPYLTRIETHOXYSILANE ON GLASS SURFACES.* JOURNAL OF COLLOID AND INTERFACE SCIENCE, 1980. **74**(2): P. 396-404.
353. ISHIDA, H., C.-H. CHIANG, AND J.L. KOENIG, *THE STRUCTURE OF AMINOFUNCTIONAL SILANE COUPLING AGENTS: 1. Γ-AMINOPROPYLTRIETHOXYSILANE AND ITS ANALOGUES.* POLYMER, 1982. **23**(2): P. 251-257.
354. SOCRATES, G., *INFRARED CHARACTERISTIC GROUP FREQUENCIES: TABLES AND CHARTS*: BOOKS ON DEMAND.
355. NAVIROJ, S., ET AL., *STRUCTURE AND ADSORPTION CHARACTERISTICS OF SILANE COUPLING AGENTS ON SILICA AND E-GLASS FIBER; DEPENDENCE ON PH.* JOURNAL OF COLLOID AND INTERFACE SCIENCE, 1984. **97**(2): P. 308-317.
356. LIEBER, E., C.N.R. RAO, AND J. RAMACHANDRAN, *THE INFRARED SPECTRA OF ORGANIC THIOCYANATES AND ISOTHIOCYANATES.* SPECTROCHIMICA ACTA, 1959. **13**(4): P. 296-299.
357. SILVERSTEIN, R.M., F.X. WEBSTER, AND D.J. KIEMLE, *SPECTROMETRIC IDENTIFICATION OF ORGANIC COMPOUNDS*2005: JOHN WILEY & SONS.
358. COLOM, X., ET AL., *STRUCTURAL AND MECHANICAL STUDIES ON MODIFIED REUSED TYRES COMPOSITES.* EUROPEAN POLYMER JOURNAL, 2006. **42**(10): P. 2369-2378.
359. MITTAL, K.L., *POLYIMIDES AND OTHER HIGH TEMPERATURE POLYMERS: SYNTHESIS, CHARACTERIZATION AND APPLICATIONS*2001: VSP.
360. KURTH, D.G. AND T. BEIN, *SURFACE REACTIONS ON THIN LAYERS OF SILANE COUPLING AGENTS.* JOURNAL NAME: LANGMUIR; (UNITED STATES); JOURNAL VOLUME: 9:11, 1993: P. MEDIUM: X; SIZE: PAGES: 2965-2973.
361. LAUNER, P.J., *INFRARED ANALYSIS OF ORGANOSILICON COMPOUNDS: SPECTRA- STRUCTURE CORRELATIONS*, IN *SILICONE COMPOUNDS REGISTER AND REVIEW*, B. ARKLES, EDITOR 1987, PETRARCH SYSTEMS INC.: NEW YORK.
362. MAYO, D.W., F.A. MILLER, AND R.W. HANNAH, *COURSE NOTES ON THE INTERPRETATION OF INFRARED AND RAMAN SPECTRA*2004: WILEY-INTERSCIENCE.
363. CULLER, S.R., H. ISHIDA, AND J.L. KOENIG, *FT—IR CHARACTERIZATION OF THE REACTION AT THE SILANE/MATRIX RESIN INTERPHASE OF COMPOSITE MATERIALS.* JOURNAL OF COLLOID AND INTERFACE SCIENCE, 1986. **109**(1): P. 1-10.
364. NABEDRYK, E., R.M. GARAVITO, AND J. BRETON, *THE ORIENTATION OF BETA-SHEETS IN PORIN. A POLARIZED FOURIER TRANSFORM INFRARED SPECTROSCOPIC INVESTIGATION.* BIOPHYSICAL JOURNAL, 1988. **53**(5): P. 671-6.
365. PIERS, A.S. AND C.H. ROCHESTER, *INFRARED STUDY OF THE ADSORPTION OF 1-AMINOPROPYLTRIALKOXYSILANES ON SILICA AT THE SOLID/LIQUID INTERFACE.* JOURNAL OF COLLOID AND INTERFACE SCIENCE, 1995. **174**(1): P. 97-103.
366. EAST, A.L.L., A.R.W. MCKELLAR, AND J.K.G. WATSON, *THE INTERMOLECULAR VIBRATIONS OF THE NO DIMER.* THE JOURNAL OF CHEMICAL PHYSICS, 1998. **109**(11): P. 4378-4383.
367. MCGOVERN, M.E., K.M. KALLURY, AND M. THOMPSON, *ROLE OF SOLVENT ON THE SILANIZATION OF GLASS WITH OCTADECYLTRICHLOROSILANE.* LANGMUIR, 1994. **10**(10): P. 3607-3614.
368. IIMURA, K.-I., Y. NAKAJIMA, AND T. KATO, *A STUDY ON STRUCTURES AND FORMATION MECHANISMS OF SELF-ASSEMBLED MONOLAYERS OF N-ALKYLTRICHLOROSILANES USING INFRARED SPECTROSCOPY AND ATOMIC FORCE MICROSCOPY.* THIN SOLID FILMS, 2000. **379**(1–2): P. 230-239.
369. CAI, C., ET AL., *GROWTH BEHAVIOR AND SURFACE TOPOGRAPHY OF DIFFERENT SILANE COUPLING AGENTS ADSORBED ON THE SILICON DIOXIDE SUBSTRATE (0001) FOR VAPOR PHASE DEPOSITION.* JOURNAL OF MATERIALS SCIENCE, 2007. **42**(15): P. 6108-6116.
370. BANGA, R., ET AL., *FTIR AND AFM STUDIES OF THE KINETICS AND SELF-ASSEMBLY OF ALKYLTRICHLOROSILANES AND (PERFLUOROALKYL)TRICHLOROSILANES ONTO GLASS AND SILICON.* LANGMUIR, 1995. **11**(11): P. 4393-4399.
371. BLUM, F.D., ET AL., *HYDROLYSIS, ADSORPTION, AND DYNAMICS OF SILANE COUPLING AGENTS ON SILICA SURFACES.* JOURNAL OF ADHESION SCIENCE AND TECHNOLOGY, 1991. **5**(6): P. 479-496.
372. BUZEK, F. AND J. RATHOUSKY, *STOICHIOMETRY AND KINETICS OF THE REACTION OF SILICA WITH ORGANOSILICON COMPOUNDS.* JOURNAL OF COLLOID AND INTERFACE SCIENCE, 1981. **79**(1): P. 47-55.
373. WASSERMAN, S.R., Y.T. TAO, AND G.M. WHITESIDES, *STRUCTURE AND REACTIVITY OF ALKYLSILOXANE MONOLAYERS FORMED BY REACTION OF ALKYLTRICHLOROSILANES ON SILICON SUBSTRATES.* LANGMUIR, 1989. **5**(4): P. 1074-1087.
374. CRAS, J.J., ET AL., *COMPARISON OF CHEMICAL CLEANING METHODS OF GLASS IN PREPARATION FOR SILANIZATION.* BIOSENSORS AND BIOELECTRONICS, 1999. **14**(8–9): P. 683-688.
375. KURTH, D.G. AND T. BEIN, *SURFACE REACTIONS ON THIN LAYERS OF SILANE COUPLING AGENTS.* LANGMUIR, 1993. **9**(11): P. 2965-2973.

376. ERICH ZYBILL, C., ET AL., *MONOMOLECULAR SILANE FILMS ON GLASS SURFACES—CONTACT ANGLE MEASUREMENTS.* JOURNAL OF ORGANOMETALLIC CHEMISTRY, 1997. **547**(1): P. 167-172.
377. FADEEV, A.Y. AND T.J. MCCARTHY, *SELF-ASSEMBLY IS NOT THE ONLY REACTION POSSIBLE BETWEEN ALKYLTRICHLOROSILANES AND SURFACES: MONOMOLECULAR AND OLIGOMERIC COVALENTLY ATTACHED LAYERS OF DICHLORO- AND TRICHLOROALKYLSILANES ON SILICON.* LANGMUIR, 2000. **16**(18): P. 7268-7274.
378. LAMPROU, D.A., ET AL., *TOWARDS THE DETERMINATION OF SURFACE ENERGY AT THE NANOSCALE: A FURTHER ASSESSMENT OF THE AFM-BASED APPROACH.* JOURNAL OF ADVANCED MICROSCOPY RESEARCH, 2010. **5**(2): P. 137-142.
379. ONOE, H., K. MATSUMOTO, AND I. SHIMOYAMA. *3D MICRO SELF-ASSEMBLY USING A HYDROPHOBIC INTERACTION CONTROLLED BY SAMS.* IN *MICRO ELECTRO MECHANICAL SYSTEMS, 2003. MEMS-03 KYOTO. IEEE THE SIXTEENTH ANNUAL INTERNATIONAL CONFERENCE ON*. 2003.
380. FRIPIAT, J.J., ET AL., *THERMODYNAMIC PROPERTIES OF ADSORBED WATER MOLECULES AND ELECTRICAL CONDUCTION IN MONTMORILLONITES AND SILICAS.* THE JOURNAL OF PHYSICAL CHEMISTRY, 1965. **69**(7): P. 2185-2197.
381. LÉONARD, A., ET AL., *STRUCTURE AND PROPERTIES OF AMORPHOUS SILICOALUMINAS. I. STRUCTURE FROM X-RAY FLUORESCENCE SPECTROSCOPY AND INFRARED SPECTROSCOPY.* THE JOURNAL OF PHYSICAL CHEMISTRY, 1964. **68**(9): P. 2608-2617.
382. L.T, Z., *SURFACE CHARACTERIZATION OF AMORPHOUS SILICA.* COLLOIDS AND SURFACES A: PHYSICOCHEMICAL AND ENGINEERING ASPECTS, 1993. **74**(1): P. 71-90.
383. HALLIWELL, C.M. AND A.E.G. CASS, *A FACTORIAL ANALYSIS OF SILANIZATION CONDITIONS FOR THE IMMOBILIZATION OF OLIGONUCLEOTIDES ON GLASS SURFACES.* ANALYTICAL CHEMISTRY, 2001. **73**(11): P. 2476-2483.
384. WIKSTRÖM, P., C.F. MANDENIUS, AND P.-O. LARSSON, *GAS PHASE SILYLATION, A RAPID METHOD FOR PREPARATION OF HIGH-PERFORMANCE LIQUID CHROMATOGRAPHY SUPPORTS.* JOURNAL OF CHROMATOGRAPHY A, 1988. **455**(0): P. 105-117.
385. OSTERHOLTZ, F.D. AND E.R. POHL, *KINETICS OF THE HYDROLYSIS AND CONDENSATION OF ORGANOFUNCTIONAL ALKOXYSILANES: A REVIEW*. JOURNAL OF ADHESION SCIENCE AND TECHNOLOGY, 1992: P. 127-149.
386. GRAF, N., ET AL., *DETERMINATION OF ACCESSIBLE AMINO GROUPS ON SURFACES BY CHEMICAL DERIVATIZATION WITH 3,5-BIS(TRIFLUOROMETHYL)PHENYL ISOTHIOCYANATE AND XPS/NEXAFS ANALYSIS.* ANALYTICAL AND BIOANALYTICAL CHEMISTRY, 2010. **396**(2): P. 725-738.
387. GRAY, R.C., J.C. CARVER, AND D.M. HERCULES, *AN ESCA STUDY OF ORGANOSILICON COMPOUNDS.* JOURNAL OF ELECTRON SPECTROSCOPY AND RELATED PHENOMENA, 1976. **8**(5): P. 343-357.
388. SARTENAER, Y., ET AL., *ADSORPTION PROPERTIES OF DECYL THIOCYANATE AND DECANETHIOL ON PLATINUM SUBSTRATES STUDIED BY SUM-FREQUENCY GENERATION SPECTROSCOPY.* SURFACE SCIENCE, 2007. **601**(5): P. 1259-1264.
389. HAIHUA, T., *ORGANIC FUNCTIONALIZATION OF SILICON SURFACES WITH ALCOHOLS, KETONES AND ISOTHIOCYANATES*, IN *CHEMISTRY*2008, NATIONAL UNIVERSITY OF SINGAPURE: SINGAPUR.
390. CISZEK, J.W., ET AL., *NEUTRAL COMPLEXES OF FIRST ROW TRANSITION METALS BEARING UNBOUND THIOCYANATES AND THEIR ASSEMBLY ON METALLIC SURFACES.* JOURNAL OF THE AMERICAN CHEMICAL SOCIETY, 2006. **128**(10): P. 3179-3189.
391. CD, W., ET AL., *NIST X-RAY PHOTOELECTRON SPECTROSCOPY DATABASE*, 2003.
392. HEBENSTREIT, E.L.D., W. HEBENSTREIT, AND U. DIEBOLD, *STRUCTURES OF SULFUR ON TIO2(100) DETERMINED BY SCANNING TUNNELING MICROSCOPY, X-RAY PHOTOELECTRON SPECTROSCOPY AND LOW-ENERGY ELECTRON DIFFRACTION.* SURFACE SCIENCE, 2001. **470**(3): P. 347-360.
393. UMEBAYASHI, T., ET AL., *BAND GAP NARROWING OF TITANIUM DIOXIDE BY SULFUR DOPING.* APPLIED PHYSICS LETTERS, 2002. **81**(3): P. 454-456.
394. ONISHI, H., ET AL., *ADSORPTION OF CH3OH, HCOOH AND SO2 ON TIO2(110) AND STEPPED TIO2(441) SURFACES.* SURFACE SCIENCE, 1988. **193**(1–2): P. 33-46.
395. SAYAGO, D.I., ET AL., *A PHOTOEMISSION STUDY OF THE SO2 ADSORPTION ON TIO2 SURFACES.* SURFACE SCIENCE, 2001. **482–485, PART 1**(0): P. 9-14.
396. RANDENIYA, L., A. MURPHY, AND I. PLUMB, *A STUDY OF S-DOPED TIO2 FOR PHOTOELECTROCHEMICAL HYDROGEN GENERATION FROM WATER.* JOURNAL OF MATERIALS SCIENCE, 2008. **43**(4): P. 1389-1399.
397. JORBÁGY, A. AND K. KIRÁLY, *CHEMICAL CHARACTERIZATION OF FLUORESCEIN ISOTHIOCYANATE-PROTEIN CONJUGATES.* BIOCHIMICA ET BIOPHYSICA ACTA (BBA) - GENERAL SUBJECTS, 1966. **124**(1): P. 166-175.
398. RANA, T.M. AND C.F. MEARES, *N-TERMINAL MODIFICATION OF IMMUNOGLOBULIN POLYPEPTIDE CHAINS TAGGED WITH ISOTHIOCYANATO CHELATES.* BIOCONJUGATE CHEMISTRY, 1990. **1**(5): P. 357-362.
399. ALBERTS, B., *MOLECULAR BIOLOGY OF THE CELL*2002: TAYLOR & FRANCIS.
400. DILL, K., R.H. LIU, AND P. GRODZINSKI, *MICROARRAYS: PREPARATION, MICROFLUIDICS, DETECTION METHODS, AND BIOLOGICAL APPLICATIONS*2008: SPRINGER.
401. WIERINGA, R.M., 2000, UNIV. OF GROMIGEN: THE NETHERLANDS.
402. AISSAOUI, N., ET AL., *SILANE LAYERS ON SILICON SURFACES: MECHANISM OF INTERACTION, STABILITY, AND INFLUENCE ON PROTEIN ADSORPTION.* LANGMUIR, 2011. **28**(1): P. 656-665.
403. HESSNER, M.J., ET AL., *IMMOBILIZED PROBE AND GLASS SURFACE CHEMISTRY AS VARIABLES IN MICROARRAY FABRICATION*, 2004, BIOMED CENTRAL LTD.
404. HOFMANN, W.K., *GENE EXPRESSION PROFILING BY MICROARRAYS: CLINICAL IMPLICATIONS*2006: CAMBRIDGE UNIVERSITY PRESS.
405. SOBEK, J., C. AQUINO, AND R. SCHLAPBACH, *PROCESSING PROTOCOLS FOR HIGH QUALITY GLASS-BASED MICROARRAYS*, IN *MICROARRAYS*, J. RAMPAL, EDITOR 2007, HUMANA PRESS. P. 53-66.
406. GINGER, D.S., H. ZHANG, AND C.A. MIRKIN, *THE EVOLUTION OF DIP-PEN NANOLITHOGRAPHY.* ANGEWANDTE CHEMIE INTERNATIONAL EDITION, 2004. **43**(1): P. 30-45.
407. WU, C.-C., ET AL., *STRATEGIES FOR PATTERNING BIOMOLECULES WITH DIP-PEN NANOLITHOGRAPHY.* SMALL, 2011. **7**(8): P. 989-1002.
408. BAMFORD, C.H. AND C.F.H. TIPPER, *DEGRADATION OF POLYMERS*1975: ELSEVIER SCIENTIFIC PUB. CO.
409. SIEGEL, S. AND H. JUDEIKIS, *EPR STUDY OF THE BIPHOTONIC NATURE OF THE SOLUTE-SENSITIZED PHOTODECOMPOSITION OF POLYDIMETHYLSILOXANE.* THE JOURNAL OF CHEMICAL PHYSICS, 1965. **43**(2): P. 343-351.
410. THOMAS, T.H. AND T.C. KENDRICK, *THERMAL ANALYSIS OF POLYDIMETHYLSILOXANES. I. THERMAL DEGRADATION IN CONTROLLED ATMOSPHERES.* JOURNAL OF POLYMER SCIENCE PART A-2: POLYMER PHYSICS, 1969. **7**(3): P. 537-549.
411. VONDRÁČEK, P. AND A.N. GENT, *SLOW DECOMPOSITION OF SILICONE RUBBER.* JOURNAL OF APPLIED POLYMER SCIENCE, 1982. **27**(11): P. 4517-4522.
412. LACOSTE, J., Y. ISRAËLI, AND J. LEMAIRE, *PHOTOAGING OF SUBSTITUTED AND UNSUBSTITUTED SILICONES*, IN *POLYMER DURABILITY*1996, AMERICAN CHEMICAL SOCIETY. P. 77-89.

413. BULLOCK, S., ET AL., *SURFACE SCIENCE OF A FILLED POLYDIMETHYLSILOXANE-BASED ALKOXYSILANE-CURED ELASTOMER: RTV11.* JOURNAL OF COLLOID AND INTERFACE SCIENCE, 1999. **210**(1): P. 18-36.
414. WEST, J.K., *THEORETICAL ANALYSIS OF HYDROLYSIS OF POLYDIMETHYLSILOXANE (PDMS).* JOURNAL OF BIOMEDICAL MATERIALS RESEARCH, 1997. **35**(4): P. 505-511.
415. DELMAN, A.D., M. LANDY, AND B.B. SIMMS, *PHOTODECOMPOSITION OF POLYMETHYLSILOXANE.* JOURNAL OF POLYMER SCIENCE PART A-1: POLYMER CHEMISTRY, 1969. **7**(12): P. 3375-3386.
416. ZIMMERMANN, C.G., *ON THE KINETICS OF PHOTODEGRADATION IN TRANSPARENT SILICONES.* JOURNAL OF APPLIED PHYSICS, 2008. **103**(8): P. 083547-9.
417. MASON, T.J., *SONOCHEMISTRY*1999: OXFORD UNIVERSITY PRESS.
418. TAMAYO, J. AND R. GARCÍA, *DEFORMATION, CONTACT TIME, AND PHASE CONTRAST IN TAPPING MODE SCANNING FORCE MICROSCOPY.* LANGMUIR, 1996. **12**(18): P. 4430-4435.
419. TAMAYO, J. AND R. GARCIA, *RELATIONSHIP BETWEEN PHASE SHIFT AND ENERGY DISSIPATION IN TAPPING-MODE SCANNING FORCE MICROSCOPY.* APPLIED PHYSICS LETTERS, 1998. **73**(20): P. 2926-2928.
420. BAR, G., ET AL., *INVESTIGATION OF THE STIFFNESS CHANGE IN, THE INDENTATION FORCE AND THE HYDROPHOBIC RECOVERY OF PLASMA-OXIDIZED POLYDIMETHYLSILOXANE SURFACES BY TAPPING MODE ATOMIC FORCE MICROSCOPY.* POLYMER, 2001. **42**(8): P. 3627-3632.
421. MEINCKEN, M., T.A. BERHANE, AND P.E. MALLON, *TRACKING THE HYDROPHOBICITY RECOVERY OF PDMS COMPOUNDS USING THE ADHESIVE FORCE DETERMINED BY AFM FORCE DISTANCE MEASUREMENTS.* POLYMER, 2005. **46**(1): P. 203-208.
422. SHEIKO, S., *IMAGING OF POLYMERS USING SCANNING FORCE MICROSCOPY: FROM SUPERSTRUCTURES TO INDIVIDUAL MOLECULES - NEW DEVELOPMENTS IN POLYMER ANALYTICS II*, M. SCHMIDT, EDITOR 2000, SPRINGER BERLIN / HEIDELBERG. P. 61-174.
423. CLÉMENT, F., ET AL., *ATOMIC FORCE MICROSCOPY INVESTIGATION OF FILLED ELASTOMERS AND COMPARISON WITH TRANSMISSION ELECTRON MICROSCOPY — APPLICATION TO SILICA-FILLED SILICONE ELASTOMERS.* POLYMER, 2001. **42**(14): P. 6259-6270.
424. HEINZ, W.F. AND J.H. HOH, *GETTING PHYSICAL WITH YOUR CHEMISTRY: MECHANICALLY INVESTIGATING LOCAL STRUCTURE AND PROPERTIES OF SURFACES WITH THE ATOMIC FORCE MICROSCOPE.* JOURNAL OF CHEMICAL EDUCATION, 2005. **82**(5): P. 695.
425. MAGONOV, S.N., V. ELINGS, AND M.H. WHANGBO, *PHASE IMAGING AND STIFFNESS IN TAPPING-MODE ATOMIC FORCE MICROSCOPY.* SURFACE SCIENCE, 1997. **375**(2–3): P. L385-L391.
426. WEISENHORN, A.L., ET AL., *MEASURING ADHESION, ATTRACTION, AND REPULSION BETWEEN SURFACES IN LIQUIDS WITH AN ATOMIC-FORCE MICROSCOPE.* PHYSICAL REVIEW B, 1992. **45**(19): P. 11226-11232.
427. BUTT, H.-J., B. CAPPELLA, AND M. KAPPL, *FORCE MEASUREMENTS WITH THE ATOMIC FORCE MICROSCOPE: TECHNIQUE, INTERPRETATION AND APPLICATIONS.* SURFACE SCIENCE REPORTS, 2005. **59**(1–6): P. 1-152.
428. PROKSCH, R. AND J. CLEVELAND, *QUANTIFYING MOLECULAR FORCES: SENSITIVITIES AND SPRING CONSTANTS WITHOUT TOUCHING A SURFACE*, A. RESEARCH, EDITOR 2005, ASYLUM RESEARCH: SANTA BARBARA. P. 1.
429. YOUNG, T. AND P. KELLAND, *A COURSE OF LECTURES ON NATURAL PHILOSOPHY AND THE MECHANICAL ARTS*1845: PRINTED FOR TAYLOR AND WALTON.
430. HERTZ, H., ON THE CONTACT OF ELASTIC SOLIDS. JOURNAL FÜR DIE REINE UND ANGEWANDTE MATHEMATIK 92, 1881: P. 156-171.
431. MARK, J.E., *POLYMER DATA HANDBOOK*1999, NEW YORK, NY: OXFORD UNIVERSITY PRESS.
432. EBENSTEIN, D.M. AND K.J. WAHL, *A COMPARISON OF JKR-BASED METHODS TO ANALYZE QUASI-STATIC AND DYNAMIC INDENTATION FORCE CURVES.* JOURNAL OF COLLOID AND INTERFACE SCIENCE, 2006. **298**(2): P. 652-662.
433. ZHAO, Y.P., X. SHI, AND W.J. LI, *EFFECT OF WORK OF ADHESION ON NANOINDENTATION.* REVIEWS ON ADVANCED MATERIALS SCIENCE, 2003. **5**(4): P. 348-353.
434. CARRILLO, F., ET AL., *NANOINDENTATION OF POLYDIMETHYLSILOXANE ELASTOMERS: EFFECT OF CROSSLINKING, WORK OF ADHESION, AND FLUID ENVIRONMENT ON ELASTIC MODULUS.* JOURNAL OF MATERIALS RESEARCH, 2005. **20**(10): P. 2820-2830.
435. GUPTA, S., ET AL., *ADHESIVE FORCES SIGNIFICANTLY AFFECT ELASTIC MODULUS DETERMINATION OF SOFT POLYMERIC MATERIALS IN NANOINDENTATION.* MATERIALS LETTERS, 2007. **61**(2): P. 448-451.
436. EBENSTEIN, D.M. AND L.A. PRUITT, *NANOINDENTATION OF BIOLOGICAL MATERIALS.* NANO TODAY, 2006. **1**(3): P. 26-33.
437. LIAO, Q., ET AL., *A HYBRID MODEL TO DETERMINE MECHANICAL PROPERTIES OF SOFT POLYMERS BY NANOINDENTATION.* MECHANICS OF MATERIALS, 2010. **42**(12): P. 1043-1047.
438. TRUONG, T.T., ET AL., *SOFT LITHOGRAPHY USING ACRYLOXY PERFLUOROPOLYETHER COMPOSITE STAMPS.* LANGMUIR, 2007. **23**(5): P. 2898-2905.
439. BÉFAHY, S.P., ET AL., *THICKNESS AND ELASTIC MODULUS OF PLASMA TREATED PDMS SILICA-LIKE SURFACE LAYER.* LANGMUIR, 2009. **26**(5): P. 3372-3375.
440. BODAS, D. AND C. KHAN-MALEK, *FORMATION OF MORE STABLE HYDROPHILIC SURFACES OF PDMS BY PLASMA AND CHEMICAL TREATMENTS.* MICROELECTRONIC ENGINEERING, 2006. **83**(4–9): P. 1277-1279.
441. EDDINGTON, D.T., J.P. PUCCINELLI, AND D.J. BEEBE, *THERMAL AGING AND REDUCED HYDROPHOBIC RECOVERY OF POLYDIMETHYLSILOXANE.* SENSORS AND ACTUATORS B: CHEMICAL, 2006. **114**(1): P. 170-172.
442. MA, K., ET AL., *WETTABILITY CONTROL AND PATTERNING OF PDMS USING UV–OZONE AND WATER IMMERSION.* JOURNAL OF COLLOID AND INTERFACE SCIENCE, 2011. **363**(1): P. 371-378.
443. BERDICHEVSKY, Y., ET AL., *UV/OZONE MODIFICATION OF POLY(DIMETHYLSILOXANE) MICROFLUIDIC CHANNELS.* SENSORS AND ACTUATORS B: CHEMICAL, 2004. **97**(2–3): P. 402-408.
444. BODAS, D. AND C. KHAN-MALEK, *HYDROPHILIZATION AND HYDROPHOBIC RECOVERY OF PDMS BY OXYGEN PLASMA AND CHEMICAL TREATMENT—AN SEM INVESTIGATION.* SENSORS AND ACTUATORS B: CHEMICAL, 2007. **123**(1): P. 368-373.
445. HU, S., ET AL., *SURFACE MODIFICATION OF POLY(DIMETHYLSILOXANE) MICROFLUIDIC DEVICES BY ULTRAVIOLET POLYMER GRAFTING.* ANALYTICAL CHEMISTRY, 2002. **74**(16): P. 4117-4123.
446. DONZEL, C., ET AL., *HYDROPHILIC POLY(DIMETHYLSILOXANE) STAMPS FOR MICROCONTACT PRINTING.* ADVANCED MATERIALS, 2001. **13**(15): P. 1164-1167.
447. ZHOU, J., N.H. VOELCKER, AND A.V. ELLIS, *SIMPLE SURFACE MODIFICATION OF POLY(DIMETHYLSILOXANE) FOR DNA HYBRIDIZATION.* BIOMICROFLUIDICS, 2010. **4**(4): P. 046504.
448. MOULDER, J.F., ET AL., *HANDBOOK OF X-RAY PHOTOELECTRON SPECTROSCOPY: A REFERENCE BOOK OF STANDARD SPECTRA FOR IDENTIFICATION AND INTERPRETATION OF XPS DATA*1995: PHYSICAL ELECTRONICS.
449. J.F. MOULDER, W.F.S., P.E. SOBOL, K.D. BOMBEN, ED. *HANDBOOK OF X-RAY PHOTOELECTRON SPECTROSCOPY.* ED. J. CHASTAIN1992., PERKIN–ELMER CORP: EDEN PRAIRIE MN.

450. SPLINTER, S.J. AND N.S. MCINTYRE, *RESOLUTION ENHANCEMENT OF X-RAY PHOTOELECTRON SPECTRA BY MAXIMUM ENTROPY DECONVOLUTION.* SURFACE AND INTERFACE ANALYSIS, 1998. **26**(3): P. 195-203.
451. MCINTYRE, N.S., ET AL., *RESOLUTION ENHANCEMENT OF X-RAY PHOTOELECTRON SPECTRA BY MAXIMUM ENTROPY DECONVOLUTION.* APPLIED SURFACE SCIENCE, 1999. **144–145**(0): P. 156-160.
452. SHARMA, V., ET AL., *SURFACE CHARACTERIZATION OF PLASMA-TREATED AND PEG-GRAFTED PDMS FOR MICRO FLUIDIC APPLICATIONS.* VACUUM, 2007. **81**(9): P. 1094-1100.
453. GABLER, C., ET AL., *CORROSION PROPERTIES OF AMMONIUM BASED IONIC LIQUIDS EVALUATED BY SEM-EDX, XPS AND ICP-OES.* GREEN CHEMISTRY, 2011. **13**(10): P. 2869-2877.
454. MITTAL, K.L., *POLYMER SURFACE MODIFICATION: RELEVANCE TO ADHESION*2009: BRILL ACADEMIC PUB.
455. SOUTO, S., ET AL., *ELECTRONIC STRUCTURE OF NITROGEN-CARBON ALLOYS (A-CN_{X}) DETERMINED BY PHOTOELECTRON SPECTROSCOPY.* PHYSICAL REVIEW B, 1998. **57**(4): P. 2536-2540.
456. AYSCOUGH, P.B., *ELECTRON SPIN RESONANCE*1985: ROYAL SOCIETY OF CHEMISTRY.
457. EGER, W., B. JAHN, AND E. ANDERS, *THE ZINC COMPLEX CATALYZED HYDRATION OF ALKYL ISOTHIOCYANATES.* JOURNAL OF MOLECULAR MODELING, 2009. **15**(4): P. 433-446.
458. BUTLER, P.J., *STRUCTURES AND ROLES OF THE POLYMORPHIC FORMS OF TOBACCO MOSAIC VIRUS PROTEIN: IX. INITIAL STAGES OF ASSEMBLY OF NUCLEOPROTEIN RODS FROM VIRUS RNA AND THE PROTEIN DISKS.* JOURNAL OF MOLECULAR BIOLOGY, 1974. **82**(3): P. 343-353.
459. RICHARDS, K.E. AND R.C. WILLIAMS, *ASSEMBLY OF TOBACCO MOSAIC VIRUS RODS IN VITRO. ELONGATION OF PARTIALLY ASSEMBLED RODS.* BIOCHEMISTRY, 1973. **12**(23): P. 4574-4581.
460. DURHAM, A.C., J.T. FINCH, AND A. KLUG, *STATES OF AGGREGATION OF TOBACCO MOSAIC VIRUS PROTEIN.* NATURE: NEW BIOLOGY, 1971. **229**(2): P. 37-42.
461. BUTLER, P.J., *THE CURRENT PICTURE OF THE STRUCTURE AND ASSEMBLY OF TOBACCO MOSAIC VIRUS.* JOURNAL OF GENERAL VIROLOGY, 1984. **65**(2): P. 253-279.
462. DURHAM, A.C. AND A. KLUG, *POLYMERIZATION OF TOBACCO MOSAIC VIRUS PROTEIN AND ITS CONTROL.* NATURE: NEW BIOLOGY, 1971. **229**(2): P. 42-46.
463. SAMBROOK, J. AND D.W. RUSSELL, *MOLECULAR CLONING: A LABORATORY MANUAL.* 3RD ED2001, COLD SPRING HARBOR, N.Y.: COLD SPRING HARBOR LABORATORY PRESS.
464. FRAENKEL-CONRAT, H., *DEGRADATION OF TOBACCO MOSAIC VIRUS WITH ACETIC ACID.* VIROLOGY, 1957. **4**(1): P. 1-4.
465. GOODING, G.V. AND T.T. HEBERT, *A SIMPLE TECHNIQUE FOR PURIFICATION OF TOBACCO MOSAIC VIRUS IN LARGE QUANTITIES.* PHYTOPATHOLOGY, 1967(57): P. 1285.
466. Y.C. LIU, Y.C.C., *FORMALDEHYDE IN FORMALDEHYDE/AGAROSE GEL MAY BE ELIMINATED WITHOUT AFFECTING THE ELECTROPHORETIC SEPARATION OF RNA MOLECULES.* BIOTECHNIQUES, 1990. **9**: P. 558-559.
467. SAMBROOK, J. AND D.W. RUSSELL, *MOLECULAR CLONING: A LABORATORY MANUAL*2001: COLD SPRING HARBOR LABORATORY PRESS.
468. MRKSICH, M. AND G.M. WHITESIDES, *PATTERNING SELF-ASSEMBLED MONOLAYERS USING MICROCONTACT PRINTING: A NEW TECHNOLOGY FOR BIOSENSORS?* TRENDS IN BIOTECHNOLOGY, 1995. **13**(6): P. 228-235.
469. LI, H., ET AL., *AMINOSILANE MICROPATTERNS ON HYDROXYL-TERMINATED SUBSTRATES: FABRICATION AND APPLICATIONS.* LANGMUIR, 2009. **26**(8): P. 5603-5609.
470. FUJITA, M., ET AL., *PATTERNING DNA ON MM SCALE ON MICA.* ULTRAMICROSCOPY, 2002. **91**(1–4): P. 281-285.
471. GEISSLER, M., ET AL., *DIRECT PATTERNING OF NIB ON GLASS SUBSTRATES USING MICROCONTACT PRINTING AND ELECTROLESS DEPOSITION.* LANGMUIR, 2003. **19**(15): P. 6283-6296.
472. BEARI, F., ET AL., *ORGANOFUNCTIONAL ALKOXYSILANES IN DILUTE AQUEOUS SOLUTION: NEW ACCOUNTS ON THE DYNAMIC STRUCTURAL MUTABILITY.* JOURNAL OF ORGANOMETALLIC CHEMISTRY, 2001. **625**(2): P. 208-216.

Appendix

A. Viral Particles Assembly Methodology (Stuttgart University- Plant Virology Group)

A.1 DNA Linker Immobilization on Aldehyde Functionalized Substrates

Materials

- DNA oligonucleotide was ordered and assembled according to the necessary sequence for the RNA binding purchased from Metabion Martinsried (Germany). *sequence will be extended in the procedure
- RNA sequence in vitro with a MEGAscript Kit from Ambion, Austin (USA).
- Only sterile 2x filtered HPLC water was used to prepare buffer solution.
- Spotting buffer 1M tris-HCl at pH 7 bought from Carl Roth (Germany).
- Saline-sodium citrate (SSC) buffer bought from Carl Roth (Germany).
- Phosphate buffered salin (PBS) buffer bought from Carl Roth (Germany).
- Sodium borohydride ($NaBH_4$) bought from Carl Roth (Germany).
- RNase inhibitor New England Biolabs (USA)
- "DIG buffer wash and block" bought from Carl Roth (Germany).
- Sodium dodecylsulfate (SDS) Sigma-Aldrich, (Germany).
- Streptavidin-alkaline phosphatase Roche; Cat #11093266910 Germany
- Diisopropylethylamine ≥99.5% (DIPEA) from Sigma-Aldrich (Germany)
- Dimethylformamide (DMF) for molecular biology, ≥99% from Sigma-Aldrich (Germany)
- Aminohexanol (≥97.0%) from Fluka (Germany)

Immobilization of DNA linker molecules was optimized on aldehyde-functionalized wafers. 5'-terminally amino-modified single stranded DNA (ssDNA) linker molecules (purchased from Metabion; Martinsried, Germany) with the following nucleotide sequences were utilized: "*5'-NH_2-GCACCACGTGTGATTACGGACACAATCCG-3*" (*TestLinker(+)_NH_2*) and "*5'-NH_2-TGGGCCCCTACCGGGGGTAACGGGGGG-3*" (*TestLinker(-)_NH_2*).

The linker molecules were diluted in 3×SSC (sodium salt citrate buffer from a 20 × SSC stock solution[463]) to the desired concentration (0.01 - 10 pmol/µl) and applied to the functionalized surfaces in a final volume of 3-5 µl. After incubation in a humid chamber for

15-30 min and a series of washing steps (2×2 min in 0.2 % SDS, 2×2 min in double distillated water (ddH_2O), 1×1 min in ddH_2O), the substrates were incubated in a solution of 0.25 % $NaBH_4$ in PBS[463] buffer : Ethanol (3:1)] under slight shaking in order to react superfluous aldehyde groups to non-reactive alcohol functions and convert Schiff bases into stable amines. For the evaluation of linker binding efficiencies, ssDNA probe molecules (Metabion) complementary in their nucleotide sequence to *TestLinker(+)_NH_2* and with a 5'-terminal biotin hapten (*5'-Biotin-CGGATTGTGTCCGTAATCACACGTGGTGC-3'*) were hybridized to the immobilized linkers. Hybridization was carried out for 16-18 h at 37°C with 5-6 ng/ml probe in 3×SSC buffer. After several washing steps (2×2 min in 0.2 % SDS, 2×2 min in ddH_2O, 1×1 min in ddH_2O), specifically hybridized biotinylated probes were detected by a chemiluminescence reaction. To this aim, the substrates were washed with DIG-washing buffer for 5 min (DIG buffers according to the DIG application manual for filter hybridization; Roche Cat # 11438425001; except that DIG buffer 3 was prepared without $MgCl_2$) and blocked for 30-40 min in DIG blocking solution. A 1/10,000 dilution of streptavidin-alkaline phosphatase (streptavidin-AP) conjugate (Roche; Cat #11093266910) in DIG blocking buffer was applied and incubated for 30 min under gentle shaking. Afterwards, substrates were washed for 2×10 min with DIG washing buffer and rinsed for 1 min with DIG buffer 3. For detection of the biotin-streptavidin-coupling, a chemoluminescence-generating substrate of alkaline phosphatase (CDP-Star; ROCHE; Cat # 12041677001) was diluted 1/500 in DIG buffer 3 and applied to the surfaces. Substrates were then sealed into transparent plastic bags, placed in an exposition cassette and incubated for 15 min at 37°C prior to the exposition of an X-ray film (SuperRX, Fujifilm) for 3-4 hours.

A.2 RNA Ligation and Induced Assembly of TMV-like Nanotubes on Unstructured and Patterned Aldehyde Functionalized Surfaces

Homogeneously functionalized and patterned DNA-linker-exposing surfaces were prepared and equipped with genetically engineered RNA strands. The amino-functionalized ssDNA linker molecule - the "RNA_anchor" - (5′-phosphate-TTAAAAAAAAAAAAAAAAA-3′NH_2) was synthesized by Metabion (Martinsried, Germany); RNA in vitro transcripts (2884 nts in length) containing the TMV origins of assembly (OAs) were prepared as described in Müller et al. [7]. The RNA transcripts were enzymatically ligated to one end of the linkers as follows: a mixture containing 2–5 ng/µL dephosphorylated RNA, 1 U/µL RNase inhibitor mix

(NEB), and 1 U/µL T4 RNA ligase 1 (NEB) was prepared in 1× T4 RNA ligase buffer (corresponding to 4500-fold enzyme excess). Prior to the addition of enzyme and inhibitor mix, the solution was heated to 95 °C for 3 min and cooled on ice. Depending on the substrate size, 50–100 µL of complete ligation mixture was applied and incubated in a humid chamber at 37 °C for 3 h. After ligation, preparations were washed in 2× in SSC/0.2% SDS (2 × 10 min), 2× in SSC (1 × 10 min), 0.2 SSC (1 × 10 min) and in ddH_2O (2 × 5 min) under vigorous shaking at RT.

Specimens were then supplemented with assembly competent TMV coat protein preparations under conditions inducing and promoting growth of TMV-like nanotubes *in situ* [7] as optimized for the two-phase system. Before starting assembly reactions, RNA-exposing silica wafers were rinsed with 50 mM SPP (sodium potassium phosphate buffer, pH 7.2) for 5–10 min. The bottoms of sterile plastic Petri dishes were covered with Parafilm, onto which Parafilm posts (about 1 mm height) were adhered to serve as support for the wafers; 50–200 µL of TMV CP (1.3 µg/µL in 50 mM SPP), depending on the wafer size, was applied between the spacers and the respective substrate placed on top, with its RNA-equipped surface pointing toward the bottom. This arrangement was incubated overnight in a humid chamber at 30 °C. The substrates were washed under shaking for 2 × 10 min in 0.2% SDS and 2 × 10 min in ddH_2O before they were dried in a nitrogen stream and analyzed by atomic force microscopy (AFM).

A.3 Hybridization of assembly-directing RNA and surface associated assembly of TMV Coat Protein on Isothiocyanate silanized substrates

All aqueous buffers were filtered sterile through a 0.2 µm membrane immediately before use. RNA was transcribed *in vitro* with the MEGAscript Kit (Ambion, Austin, USA) following the manufacturer's protocol. As a template, a shortened derivative of the plasmid p843pe35TMVr.1' was created by enzymatic restriction hydrolysis. The formation of an additional *Sna*BI restriction site, which resulted from the mutation T3391C in one of the clones, was used to create a deletion by enzymatic restriction hydrolysis with *Sna*BI (New England Biolabs, USA) and religation (T4 DNA ligase, New England Biolabs, USA). The resulting plasmid p843peTMVΔ9353-3391 was used as a template for transcription after linearization with *Bsi*WI (New England Biolabs, USA). This resulted in a 2884 nts long RNA molecule containing the OAs of TMV and a 3' end sequence complementary to the anchor DNA oligomer. For hybridization to the surface-bound DNA oligomers, 50 ng/µl RNA final concentration (f.c.) was first partially denatured in 3x saline-sodium citrate (SSC) buffer [463]

at 65 °C for 5 min. After addition of murine RNase inhibitor (New England Biolabs, USA) to 1 U/µl f.c., 20 µl of this hybridization solution were applied per cm2 surface area and covered with a baked glass cover slip. Hybridization was performed for about 20 h at 37 °C in a humid chamber. After three washing steps in 2x SSC containing 0.2 % w/V SDS, 2x SSC and 0.2x SSC each for 10 min, the RNA-equipped substrates were equilibrated in 75 mM sodium-potassium phosphate (SPP) buffer. TMV CP was prepared from virus particles [224, 464] isolated from infected plants [465] and incubated for at least 48 h in 75 mM SPP buffer pH 7.2 at room temperature at a concentration of about 10 mg/ml. To induce assembly, about 40 µl of 1.3 mg/ml TMV CP in 75 mM SPP buffer pH 7.2 were applied to a cover slip per cm2 of RNA-equipped surfaces. The wafer was placed upside down onto the drop of TMV CP solution on a glass cover slip and incubated in a humid chamber for about 20 h, otherwise indicated. After assembly the surfaces were washed twice for 3 min in 0.1 % (w/V) SDS and twice for 10 min in water, before they were dried under a stream of nitrogen

A.4 Analysis of Intermediate RNA States in the Course of Bottom-Up Assembly.

After enzymatic treatment with Antarctic Phosphatase in vitro, and again after subsequent incubation with T4 RNA ligase 1 in situ on linker-equipped wafers (see above), excess RNA-containing solution was collected and divided into aliquots, which were subjected to different procedures and analyzed in agarose gels, or used as scaffolds for in vitro encapsidation of scaffold RNA in solution. Prior to electrophoresis, one of each portions was treated only with denaturating RNA sample buffers [466], whereas a second portion was treated with phenol/chloroform to extract proteins adsorbed to the RNA [467]. The samples were diluted to a volume of 200 µl and, after phenol extraction, concentrated to the original volume using n-butanol [467]. 50-500 ng of RNA each were applied for sample preparation, separated on 1 % agarose gels in 1xTBE buffer for 2 h at 5 V/cm, and stained with ethidium bromide. An aliquot of the RNA ligation mixture incubated with both enzymes was combined with assembly-competent protein directly after its collection from the wafer, and analyzed by transmission electron microscopy after negative staining, as well as on wafers by AMF to determine the length distribution of assembly products.

B. Microcontact-printing of Silanes

Silanes can be microcontact printed directly onto hydroxylated glass, silicon or other oxidic material [48, 468]. Previous studies reported that aminosilanes are inconvenient "inks" for μCP due to their low affinity to PDMS and the high tendency to hydrolysis and polymerization under ambient conditions; only few groups reported the direct patterning of aminosilanes on SiO_2 or glass substrates by μCP, in which the aminosilanes are usually dissolved in an organic solvent used as "ink"[130, 469-471].

It has been reported that the hydrolysis and the condensation of aminopropyltriethoxy silane (APTES) in aqueous solution are both auto catalyzed and the hydrolysis completes in a few minutes [472]. Nevertheless, in the dilute APTES aqueous solution (3% by volume) , the concentration of reactive silanol groups is still more than 50% even after 80 h of condensation [472]. Although APTES aqueous solution has been used as "ink" in reactive μCP by using a wet agarose stamp, it is difficult to fabricate patterns with the small feature size (e.g., less than 20 μm), because of the lateral diffusion of the molecules induced by the wet stamp surface [469]. In this case we have also stamped the hydroxyl rich surface of silica with a derivative isothiocyanate silane with methoxy anchor (ITCPTMS) groups which are even more reactive towards the oxidic surfaces than those silanes with an ethoxy anchor group. However, this experiment showed that the μCP of the ITC silane was not as accurate to shape and size of the features as those created by other patterning methods as e.g. Dip Pen Nanolithography, Polymer blend masking, UV/O_3 direct oxidation of polymers which is in agreement with the results shown in literature for other alkoxy silanes. Figure 92 shows two AFM topography images of the isothiocyanate propyl trimethoxy silane printed directly on the silica wafer. A completely defined lateral resolution cannot be achieved as the silane molecules are able to move across the water layer on top of the silica creating a smearing of the molecules across the substrate.

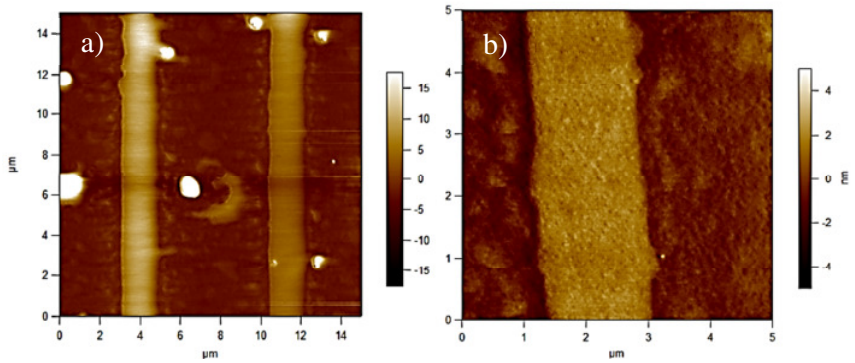

Figure 92.- AFM topography images of microcontact printed isothiocyanate silane on silica wafer. a) surface pattern prpared with a line gradient stamp shown in Figure 6 , b) a zoom into the left line in a).